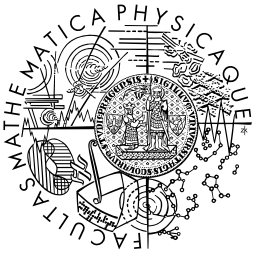

FACULTY
OF MATHEMATICS
AND PHYSICS
Charles University

DOCTORAL THESIS

Vít Orava

Modelling of heterogeneous catalytic reactions in chemical reactors

Mathematical institute of Charles University

Supervisor of the doctoral thesis:	RNDr. Jaroslav Hron, PhD.
Study programme:	Physics
Study branch:	Mathematical and Computer Modelling

Prague 2018

I declare that I carried out this doctoral thesis independently, and only with the cited sources, literature and other professional sources.

I understand that my work relates to the rights and obligations under the Act No. 121/2000 Sb., the Copyright Act, as amended, in particular the fact that the Charles University has the right to conclude a license agreement on the use of this work as a school work pursuant to Section 60 subsection 1 of the Copyright Act.

In ..... date ..... signature of the author

Title: Modelling of heterogeneous catalytic reactions in chemical reactors

Author: Vít Orava

Institute: Mathematical institute of Charles University

Supervisor: RNDr. Jaroslav Hron, PhD., Mathematical institute of Charles University

Abstract: This thesis consists of two parts discussing modelling of heterogeneous catalytic reactors.

In the first one, an industrial prototype of a fluidized bed reactor serving as a hydrogen generator based on endothermic decomposition of formic acid is studied. After initial determination of the main reactor characteristics a system of nine constituents is derived and, consequently, reduced to a three phase flow. The solid and bubble particles immersed in a liquid are modelled by the Basset-Boussinesq-Ossen equation. Furthermore, an averaging technique is used to derive a three phase Euler-Euler model. Finally, numerical computations with a verification towards the measurements and a CFD analysis are proceeded.

The second part discusses interfacial transport phenomena between a bulk and catalytic surfaces of a reactor mediated via the boundary conditions. The constitutive relations, that by construction comply with the second law of thermodynamics, follow from the specification of suitable thermodynamic potentials together with an identification of the bulk and surface entropy productions. The derived model is suitable for further analysis providing clear guidelines for the incorporation of the Langmuir-type adsorption model as well as other sorption models.

Keywords: Heterogeneous catalysis, multi-phase flow, Euler-Euler model, fluidized bed reactor, interfacial transport phenomena.

I would like to dedicate this thesis to my wife Petra and my newborn daughter Veronika. To the first one for her understanding when I needed to work late or during the weekends, to the second one for her smile which gave me strength every morning I left to work.

Furthermore, I would like to thank to my colleagues and friends, namely to the consultant of the thesis and co-author of my two publications Ondřej Souček Ph.D.; to my ex-colleague at ICP ZHAW, who dragged me into the HyForm project and the Swiss Alps, Peter Cendula; to my very good friend and colleague, with whom I discussed not just scientific but many life issues, MSc. Jan Blechta; to my ex-supervisor and head of the department of Mathematic modelling at MFF CUNI Prof. Josef Málek; to my ex-chief at ICPF CAS Doc. Marek Růžička; and, finally, to my current supervisor Jaroslav Hron Ph.D.

Contents

Preface

This Ph.D. thesis consists of two parts. In both parts a modelling of heterogeneous catalytic reactors is discussed but from two different perspectives. The first one, named "Multi-phase modelling of a reactive flow in fluidized bed reactors", represents an industrial application study when the heterogeneous nature of the reactor is suppressed by the volume averaging technique resulting into standard PDE-system in bulk only. This approach is suitable for modelling of macro-scale heterogeneous reactors when the area of the surfaces exceeds a numerically feasible threshold for direct interface tracking/capturing and an averaging technique need to be used.

On the other hand, the second part, named "A continuum model of heterogeneous catalysis: thermodynamic framework for multicomponent bulk and surface phenomena coupled by sorption", belongs in scope of theoretical studies which may be further applied for modelling of heterogeneous reactive systems. The surface phenomena are modelled along the bulk phenomena, i.e. without the averaging. This approach is possible for systems with relatively low and immobile surface area. The coupling of the superficial and bulk phenomena is mediated via boundary conditions.

The first part of the thesis concludes the work of V.O. at ICP ZHAW in Switzerland during his Ph.D. study which was a part of the HyForm project together with groups from EPFL, PSI and Granit SA. The two-years project, with one year of prolongation, was supported by CTI and Swisselectric Reseach. The aim of the project was a construction of a lab-scale prototype of an electric generator based on environmentally harmless endothermic decomposition of formic acid whose product feeds a PEM fuel cell. The decomposition occurs in a fluidized bed reactor whose modelling was the responsibility of V.O. and P. Cendula. A preliminary result of the modelling part was published in the article titled *Multi-phase modeling of non-isothermal reactive flow in fluidized bed reactors* by V.O., O. Souček and P. Cendula in the Journal of Computational and Applied Mathematics, cf. [75]. The final outcome of the project is summarized in the article *Heterogeneous Catalytic Reactor for Hydrogen Production from Formic Acid and Its Use in Polymer Electrolyte Fuel Cells* by Yuranov et al. in the ACS Sustainable Chemistry & Engineering, cf. [115].

The second part of the thesis is a preprint of the same name article by O. Souček, V.O., J. Málek and D. Bothe which is under review in the International Journal of Engineering Science. The article originally arose as a continuation of the V.O. diploma thesis, supervised by J. Málek at MFF CUNI and D. Bothe at TU Darmstadt. Consequently, joining of O. Souček as a co-author gave rise to a self-consistent study on the modelling of active surfaces which, I believe, will serve as a valuable guidance for further modelling of heterogeneous catalysis.

Comments on the contents of the thesis:

The first part of the thesis consists of four chapters and two Appendices. Chapter 1 discusses an overall introduction to modelling of fluidized bed reactors focusing on chemical reactions and other transformations during the thermal decomposition of a liquid formic acid into gaseous mixture of hydrogen and carbon dioxide.

Chapter 2 treats the Basset-Boussinesq-Ossen (BBO) equation describing a motion of particles in fluid. The basic concept of the BBO equation and the consequent application to the investigated fluidized bed reactor are presented.

Chapter 3 concerns a derivation of a PDE-system based on balancing of partial masses, partial velocities and a common temperature. The model of originally nine constituents is reduced to three phase flow. Using the form of reduced BBO equation derived in the second chapter, the partial velocities of solid and gaseous objects may be expressed in an algebraic form depending on the liquid velocity only. Due to the application of the volumetric averaging technique, the momentum balance adopts the form of Reynolds-averaged Navier-Stokes (RANS) equation and an additional closure need to be used. This is done by multiphase version of the $k - \varepsilon$ model.

Chapter 4, the last chapter of the first part, describes numerical implementation of the model, verification of the results towards the measurements and CFD analysis of the system with consequent design and up-scale guidelines.

Finally, Appendix A concerns a brief introduction to the theory of volume averaging technique applied in Chapter 3.

The second part of the thesis consists of three chapters and two Appendices. The first chapter of the second part, i.e. Chapter 5, is a brief introduction to the problematic of modelling on active surfaces together with definitions of the bulk and surface variables.

Chapter 6 recalls partial balances of mass and a common balance of momenta, energy and entropy for a control volume containing active interfaces, i.e. both bulk and surface balances need to be considered. Moreover, suitable boundary conditions are introduced.

Chapter 7 provides essential closures in scope of Classical Irreversible Thermodynamic (CIT) for bulk as well as for active surfaces. Two possible transfer models are introduced together with eventual further simplification to the standard Langmuir adsorption model commonly used in chemical engineering.

Appendix B introduces a statistical lattice model for surface free energy. Finally, Appendix C provides very elegant derivation of the Euler relations in the bulk and on the surface.

List of Symbols

Latin letter	Explanation
A_α, ${}^{\Sigma}\mathrm{A}_\alpha$	α-th bulk constituents and their surface counterparts
A_N	solvent
${}^{\Sigma}\mathrm{A}_0$	surface vacancies
$\mathcal{A}^\zeta$, ${}^{\Sigma}\mathcal{A}^\zeta$	affinity of the ζ-th bulk, resp. surface chemical reaction
$\mathbf{b}$, ${}^{\Sigma}\mathbf{b}$	specific density of bulk and surface forces
$\mathbf{b}_\alpha$, ${}^{\Sigma}\mathbf{b}_\alpha$	specific bulk and surface force densities acting on α-th constituent
$\mathbf{b}_\alpha^{\mathrm{M}}$, ${}^{\Sigma}\mathbf{b}_\alpha^{\mathrm{M}}$	bulk and surface specific molar force acting on α-th constituent
${}^{\Sigma}$	surface curvature tensor
c_α, ${}^{\Sigma}c_\alpha$	bulk and surface mass fraction (mass concentration) of α-th constituent
c_α^{M}, ${}^{\Sigma}c_\alpha^{\mathrm{M}}$	bulk and surface molar concentration of α-th constituent
${}^{\mathrm{d}\Sigma}c_\alpha^{\mathrm{M}}$	surface molar concentrations of α-th constituent on $\mathrm{d}\Sigma$
c^{M}, ${}^{\Sigma}c^{\mathrm{M}}$	sum of bulk and surface molar concentrations
${}^{\mathrm{d}\Sigma}c^{\mathrm{M}}$	sum of surface molar concentrations on $\mathrm{d}\Sigma$
$\mathbf{d}_\alpha^{\mathrm{diff}}$	bulk diffusional driving force in Maxwell-Stefan equations acting on α-th constituent
$\mathrm{D}_{\alpha\beta}$	Maxwell-Stefan diffusivity matrix
${}^{\Sigma}$,	symmetric part of the bulk and surface velocity gradient
d, ${}^{\Sigma}$ d	deviatoric (traceless) part of and ${}^{\Sigma}$
div, div^{Σ}	bulk and surface divergence operators
e, ${}^{\Sigma}e$	bulk and surface specific internal energies
e^{M}, ${}^{\Sigma}e^{\mathrm{M}}$	bulk and surface molar internal energies
$f_{\alpha\beta}$, ${}^{\Sigma}f_{\alpha\beta}$	bulk and surface Maxwell-Stefan friction coefficient matrix
${}^{\mathrm{d}\Sigma}F$	Helmholtz free energy of $\mathrm{d}\Sigma$
g, ${}^{\Sigma}g$	specific bulk and surface Gibbs' free energies
g^{M}, ${}^{\Sigma}g^{\mathrm{M}}$	bulk and surface molar Gibbs' free energies
h, ${}^{\Sigma}h$	specific bulk and surfaces enthalpies of the mixture as a whole
h_α, ${}^{\Sigma}h_\alpha$	specific bulk and surfaces enthalpies of the α-th constituent
${}^{\Sigma}\mathrm{H}$	mean surface curvature
$\mathbf{J}_\eta$, ${}^{\Sigma}\mathbf{J}_\eta$	bulk and surface entropy fluxes
$\mathbf{J}_e$, ${}^{\Sigma}\mathbf{J}_e$	bulk and surface energy fluxes
$\mathbf{J}_\alpha^{\mathrm{diff}}$, ${}^{\Sigma}\mathbf{J}_\alpha^{\mathrm{diff}}$	bulk and surface diffusive fluxes of α-th constituent
$\mathbf{J}_\alpha^{\mathrm{M,diff}}$, ${}^{\Sigma}\mathbf{J}_\alpha^{\mathrm{M,diff}}$	bulk and surface molar diffusive fluxes of α-th constituent
k	Boltzmann constant
K, K_0	index sets of bulk species, surface species (including vacancies)
$K^{\mathrm{non-ad}}$	index set of non-adsorbing species
$\mathcal{K}_\zeta^{\mathrm{chem}}$, ${}^{\Sigma}\mathcal{K}_\zeta^{\mathrm{chem}}$	equilibrium constant of ζ-th bulk and surface chemical reaction
$\mathcal{K}_\alpha^{\mathrm{sor}}$	sorption equilibrium constant for α-th constituent
k_ζ^f, k_ζ^b	forward and backward reaction rate coefficients of ζ-th bulk chemical reaction
${}^{\Sigma}k_\zeta^f$, ${}^{\Sigma}k_\zeta^b$	forward and backward reaction rate coefficients of ζ-th surface chemical reaction
${}^{\Sigma}k_\alpha^{\mathrm{ad-sor}}$, ${}^{\Sigma}k_\alpha^{\mathrm{de-sor}}$	adsorption and desorption rate coefficients

$\mathbb{L}$, ${}^{\Sigma}\mathbb{L}$	bulk and surface thermo-diffusional coupling matrices
$N_\alpha(V)$, ${}^{\Sigma}N_\alpha(S)$	number of moles of A_α constituent in the given volume element V, resp. surface element S
P, ${}^{\Sigma}\mathrm{P}$	bulk and surface mean normal stresses, i.e. isotropic parts of the bulk and surface Cauchy stress tensors
p, ${}^{\Sigma}p$	bulk thermodynamic pressure and surface pressure
M_α	molar mass of molecule A_α
$\mathcal{M}_b$	molar mass of b-th atom
$\mathbf{n}$, $\mathbf{n}^{\Sigma}$	(outer) unit normal to Ω and Σ
N_A	Avogadro number
${}^{\mathrm{d}\Sigma}\mathrm{N}_\alpha$	number of surface molecules of α-th constituent on $\mathrm{d}\Sigma$
${}^{\mathrm{d}\Sigma}\mathrm{N}_S$	number of adsorption sites on $\mathrm{d}\Sigma$
${}^{\Sigma}\mathbb{I}$	surface projection tensor
s_e, ${}^{\Sigma}\mathrm{s}_e$	bulk and surface internal energy sources on Σ
s_η, ${}^{\Sigma}\mathrm{s}_\eta$	bulk and surface entropy sources
${}^{\Sigma}q$	surface molecular partition function
r_α, ${}^{\Sigma}r_\alpha$	bulk and surface rates of production of α-th constituent in chemical reactions
r_α^{M}, ${}^{\Sigma}r_\alpha^{\mathrm{M}}$	bulk and surface molar rates of production of α-th constituent in chemical reactions
R	universal gas constant
$\mathcal{R}_\zeta^f$, $\mathcal{R}_\zeta^b$	forward and backward reaction rates of ζ-th bulk chemical reactions
$\mathcal{R}_\zeta$	${}^{\Sigma}\mathcal{R}_\zeta^f - {}^{\Sigma}\mathcal{R}_\zeta^b$
${}^{\Sigma}\mathcal{R}_\zeta^f$, ${}^{\Sigma}\mathcal{R}_\zeta^b$	forward and backward reaction rates of ζ-th surface chemical reactions
${}^{\Sigma}\mathcal{R}_\zeta$	${}^{\Sigma}\mathcal{R}_\zeta^f - {}^{\Sigma}\mathcal{R}_\zeta^b$
${}^{\Sigma}s_\alpha$	surface sorption rate of α-th constituent
${}^{\Sigma}s_\alpha^{\mathrm{M}}$	surface molar sorption rate of α-th constituent
$\mathbb{S}$, ${}^{\Sigma}\mathbb{S}$	deviatoric (traceless) parts of tensors $\mathbb{T}$, ${}^{\Sigma}\mathbb{T}$
$\mathrm{S}^{b\alpha}$	matrix capturing the atomic composition of A_α
$\mathbb{T}$, ${}^{\Sigma}\mathbb{T}$	bulk and surface Cauchy stress tensors
$\mathbb{T}^{\mathrm{e}}$	bulk extra stress tensor
$\mathbf{u}_\alpha^{\mathrm{diff}}$	bulk diffusive velocity of α-th constituent with respect to barycentric velocity
$\mathbf{v}_\alpha$, ${}^{\Sigma}\mathbf{v}_\alpha$	bulk and surface velocities of α-th constituent
$\mathbf{v}$, ${}^{\Sigma}\mathbf{v}$	barycentric bulk and surface velocities
${}^{\mathrm{d}\Sigma}W$	grand thermodynamic potential
x_α, ${}^{\Sigma}x_\alpha$	bulk and surface molar fractions of α-th constituent
${}^{\mathrm{d}\Sigma}x_\alpha$	surface molar fraction of α-th constituent on $\mathrm{d}\Sigma$
Z, ${}^{\Sigma}Z$	number of bulk and surface chemical reactions
$[\![\phi]\!]$	jump of ϕ quantity across an interface ($[\![\phi]\!] := {}^{+}\phi - {}^{-}\phi$)

Greek letter	Explanation
β^ζ, ${}^{\Sigma}\beta^\zeta$	bulk and surface chemical rate constant of ζth reaction
${}^{\Sigma}\gamma$, σ	surface tension
ζ_α	chemical activity of α-th constituent
η, ${}^{\Sigma}\eta$	specific bulk and surface entropies

η^{M}, ${}^{\Sigma}\eta^{\mathrm{M}}$	bulk and surface molar entropies
ϑ, ${}^{\Sigma}\vartheta$	bulk and surface temperatures
${}^{\mathrm{d}\Sigma}\vartheta$	local surface thermodynamic temperature on $\mathrm{d}\Sigma$
λ, ${}^{\Sigma}\lambda$	bulk and surface volumetric viscosity
μ_α, μ_α^{M}	bulk and surface chemical potentials of α-th constituent
${}^{\Sigma}\bar{\mu}_\alpha^{\mathrm{M}}$	${}^{\Sigma}\mu_\alpha^{\mathrm{M}} - {}^{\Sigma}\mu_0^{\mathrm{M}}$
$\mu_{\alpha,\beta}^{\mathrm{M}}$	$\mu_\alpha^{\mathrm{M}} := \frac{M_\alpha}{M_\beta}\mu_\beta^{\mathrm{M}}$
${}^{\Sigma}\mu_\alpha^{\mathrm{M}}$	surface molar chemical potential of α-th constituent
${}^{\mathrm{d}\Sigma}\mu_\alpha^{\mathrm{M}}$	local surface molar chemical potential of α-th on $\mathrm{d}\Sigma$
${}^{\mathrm{d}\Sigma}\mu_\alpha^{\mathrm{m}}$	local molecular surface chemical potential of α-th const. on $\mathrm{d}\Sigma$
ν, ${}^{\Sigma}\nu$	bulk and surface shear viscosities
$\delta_\alpha^{\zeta,f}$, $\delta_\alpha^{\zeta,b}$, δ_α^{ζ}	forward, backward and combined stoichiometric coefficients of ζ-th bulk chemical reaction
${}^{\Sigma}\delta_\alpha^{\zeta,f}$, ${}^{\Sigma}\delta_\alpha^{\zeta,b}$, ${}^{\Sigma}\delta_\alpha^{\zeta}$	forward, backward and combined stoichiometric coefficients of ζ-th surface chemical reaction
${}^{\mathrm{d}\Sigma}\Xi$	grand-canonical partition sum on patch $\mathrm{d}\Sigma$
$\Upsilon^{(\mathrm{A})}$, $\Upsilon^{(\mathrm{B})}$	kinetic factors for Transfer models A and B, respectively
Λ	Lagrange multiplier in the bulk Maxwell-Stefan equations
Π_η, ${}^{\Sigma}\Pi_\eta$	bulk and surface entropy productions
${}^{\Sigma}\Pi_\eta^{\mathrm{i}}$, ${}^{\Sigma}\Pi_\eta^{\mathrm{t}}$	surface entropy production due to intrinsic surface processes and transfer processes
Π_η^{mech}, ${}^{\Sigma}\Pi_\eta^{\mathrm{i,mech}}$	bulk and surface entropy productions due to mechanical processes
Π_η^{diff}, ${}^{\Sigma}\Pi_\eta^{\mathrm{i,diff}}$	bulk and surface entropy productions due to thermo-diffusion (heat transfer and mass diffusion)
Π_η^{chem}, ${}^{\Sigma}\Pi_\eta^{\mathrm{i,chem}}$	bulk and surface entropy productions due to chemical reactions
${}^{\Sigma}\Pi_\eta^{\mathrm{i,diff}}$, ${}^{\Sigma}\Pi_\eta^{\mathrm{i,chem}}$	surface entropy productions due to mechanical dissipation, thermo-diffusion and chemical reactions
$\Pi_\eta^{\mathrm{diff-m}}$, ${}^{\Sigma}\Pi_\eta^{\mathrm{i,diff-m}}$	bulk entropy production due to mass diffusion
${}^{\Sigma}\Pi_\eta^{\mathrm{sor(A,B)}}$	surface entropy production due to sorption (Models A and B)
${}^{\Sigma}\Pi_\eta^{\mathrm{fric(A,B)}}$	surface entropy production due to friction (Models A and B)
${}^{\Sigma}\Pi_\eta^{\mathrm{et(A,B)}}$	entropy production due to energy transfer between bulk and surface (Models A and B)
ρ_α, ρ_α^{Σ}	bulk and surface partial density of α-th constituent
ρ, ρ^{Σ}	bulk and surface mixture densities
Σ, $\mathrm{d}\Sigma$	active surface and its element
$\tau_{\alpha\beta}$	Maxwell-Stefan interaction coefficient matrix
ψ, ${}^{\Sigma}\psi$	specific bulk and surface Helmholtz free energies
ψ^{M}, ${}^{\Sigma}\psi^{\mathrm{M}}$	bulk and surface molar Helmhotz free energies
Ω	bulk domain
$\partial\Omega$	boundary of Ω
∇, ∇^{Σ}	bulk and surface gradient

Part I

Modelling of multi-phase reactive flow in fluidized bed reactors

1. Introduction to the problem

In this section a basic concept of the examined fluidized bed reactor is presented. Starting with simple and better-known reactors, the fluidized bed reactor principle is introduced and, consequently, discussed on a concrete application. Alongside a physical concept of the modelling, basic chemistry and thermodynamic of the reactor are discussed.

1.1 Fluidized bed reactors

1.1.1 Motivation

There is great diversity in application, shape and working regime of multiphase chemical reactors. To begin with, we present three groups of commonly used multiphase reactors, distinguished by the operating principles.

One of the representative of multiphase reactors are bubble-column reactors where bubbles ascent through liquid. The bubbles are typically injected to a reactor by a distributor and they are usually subjected to purely mechanical effects, such as adiabatic expansion and mass exchange via the interface. These reactors contain mainly two phases, no chemical reaction takes place and the flow is commonly assumed to be isothermal. As an industrial example, we mention the bubble column reactors for oxidation, polymerization, hydrogenation etc., commonly used in manufacturing of synthetic fuels.

Second big group of multiphase reactors are the packed bed reactors. Here, the main body of the reactor is usually filled by a (rigid) porous medium which is being penetrated by a fluid. The inner structure of packed bed reactors is considered as immobilised, formed by a continuous or closely packed matter. The packed bed reactors are widely used e.g. in petroleum industry; cleaning of drinking water etc.

Fluidized bed reactors posses something from both previously mentioned. A body of fluidized bed reactor is partially filled by (discrete, floating) particles which undergo stirring due to a movement of other particles or a flow of the surrounding continuous phase. In some cases, the reactor may change the behaviour and transfers from packed bed to fluidized bed (or vice versa). This phenomena is called fluidization and it is often part of an initiation process of fluidized bed reactors (especially in case of sand bed reactors of filters), usually accompanied by the characteristic pressure drop profile (Figure (1.1)).

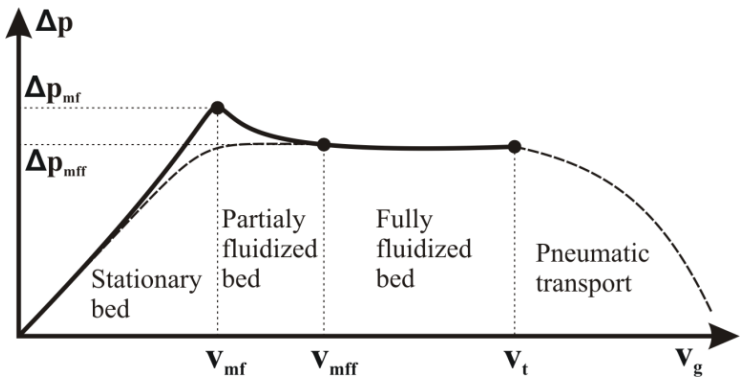

Figure 1.1: Fluidization of a fluidized bed reactor. Adopted from [54].

A common example of a three-phase fluidized bed reactor is an aeration tank for water treatment. It is a biological reactor where gas (usually air or oxygen) is being injected in the form of bubbles into a mixture of waste-water and micro-organisms. This helps to develop biological flocs which reduce the organic content of the waste-water.

The examined fludized bed reactor serving as a hydrogen generator works, however, little bit different. In contrast to bubble columns or aeration tanks, the bubbles are not injected into the reactor, but they are produced inside. The reactor is filled and constantly supplied by a liquid formic acid. Besides the liquid, solid catalytic particles of a spherical shape are present. On the surface of the particles, a molecule of the acid decomposes to a molecule of dissolved hydrogen and carbon dioxide. Once the surrounding liquid becomes saturated by the reaction product, gaseous bubbles are formed. The bubbles undergo possibly rapid growth and ascent to the liquid surface on the top of the reactor. (This phenomena is very similar to degassing of a mineral water/beer.) Consequently, the gas leaves the reactor through a pressure valve and continues to the connected PEM fuel cell.

Since the decarboxylation of formic acid is an endothermic reaction, an external heat source need to be provided, e.g. by immersed heating tubes. Consequently, the resulting temperature gradients induce thermal (natural) convection which mixes the solid particles together with the formic acid and forms a suspension.

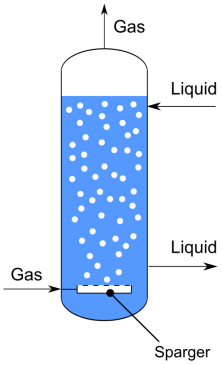

Bubble column reactor:
liquid gas
Dissolution of the gas into the liquid.

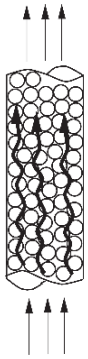

Packed/fixed bed:
fluid ^{solid} fluid
Heterogeneous catalysis in porous **immobilized** macro-structure

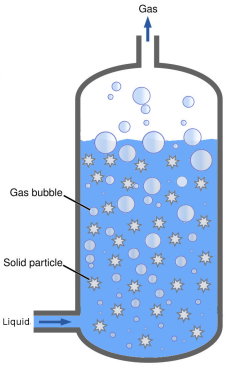

Three-phase fluid. bed:
liquid ^{solid} gas
Heterogeneous catalysis on **moving** micro-structure.

1.1.2 Hydrogen generator for PEMFC

In the recent years, proper understanding and optimization of the process of hydrogen production at the industrial scale has become a topic of utmost importance. This is mainly due to the primal role of hydrogen as a fuel in most types of fuel cells whose application in various industry segments has been growing rapidly, see [22]. Production of hydrogen by formic acid decomposition is one promising route to overcome inherently difficult and inefficient storage of hydrogen itself, cf. [35].

Formic acid is a non-hazardous liquid with the highest content of hydrogen from all carboxylic acids. [1] This makes it an ideal source of hydrogen which can be effectively produced by heterogeneous catalysis under presence of certain noble metal (e.g. Ruthenium). This is possible for example in a fluidized bed reactor. In this reactor the gaseous

[1] Acids containing a carboxylic group $COOH$

bubbles, filled by mixture of hydrogen and carbon dioxide, are produced enabling direct use in commercial PEM fuel cells (Figure (1.2)).

The development of a hydrogen generator along with a PEM fuel cell represents very attractive technological field with a plethora of possible industrial applications, e.g. in mobile (automotive) or decentralised power sources with fixed-site installations for power grid backup generation and many other. A proper CFD model of the reactor with reasonable complexity, tractable by numerical simulations, may provide valuable means for understanding and optimal performance of the reactor in an industrial application.

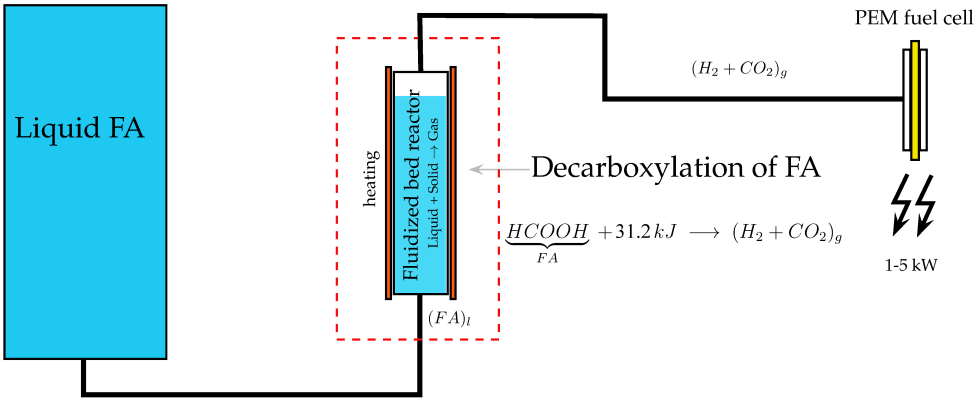

Figure 1.2: A sketch of the generator coupled to PEMFC.

1.2 Problem description

1.2.1 Reactor design specifications

During the development of the fluidized bed reactor for the HyForm project, we investigated several prototypes using various catalyst, reactor shapes and heating systems. In this work, we focus on the reactor which showed the most reliable measurements simultaneously allowing observations of the ongoing phenomena.

The reactor has a simple cylindrical shape with the inner diameter 70 mm, and length 460 mm (Figure (1.3)). The bottom and top of the reactor are made of Inconel 625 steel and the main body is made of thick transparent high-pressure (up to 10 atm) glass allowing visual observations or covered by an insulation layer. The heating system is formed by several connected hollow U-shaped Inconel 625 tubes with inner diameter 3 mm and outer diameter 4.75 mm.

Within the heating tubes flows a low viscosity oil which is externally heated in a thermostat and driven by a compressor (pump). Except the known temperature in the thermostat, there are two more sensors, namely on the inlet and on the outlet of the heating system.

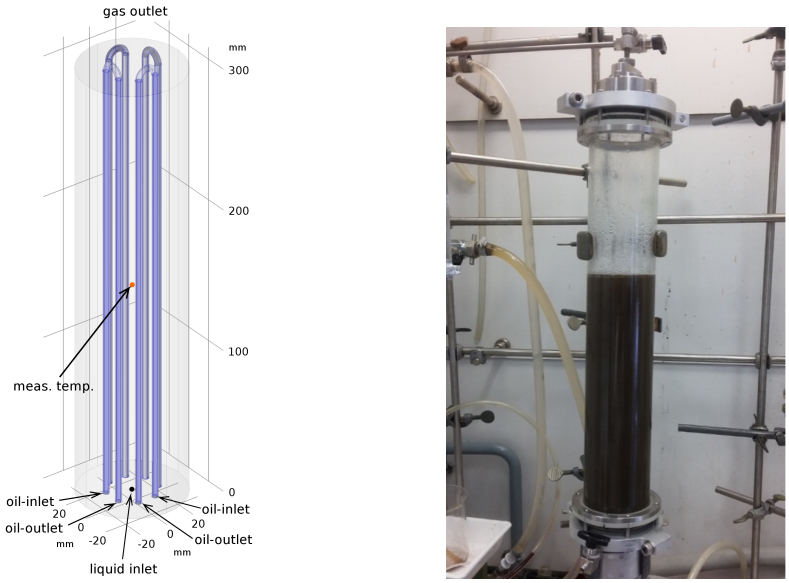

Figure 1.3: Reactor interior with highlighted heating tubes (left) and the lab installation.

The level of liquid is approximately at the height 300 mm, hence, the reactor volume is little more than 1 L. The formic acid is injected via a nozzle located in the centre of the bottom plate and the flow rate is regulated by a pump. Since the mass transfer of the liquid into the gas is relatively slow, its upper surface level may be considered as constant and we can model the reactor interior as a constant control volume avoiding the difficulties with a free surface flow.

The catalytic particles consist of support and catalytic coating. As the support serves commercial GPPS polystyrene with density 1.05 $\frac{\mathrm{g}}{\mathrm{mL}}$ and approximately spherical shape having the characteristic diameter 100 μm. Nevertheless, the process of catalytic coating cause a certain damage on the particle and we may experience irregular shapes (Figure (1.4)).

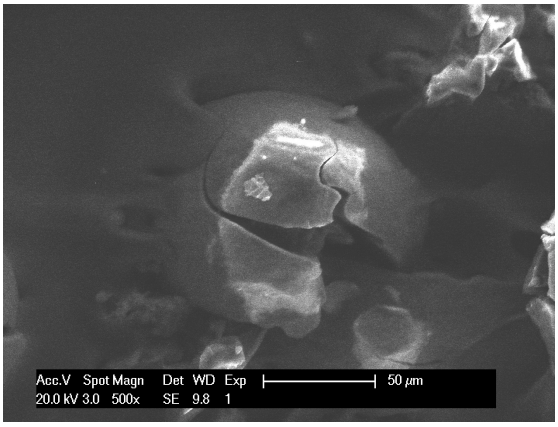

Figure 1.4: A SEM image of a damaged catalytic particle.

The catalytic particles stay all the time within the reactor, i.e. there is no inflow/outflow neither sink/source. Since their density is similar (little higher) to the density of the surrounding liquid, once the liquid starts to circulate due to the thermal convection, the particles circulate along.

The construction of the prototype lab-scale reactor and its examination towards industrial applications was a part of the Swiss project HyForm supported by CTI and Swisselectric Research. The manufacturing, installation and experimental measurements of the reactor system was made by Martin Grasemann, Andrew Dalebrook and Igor Yuranov at EPFL under supervisory of prof. Gábor Laurenczy. The modelling part including verification and optimal design guidelines was in charge of V.O. and Peter Cendula at ZHAW. For further details we refer to [115].

1.2.2 Hydrogen production principle

The purpose of the reactor is a decomposition of the liquid formic acid into a gaseous mixture of hydrogen and carbon dioxide which escape through the top of the reactor. The process as a whole can be summarized in the following steps:

1. A highly concentrated aqueous solution of formic acid (typically $97-99\,\%\text{mol}$)[2] enters the reactor.
2. A molecule of formic acid adsorbs onto the catalytic surface of the particle and forms a chemical bond with the catalyst (Ruthenium).
3. The catalyst decomposes the adsorbed molecule of formic acid into the molecule of hydrogen and carbon dioxide.
4. The molecules of hydrogen and carbon dioxide unbind the catalyst and desorb from the catalytic surface into the surrounding liquid in the form of dissolved gas.
5. Once, the liquid becomes saturated, the dissolved gas starts to evaporate into nucleating bubbles. The bubbles undergo rapid growth and ascend to the liquid surface.
6. The gas leaves the reactor through a pressure valve situated on the top of the reactor and continues to the adjacent PEM fuel cells.

The steps 2-5 may be written in the chemical equation as [3]

$$\underbrace{HCOOH_{(l)} \longrightarrow \overbrace{HCOOH^*}^{\text{chemical reaction}}}_{\text{adsorption}} \overset{Cat_{(s)}}{\longrightarrow} \underbrace{H_2^* + CO_2^* \longrightarrow \overbrace{H_{2(d)} + CO_{2(d)}}^{\text{vaporization}} \longrightarrow H_{2(g)} + CO_{2(g)}}_{\text{desorption}}$$

or, in a compact way, as

$$HCOOH_{(l)} \overset{Cat_s}{\longrightarrow} H_{2(g)} + CO_{2(g)}.$$

Moreover, along the dissolved gas evaporation, the system experiences also the evaporation of liquid water and formic acid. This may be represented as

$$H_2O_{(l)} \longrightarrow H_2O_{(g)} \tag{1.1a}$$

$$FA_{(l)} \longrightarrow FA_{(g)}. \tag{1.1b}$$

[2] The symbol "%mol" denotes molar fraction of the solution, i.e. the amount of a constituent (expressed in moles) divided by the total amount of all constituents in a mixture. Analogously, we understand also mass fraction (weighted) denoted by "wt." and volume fraction "vol.".

[3] The lower indices of a constituent denote the phase type, namely (l) is liquid, (s) is solid, (g) is gas. Moreover, (d) denotes dissolved gas and "*" an adsorbed species.

Let us mention one important fact concerning a mixture of formic acid and water. These two liquids tends to form an azeotrope, i.e. due to the evaporation/boiling a mixture of constant ratio of formic acid and water is formed. To ensure relatively constant production of the gaseous hydrogen, the reactor is initially filled by the formic acid/water azeotrope. For more information, see Remark (1.2.2).

1.2.3 Chemical reactions

Catalytic reactions: Generally speaking, catalyst acts as a reaction medium, i.e. it enters the reaction; decreases the activation energy by formation of an additional reaction step (Figure (1.5)); but it does not form the final product of the reaction. In the ideal case, the catalyst neither drains nor deactivates.

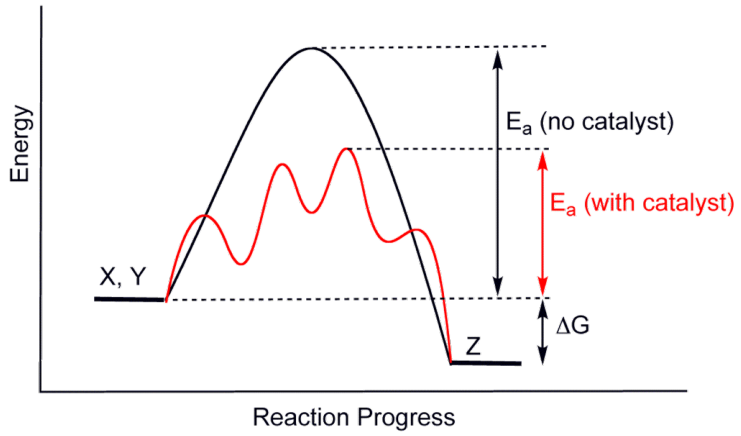

Figure 1.5: Decrease in the activation energy under catalyst. Source en.wikipedia.org.

A simple chemical reaction of two species A, B forming a product C:

$$A + B \to C$$

undergoes in a presence of a catalyst X several intermediate steps which may be expressed as a system of consequent reactions:

$$\begin{aligned} A + X &\to AX \\ B + AX &\to ABX \\ ABX &\to XC \\ XC &\to X + C. \end{aligned}$$

Although the catalyst is consumed in the first step of the reaction, it is subsequently produced in the fourth step, so it does not occur in the overall reaction equation.

Kinetic regime of a reactor:

Performance of multi-phase reactors depends on many factors - not just a speed of chemical reactions but also transport processes such as a mass transfer between the phases or diffusion of the constituents.

From this perspective, we distinguish a kinetic and diffusive regime of a reactor. The first one is characterised by fast transport processes when the reactor performance is mostly

limited by the chemical reaction. The diffusive regime is, on the other hand, limited by a speed of transport processes rather that rate of chemical reactions.

In our particular case, we consider the reactor being in the kinetic regime limited by the decarboxylation of the formic acid. This assertion is supported by the fact that the reactor production rate follows the exponential temperature dependency predicted by the Arrhenius equation. [4] Other processes, such as diffusion of the dissolved gases and consequent gas-liquid interfacial transfer, are, therefore, considered much quicker.

There are several important consequences of the kinetic reactor setting. Since the mass transfer is not limited by the diffusion, we can assume that the reaction product is quickly (and more or less uniformly) distributed within the whole reactor volume. Thus, its concentrations may be fairly approximated as constant.

Thermodynamics of the reactions:

The decarboxylation of formic acid is described by the following change in thermodynamic potentials

$$HCOOH_{(l)} \longrightarrow H_{2(g)} + CO_{2(g)} \tag{1.2}$$
$$\Delta G^{\Theta} = -32.9\ \tfrac{\mathrm{kJ}}{\mathrm{mol}},\ \Delta H^{\Theta} = 31.2\ \tfrac{\mathrm{kJ}}{\mathrm{mol}},\ \Delta S^{\Theta} = 215\ \tfrac{\mathrm{J}}{\mathrm{mol\cdot K}}.$$ [5]

It expresses that the reaction is being spontaneous and endothermic (consumes heat). The equilibrium constant [6] can be calculated from the change of Gibbs free energy as

$${}^{eq}K^{\Theta} := \frac{[H_2][CO_2]}{[HCOOH]} = e^{-\frac{\Delta \mathrm{G}^{\Theta}}{\mathrm{RT}}} \tag{1.3}$$

where the bracket $[\cdot]$ denotes the molar concentration of the species. Using the value of Gibbs energy for the FA-decarbolylation, we obtain ${}^{eq}K^{\Theta} \approx 5.8 \cdot 10^5$.

The enthalpy change of the reaction is typically considered to be independent of pressure once the reaction occurs at constant pressure. This can be viewed from the thermodynamic identity

$$\Delta H = T\Delta S + V\Delta p \overset{\Delta p=0}{=} T\Delta S.$$

On the other hand, the enthalpy change of the reaction depends on the temperature.

Following the Shomate Equation for gases [17] in the form

$$\Delta H = H - H^{\Theta} = A\,t + B\frac{t^2}{2} + C\frac{t^3}{3} + D\frac{t^4}{4} + \frac{E}{t} - F, \tag{1.4}$$

with coefficients commonly available in the literature (e.g. [17]), we obtain the (minor) dependency of the reaction enthalpy on the temperature (Figure (1.6)).

[4] The Arrhenius equation describes (empirically) the temperature dependence of reaction rates at ideal conditions, cf. [4, 22.5].

[5] The values of standard state variables of the reaction, namely, the Gibbs free energy G^{Θ}, the enthalpy H^{Θ} and the entropy S^{Θ} are valid for one mole of each substance being in its standard states and the STP condition - standard temperature (298 K) and pressure (1 atm).

[6] The equilibrium constant of a chemical reaction is the value of reaction quotient when the reaction has reached its equilibrium. i.e. the forward and backward chemical rates equal.

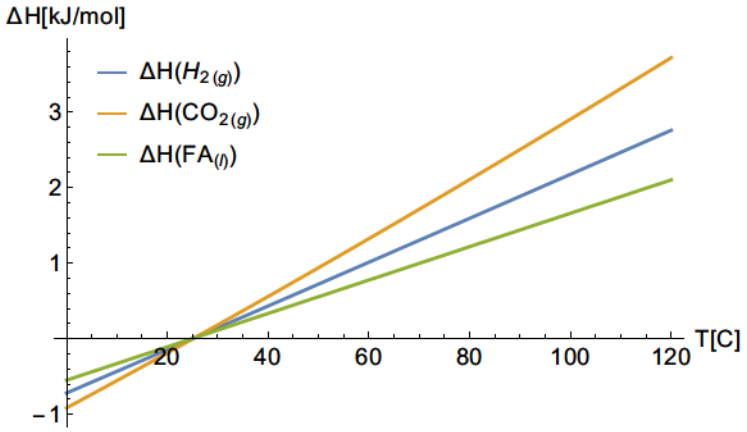

Figure 1.6: The temperature dependence of the enthalpy change for hydrogen, carbon dioxide molecule and formic acid.

Using the additivity of the enthalpies, i.e.

$$\Delta H = \sum \nu_\alpha \Delta H_\alpha,$$

where ν_α denotes stoichiometric coefficients of the reaction, we obtain the change of enthalpy of reaction $\Delta H = 3.42\,\frac{\text{kJ}}{\text{mol}}$ at 100 °C. From this, we derive the enthalpy of reaction for the decarboxylation of formic acid at 100 °C having a value approximately $36.32\,\frac{\text{kJ}}{\text{mol}}$.

The Van't Hoff equation follows the relation

$$\frac{\mathrm{d}\ln {}^{eq}K^{\Theta}}{\mathrm{d}T} = -\frac{\Delta H^{\Theta}}{R}. \tag{1.5}$$

The integration between the temperatures T_1 ans T_2 gives

$$\ln\left(\frac{K_2}{K_1}\right) = \frac{\Delta H^{\Theta}}{R}\left(\frac{1}{T_1} - \frac{1}{T_2}\right) \tag{1.6}$$

where K_1, K_2 are the equilibrium constants at the temperature T_1 and T_2. Consequently, tt $T = 373\text{K}$ the equilibrium constant for decarboxylation of formic acid correspond to ${}^{eq}K^{373K} \approx 7.3 \cdot 10^6$.

Now, we define the extent (evolution) of the reaction as [7]

$$\mathrm{d}\xi := \frac{\mathrm{d}[A_\alpha]}{\nu_\alpha M_\alpha} \tag{1.7}$$

where ν_α stands for stoichiometric coefficient of the species A_α. Note, that any reaction r of n-species $A_1, \ldots, A_n$ written in the form

$$\nu_1^f A_1 + \nu_2^f A_2 + \ldots + \nu_n^f A_n \qquad \nu_1^b A_1 + \nu_2^b A_2 + \ldots + \nu_n^b A_n,$$

where $\nu_\alpha := \nu_\alpha^f - \nu_\alpha^b, \alpha = 1, \ldots, n$, satisfies the following relation:

$$\frac{\mathrm{d}[A_\alpha]}{\nu_\alpha M_\alpha} = \frac{\mathrm{d}[A_\beta]}{\nu_\beta M_\beta}, \ \forall \alpha, \beta \in \{1, \ldots, n\}.$$

[7] Strictly speaking, one should consider instead of molar concentration $[A_\alpha]$ a generalized quantity called activity $a_\alpha([A_\alpha])$. However, for elementary (one-step) reaction, this quantity is commonly considered as an identity.

Considering the reaction at constant pressure and temperature, we use the Van't Hoff equation (1.5) and the relation (1.3) to obtain the dependence of change of Gibbs free energy as

$$\Delta G = \left(\frac{\mathrm{d}G}{\mathrm{d}\xi}\right)_{T,p} = \Delta G^{\Theta} + RT \ln Q \tag{1.8}$$

where $Q := \Pi_{\alpha=1}^{n} [A_\alpha]^{\nu_\alpha}$ is the reaction quotient.

The reactor is an open system constantly held out of equilibrium, the characteristic molar concentrations correspond approximately to

$$c_{FA_{(l)}} \approx 26 \,\frac{\mathrm{mol}}{\mathrm{L}},\ \mathrm{c}_{\mathrm{H}_{2(\mathrm{d})}}, \mathrm{c}_{\mathrm{CO}_{2(\mathrm{d})}} \ll 1 \,\frac{\mathrm{mol}}{\mathrm{L}}.$$

This gives the following value for reaction coefficient and change of Gibbs free energy:

$$Q \ll 1,\ \Delta G < -43.4 \,\frac{\mathrm{kJ}}{\mathrm{mol}}.$$

Once $Q < {}^{eq}K^{373K}$ and $\Delta G < 0$ the reaction at the specific condition within the reactor proceeds (is spontaneous) in the desired forward direction.

Side reactions: The decarboxylation of formic acid has been very well utilized on a noble-metal-based heterogeneous catalyst (e.g. Ru, Pd, Au) which is practically CO-free, cf. [35]. However, besides the main chemical reaction, there are always also other chemical reactions but, typically, with much lower reaction rate.

Generally speaking, the molecules of incoming formic acid and water may decompose or compose to many different molecules formed by the atoms of hydrogen, carbon and oxygen. In the recent reactor conditions, we detected (apart of the decarboxylation product), also traces of CO. This indicates that there is at least one more reaction present. Various authors discuss this issue where traces of another strong acid or a nickel/copper reactor wall may significantly increase the rate of the unwanted side-reactions. Especially the rate of decarbonylation of FA, whose product (CO) may poison the fuel-cell membrane, can play a crucial role. For more information, we refer to (1.2.1) or [65, pp. 90],[114], [46] etc.

Nevertheless, for our purposes we do not need to consider any other chemical reaction than the decarboxylation of formic acid.

Remarks:

1.2.1 Side-reactions. *Another possible decomposition of FA is its decarbonylation, i.e. the reaction*

$$HCOOH \longrightarrow CO + H_2O.$$

This reaction often accompanies the decarboxylation. Moreover, we may consider also another possibilities, e.g. involving a formation of intermediate product.

To give a a more rigorous answer, let us assume a presence of the following chemical species in the reactor: $HCOOH, H_2, CO_2, H_2O, CO, HCHO$, *i.e.* $z = 3$ *different atoms*

and $n = 6$ different molecules:

$$\begin{aligned} z = 3 : \beta &= 1 \dots H \\ \beta &= 2 \dots C \\ \beta &= 3 \dots O \end{aligned}$$

$$\begin{aligned} n = 6 : \alpha &= 1 \dots HCOOH \\ \alpha &= 2 \dots H_2 \\ \alpha &= 3 \dots CO_2 \\ \alpha &= 4 \dots H_2O \\ \alpha &= 5 \dots CO \\ \alpha &= 6 \dots HCHO \end{aligned}$$

Now, we can construct the reaction composition matrix $T^{\alpha,\beta} \in R^{z \times n}$:

$$T = \begin{pmatrix} 2 & 2 & 0 & 2 & 0 & 2 \\ 1 & 0 & 1 & 0 & 1 & 1 \\ 2 & 0 & 2 & 1 & 1 & 1 \end{pmatrix}.$$

Moreover, we determine its orthogonal-subspace reaction matrix P where

$$P^T = \begin{pmatrix} -1 & 1 & 1 & 0 & 0 & 0 \\ -1 & 0 & 0 & 1 & 1 & 0 \\ -2 & 0 & 1 & 1 & 0 & 1 \end{pmatrix}.$$

This gives us the three possible independent reactions (the rows), namely

$$HCOOH \quad H_2 + CO_2 \tag{1.9a}$$
$$HCOOH \quad H_2O + CO \tag{1.9b}$$
$$2HCOOH \quad H_2O + CO_2 + HCHO \tag{1.9c}$$

and we may list some of the important linear combinations corresponding to intermediate steps (excluding $HCOOH$ as the reactant)

$$\begin{aligned} H_2O + CO \quad & H_2 + CO_2. \\ H_2 + CO \quad & HCHO \\ H_2O + 2CO \quad & CO_2 + HCHO \\ 2H_2 + CO_2 \quad & H_2O + HCHO. \end{aligned}$$

This procedure represent an elegant algebraic tool how to list possible reactions for given (detected) molecules.

1.2.2 Azeotrope. *An azeotrope is, so called, a constantly boiling mixture, i.e. the molar concentration of mixture equals the molar concentration of evaporated steam, thus, its composition can not be altered by distillation. Mixture of liquid water and formic acid forms an azeotrope. Its mass fraction ratio at $p = 1\,\mathrm{atm}$ corresponds to*

$$R^{FA}_{H_2O}(p) := \frac{w_{FA_g}}{w_{H_2O_{(g)}}} \overset{eq}{=} \frac{w_{FA_{(l)}}}{w_{H_2O_{(l)}}} \approx \frac{77.6}{22.4}$$

The pressure dependence of the ratio is relatively significant, hence, we approximate the value by fitting the available data, cf. [42], with the basis functions $1, \sqrt{x}, x$ *(Figure* (1.7) *and Table* (1.1)*).*

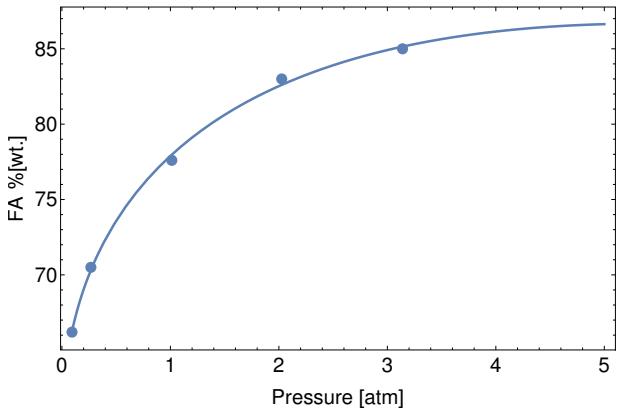

Figure 1.7: The estimated dependence of the azeotropic ratio on the pressure.

p [atm]	1	1.5	2	2.5	3	4	5
$R^{FA}_{H_2O}$ [%wt]	78	81	83	84	85	86	87
$R^{FA}_{H_2O}$ [%mol]	58	62	65	67	69	71	72

Table 1.1: The estimated dependence of the azeotropic ratio $R^{FA}_{H_2O}$ on the pressure.

Since the formic acid is consumed by the reaction, the azeotropic ratio is not exactly achieved in our case and $R^{FA}_{H_2O} \leq {}^{eq}R^{FA}_{H_2O}$*. Therefore, we should expect (slightly) more water vapour than in equilibrium, i.e. the rate of evaporation of water grows at the expense of formic acid (Figure* (1.2)*).*

BP temp.[°C]	102.3	105.9	107.1	107.6	107.1	106.0	104.2	101.8
[%mol] liquid	4.05	21.8	32.1	41.1	52.2	63.2	74.0	90.0
[%mol] vapour	2.45	16.2	27.9	40.5	56.7	71.8	83.6	95.1

Table 1.2: Amount of H_2O in liquid and vapour of equilibrated FA-azeotrope at boiling point (BP) and pressure 1 atm

1.2.3 Reactor auto-regulation. *If the evaporation rate is not sufficient, the reactor is being filled by the water decreasing the reaction rate - the catalytic surfaces are occupied by the adsorbed molecules of water. In other words, the reactor partially compensates the higher water content by increasing its evaporation rate. However, this auto-regulation works within limited ranges only and too much water can virtually kill the reaction. To avoid this scenario, one should always use as pure formic acid solution as possible.*

Once the water content increases, a solution to suppress the higher water content is allowing the system to reach its boiling point and, thus, rapidly increases the evaporation ratio. This process drives the ratio $R^{FA}_{H_2O}(p)$ *back to the azeotropic equilibrium value.*

1.2.4 Catalysis of reversible reactions. *Generally speaking, all reactions proceed in both directions. The catalyst speeds up the reaction in the both direction maintaining the equilibrium ratio unchanged, i.e.* ΔG *remains the same.*

1.2.5 Nucleation. *Once a molecule of H_2 or CO_2 is produced, it tends to a natural physical configuration given by the state-variable-couple (T, p). However, one molecule does not form a phase but a phase needs to nucleate, i.e. form a cluster (aggregate) of many molecules which overcome a certain energy threshold forming a new phase (bubble).*

Note, that one of the factor limiting the minimum bubble size is the pressure jump generated by the surface tension σ. It is commonly modelled by the Young-Laplace equation

$$\Delta p = p_g - p_l = \frac{2\sigma}{r} \tag{1.11}$$

where r is a radius of (spherical) bubble. Until the nucleation happens, the molecules do not form any phase but they adopt the phase of the solution, i.e. liquid in our case.

1.2.6 Evaporation rate. *Besides the main mass transfer between the dissolved gases $H_{2(d)}$, $CO_{2(d)}$ and the bubble, we need to consider also evaporation of the liquid across the bubble surface. These rates are commonly modelled by the Noyes-Whitney equation [73]:*

$$m_{gl}\left[\tfrac{\mathrm{kg}}{\mathrm{s}}\right] := \int_{\Sigma_{gl}} k_{gl}\left(\rho_g^{\Sigma} - \rho_g\right) \mathrm{d}S \tag{1.12}$$

where $k_{gl} = \frac{D_g}{\delta_{gl}}\left[\frac{\mathrm{m}}{\mathrm{s}}\right]$ is the speed of mass transfer; $D_g\left[\frac{\mathrm{m}^2}{\mathrm{s}}\right]$ the diffusion coefficient of the gaseous molecule, $\delta_{gl}\,[\mathrm{m}]$ is the thickness of the interface (usually assumed to be constant), $\rho_k^{\Sigma}\left[\frac{\mathrm{kg}}{\mathrm{m}^3}\right]$ is the k-th density of the substance on the interface Σ_{gl} and $\rho_k\left[\frac{\mathrm{kg}}{\mathrm{m}^3}\right]$ is its (mixture) density in the bulk. Using the Henry's law, cf. [41], together with the Dalton's law [21] and the equation of state for ideal gases (3.11)*, we can use the Henry (atmospheric) constant* [8] *$H_k^{cp} = \frac{c_{k(d)}}{p_{k(g)}}$ obtaining*

$$m_{gl}^k = \pm A_{\Sigma_{gl}} k_{gl}^{cp}\left(\frac{c_{k(d)}}{H_k^{cp}} - p_{k(g)}\right),\ k = H_2, CO_2, FA, H_2O \tag{1.13}$$

where $k_{gl}^{cp} = k_{gl}\frac{M_k}{RT}$.

[8] All Henry's constants describe values in the equilibrium state. In case of the atmospheric Henry's constant, $c_{k(d)}$ stands for the mass fraction of the dissolved k-th component in the liquid phase equilibrated with the gas phase (bubble) having the partial pressure $p_{k(g)}$.

2. Motion of a particle in fluid

In this chapter the fundamentals of a particle motion in fluid based on the classical approach using the BBO equation is given. The acting forces, such as the pressure-gradient force, gravity, buoyancy, drag, Basset force, added mass force, wall force or lift force are discussed. Finally, along the mass transfer via the bubble interface, collective effects are introduced and implemented into the system. [1]

2.1 Introduction

Dynamics of a particle in fluid [2] was studied by many authors. As the pioneering work one may consider the results of Stokes [107], Boussinesq [13], Basset [5] and Oseen [76] who laid the foundations of the BBO equation which is by many authors regarded as the fundamental relation applicable in many (but not all) cases. [3]

Later on, many great physicists introduced a complex description of the bubble fluid dynamics, e.g. one of the first complex work in the field by Lamb [55]; popular courses of Landau & Lifshitz presented in late 1930s in USSR and published later in English [60]; or considerable work of Batchelor [6]. Choosing one representative example, we highlight the work of Clift et. al. [18],[19] which represents great review of the theory supported by many experiments. From the later results, we would like to emphasize the work of Tomiyama [109] and the extensive monograph on Chemical Reactor Modelling by Jakobsen [48].

2.1.1 BBO equation

The motion of a small particle in an incompressible fluid can be conveniently described by the Newton's second law. Here, we assume that the particle behaves as a rigid sphere neglecting its internal flow and other quantity variations (e.g. pressure or density). In the scope of multi-phase continuum mechanics, this approach is known as Euler-Lagrange approach.

We express the second Newton's law, cf. [48], as

$$\frac{\mathrm{d}}{\mathrm{d}t}(\mathrm{m_p}\mathbf{v}_\mathrm{p}) = \mathrm{F_p^S} + \mathrm{F_p^V} \tag{2.1}$$

where $\mathrm{m_p}$ is the mass of the particle p moving by the velocity $\mathbf{v}_p$ and F_p^S, F_p^V are resultants of the surface and volumetric forces acting on the particle.

Usually, the only considered volume field force, acting on the particle immersed in a continuous fluid, is the gravitation force, i.e.

$$F_p^V = F_p^G = \int_{V_p} \rho_p \mathbf{g}\,\mathrm{dV} = \rho_f \mathbf{g} V_p.$$

[1] Within this chapter we introduce several plots which were generated by Wolfram Mathematica software. For more information about the numerical implementation see the section (4.1)

[2] The term "particle" represents both solid particles and gaseous bubbles. Similarly, "fluid" stands for a liquid as well as a gas. When we do not need to distinguish the concrete ensemble, we use subscription "p" for particle and "f" for fluid. Otherwise, we use subscription "s" for solid particles, "g" for gaseous bubbles and "l" for liquid.

[3] According to Lott, cf. [62]: *"The linear split of the net drag force acting on the particle is not always valid as there can be non-linear interactions between the various forces. Such interactions are not well understood, but are typically small enough to be neglected for many conditions."*

The total hydrodynamic surface force F^S, exerted by a continuous fluid on a particle, is defined as

$$F_p^S = -\int_{\partial V_p} \quad_f \cdot \mathbf{n}\,\mathrm{dS}. \tag{2.2}$$

Here, $\quad_f = p_f \;+\; \overset{d}{}_f$ stands for the total stress tensor with the isotropic pressure part p_f and the extra stress $\overset{d}{}_f$; and $\mathbf{n}$ is the outward directed unit normal vector to the particle surface ∂V_p.

In our case, we do not consider any external pressure-gradient force in our case and, thus, we may decompose the pressure field into the hydrostatic and hydrodynamic part:

$$p_f = \rho_f \mathbf{g} \cdot \mathbf{r} + p_f^{dyn} \tag{2.3}$$

where $\mathbf{r}$ corresponds to the position vector. The surface force can be rewritten as

$$\begin{aligned} F^S &= -\int_{\partial V_p} \left((\rho_f \mathbf{g} \cdot \mathbf{r} + p_f^{dyn}) \;+\; \overset{d}{}_f \right) \cdot \mathbf{n}\,\mathrm{dS} \\ &= \int_{V_p} \rho_f \mathbf{g}\,\mathrm{dV} - \int_{\partial V_p} (p_f^{dyn} + \overset{d}{}_f)\,\mathrm{dS} \\ &= F_p^B + F_p^{hydr}. \end{aligned} \tag{2.4}$$

The net hydrodynamic force (sometimes referred as a generalized drag) is usually further divided into numerous contributions like the dynamic pressure gradient, steady drag, added mass, lift, Basset history, and the wall forces:

$$F_p^{hydr} = F_p^{dyn} + F_p^D + F_p^{AM} + F_p^L + F_p^{BA} + F_p^W,$$

hence,

$$\frac{\mathrm{d}}{\mathrm{d}t}(m_p \mathbf{v}_p) = F_p^G + F_p^B + F_p^{pg} + F_p^D + F_p^{AM} + F_p^L + F_p^{BA} + F_p^W. \tag{2.5}$$

This equation is one of the possible version of BBO (Basset-Boussinesq-Oseen) equation, cf. [30].

As the next step, we distinguish the forces according to the following manner:

- **Steady:** buoyancy and gravity forces. These forces are steady, independent of motion.
- **Inertial:** inertia, added mass and Basset forces. These forces are consequences of a particle/fluid acceleration. They are significant usually for a short time-range on the beginning of motion. Then, their influence decreases rapidly and may be often neglected.
- **Dynamic:** drag, pressure gradient, lift, and wall forces. These forces increase with particle velocity. They typically act during the whole time-range.

2.1.2 Characteristic values

In the sequel, we describe the influence of the individual forces for different flow regimes and neglect those whose characteristic values are strictly less than 5 % of the overall cause - this relation will be denoted as " $\ll$ ". To do so, we need to specify the characteristic values of the system. These values are taken from the literature (cf. [37], [40]), measured

in an experiment or estimated from the results of the CFD modelling. We list them in the following tables (2.1), (2.2), (2.3).

Symbol	Explanation	Value	Unit
$\overline{R}^{FA}_{H_20}$	Azeotropic (mass) ratio of FA and H_2O	0.69	[1]
$\overline{\rho}^{true}_l$	Material density of the liquid at 100 ℃	1070	$\mathrm{kg{\cdot}m^{-3}}$
$\overline{\rho}^{true}_g$	Material density of the gas at STP	1	$\mathrm{kg{\cdot}m^{-3}}$
$\overline{\rho}^{true}_s$	Effective density of the solid	1080	$\mathrm{kg{\cdot}m^{-3}}$
$\overline{\mu}_l$	Viscosity of the liquid	$1 \cdot 10^{-3}$	Pa·s
$\overline{\alpha}_l$	Thermal exp. coeff. of the liquid	$1 \cdot 10^{-3}$	$\mathrm{K^{-1}}$
$\overline{k}_l$	Thermal conductivity of the liquid	0.2	$\mathrm{W{\cdot}m^{-1}{\cdot}K^{-1}}$
$\overline{\sigma}_l$	Surface tension of the liquid	0.04	$\mathrm{N{\cdot}m^{-1}}$
g	Gravitation constant	9.81	$\mathrm{m{\cdot}s^{-2}}$
ν^0_l	Viscous frequency factor	$5.17 \cdot 10^{-6}$	Pa·s
E^{ν}_a	Viscous activation energy	14.27	$\mathrm{kJ{\cdot}mol^{-1}}$

Table 2.1: Table of the characterictic material values for the system.

Symbol	Explanation	Value	Unit
$\overline{\mathbf{v}}_l$	Characteristic velocity magnitude of the liquid	0.01	$\mathrm{m{\cdot}s^{-1}}$
$\overline{\mathbf{v}}_g$	Characteristic velocity magnitude of the gas	0.1	$\mathrm{m{\cdot}s^{-1}}$
$\overline{r}_g$	Characteristic radius of the bubbles	$1 \cdot 10^{-3}$	m
$\overline{r}_s$	Characteristic radius of the solid cat. particles	$5 \cdot 10^{-5}$	m
L	Characteristic length (size) of the reactor	0.1	m
t_r	Characteristic occupation time of a bubble in the reactor	2.1	s

Table 2.2: Table of the characterictic observed values for the system.

Symbol	Explanation	Value	Unit
$\overline{k}^{\dot{m}}_{gl}$	Estimated mass transfer coefficient	$5 \cdot 10^{-4}$	$\mathrm{m{\cdot}s^{-1}}$
r_0	Estimated initial radius of bubbles	$1 \cdot 10^{-4}$	m
$\overline{\mathbf{v}}^{slip}_{ls}$	Slip velocity magnitude of liquid and solid phase	$1 \cdot 10^{-3}$	$\mathrm{m{\cdot}s^{-1}}$
$\lvert\overline{\nabla\phi_g}\rvert$	Characteristic gas-fraction gradient	0.1	$\mathrm{m^{-1}}$

Table 2.3: Table of the characterictic simulated values for the system.
[4]

Now, we introduce the non-dimensional Reynolds number for continuous phase (liquid) and particle Reynolds number for discrete phases - rigid particles and gas bubbles. It expresses the ratio of the inertial and viscous forces and characterizes the flow pattern

[4]The values were extracted from CFD-modelling results using typical boundary and initial conditions for $T_{set} = 100\,$℃, cf. section 4.3.3.

(laminar or turbulent):

$$Re_l = \frac{\overline{\rho}_l \overline{\mathbf{v}}_l L}{\overline{\mu}_l} \approx \frac{10^3 \cdot 10^{-2} \cdot 10^{-1}}{10^{-3}} \approx 1000 \tag{2.6a}$$

$$Re_s = \frac{\overline{\rho}_l \overline{\mathbf{v}}_{ls}^{slip} 2\overline{r}_s}{\overline{\mu}_l} \approx \frac{10^3 \cdot 10^{-3} \cdot 10^{-4}}{10^{-3}} \approx 0.1 \tag{2.6b}$$

$$Re_g = \frac{\overline{\rho}_l \overline{\mathbf{v}}_{gl}^{slip} 2\overline{r}_g}{\overline{\mu}_l} \approx \frac{10^3 \cdot 10^{-1} \cdot 2 \cdot 10^{-3}}{10^{-3}} \approx 200. \tag{2.6c}$$

2.1.1 Effective density of a catalytic particle. *The density of the solid catalytic particles outside of the reactor is a little higher than density of the liquid. However, it does not need to be the case once the reaction occurs.*

Taking the density of the GPPS [5] *catalytic support* $1050\ \frac{\mathrm{kg}}{\mathrm{m}^3}$ *and assuming the coating of Ruthenium having density* $12410\ \frac{\mathrm{kg}}{\mathrm{m}^3}$ *and occupying* $1\%[vol]$*, we obtain the resulting density at characteristic temperature approximately* $1170\ \frac{\mathrm{kg}}{\mathrm{m}^3}$*. However, the stuck micro-bubbles buoy the particle and the appropriate density is lower. We call the density of catalytic particles with stuck micro-bubbles the effective density of the solid particles* $\overline{\rho}_s^{true}$ *and we estimate its value* $1080\ \frac{\mathrm{kg}}{\mathrm{m}^3}$*.* [6]

2.1.2 Intensive and extensive force. *We introduce an intensive (density) quantity* f_i *of an extensive force* F_i *via the mutual relation* $F_i = \int_{V_p} f_i \,\mathrm{d}V$*.*

2.2 Cause of the motion

The force-cause, which we denote $f_{C_{gl}}$ for gas-liquid systems and $f_{C_{ls}}$ for liquid-solid systems, is usually considered as a composition of the gravitation, buoyancy and pressure gradient force.

2.2.1 Pressure-gradient force

The pressure gradient force, sometimes call the Taylor force, is the force induced by a local movement of the surrounding continuous phase (liquid). It is significant for high speed flows, e.g. propellers, turbines etc., but commonly negligible in other applications. Assuming no-slip condition for the liquid velocity on the wall and $\overline{\mathbf{v}}_l$ velocity magnitude at the same height but in the centre of the reactor, the characteristic pressure gradient may be estimated by Bernoulli equation as

$$\frac{\mathbf{v}_f^2}{2} + \mathbf{g}z + \frac{p_f}{\rho_f} = const.$$

This results into the following pressure gradient forces for the liquid

$$|f^{pg}| = |\nabla p^{dyn}| \approx \left| \frac{p_l^{centre} - p_l^{wall}}{L} \right| = \left| \frac{\frac{1}{2}\rho_l[(\overline{\mathbf{v}}_l)^2 - (\mathbf{v}_l^{wall})^2]}{L} \right| \approx 0.5\,\frac{\mathrm{N}}{\mathrm{m}^3}.$$

[5] General purpose polystyrene.

[6] Let us mention that once the effective density fluctuates around the liquid density, we may experience a self-mixing effect. However, we may experience also an unwanted aggregation when the particles stick together wrapped by gas to decrease the surface tension. The caught particles become, basically, chemically inactive and we experience a drastic decrease in the reactor performance.

This force acts on the liquid phase as well as on the immersed particles.

2.2.2 Gravity & buoyancy

In a gas-liquid system, the dominant force is typically the buoyancy of the particle, since

$$|f_g^B| \approx 10000 \,\frac{\mathrm{N}}{\mathrm{m}^3} \gg |\mathrm{f_g^G}| \approx 10 \,\frac{\mathrm{N}}{\mathrm{m}^3}$$

and the cause-force for gas-liquid system may be taken as

$$|f_{C_{gl}}| \approx |f_g^B| \approx 10000 \,\frac{\mathrm{N}}{\mathrm{m}^3}.$$

The situation slightly differs in the solid-liquid system since the buoyancy and gravitation have a comparable magnitudes. However, for the solid-liquid density difference $\Delta\rho_{gl} \approx 10 \,\frac{\mathrm{kg}}{\mathrm{m}^3}$ the force difference corresponds to $|f^G - f^B| \approx 100 \,\frac{\mathrm{N}}{\mathrm{m}^3}$ which is still fairly dominant over the pressure gradient force and we take it as the estimate for the cause force

$$f_{C_{ls}} = |f_s^G - f_s^B| \approx 100 \,\frac{\mathrm{N}}{\mathrm{m}^3}.$$

2.2.3 Initial bubble radius

Since the surface of the solid particles is damaged by the process of catalytic coating, cf. fig. (1.4), it is impossible to define any characteristic size of a pore, resp. size of a surface-cavity. Nevertheless, once a bubble detaches from the particle, it undergoes a significant growth with the final diameter practically independent of the initial one. From this reason, it is satisfactory to employ an approximation valid for the bubble detaching from a cavity in a still liquid.

This situation was studied by Jones et al. [49] balancing the drag, surface tension, inertial, pressure and buoyancy force. If the bubble grows relatively slowly, we may neglect influence of drag, inertial and pressure force. Moreover, for bubbles with a radius $> 10\,\mu$m, the pressure force (usually modelled by Young-Laplace relation, see (1.11)) is negligible as well. This results into a balance of surface tension force and buoyancy

$$2\pi r_d \sigma_{gls} \sin\alpha = (\rho_l - \rho_g)\mathbf{g}\frac{4}{3}\pi r_g^3$$

where r_d denotes the detachment radius, σ_{gls} is the surface tension at the gas-liquid-solid junction and α is the contact angle, cf. Figure (2.1).

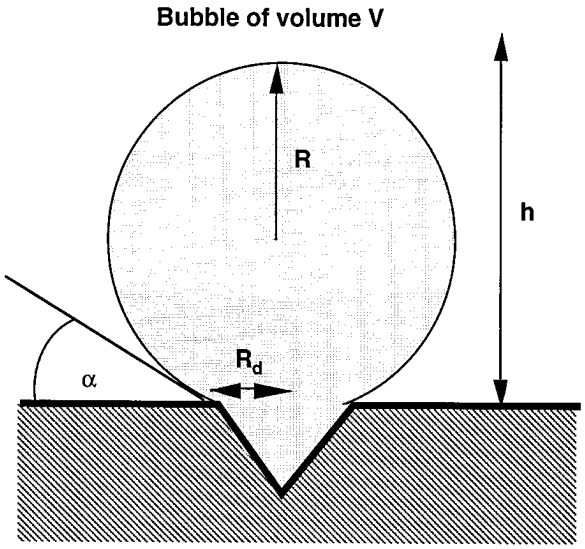

Figure 2.1: Schematic picture of the bubble detachment from a surface-cavity. Adopted from [49].

Using the characteristic values $r_d = 10\,\mu\text{m}$, $\sigma_{gls} = 0.04\,\frac{\text{N}}{\text{m}}$, $\alpha = 60°$, we obtain $r_g \approx 300\,\mu\text{m}$. This is, actually, the upper bound of the bubble-radius since we have not considered any flow around the particle which would, certainly, lower the value.

Remarks:

2.2.1 Boussinesq approximation. *A liquid is very often modelled as an incompressible medium due to the small volume-expansion coefficient and practically negligible density-variation due to a pressure change. However, the temperature change can play the fundamental role although its magnitude may be small. Typical example is the thermal convection which is driven by the difference of buoyancy force (i.e. the change of density) in the hotter and colder regions of the liquid.*

To model the thermal convection of an isothermally incompressible fluid (i.e. the density independent of pressure), Boussinesq [13] suggested a correction in the momentum balance of incompressible fluid allowing a response on a density change due to the variation of temperature. It appears in none but the gravity term where the density adopts the form

$$\rho_l(T) \stackrel{def}{=} \rho_l^0 + \alpha_l \rho_l^0 (T - T^0) = \rho_l^0 (1 + \alpha_l \Delta T).$$

Here, the coefficient α_l represents the volumetric expansion for the liquid and ρ_l^0 stands for the density at the STP condition ($T = 298\,\text{K}, p = 1\,\text{atm}$).

2.3 The consequences of the motion

Drag force is very often the dominant and the only considered consequent force - equilibrating buoyancy and gravitation force. The inertia of a particle, moving through a fluid with higher or comparable density, is usually negligible and the drag may be treated as steady. However, once we need to take into account an acceleration of the particle, we have to treat the effect of added mass and an unsteady drag force.

2.3.1 Steady drag force

When the system posses very low particle Reynolds number ($Re_p < 1$), it can be conveniently approximate by the Stokes' regime, cf. [107]. In such a case, the drag force follows the analytical formula:

$$F_D = 6\pi\mu_f r_g \mathbf{v}_{pf}^{slip}. \tag{2.7}$$

For $Re > 1$ the Stokes' regime is not applicable any more and the drag force need to be expressed in the general formula rising from empirical correction of Bernoulli principle, cf. [48, 5.2.1]:

$$F_D = \frac{1}{2} C_D A_{\Sigma_{pf}} \rho_f |\mathbf{v}_{pf}^{slip}| \mathbf{v}_{pf}^{slip} \tag{2.8}$$

where C_D stands for the empirical drag coefficient - usually a function of Reynolds particle number Re_p. Its values are typically tabulated by measurements when a rigid sphere falls in a column filled by a still liquid and the flow is assumed to be steady. In this case, the influence of the wall forces is simply neglected (the situation corresponds to an unbounded domain) or the wall correction coefficient in the drag force is introduced, cf. [77, 5.II.A.3], [63]. The BBO equation reduces to the buoyancy-drag balance

$$F_D = F_B$$

Using the ansatz (2.8), we obtain for a spherical particle the relation

$$C_D = \frac{4}{3} d_p \frac{\rho_p - \rho_f}{\rho_f} \frac{\mathbf{g}}{|\mathbf{v}_{pf}^{slip}| \mathbf{v}_{pf}^{slip}} \tag{2.9}$$

where $\mathbf{v}_{pf}^{slip} = \frac{s}{t}$ is the measurable variable (measured time t at the given bubble trajectory length s).

There exist a huge amount of various drag formulae fitting different (and sometimes questionable) measurements, cf. Figure (2.2), and we refer to paper of Brown and Lawler [15], who summarized and statistically analysed several commonly used relations. As the authoritative result is often considered the classical work of Clift [19] who fitted the measurement data using formula

$$C_D = \frac{K_1}{Re_p} + \frac{K_2}{Re_p^2} + K_3$$

separated in the 8 different ranges according to the Re_p magnitude. He succeeded to fit the data in the range $0 < Re_p < 10^5$ within the standard deviation 0.0174, and 98.1 % of the measurements with less than 10 % deviation from the modelled values.

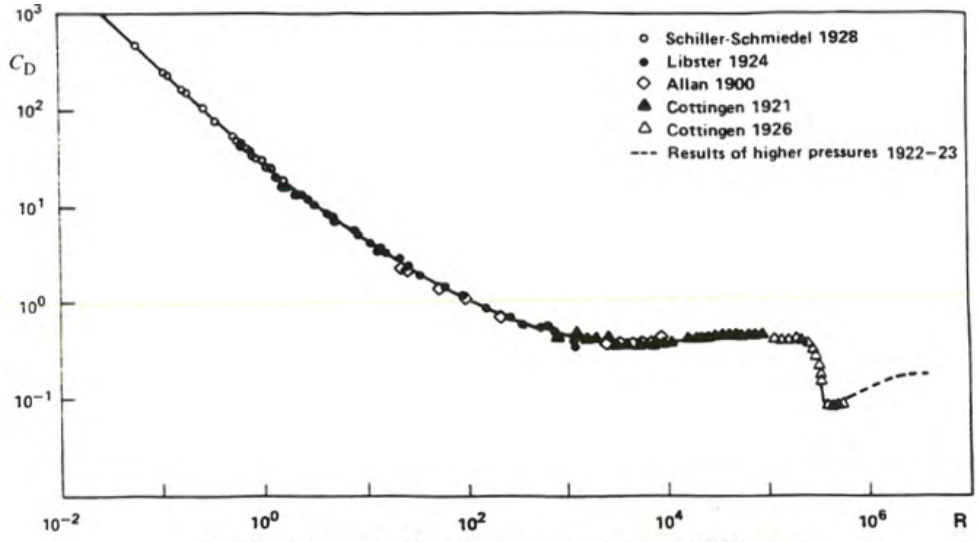

Figure 2.2: Dependence of the drag coefficient C_D on the solid particle Reynolds number Re_p; adopted from [36].

Once we restrict the problem to a smaller range of Reynolds numbers, we can conveniently use a one-formula-approach applicable for for rigid spheres falling into a still liquid. For $0 < Re_p < 1000$ the result of Schiller and Naumann [88], suggesting

$$C_D = \frac{24}{Re_p}\left(1 + 0.15 Re_p^{0.687}\right), \tag{2.10}$$

is commonly accepted.

2.3.2 Unsteady drag and Basset force

In the most of the experiments, the drag force is measured in the steady flow regime. The generalization to the unsteady drag is commonly proceeded by the introduction of the Basset history force which represents the delay in the boundary-layer (wake) evolution. Since the force is very often negligible for all but high acceleration motions (propellers, turbines), it is usually a priori omitted which may be, consequently, justified by a posterior analysis.

The general prescription of the force follows

$$f_p^{BA} = \mu_f d_p \int_0^t K(t-\tau)\left(\frac{\mathrm{d}\mathbf{v}_p}{\mathrm{d}t} - \frac{\mathrm{d}\mathbf{v}_f}{\mathrm{d}t}\right)\mathrm{d}\tau$$

where $K(t-\tau)$ depends on the diffusion process of the vorticity. Neglecting the acceleration of the surrounding fluid, the relation proposed by Clift [19, 11.2] reads

$$f_p^{BA} = -\frac{3}{2} d_p^2 \sqrt{\pi \rho_L \mu_l} \int_0^t \frac{\mathrm{d}\mathbf{v}_p}{\mathrm{d}t}(t-\tau)^{-\frac{1}{2}}\,\mathrm{d}\tau.$$

Employing the characteristics values, we obtain

$$|f_l^{BA}| \approx -\frac{3}{2} 4 \cdot 10^{-6}\sqrt{\pi \cdot 10^3 \cdot 10^{-3}} \cdot 20 \cdot 1\mathrm{N} \approx 4 \cdot 10^{-4}\mathrm{N} \ll |f_{gl}^C|$$

$$|f_s^{BA}| \approx -\frac{3}{2} 1 \cdot 10^{-8}\sqrt{\pi \cdot 10^3 \cdot 10^{-3}} \cdot 20 \cdot 1\mathrm{N} \approx 1 \cdot 10^{-6}\mathrm{N} \ll |f_{ls}^C|.$$

Hence, the Basset history force can be considered as negligible in our case.

2.3.3 Added-mass force

The added mass force, or sometimes called virtual mass force, is the inertia of the surrounding fluid which needs to be accounted in the force balance of the particle. Citting Techet [108]: *"When a body moves in a fluid, some amount of fluid must move around it. When the body accelerates, so too must the fluid. Thus, more force is required to accelerate the body in the fluid than in a vacuum. Since force equals mass times acceleration, we can think of the additional force in terms of an imaginary added mass of the object in the fluid."*

According to the previous description, we define

$$F = m\frac{\mathrm{d}}{\mathrm{d}t}\mathbf{v}_p = (m_p + m_{AM})\frac{\mathrm{d}}{\mathrm{d}t}\mathbf{v}_p \overset{def}{=} \underbrace{V_p\rho_p\frac{\mathrm{d}\mathbf{v}_p}{\mathrm{d}t}}_{F_I} + \underbrace{C_{AM}V_p\rho_p\frac{\mathrm{d}\mathbf{v}_p}{\mathrm{d}t}}_{F_{AM}} \tag{2.11}$$

where F_I stands for inertial force; F_{AM} is the added mass force; and C_{AM} is the added mass coefficient. There is an analytical solution for C_{AM} of a rigid sphere (and ellipsoid) in the case of creeping or potential flow, see Clift [19, 11.2]. However, no analytical solution is available for more complex shapes (e.g. bubble cap). In this case, we may calculate the added mass coefficient numerically, cf. [94], [78] as follows.

Let us treat the situation when particle is immersed in a still liquid. On the beginning of the motion, the buoyancy balance the inertia and added mass force. All other forces are negligible. Any movement of a particle immediately generates a velocity field of surrounding liquid. This velocity field has a kinetic energy which corresponds to a work which is done by added mass force by displacing the particle. Simply by integrating the kinetic energy over the region and measuring the bubble displacement (usually in the centre of mass), we may calculate the added mass force.

This force is commonly negligible for systems where the discrete phase has much higher density than the surrounding continuous phase (e.g. drops in air). On the other hand, for the opposite situation (e.g. bubbles in water) it is the dominant consequential force during the initiation of the motion (typically for time $< 10^{-3}$ s). In this situation, the analytical values of added mass coefficient C_{AM} in a still liquid are usually good approximation since the flow may be considered potential due to the slow development of the bubble-wake.

There are a few other situations when the added mass force has to be taken into account. One example is a rapid expansion of a freely moving bubble due to a very quick pressure-change [7] or rapid mass transfer (e.g. boiling). Another example is a change of the bubble-shape. [8]

2.3.4 Lift force

The lift force is usually considered in the form, cf. [48, 5.2.6],

$$F_L = C_L\rho_f V_p(\mathbf{v}_f - \mathbf{v}_p) \times (\nabla \times \mathbf{v}_f). \tag{2.12}$$

[7] For example a release of a cork in a bottle of champagne.

[8] Some authors denote the force contribution of the volume change as a part of the added mass force, i.e. the so called Kelvin impulse, cf. [74]. Nevertheless, we follow the common definition (2.11) excluding the volume change effect whose contribution will be covered in an extra term.

Such a defined lift force needs to be considered for rotational flows only (i.e. $\nabla \times \mathbf{v}_f \neq \mathbf{0}$). Here, we usually distinguish the situations when the rotation is induced by particle-rotation in a uniform flow (Magnus force) or it is induced by the flow pattern, e.g. shear flow. In the particular fluidized bed reactor, we consider only the latter one caused by the thermal convection and the no-slip condition on the reactor walls.

Focusing on the characteristic value of the force, we approximate $C_L \approx \frac{1}{2}$ and the vorticity $|\nabla \times \mathbf{v}_f| \approx \frac{|\mathbf{v}_f|}{L_{rot}}, L_{rot} \approx 10^{-1}$ m. Consequently, we obtain for the following values

$$|f_{gl}^L| = 0.5 \cdot 1000 \cdot 0.1 \cdot \frac{0.1}{0.1}\,\mathrm{N} \approx 50\,\mathrm{N} \ll |f_{C_{gl}}|,$$

resp.

$$|f_{ls}^L| = 0.5 \cdot 10 \cdot 0.01 \cdot \frac{0.01}{0.1}\,\mathrm{N} \approx 5\,\mathrm{mN} \ll |f_{C_{ls}}|.$$

2.3.5 Wall force

A particle moving near a wall is subject of several effects. One of them is an increase of the added mass, since the demand on displacing the surrounding liquid increases due to the viscosity and the no-slip condition on the wall. However, this effect has generally lower magnitude than the other wall effect - the wall lubrication. Although the wall lubrication may be neglected in some cases, it can lead to an incorrect behaviour in others.

A simple, commonly used pressure-drag balance for a spherical particle with diameter d_p moving in a fluid (in Stokes regime) reduces to an explicit relation for the slip velocity in the form

$$\mathbf{v}_{pf}^{slip} = \frac{(\rho_p - \rho_f) d_p^2 \mathbf{g}}{18 \mu_f}.$$

This approach is convenient in the case of bubble column reactors of a simple cylindrical shape when the boundaries are parallel to the flow, however, it is incorrect when the boundary has a different orientation (Figure (2.3)).

Figure 2.3: Correct behaviour on the left side and non-physical behaviour on right - penetrating of the ascending particle through the boundary having different orientation that the particle-flow.

To prevent the model from this inconsistency, a wall force has to be introduced. Antal et al [3] was one of the first authors proposing the wall lubrication force in the form

$$F_W = C_W \frac{\rho_f |\mathbf{v}_{pf}^{slip}{}_{||}|^2}{r_g} \mathbf{n}_W$$

where C_W is the wall lubrication coefficient; ${\mathbf{v}_{pf}^{slip}}_{||} = (\mathbf{v}_p - \mathbf{v}_f) - [(\mathbf{v}_p - \mathbf{v}_f) \cdot \mathbf{n}_W]\mathbf{n}_W$ is the slip velocity component tangential to the wall; and $\mathbf{n}_W$ is the unit normal pointing away from the wall.

The model was lately modified by Tomiyama [109], and Jakobsen [48, 5.2.5] who proposed for flows characterized by ${\mathbf{v}_{pf}^{slip}}_{||} \approx \mathbf{v}_{pf}^{slip}$ (e.g. bubbly flow) the following simplified form:

$$F_W = C_w \rho_f \frac{|\mathbf{v}_p - \mathbf{v}_f|^2}{r_p} \mathbf{n}_W, \; C_w = \max\left\{0, C_{w_1} + C_{w_2}\frac{r_p}{y_0}\right\}. \tag{2.13}$$

wher the parameter values

$$C_{w_1} = -0.05, \, C_{w_2} = 0.35$$

represent the empirical best fit. Since the wall force acts only in a narrow region near the boundaries, it is often not explicitly considered in the bulk but implemented as a kind of generalized boundary condition. This is also the case of our implementation in Comsol Multiphysics.

2.3.6 Bubble deformation

In the case of the gaseous bubbles, we are interested also in a change of bubble-shape. Due to the effect of surface tension, the bubble surface tends to minimize its area, i.e. form a sphere, however, the shape is, consequently, deformed by hydrodynamic forces. The dimensionless number expressing the corresponding ratio is called the Eötvös number:

$$Eö = \frac{(\rho_l - \rho_g)\mathbf{g} d_g^{e\,2}}{\sigma_{gl}}$$

where d_g^e is the equilibrated diameter of the bubble. [9] For $Eö \ll 1$, the bubble remains practically spherical. On the other hand, when $Eö \gg 1$, the influence of the surface tension forces decreases and the bubble significantly deform to a spherical cap or possibly breaks-up.

The shape of the bubble may be characterized by the combination of Eötvös and Reynolds number, cf. [19]:

[9] The equilibrated diameter d_g^e corresponds to diameter of a spherical bubble with the same volume as the original bubble.

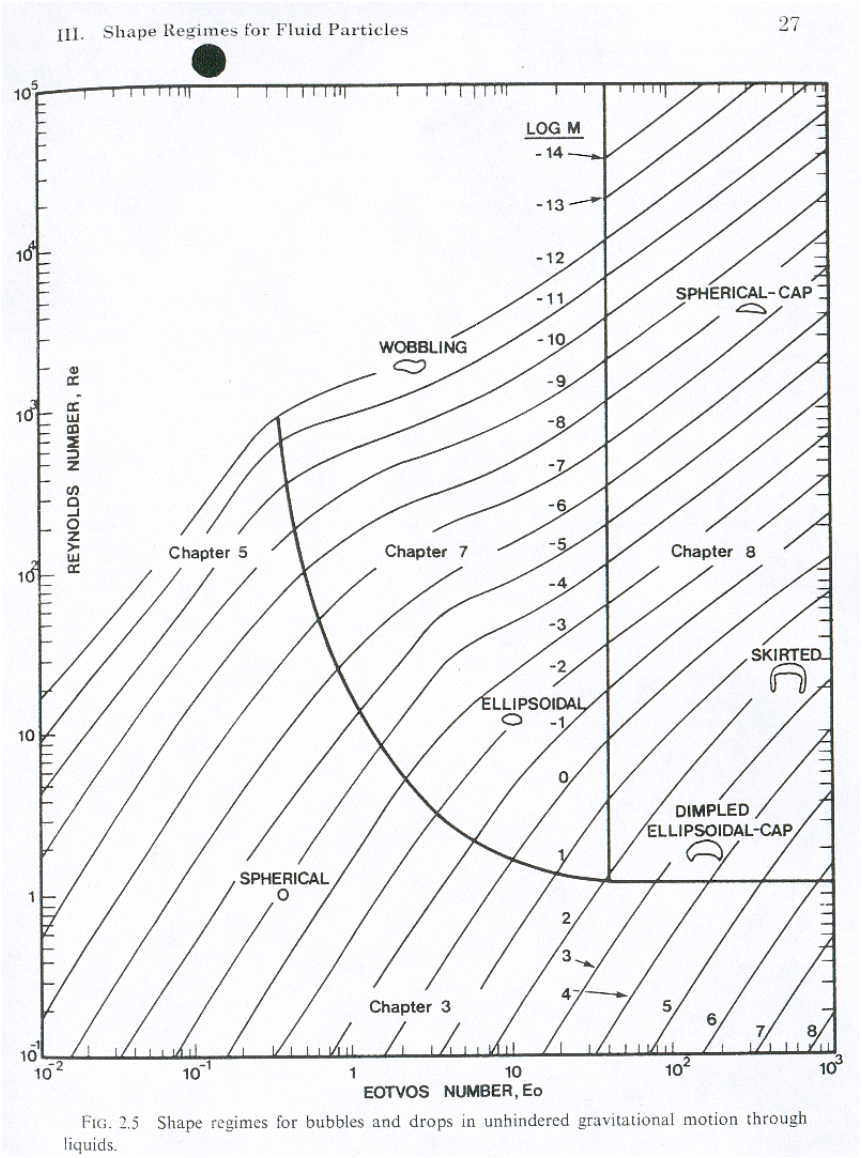

Figure 2.4: The shape of bubbles depending on the Reynolds and Eotvos (ev. Morton) number. Adopted from [18].

As long as the system is situated in the lower-left part of the Figure (2.4), which is typical for spherical and elliptic bubbles, [10] the influence of the Reynolds number may be neglected. The shape of the bubble and, in particular, the axial ratio can be estimated by the bubble-ellipticity

$$E = \frac{a}{b} \approx \frac{1}{1 + 0.163 E\ddot{o}^{0.757}} \tag{2.14}$$

where a is the length of the vertical axes and b the horizontal axes (Figure (2.5)). Consequently, the change of the surface area, drag, added mass and lift coefficients may be discussed.

[10] In the case of strictly vertical ascent, the bubble shape can be conveniently approximated by a spheroid, i.e. an ellipsoid with two equal semi-diameters.

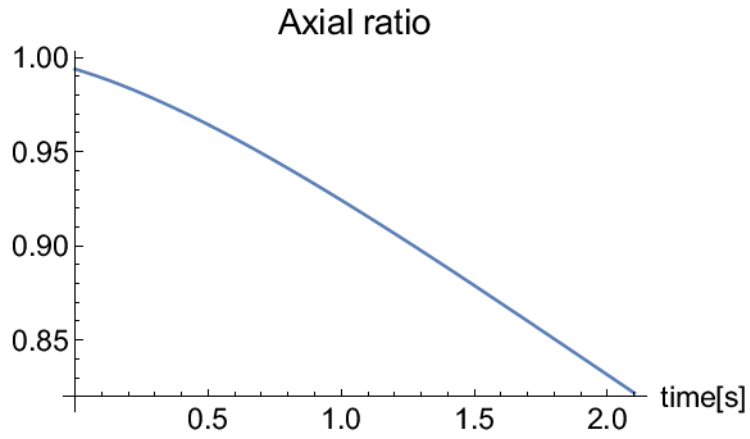

Figure 2.5: Change of the bubble axial-ratio E with the time. Minimum value at the reactor occupancy time $t = t_r$ and $d_e = 3\,\text{mm}$ is approximately $E_{min} = 0.82$.

2.3.7 Bubble vs. solid-particle motion

In the case of solid-liquid interface, the surrounding fluid molecules stick to the solid surface due to the surface roughness, thus, no-slip condition is applicable. However, in the case of a bubble, the situation is different.

A rising bubble in a pure liquid has a mobile interface and, thus, the drag coefficient is much lower (slip velocity is higher). On the other hand, the presence of a small amount of surfactant [11] may strongly influence the interface behaviour which may quickly become immobile and liquid "sticks" to the bubble surface again. However, for expanding bubbles (non-material interface) the "stick" condition holds in the tangential direction only. Thus, we write the corresponding condition as

$$\mathbf{v}_{l||} = \mathbf{v}_{gl_{||}} = \mathbf{v}_{g_{||}} \text{ on } \Sigma_{gl} \tag{2.15}$$

where $\mathbf{v}_{||}$ denotes the tangential component of the velocity.

Bubbles have usually negligible momentum, thus, the generated turbulent wake disturbs the straight upward trajectory for relatively small Reynolds numbers generating a zig-zag and, lately, also a helical motion. This phenomena significantly increases the effective drag of the bubble and the drag-coefficient-plateau (when the drag is independent of the slip velocity) occurs much sooner than in the case of rigid particle motion.

As a consequence, the drag coefficient for a bubble at low Reynolds number is significantly lower that in the case of rigid particle but for a higher Reynolds number the situation is opposite. This effect was studied for example by Karamanev [50] or Tomiyama [109] who suggested a modification of the original model of Schiller-Naumann [88].

The modification for pure systems follows

$$C_D = \max\left\{\min\left\{\frac{24}{Re_p}\left(1 + 0.15Re_p^{0.687}\right), \frac{48}{Re_p}\right\}, \frac{8}{3}\frac{E\ddot{o}}{E\ddot{o}+4}\right\},$$

for slightly contaminated systems

$$C_D = \max\left\{\min\left\{\frac{24}{Re_p}\left(1 + 0.15Re_p^{0.687}\right), \frac{72}{Re_p}\right\}, \frac{8}{3}\frac{E\ddot{o}}{E\ddot{o}+4}\right\},$$

[11] Any chemical compound which has surface activity, e.g. an organic compound that is amphiphilic.

and for highly contaminated systems

$$C_D = \max\left\{\frac{24}{Re_p}\left(1+0.15Re_p^{0.687}\right), \frac{8}{3}\frac{E\ddot{o}}{E\ddot{o}+4}\right\}. \tag{2.16}$$

In our particular case, we use smoothed (locally by the error function) Tomiyama's correction for contaminated system (Figure (2.6)).

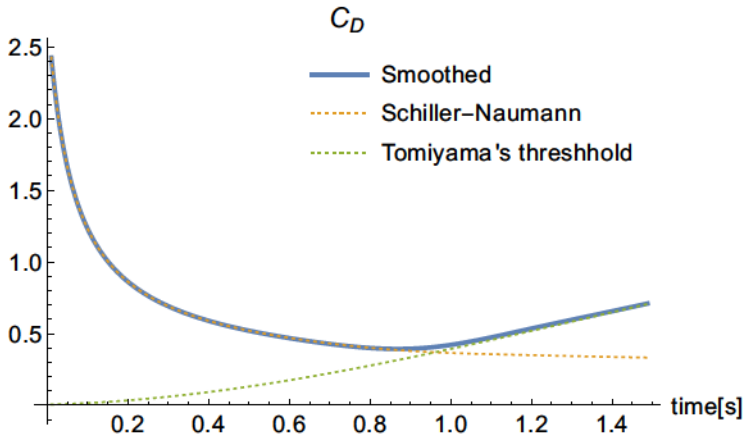

Figure 2.6: The evolution of the drag coefficient C_D.

where the Reynolds particle number posses the following profile

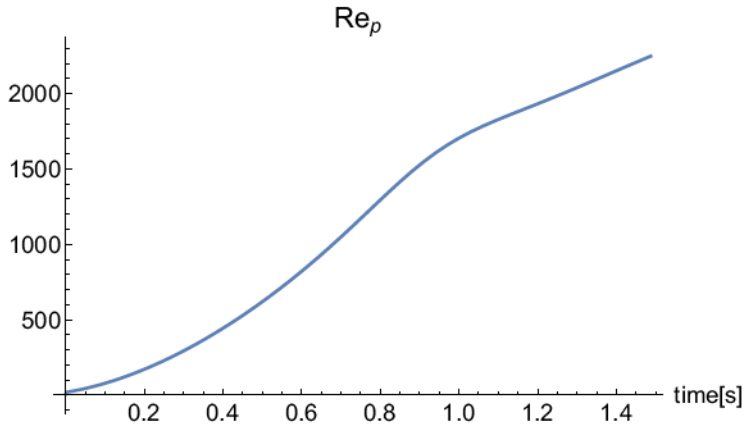

Figure 2.7: Reynolds particle number $\mathrm{Re_p}$

Remarks:

2.3.1 The change of the added mass coefficient. *To determinate the added mass coefficient for a spheroidal shape ($E < 1$), we may use the formula of Lamb, cf. [55]:*

$$C_{AM} = \frac{E\,\mathrm{ArcCos}(E) - \sqrt{1-E^2}}{E^2\sqrt{1-E^2} - E\,\mathrm{ArcCos}(E)},$$

resulting into a variation of the added mass coefficient (Figure (2.8)). However, since in our case the added mass is significant during the initiation only, we may neglect this effect.

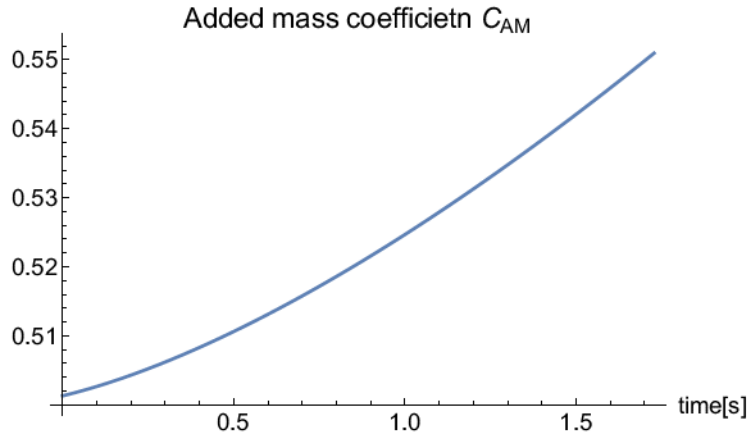

Figure 2.8: Change of the added mass coefficient C_{AM}.

2.3.2 The change of the surface area. *The surface area of the spheroid increases with the axial ratio drop according to [113] as*

$$S = \frac{\pi}{2} d_e^2 \, E^{-\frac{2}{3}} \left(1 + \frac{E^2}{\sqrt{1-E^2}} \operatorname{ArcTanh}(\sqrt{1-E^2}) \right).$$

Taking the minimum axial ratio value $E_{min} = 0.82$, the surface area difference of the sphere and the spheroid is less than $1\,\%$, hence, negligible.

2.3.3 Change of the drag coefficient. *According to Haider-Levenspiel, cf. [38, p. 737], the drag coefficient C_D of the spheroidal bubble may be estimated according to the relation*

$$C_D = \frac{24}{Re_p} \left(1 + A(S) Re_p^{B(S)} \right) + \frac{C(S)}{\left(1 + \frac{D(S)}{Re_p} \right)}$$

where the empirical parameters A, B, C, D are functions of the bubble-axial ratio S

$$\begin{aligned} A(S) &= e^{2.3288 - 6.4581S + 2.4486S^2} \\ B(S) &= 0.0934 + 0.5565S \\ C(S) &= e^{4.905 - 13.8944S + 18.4222S^2 - 10.2599S^2} \\ D(S) &= e^{1.4681 + 12.2584S + 20.7322S^2 + 15.8855S^3}. \end{aligned}$$

Here, S denotes the sphericity defined as ratio of the surface-area of the sphere having the same volume as the particle and the surface-area of the particle. For spheroiod, the sphericity and ellipticity satisfy $S = E^{\frac{2}{3}}$.

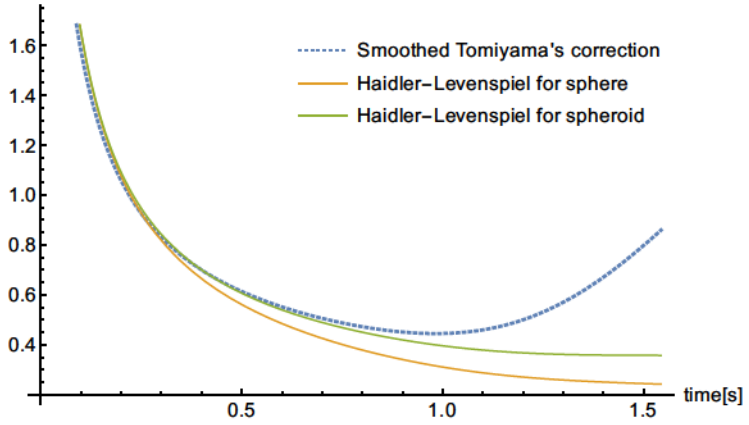

Figure 2.9: Change of the drag coefficient C_D depending on the time-changing sphericity.

As we can see in the Figure (2.9)*, some difference between the spherical and ellipsoidal bubble occurs. However, this effect is basically negligible as long as we consider the (smoothed) drag-correction proposed by Tomiyama [109].*

2.4 Mass transfer

2.4.1 The rocket equation

Once the mass change of the object needs to be taken into account, the Newton's second law is no longer applicable - a bubble allowing mass transfer can not be considered as a closed system. [12] However, a simple generalization provides, so called, the rocket equation, cf. [20]. [13]

Consider a system of two bodies, one with mass m, velocity $\mathbf{v}$ and the second with mass $\mathrm{d}m$ and velocity $\mathbf{u}$. The total momentum equals to

$$P(t) = m\mathbf{v} + \mathbf{u}\,\mathrm{d}m.$$

Assuming a perfect inelastic (plastic) collision at $t + \mathrm{d}t$, the final momentum equals

$$P(t + \mathrm{d}t) = (m + \mathrm{d}m)(\mathbf{v} + \mathrm{d}\mathbf{v})$$

and we may define the resultant of the all external forces as

$$F_{ext} \overset{def}{=} \frac{\mathrm{d}P}{\mathrm{d}t} = \frac{m\,\mathrm{d}\mathbf{v} - (\mathbf{u} - \mathbf{v})\,\mathrm{d}m}{\mathrm{d}t} = m\frac{\mathrm{d}\mathbf{v}}{\mathrm{d}t} - (\mathbf{u} - \mathbf{v})\frac{\mathrm{d}m}{\mathrm{d}t}.$$

Now, we apply the relation on the gas-suspension system, where $\mathbf{v} = \mathbf{v}_g, \mathbf{u} = \mathbf{v}_l$ and $\mathbf{v}_l - \mathbf{v}_g = -\mathbf{v}_{gl}^{slip}$:

$$F_{ext} = m_g \frac{\partial}{\partial t}\mathbf{v}_g + \underbrace{m_{AM}\frac{\partial}{\partial t}\mathbf{v}_g}_{F_{AM}} + \underbrace{\mathbf{v}_{gl}^{slip}\frac{\mathrm{d}m_g}{\mathrm{d}t}}_{F_{\dot{m}}} = F^B + F_D^{st} + F_W \tag{2.17}$$

[12] Citing Halliday & Resnick [39]: *"It is important to note that we cannot derive a general expression for Newton's second law for variable mass systems by treating the mass in $F = \frac{\mathrm{d}P}{\mathrm{d}t} = \frac{\mathrm{d}}{\mathrm{d}t}(m\mathbf{v})$ as a variable. [...] We can use $F = \frac{\mathrm{d}P}{\mathrm{d}t}$ to analyze variable mass systems only if we apply it to an entire system of constant mass having parts among which there is an interchange of mass."*

[13] The designation "rocket equation" has a historical reasons, although, it is applicable to any system gaining or loosing its matter and we will demonstrate it on the plastic collision of two bodies.

where we denoted the mass transfer force $F_{\dot{m}}$ depending on the volume and density change.

2.4.2 Interfacial mass transfer

If the system does not undergo a significant pressure change, the density change due to the hydrostatic pressure or surface tension is negligible and we obtain for spherical bubble with use of the Henry's law (1.13) the following expressions

$$\begin{aligned}\frac{\mathrm{d}m_g}{\mathrm{d}t} &= \frac{\mathrm{d}\rho_g}{\mathrm{d}t}V_g + \rho_g\frac{\mathrm{d}V_g}{\mathrm{d}t} = \rho_g 4\pi r_g^2\frac{\mathrm{d}r_g}{\mathrm{d}t} \\ &\overset{1.12}{=} \int_{\Sigma_{gl}} k_{gl}(\rho_g^{\Sigma} - \rho_g)\,\mathrm{d}S \overset{1.13}{=} \sum_k A_{\Sigma_{gl}} k_{gl_k}^{cp}\left(\frac{c_{k_{(d)}}}{H_k^{cc}} - p_{\rho_{k_{(g)}}}\right).\end{aligned} \tag{2.18}$$

The partial pressure of the species $p_{\rho_{k_{(g)}}}$ in the gas phase (bubble) may be WLOG considered as constant. The mass fraction of dissolved gas within the liquid may generally vary. However, since the dissolved gas circulates together with the liquid and it is object of further dispersion (movement of solid particles and ascending bubbles) and diffusion effects, we consider its concentration constant as well. This is in accordance with the kinetic regime of the reactor.

Together with the assumption of constant concentration-composition of the produced gas, see section 3.2.2, we can treat the gas-liquid mass transfer rate k_{gl} as a constant. Moreover, in this setting we may identify the mass transfer rate with the (averaged) chemical rates:

$$\langle R_{gl}^{\Sigma}\rangle_{V_r} = \frac{1}{V_r}\int_{V_r}\left(\left(1 + R_{H20}^{FA}\right)\phi_{H20_{(l)}}^{in} + 1\right)\rho_l^{true} A\, e^{\frac{-E_a}{RT}} R_{H_20}^{FA}\phi_l\phi_s\,\mathrm{d}V. \tag{2.19}$$

Defining the speed of the mass transfer $k_{gl}^{\dot{m}}\,[\frac{\mathrm{m}}{\mathrm{s}}] \overset{def}{=} k_{gl}\frac{\rho_g^{\Sigma}-\rho_g}{\rho_g}$, we specify the growth of the bubble as

$$\frac{\mathrm{d}r_g}{\mathrm{d}t} = k_{gl}^{\dot{m}} \;\Rightarrow\; r_g(t) = k_{gl}^{\dot{m}}\,t + r_0. \tag{2.20}$$

[14] The mass transfer force, consequently, adopts the form

$$F_{\dot{m}} = A_{\Sigma_{gl}}\rho_g k_{gl}^{\dot{m}}\mathbf{v}_{gl}^{slip}. \tag{2.21}$$

The BBO force balance mat be written as

$$F_{ext} \approx F_{AM} = F^B + F_D^{st} + F_{\dot{m}} \tag{2.22}$$

which yields the relation

$$C_{AM}V_g\rho_l\frac{\mathrm{d}\mathbf{v}_g}{\mathrm{d}t} = -V_g\rho_l\mathbf{g} + A_{\Sigma_{gl}}^{cs}\rho_l C_D|\mathbf{v}_{gl}^{slip}|\mathbf{v}_{gl}^{slip} - A_{\Sigma_{gl}}\rho_g k_{gl}^{\dot{m}}\mathbf{v}_{gl}^{slip} \tag{2.23}$$

where $A_{\Sigma_{gl}}^{cs} = \pi r_g^2$ is the cross section area of the bubble. Consequently, we obtain

$$\frac{\mathrm{d}\mathbf{v}_g(t)}{\mathrm{d}t} = -2\mathbf{g} + \frac{3}{2}\frac{C_D(r_g(t),\mathbf{v}_{gl}^{slip}(t))}{r_g(t)}|\mathbf{v}_{gl}^{slip}(t)|\mathbf{v}_{gl}^{slip}(t) - \frac{6k_{gl}^{\dot{m}}\frac{\rho_g}{\rho_l}}{r_g(t)}\mathbf{v}_{gl}^{slip}(t). \tag{2.24}$$

However, since the bubble radius $r_g \geq r_0 \approx 0.1\,\mathrm{mm}$, the mass transfer term is small enough to be neglected in the sequel (Figure (2.10)).

[14] The value $k_{gl}^{\dot{m}} \approx 5\cdot 10^{-4}$ [m/s] is estimated from the simulation together with experimentally observed final bubble diameter ($d_{max} \approx 3\,\mathrm{mm}$).

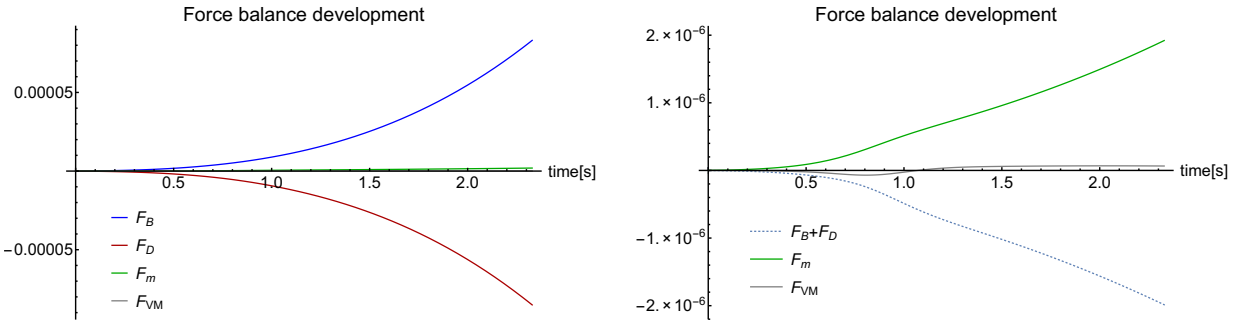

Figure 2.10: Force balance development for $k_{gl}^{\dot{m}} = 5 \cdot 10^{-4}\,\mathrm{m}\cdot\mathrm{s}^{-1}$, the reactor height $h = 0.3\,\mathrm{m}$, final bubble diameter 3 mm.

Remarks:

2.4.1 Massive mass transfer. *There are several examples, when the mass transfer via the bubble interface is much higher and the mass transfer force is not negligible any more. One of the typical example is boiling. Estimating the value of the mass transfer rate for boiling $k_{gl}^{\dot{m}} \approx 1 \cdot 10^{-2}$, the mass transfer force (and added mass force) starts to play a role (Figure (2.11)).*

However, the final bubble diameter of a spherical bubble would be approx. 17.4 mm *which is physically unrealistic and one needs too use a different approach (including bubble break-up) to describe such fast mass transfer.*

2.4.2 Remark. *The volume change, resp. $\frac{\mathrm{d}r_g}{\mathrm{d}t}$, may be computed by the Rayleigh-Plesset equation which is the one-dimensional NS equation in the spherical coordinates.*

Let us now switch to a little bit different situation when the bubble is slowly inflated surrounded by a liquid (in an unbounded domain). The whole system is spherically symmetric with the centre in the middle of the bubble. The NS equation

$$\rho_l \frac{\mathrm{d}\mathbf{v}_l}{\mathrm{d}t} = -\nabla p_l + \mu_l \Delta \mathbf{v}_l + \dot{m}_l \mathbf{v}_l, \tag{2.25}$$

may be, consequently, transformed into the form

$$\frac{p_g - p_l}{\rho_l} = r_g \frac{\mathrm{d}^2 r_g}{\mathrm{d}t} + \frac{3}{2}\left(\frac{\mathrm{d}r_g}{\mathrm{d}t}\right)^2 + \frac{4\nu_l}{r_g}\frac{\mathrm{d}r_g}{\mathrm{d}t} + \frac{2\sigma_{gl}}{\rho_l r_g} + \frac{2}{3}\frac{k_{gl}(\rho_g - \rho_g^{\Sigma})}{\rho_l}\frac{\mathrm{d}r_g}{\mathrm{d}t}. \tag{2.26}$$

As long as we do not treat massive mass transfer (e.g. boiling), we may apply the equilibrium Young-Laplace relation

$$\Delta p_{gl} = \frac{2\sigma_{gl}}{r_g}$$

and omit the second-time-derivative term together with the viscous term. As a consequence, we obtain

$$\left(\frac{\mathrm{d}r_g}{\mathrm{d}t}\right)^2 = k_{gl}\frac{\rho_g - \rho_g^{\Sigma}}{\rho_l}\frac{\mathrm{d}r_g}{\mathrm{d}t}, \tag{2.27}$$

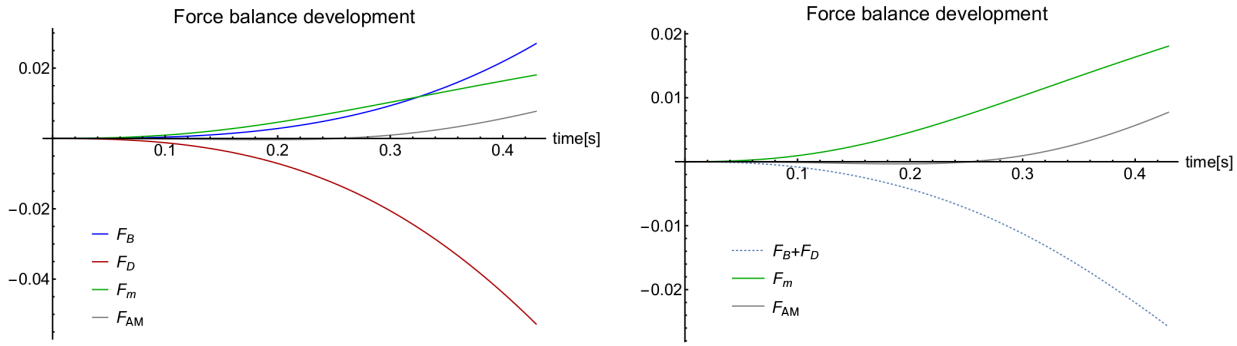

Figure 2.11: The force balance development for $k_{gl}^{\dot{m}} \approx 1 \cdot 10^{-2}$, reactor height $h = 0.4\,\mathrm{m}$, final bubble diameter $17,4\,\mathrm{mm}$.

hence,

$$r_g(t) = \int_0^t k_{gl} \frac{\rho_g - \rho_g^{\Sigma}}{\rho_l} \,\mathrm{d}t + r_0 \approx k_{gl}^{\dot{\boldsymbol{m}}}\, t + r_0, \tag{2.28}$$

which coincides with the adopted parametrization of $r_g(t)$*, cf.* (2.20)*.*

2.5 The three-phase system

2.5.1 Solid-liquid system

Let us consider a rigid spherical particle with constant density ρ_s^{true} and diameter d_s immersed into homogeneous incompressible liquid with constant density ρ_l^{true}. The particle Reynolds number corresponds to $Re_p \approx 0.1$, cf. (2.6), and the flow can be conveniently approximated by the Stokes regime (flow) when the inertia of the particle is negligible, cf. [48, 5.2.1]. The BBO force balance (2.5) reduces to the form

$$0 = F^G + F^B + F_D. \tag{2.29}$$

The drag force, satisfying the Stokes's ansatz

$$F_D = 6\pi\mu_l r_g \mathbf{v}_{ls}^{slip}, \tag{2.30}$$

allows the explicit relation for the slip velocity

$$\mathbf{v}_{ls}^{slip} = \frac{2}{9} \frac{(\rho_s - \rho_l) r_s^2 \mathbf{g}}{\mu_l}. \tag{2.31}$$

The boundary condition ($\mathbf{v}_{ls}^{slip}{}_{|wall} = 0$) is enforced by the wall force acting near the boundaries and the force balance adopts the form

$$C_w \frac{|\mathbf{v}_{sl}^{slip}|^2}{r_s} \mathbf{n}_W + \frac{9}{2} \frac{\nu_l \mathbf{v}_{ls}^{slip}}{r_s^2} + \frac{\rho_s^{true} - \rho_l^{true}}{\rho_l^{true}} \mathbf{g} = 0. \tag{2.32}$$

2.5.2 Gas-liquid system

Considering a bubble with a constant density ρ_g^{true} and radius r_g, the BBO balance reduces to [15]

$$F_{AM} = F^B + F_D. \tag{2.33}$$

The particle Reynolds number corresponds to $Re_p \approx 300$, cf. (2.6), thus, the Stokes regime is not applicable any more, and we need to use the general drag force prescription in the form:

$$F_D = \frac{1}{2} C_D A_{\Sigma_{gl}} \rho_l |\mathbf{v}_{gl}^{slip}| \mathbf{v}_{gl}^{slip}, \tag{2.34}$$

where $A_{\Sigma_{gl}} = \pi r_s^2$ is the cross section area. Employing the Tomiyama correction of the Schiller-Naumann drag coefficient, cf. [109],

$$C_D = \max\left\{ \frac{24}{Re_p}\left(1 + 0.15 Re_p^{0.687}\right), \frac{8}{3}\frac{E\ddot{o}}{E\ddot{o}+4} \right\},$$

the force balance reads

$$C_{AM} \frac{\mathrm{d}\mathbf{v}_{gl}^{slip}}{\mathrm{d}t} = \frac{C_D}{r_g} |\mathbf{v}_{gl}^{slip}| \mathbf{v}_{gl}^{slip} + \frac{8}{3}\mathbf{g}.$$

Unlike the case of solid particles, here, we need to consider several time-ranges to characterize the corresponding force balances and flow regimes. Concretely:

1. The first regime, an initialization of the motion, occurs for $t \in \langle 0, 1 \cdot 10^{-3} \rangle$. This regime is characterized by a rapid but short, nearly constant acceleration, cf. fig. (2.13). The dominant (consequential) force is clearly the added mass force, i.e. the effect of displacement of the surrounding liquid. Since $\mathbf{v}_{gl}^{slip}$ is practically zero, the drag is negligible and the force balance follows

$$F_{AM} = F^B.$$

2. The second (transient) regime occurs at $t \in \langle 10^{-3}, 10^{-2} \rangle$. The acceleration decreases as the drag force starts to play a role. The force balance follows

$$F_{AM} = F^B + F_D.$$

3. The third regime occurs at $t \in \langle 10^{-2}, 1.7 \rangle$. Here (and later on) the acceleration is low (the inertial forces are practically negligible), cf. fig. (2.13), but the growth of the bubble drives an increase in the buoyancy and slip velocity. The growth is initially linear ($C_D \approx \frac{24}{Re_p}$, $|\mathbf{v}_{gl}^{slip}| \approx Ct$) and, lately, becomes sub-linear ($C_D \approx \frac{3.6}{Re_p^{\frac{1}{3}}}$, $|\mathbf{v}_{gl}^{slip}| \approx Ct^{\frac{2}{3}}$). The force balance follows

$$0 = F^B + F_D.$$

4. In the last regime ($t > 1.7\,\mathrm{s}$), the growth of the bubble continuous in the sub-linear regime but the drag coefficient is reaching its plateau (Newtonian regime) or even rising again due to the bubble-deformation. As a consequence, the bubble velocity stagnate or even decreases, see fig. (2.12). The force balance still follows

$$0 = F^B + F_D.$$

[15] Note that, in contradiction to the solid-liquid system, we neglect the gravitation of the bubble but consider the added mass force since the liquid has much higher density than the gas.

As we can see from the previous consideration, there is a tiny time region when the added mass force need to be taken into account. Referring to $t_r = 2.1\,\mathrm{s}$ as the characteristic reactor occupation time, the magnitude of the added mass time region is less than 1% and will be neglected in the sequel. Consequently, the force balance may be expressed as $F_D = -F^B$, i.e.

$$\frac{C_D}{r_g}|\mathbf{v}_{gl}^{slip}|\mathbf{v}_{gl}^{slip} = -\frac{8}{3}\mathbf{g}. \tag{2.35}$$

From this relation, we may explicitly express the slip velocity as

$$\mathbf{v}_{gl}^{slip} = \sqrt{\frac{8}{3}\frac{r_g|\mathbf{g}|}{C_D}}\,\mathbf{e}_z \tag{2.36}$$

or, with the contribution of the wall force, as

$$\frac{C_w}{r_g}|\mathbf{v}_{gl}^{slip}|^2\mathbf{n}_W + \frac{C_D}{r_g}|\mathbf{v}_{gl}^{slip}|\mathbf{v}_{gl}^{slip} = -\frac{8}{3}\mathbf{g}. \tag{2.37}$$

The evolution of the slip velocity and the acceleration may be seen in the Figure (2.12) and (2.13).

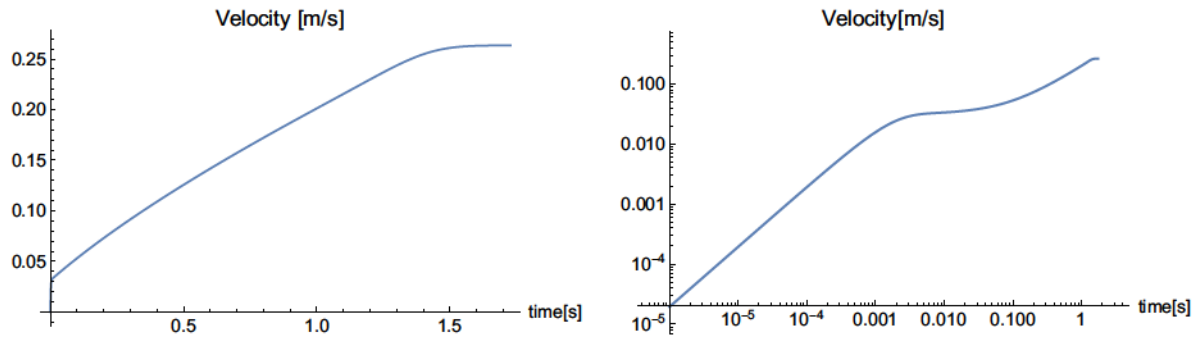

Figure 2.12: The evolution of the slip velocity $\mathbf{v}_{gl}^{slip}$ (left) and its Log-Log plot (right).

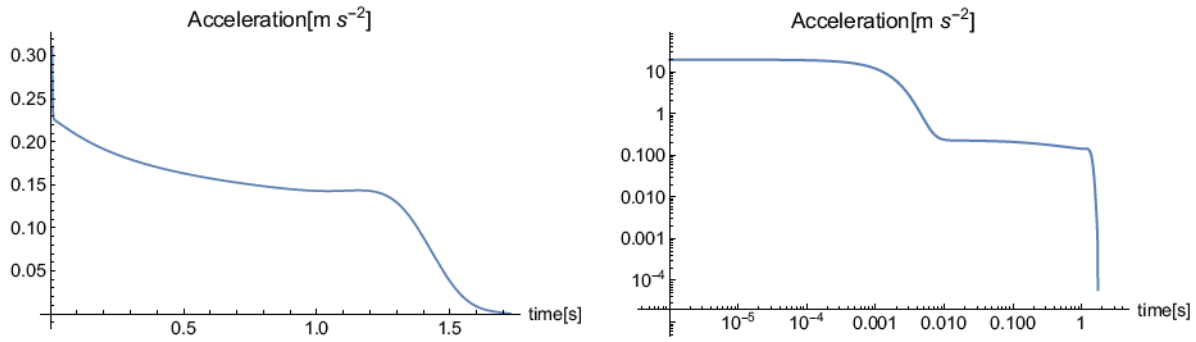

Figure 2.13: The evolution of the bubble acceleration (left) and its Log-Log plot (right).

Remarks:

2.5.1 Boundary layer thickness. *Note, that the wall force coefficient C_W is zero outside of the wall layer with the thickness $y_0(t)$. This value is not constant but differs with the reactor height and bubble radius:*

$$C_w = 0 \Leftrightarrow y \geq y_0(t) = \frac{C_{w_2}}{C_{w_1}} r_g(t).$$

Once we assume no bubble coalescence (neither break-up) together with assumption that most of the bubbles are formed near the bottom of the reactor, the boundary layer undergoes the development depicted in the Figure (2.14).

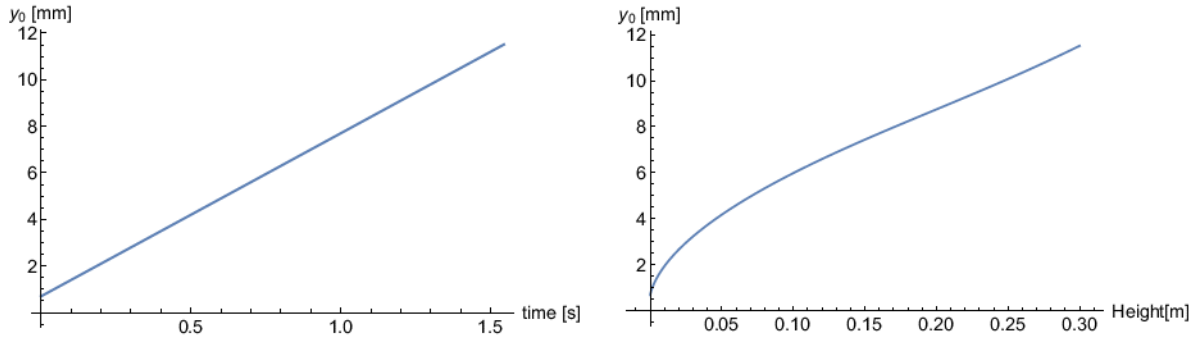

Figure 2.14: Wall layer thickness y_0 depending on time (left), resp. height (right).

2.6 Collective effects

Up to now we have been taking into account various effects acting on a single particle flow in a fluid but we didn't include any effect arising from a collective (swarm) behaviour. We need to consider for dense dispersed systems mutual interactions of the dispersed particles (collisions) as well as interactions mediated via the continuous phase.

These effects have been described by various authors e.g. [83], [112], [91], [52]. In our case of the three phase flow, we need to distinguish two significant collective effects. Firstly, the interaction of solid-liquid phase forming a suspension. Secondly, the interaction of solid-solid and gas-solid (mediated via the liquid).

The gas-gas (or bubble-bubble) interaction will be neglected due to the low concentration of the randomly popped up bubbles moving mostly in vertical direction, cf. [94], [93], [78].

2.6.1 Collective slip velocity

The introduced relation (2.36) holds for a single ascending bubble popping up in the bottom of the reactor. However, we treat a system where bubbles pop up in the whole reactor volume. Once the reactor operates in the kinetic regime, we may assume an uniform concentration of new bubbles and, thus, we may express the collective slip velocity as a reaction-occupancy time average, i.e.

$$\overline{\mathbf{v}}_{gl}^{slip}(t) = \frac{1}{|t_r|} \int_0^{t_r} \mathbf{v}_{gl}^{slip}(\tau)\, \mathrm{d}\tau. \tag{2.38}$$

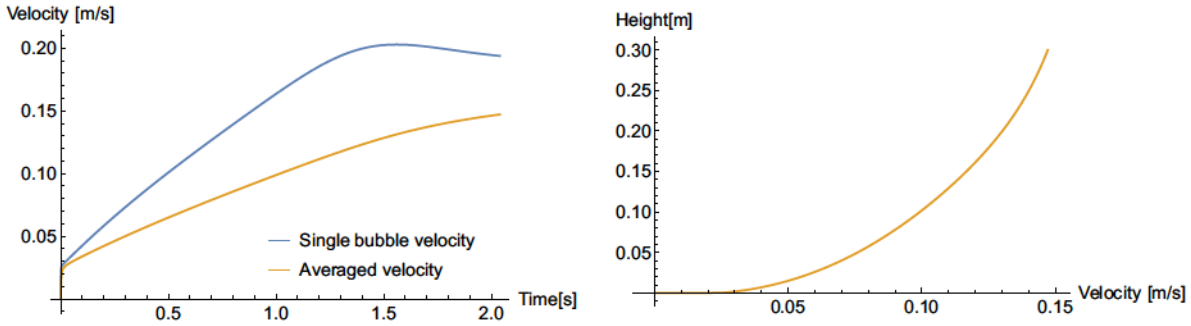

Figure 2.15: The single-bubble slip velocity and averaged (swarm) velocity comparison (left). The averaged (swarm) velocity increasing with height (right).

2.6.2 Collective interfacial area

Once we know the evolution of bubble radius r_g, we can calculate the interfacial surface area of a single bubble as $A_{\Sigma_{gl}}(t) = 4\pi r_g^2(t)$. Analogously to the collective slip velocity (2.39), taking the time average of $A_{\Sigma_{gl}}(t)$, we obtain the collective interfacial surface area in the form

$$\overline{A}_{\Sigma_{gl}}(t) \overset{def}{=} \frac{1}{|t_r|}\int_0^{t_r} A_{\Sigma_{gl}}(\tau)\,\mathrm{d}\tau = \frac{1}{|t_r|}\int_0^{t_r} 4\pi(k_{gl}^{\dot{m}}\,\tau + r_0)^2\,\mathrm{d}\tau. \tag{2.39}$$

Since the specific interface mass transfer rate is constant within the whole reactor volume (cf. the kinetic regime (1.2.3)), the mass transfer rate depends linearly on the interfacial area, i.e.

$$\dot{m}_{gl} = \frac{\overline{A}_{\Sigma_{gl}}}{\langle \overline{A}_{\Sigma_{gl}} \rangle_{V_r}} \langle R_{gl}^{\Sigma} \rangle_{V_r} \tag{2.40}$$

and we may write the partial mass balance for the gas phase as

$$\partial_t(\phi_g \rho_g^{true}) + \mathrm{div}(\phi_g \rho_g^{true} \mathbf{v}_g) = \dot{m}_{gl}.$$

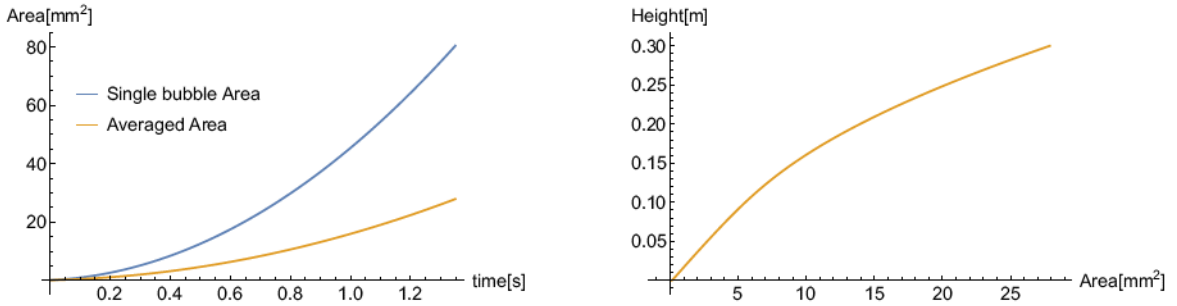

Figure 2.16: Single bubble interfacial-area and collective interfacial-area comparison (left). Dependence of the interfacial-area on the height of the reactor (right).

2.6.3 Suspension: solid-liquid interaction

To model the collective effect of solid-liquid interaction, we follow the approach of Krieger & Dougherty [51]. They represented the effects by introducing the effective suspension-viscosity, dependent on the solid particle concentration, as

$$\nu_{ls} = \nu_l \left(1 - \frac{\phi}{\phi_{max}}\right)^{-2.5\phi_{max}} . \tag{2.41}$$

Here $\phi = \frac{\phi_s}{\phi_{ls}}$; ϕ_{max} is an empirical value corresponding to maximum packing [16] and ν_l is the kinematic viscosity of clear liquid ($\phi = 0$). Moreover, let us assert the viscosity dependence on temperature by the Arrhenius equation for molecular kinetics [68]

$$\nu_l(T) = \nu_l^0 \, e^{\frac{E_a^\nu}{RT}} \tag{2.42}$$

where ν_l^0 correspond to viscous equivalent of frequency factor and E_a^ν is a viscous equivalent of the activation energy.

2.6.4 Drift diffusion

Treating the turbulent (averaged) three-phase flow, one needs to take into account also a drift diffusion (Figure (2.17)). It is commonly a representation of two phenomena: firstly, the rising bubbles cause local flow-eddies which drift the surrounding fluid; secondly, the solid particles mutually collide. [17]

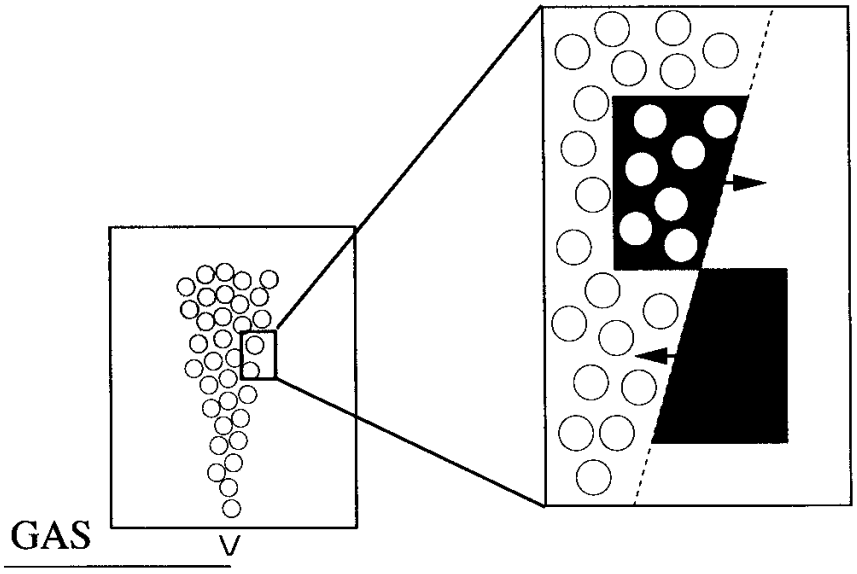

Figure 2.17: Drift diffusion of the solid particles, adopted from [103].

According to Simonin [95] and lately by Sokolichin [103], we consider a collective slip velocity field consisting of a single particle velocity and a drift velocity where the latter

[16] For random packing of small uniform spheres in cube $\phi_{max} \approx 0.64$ which is used also in our case.
[17] We do not consider any gas-solid interaction.

one depends on the gradient of volume fraction:

$$\mathbf{v}_g - \mathbf{v}_l = \mathbf{v}_{gl}^{slip} + \mathbf{v}_{gl}^{drift} \ , \ \mathbf{v}_s - \mathbf{v}_l = \mathbf{v}_{ls}^{slip} + \mathbf{v}_{ls}^{drift}$$
$$\mathbf{v}_{gl}^{drift} = -\frac{\nu_l^{turb}}{\rho_l}\frac{1}{\phi_g}\nabla\phi_g \ , \ \mathbf{v}_{ls}^{drift} = -\frac{\nu_l^{turb}}{\rho_l}\frac{1}{\phi_s}\nabla\phi_s.$$

Nevertheless, since we typically have $|\nabla\phi_g| < 0.1$ and $\rho_g^{true} \ll \rho_l^{true}$, the drift-velocity term may be neglected in case of the gas phase but need to be considered for the solid phase. Thus, the mass balance (3.27c) adopts the form

$$\partial_t(\phi_s\rho_s^{true}) + \mathrm{div}(\phi_s\rho_s^{true}\mathbf{v}_s) = \mathrm{div}\left(\frac{\rho_s}{\rho_l}\nu_l^{turb}\nabla\phi_s\right). \tag{2.44}$$

To conserve mass of the mixture as a whole, one need to consider also corresponding counterparts in the mass balance of the liquid. This can be elegantly implicitly satisfied once the balance of a whole mixture is employed, i.e.

$$\mathrm{div}(\phi_l\mathbf{v}_l + \phi_g\mathbf{v}_g + \phi_s\mathbf{v}_s) = 0. \tag{2.45}$$

3. Balance equations

In this chapter, a volume averaging technique to derive an equation-system modelling the decarboxilation of formic acid in the fluidized bed reactor is introduced. An overview of the technique is followed by the application on the balance equations. Consequently, the constituent relations derived in the Chapter 2 are used to obtain the final model suitable for numerical computations.

3.1 Multi-fluid volume-averaging

3.1.1 Motivation

From perspective of continuum mechanics, we treat a system where the liquid represents a continuous phase and the particles (bubbles and catalytic particles) represent two discrete phases. The interfaces between them may have both material or non-material character. Depending on the complexity of the geometry, we can track the interfaces or apply an averaging (or mixture) techniques. In our case, the reactor is filled by too many interfaces to track them all, thus, it is necessary to use an averaging technique.

Following the terminology of Brennen [14], we need to treat the problem as a dispersed multiphase flow. Thus, we do not search for variables determining single dispersed particles but for some kind of its general representation which keeps the major information of the flow, e.g. an average of the quantities. Quoting Jakobsen [48]:

There are two main strategies that have been used deriving the existing macroscopic models, denoted the averaging and mixture approaches, respectively. The averaging approach consists of the postulation of local instantaneous conservation equations prior to the application of an averaging procedure deriving macroscopic Eulerian multi-fluid models. In the mixture approach the mixture properties are postulated directly at the macroscopic scales, and a set of macroscopic balance equations is formulated based on the conventional conservation laws and the mixture properties. So, in this particular modeling concept the control volume and the averaging volume coincide.

The averaging approach might be considered fundamental and preferred compared to the mixture approach, because averaging provides certain advantages as the resulting macroscopic variables are explicitly related to the local variables.

In this work we give a brief awareness about a volume averaging technique, sometimes called, the spatial averaging. For more details we refer to e.g. Appindix A, [48] or [71].

3.1.2 Averaging procedure

The main requirement for an application of the volume averaging is a proper scale-separation, i.e.

$$\text{Volume of dispersed particle } V_p \ll \text{ Averaging control volume } V \ll \text{ Reactor volume } V_r.$$

Here, the relation $\ll$ is understand in a sense of much lower magnitude. Assuming the proper scale separation [1] , a discontinuous dispersed-object-quantity ψ may be well represented by its average which is already continuous. [2]

In case of heterogeneous catalysis it is important to take into account also surface phenomena. The averaging procedure than reduces the unknown set of n volumetric and m surface variables to a set of n averaged variables. Although we lost the exact information about the surface variables, their influence on the volumetric (averaged) quantity is negotiated via a closure term within the averaged balance equation.

The volume averaging operator for a function ψ of an immiscible k-th phase is defined as

$$\langle \psi_k \rangle_V \stackrel{def}{=} \frac{1}{V} \int_V \chi_k \psi \, \mathrm{dV} = \frac{1}{V} \int_{V_k(t)} \psi_k \, \mathrm{dV} \tag{3.1}$$

where $\chi_k(t)$ is the phase indicator function which equals 1 in the region occupied by phase k, denoted by $V_k(t)$, and 0 elsewhere. Note that the averaging control volume V is independent of time but the phase averaged volume $V_k(t)$ is not. In addition to the volume averaging operator, we define also the deviation (fluctuation) operator as

$$\widehat{\psi}_k \stackrel{def}{=} \psi_k - \langle \psi_k \rangle_V. \tag{3.2}$$

and the volume fraction ϕ_k of the k-th phase as

$$\phi_k(t) \stackrel{def}{=} \frac{V_k(t)}{V} = \frac{\int_V \chi_k(t) \, \mathrm{dV}}{V}. \tag{3.3}$$

For the volume averaging operator we directly obtain the relation

$$\langle \psi_k \rangle_V = \phi_k \langle \psi_k \rangle_{V_k}.$$

A derivation of transport equation for a multiphase body may be found in Appendix A.3, [98, 1.3] or [48, 3.4]. Here, we only recall the results, i.e. the *transport equation for the k^{th}-phase* (A.30) as

$$\begin{aligned} &\frac{\partial(\phi_k \langle \rho_k \psi_k \rangle_{V_k})}{\partial t} + \mathrm{div}(\phi_k \langle \rho_k \mathbf{v}_k \psi_k \rangle_{V_k}) + \mathrm{div}(\phi_k \langle \mathbf{J}_k \rangle_{V_k}) \\ &\quad = \phi_k \langle R_k \rangle_{V_k} - \sum_{\substack{l=1 \\ l \neq k}}^{m} A_{\Sigma_{kl}} \langle (\dot{\boldsymbol{m}}_k^{kl} \psi_k + \mathbf{J}_k) \cdot \mathbf{n} \rangle_{\Sigma_{kl}}. \end{aligned} \tag{3.4}$$

and the vectorial version of (A.31) as

$$\begin{aligned} &\frac{\partial(\phi_k \langle \rho_k \boldsymbol{\psi}_k \rangle_{V_k})}{\partial t} + \mathrm{div}(\phi_k \langle \rho_k \mathbf{v}_k \otimes \boldsymbol{\psi}_k \rangle_{V_k}) + \mathrm{div}(\phi_k \langle \mathbf{J}_k \rangle_{V_k}) \\ &\quad = \phi_k \langle R_k \rangle_{V_k} - \sum_{\substack{l=1 \\ l \neq k}}^{m} A_{\Sigma_{kl}} \langle (\dot{\boldsymbol{m}}_k^{kl} \otimes \boldsymbol{\psi}_k + \mathbf{J}_k) \cdot \mathbf{n} \rangle_{\Sigma_{kl}}. \end{aligned} \tag{3.5}$$

[1] The scale separation in case of the investigated fluidized reactors, concretely $V^{\text{Å}} \ll V_p \ll V \ll V_r$, results from the following characteristic values: $V^{\text{Å}} \sim 10^{-30}\,\mathrm{m}^3$ of atom (molecule), $V^p \sim 10^{-14} - 10^{-8}\,\mathrm{m}^3$ size of a dispersed particles (bubbles, solid particles), V an arbitrary averaging (control) volume and $V_r \sim 10^{-3}\,\mathrm{m}^3$ the volume of the reactor.

[2] Since the averaging control volume is arbitrary small, it can be identified with a space point.

3.1.3 Averaged mass balance

In the previous section, we introduced the volume averaging which is not multiplicative, i.e. generally $\langle ab \rangle \neq \langle a \rangle \langle b \rangle$. Since the balance equations contain non-linear terms, we introduce also the *mass-weighted volume average* of the quantity ψ_k as

$$\langle \psi_k \rangle_{V_k}^{\rho_k} \stackrel{def}{=} \frac{\langle \rho_k \psi_k \rangle_{V_k}}{\langle \rho_k \rangle_{V_k}} = \frac{\int_{V_k} \rho_k \psi_k dV}{\int_{V_k} \rho_k dV} \tag{3.6a}$$

$$\widehat{\psi}_k^{\rho_k} \stackrel{def}{=} \psi_k - \langle \psi_k \rangle_{V_k}^{\rho_k}. \tag{3.6b}$$

Note that $\langle \widehat{\psi}_k^{\rho_k} \rangle_{V_k} = \langle \widehat{\psi}_k \rangle_{V_k}^{\rho_k} = 0$. Moreover, in case of constant density ρ_k both averages coincide.

Substituting $\psi_k = 1, R_k = R_k^V$ to the equation (3.4) and neglecting the volumetric molecular fluxes $\mathbf{J}_k$, we obtain

$$\frac{\partial (\phi_k \langle \rho_k \rangle_{V_k})}{\partial t} + \langle \mathrm{div}(\phi_k \langle \rho_k \mathbf{v}_k \rangle) \rangle_{V_k} = \phi_k \langle R_k^V \rangle_{V_k} - \sum_{\substack{l=1 \\ l \neq k}}^{m} A_{\Sigma_{kl}} \langle \dot{\boldsymbol{m}}_k^{kl} \cdot \mathbf{n} \rangle_{\Sigma_{kl}}.$$

To obtain the mass balance in the standard form, we denote the density of k-th phase averaged over the phase volume V_k as the material density [3] , i.e.

$$\langle \rho_k \rangle_{V_k} \stackrel{def}{=} \rho_k^{true}.$$

and

$$\mathbf{v}_k \stackrel{def}{=} \langle \mathbf{v}_k \rangle_{V_k}^{\rho_k}.$$

Furthermore, we identify also

$$R_k^V \stackrel{def}{=} \langle R_k^V \rangle_{V_k}, \; \dot{m}_k^{kl} \stackrel{def}{=} \langle \dot{\boldsymbol{m}}_k^{kl} \cdot \mathbf{n} \rangle_{\Sigma_{kl}}$$

and the *averaged partial mass balance for the k-th phase* may be, consequently, expressed as

$$\frac{\partial \phi_k \rho_k^{true}}{\partial t} + \mathrm{div}(\phi_k \rho_k^{true} \mathbf{v}_k) = \phi_k R_k^V - \sum_{\substack{l=1 \\ l \neq k}}^{m} A_{\Sigma_{kl}} \dot{m}_k^{kl}. \tag{3.7}$$

3.1.4 Averaged momentum balance

Substituting $\psi_k = \mathbf{v}_k, \mathbf{J}_k = -\ _k, R_k = \rho_k \mathbf{g} + R_k^V \mathbf{v}_k$ into (3.5), we obtain the relation

$$\begin{aligned} &\frac{\partial (\phi_k \langle \rho_k \mathbf{v}_k \rangle_{V_k})}{\partial t} + \mathrm{div}\left(\phi_k \langle \rho_k \mathbf{v}_k \otimes \mathbf{v}_k \rangle_{V_k}\right) - \mathrm{div}(\phi_k \langle\ _k \rangle_{V_k}) = \\ &\phi_k \langle \rho_k \mathbf{g} + R_k^V \mathbf{v}_k \rangle_{V_k} - \sum_{\substack{l=1 \\ l \neq k}}^{m} A_{\Sigma_{kl}} \left\langle \left(\dot{\boldsymbol{m}}_k^{kl} \otimes \mathbf{v}_k +\ _k\right) \cdot \mathbf{n} \right\rangle_{\Sigma_{kl}}. \end{aligned} \tag{3.8}$$

Using the tensor identity

$$(\mathbf{a} \otimes \mathbf{b}) \cdot \mathbf{c} = (\mathbf{a} \cdot \mathbf{b})\, \mathbf{c}; \;\; \mathbf{a}, \mathbf{b}, \mathbf{c} \in \mathbf{R^3},$$

[3] In the mixture theory, is is commonly addressed as a "true" density of the phase.

yields

$$\langle \dot{\boldsymbol{m}}_k^{kl} \otimes \mathbf{v}_k \cdot \mathbf{n} \rangle_{\Sigma_{kl}} = \langle (\dot{\boldsymbol{m}}_k^{kl} \cdot \mathbf{n})\, \mathbf{v}_k \rangle_{\Sigma_{kl}} = \dot{m}_k^{kl} \langle \mathbf{v}_k \rangle_{\Sigma_{kl}}^{\rho_{kl}^{\Sigma}}$$

where

$$\langle \mathbf{v}_k \rangle_{\Sigma_{kl}}^{\rho_{kl}^{\Sigma}} \stackrel{def}{=} \frac{\langle \rho_k^{\Sigma} \mathbf{v}_k \rangle_{\Sigma_{kl}}}{\langle \rho_k^{\Sigma} \rangle_{\Sigma_{kl}}}.$$

Applied on the averaged momentum balance, we have

$$\begin{aligned} &\frac{\partial (\phi_k \langle \rho_k \rangle_{V_k} \langle \mathbf{v}_k \rangle_{V_k}^{\rho_k})}{\partial t} + \operatorname{div}\left(\phi_k \langle \rho_k \rangle_{V_k} \langle \mathbf{v}_k \otimes \mathbf{v}_k \rangle_{V_k}^{\rho_k}\right) + \operatorname{div}(\phi_k \langle \quad_k \rangle_{V_k}) = \\ &\phi_k \langle \rho_k \rangle_{V_k} \mathbf{g} + \langle R_k^V \rangle_{V_k} \langle \mathbf{v}_k \rangle_{V_k}^{\rho_k} - \sum_{\substack{l=1 \\ l \neq k}}^{m} A_{\Sigma_{kl}} \left(\dot{m}_k^{kl} \langle \mathbf{v}_k \rangle_{\Sigma_{kl}}^{\rho_{kl}^{\Sigma}} + \langle \quad_i \cdot \mathbf{n} \rangle_{\Sigma_{kl}} \right). \end{aligned} \tag{3.9}$$

Although we got rid of the non-linear term $\langle \rho_k \mathbf{v}_k \rangle_{V_k}$ in the mass balance, it is not possible here, since the non-linearity is quadratic and an introduction of a new averaging would lead to under-determined equation system. The quadratic term

$$\langle \mathbf{v}_k^i \mathbf{v}_k^j \rangle_{V_k} = \langle (\langle \mathbf{v}_k^i \rangle_{V_k}^{\rho_k} + \widehat{\mathbf{v}}_k^i)(\langle \mathbf{v}_k^j \rangle_{V_k}^{\rho_k} + \widehat{\mathbf{v}}_k^j) \rangle_{V_k} = \langle \mathbf{v}_k^i \rangle_{V_k}^{\rho_k} \langle \mathbf{v}_k^j \rangle_{V_k}^{\rho_k} + \langle \widehat{\mathbf{v}}_k^i \widehat{\mathbf{v}}_k^j \rangle_{V_k}.$$

implies a need of an additional closures for convection term (usually referred as the Reynolds stress tensor). Moreover in case of the momentum balance, we need also a closure for the interfacial momentum transfer term $\dot{m}_k^{kl}$ as well as in the averaged liquid velocity term on the gl-interface $\langle \mathbf{v}_k \rangle_{\Sigma_{kl}}^{\rho_{kl}^{\Sigma}}$.

Dropping the averaging brackets

$$_k \stackrel{def}{=} \langle \quad_k \rangle_{V_k}; \quad {}_k^{Re} \stackrel{def}{=} \langle \rho_k \rangle_{V_k} \langle \widehat{\mathbf{v}}_k^i \widehat{\mathbf{v}}_k^j \rangle_{V_k}^{\rho_k}, \quad \rho_k^{true} \stackrel{def}{=} \langle \rho_k \rangle_{V_k}$$

and applying the notation introduced in the previous section, we may write the *averaged partial momentum balance for the k-th phase* as

$$\begin{aligned} &\frac{\partial (\phi_k \rho_k^{true} \mathbf{v}_k)}{\partial t} + \operatorname{div}\left(\phi_k \rho_k^{true} \mathbf{v}_k \otimes \mathbf{v}_k\right) + \operatorname{div}\left(\phi_k (\quad_k + \quad_k^{Re})\right) = \\ &+\phi_k \rho_k^{true} \mathbf{g} + R_k^V \langle \mathbf{v}_k \rangle_{V_k}^{\rho_k} - \sum_{\substack{l=1 \\ l \neq k}}^{m} A_{\Sigma_{kl}} \left(\dot{m}_k^{kl} \langle \mathbf{v}_k \rangle_{\Sigma_{kl}}^{\rho_{kl}^{\Sigma}} + \langle \quad_i \cdot \mathbf{n} \rangle_{\Sigma_{kl}} \right). \end{aligned} \tag{3.10}$$

Remarks:

3.1.1 Mixture theory. *There are several definitions of the volume fraction quantity in a system containing more different fluids. The phase indicator function is a convenient tool in case of immiscible fluids separated by interfaces. On the other hand, this function is not clearly defined for a mixture of miscible fluids. Therefore, we introduce also a concept commonly used in the theory of mixtures:*

Let us consider a volume element of the mixture (of n constituents) with the volume V. We introduce the following measures: $M_k(V)$ - denoting the denoting the mass of the k-th phase in the given volume element V, $\forall k = 1, \ldots, n$. Assuming absolute continuity of these measures with respect to the corresponding volume measure, we define the (mixture) density as

$$M_\alpha(B) \stackrel{def}{=} \int_B \rho_\alpha \, \mathrm{dV}, \ \forall k = 1, \ldots, n.$$

Moreover, knowing the material (true) density of the constituents ρ_k^{true}, we may define also their volume fraction as

$$\phi \stackrel{def}{=} \frac{\rho_k}{\rho_k^{true}}.$$

3.1.2 Mixture of ideal gases. *Having a mixture of N ideal gases at temperature T, volume V and pressure p, the volume fraction of all constituents are the same since they always fill the whole volume. Nevertheless, we may measure their amount by their partial pressures p_α. These commonly satisfy the Dalton's additivity law, cf. [92],*

$$p = \sum_{\alpha=1}^{N} p_\alpha.$$

Consequently, we may define the (material) density of the gas by equation of state for ideal gases:

$$\rho_k = \frac{p_k M_k}{RT}. \tag{3.11}$$

and, applied in our case, we obtain

$$\phi_g = \phi_{H_{2(g)}} = \phi_{CO_{2(g)}},\ \rho_g = \frac{p_{H_{2(g)}} M_{H_2} + p_{CO_{2(g)}} M_{CO_2}}{RT}.$$

3.1.3 Volume-additivity. *If it is not written otherwise, we assume that liquids satisfy the volume additivity constrain. Taking two liquids with volume V_1, V_2 and mixing them together, the resulting volume is $V = V_1 \cup V_2$. This is generally valid for the immiscible liquids and good approximation for most of the miscible fluids (also for formic acid - water mixture, cf. [37, 2-114]), however, it does not hold always (e.g. ethanol and water).*

3.2 Balance of mass

3.2.1 Partial momenta: nine-constituents system

Let us recall all nine constituents within the reactor sorted by the phase type:

$$\begin{aligned} \text{Liquid: } & FA_{(l)}, H_2O_{(l)} \\ \text{Gas: } & FA_{(g)}, H_2O_{(g)}, H_{2(g)}, CO_{2(g)} \\ \text{Dissolved gas: } & H_{2(d)}, CO_{2(d)} \\ \text{Solid: } & Cat_{(s)} \end{aligned}$$

and the averaged partial mass balance for the k-th phase (3.7):

$$\frac{\partial \phi_k \rho_k^{true}}{\partial t} + \operatorname{div}(\phi_k \rho_k^{true} \mathbf{v}_k) = \phi_k R_k^V - \sum_{\substack{l=1 \\ l \neq k}}^{m} A_{\Sigma_{kl}} \dot{m}_k^{kl}.$$

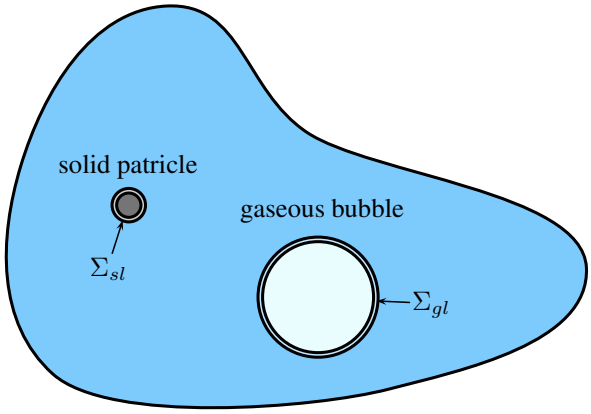

Figure 3.1: A schematic figure of the control (averaging) volume.

In case of the fluidized bed reactor, we treat three different phases distinguishing three kinds of interfaces: solid-liquid (sl), gas-liquid (gl) and gas-solid (gs); cf. Figure (3.1). From the problem description in Chapter 1, we postulate the following assumptions:

1. The solid particles are treated as an idealized catalyst. Thus, we may express its (mass) conservation as
$$\partial_t(\phi_{Cat_{(s)}}\rho^{true}_{Cat_{(s)}}) + \operatorname{div}(\phi_{Cat_{(s)}}\rho^{true}_{Cat_{(s)}}\mathbf{v}_{Cat_{(s)}}) = 0.$$

2. No homogeneous reaction is considered, hence,
$$R^V_k \approx 0, \forall k.$$

3. The only considered heterogeneous reaction is the decarboxilation of $FA_{(l)}$:
$$FA_{(l)} \xrightarrow{Cat_{(s)}} H_{2(d)} + CO_{2(d)},$$
thus,
$$\dot{m}^{ls}_{H_{2(d)}} = \frac{M_{H_2}}{M_{FA}}\dot{m}^{ls}_{FA_{(l)}},\ \dot{m}^{ls}_{CO_{2(d)}} = \frac{M_{CO_2}}{M_{FA}}\dot{m}^{ls}_{FA_{(l)}}.$$

Consequently, we may express the mass balances as

$$\partial_t(\phi_{FA_{(g)}}\rho^{true}_{FA_{(g)}}) + \operatorname{div}(\phi_{FA_{(g)}}\rho^{true}_{FA_{(g)}}\mathbf{v}_{FA_{(g)}}) = A_{\Sigma_{gl}}\dot{m}^{gl}_{FA} \tag{3.12a}$$
$$\partial_t(\phi_{H_2O_{(g)}}\rho^{true}_{H_2O_{(g)}}) + \operatorname{div}(\phi_{H_2O_{(g)}}\rho^{true}_{H_2O_{(g)}}\mathbf{v}_{H_2O_{(g)}}) = A_{\Sigma_{gl}}\dot{m}^{gl}_{H_2O} \tag{3.12b}$$
$$\partial_t(\phi_{H_{2(g)}}\rho^{true}_{H_{2(g)}}) + \operatorname{div}(\phi_{H_{2(g)}}\rho^{true}_{H_{2(g)}}\mathbf{v}_{H_{2(g)}}) = A_{\Sigma_{gl}}\dot{m}^{gl}_{H_2} \tag{3.12c}$$
$$\partial_t(\phi_{CO_{2(g)}}\rho^{true}_{CO_{2(g)}}) + \operatorname{div}(\phi_{CO_{2(g)}}\rho^{true}_{CO_{2(g)}}\mathbf{v}_{CO_{2(g)}}) = A_{\Sigma_{gl}}\dot{m}^{gl}_{CO_2} \tag{3.12d}$$

$$\partial_t(\phi_{FA_{(l)}}\rho^{true}_{FA_{(l)}}) + \operatorname{div}(\phi_{FA_{(l)}}\rho^{true}_{FA_{(l)}}\mathbf{v}_{FA_{(l)}}) = -A_{\Sigma_{ls}}\dot{m}^{ls}_{FA} - A_{\Sigma_{gl}}\dot{m}^{gl}_{FA} \tag{3.12e}$$
$$\partial_t(\phi_{H_2O_{(l)}}\rho^{true}_{H_2O_{(l)}}) + \operatorname{div}(\phi_{H_2O_{(l)}}\rho^{true}_{H_2O_{(l)}}\mathbf{v}_{H_2O_{(l)}}) = -A_{\Sigma_{gl}}\dot{m}^{gl}_{H_2O} \tag{3.12f}$$
$$\partial_t(\phi_{H_{2(d)}}\rho^{true}_{H_{2(d)}}) + \operatorname{div}(\phi_{H_{2(d)}}\rho^{true}_{H_{2(d)}}\mathbf{v}_{H_{2(d)}}) = \frac{M_{H_2}}{M_{FA}}A_{\Sigma_{ls}}\dot{m}^{ls}_{FA} - A_{\Sigma_{gl}}\dot{m}^{gl}_{H_2} \tag{3.12g}$$
$$\partial_t(\phi_{CO_{2(d)}}\rho^{true}_{CO_{2(d)}}) + \operatorname{div}(\phi_{CO_{2(d)}}\rho^{true}_{CO_{2(d)}}\mathbf{v}_{CO_{2(d)}}) = \frac{M_{CO_2}}{M_{FA}}A_{\Sigma_{ls}}\dot{m}^{ls}_{FA} - A_{\Sigma_{gl}}\dot{m}^{gl}_{CO_2} \tag{3.12h}$$

3.2.2 Additional assumptions:

Now we employ the fact that we are interested in continuous performance only, i.e. we do not consider an initiation of the rector. This implies the following:

1. We omit phenomena with very small relaxation time, such as evolution of the surface species and their transport along the interfaces. [4] The equation (A.21b) reduces to

$$0 = R^{\Sigma}_{kl} + [\![\dot{\boldsymbol{m}}^{kl}_i]\!]^k_l, \ \forall l \neq k. \tag{3.13}$$

2. The liquid is already saturated by the dissolved gases and the reactor operates in a kinetic regime (sec. 1.2.3), i.e.

$$\underbrace{FA_{(l)} \longrightarrow FA^*_{(l)}}_{\text{fast adsorption}} \overbrace{\overset{Cat_{(s)}}{\longrightarrow}}^{\text{slow reaction}} \underbrace{H^*_{2(d)} + CO^*_{2(d)} \longrightarrow H_{2(d)} + CO_{2(d)}}_{\text{fast desorption}} \overbrace{\longrightarrow H_{2(g)} + CO_{2(g)}}^{\text{fast vaporization}}.$$

   Consequently, we may identify the vaporization rate and the chemical rate of hydrogen and carbon dioxide

$$\begin{aligned} A_{\Sigma_{ls}} \dot{m}^{ls}_{H_2} &= A_{\Sigma_{gl}} \dot{m}^{gl}_{H_2} && (3.14a)\\ A_{\Sigma_{ls}} \dot{m}^{ls}_{CO_2} &= A_{\Sigma_{gl}} \dot{m}^{gl}_{CO_2} && (3.14b)\\ A_{\Sigma_{ls}} \dot{m}^{ls}_{FA} &= A_{\Sigma_{ls}} \dot{m}^{ls}_{H_2} + A_{\Sigma_{ls}} \dot{m}^{ls}_{CO_2} && (3.14c)\\ &= A_{\Sigma_{gl}} \dot{m}^{gl}_{H_2} + A_{\Sigma_{gl}} \dot{m}^{gl}_{CO_2} && (3.14d) \end{aligned}$$

   and

$$\frac{\dot{m}^{gl}_{H_2}}{\dot{m}^{gl}_{CO_2}} = \frac{\dot{m}^{ls}_{H_2}}{\dot{m}^{ls}_{CO_2}} = \frac{M_{H_2}}{M_{CO_2}} \implies \frac{[H_{2(g)}]}{[CO_{2(g)}]} = \frac{1}{1}.$$

3. We assume that liquid formic acid and water already formed an azeotrope (sec. 1.2.2) which is constant. Moreover, the amount of in-coming (prescribed by a boundary condition) has to equal the amount of out-coming water. These may be expressed as

$$\begin{aligned} \frac{[FA_{(l)}]}{[H_2O_{(l)}]} = \frac{[FA_{(g)}]}{[H_2O_{(g)}]} &= \frac{M_{H_2O}}{M_{FA}} R^{FA}_{H_20} && (3.15a)\\ A_{\Sigma_{in}} \dot{m}^{in}_{H_2O_{(l)}} &= A_{\Sigma_{out}} \dot{m}^{out}_{H_2O_{(l)}}. && (3.15b) \end{aligned}$$

   Together with the preceding, we obtain

$$\begin{aligned} A_{\Sigma_{gl}} \dot{m}^{gl}_{H_2O_{(l)}} &= A_{\Sigma_{in}} \dot{m}^{in}_{H_2O_{(l)}} && (3.16a)\\ A_{\Sigma_{gl}} \dot{m}^{gl}_{FA_{(l)}} &= A_{\Sigma_{ls}} \dot{m}^{ls}_{FA_{(l)}} + R^{FA}_{H_20} A_{\Sigma_{in}} \dot{m}^{in}_{H_2O_{(l)}} && (3.16b) \end{aligned}$$

[4] This assumption is commonly applicable for solid-liquid interfaces as well as gas-liquid once we consider contaminated interfaces.

In terms of partial mass balances (3.12), we write a consequence of the previous assumptions as:

$$\partial_t(\phi_{FA_{(l)}}\rho^{true}_{FA_{(l)}}) + \mathrm{div}(\phi_{FA_{(l)}}\rho^{true}_{FA_{(l)}}\mathbf{v}_l) = -A_{\Sigma_{ls}}\dot{m}^{ls}_{FA} - R^{FA}_{H_20}A_{\Sigma_{gl}}\dot{m}^{H_20}_{gl} \tag{3.17a}$$

$$\partial_t(\phi_{H_2O_{(l)}}\rho^{true}_{H_2O_{(l)}}) + \mathrm{div}(\phi_{H_2O_{(l)}}\rho^{true}_{H_2O_{(l)}}\mathbf{v}_l) = -A_{\Sigma_{gl}}\dot{m}^{H_20}_{gl} \tag{3.17b}$$

$$\partial_t(\phi_{H_{2(d)}}\rho^{true}_{H_{2(d)}}) + \mathrm{div}(\phi_{H_{2(d)}}\rho^{true}_{H_{2(d)}}\mathbf{v}_l) = 0 \tag{3.17c}$$

$$\partial_t(\phi_{CO_{2(d)}}\rho^{true}_{CO_{2(d)}}) + \mathrm{div}(\phi_{CO_{2(d)}}\rho^{true}_{CO_{2(d)}}\mathbf{v}_l) = 0. \tag{3.17d}$$

4. Finally, the kinetic regime of the reactor determinates also the characteristic values of the dissolved gas concentration since they are expected to be close to equilibrium. For their estimation, we take the equilibrium Henry's constant giving the mass fraction [5] $w_{CO_{2(d)}} = 2.1 \cdot 10^{-3}$ and $w_{H_{2(d)}} = 2.3 \cdot 10^{-6}$ for $H_{2(d)}$, cf. [40].

   Moreover, an influence of the dissolved gas on the material (mechanical) properties of the solvent is very often negligible, thus, we omit them also here. Consequently, the partial mass balances (3.12) may be expressed as

$$\partial_t(\phi_{FA_{(l)}}\rho^{true}_{FA_{(l)}}) + \mathrm{div}(\phi_{FA_{(l)}}\rho^{true}_{FA_{(l)}}\mathbf{v}_l) = -A_{\Sigma_{ls}}\dot{m}^{ls}_{FA} - R^{FA}_{H_20}A_{\Sigma_{gl}}\dot{m}^{H_20}_{gl} \tag{3.18a}$$

$$\partial_t(\phi_{H_2O_{(l)}}\rho^{true}_{H_2O_{(l)}}) + \mathrm{div}(\phi_{H_2O_{(l)}}\rho^{true}_{H_2O_{(l)}}\mathbf{v}_l) = -A_{\Sigma_{gl}}\dot{m}^{H_20}_{gl} \tag{3.18b}$$

$$\phi^m_{H_{2(d)}} \approx 0 \approx \phi^m_{CO_{2(d)}}. \tag{3.18c}$$

3.2.3 Three-phase system

A natural consequence of the previous assumptions is a reduction of the system into three immiscible phases (fluids) with distinguished velocity-fields and concentrations. Then, a classical multi-fluid (mixture) theory may be applicable.

In this sense, we consider gas, liquid and solid phase with corresponding volume fractions ϕ_g, ϕ_l, ϕ_s filling the entire control volume, i.e.

$$\phi_g + \phi_l + \phi_s = 1.$$

To balance partial masses and momenta we need to define corresponding densities and velocities. However, the situation complicates in the case of the gas and liquid phase since they are actually composition of other miscible fluids. We proceed as follows:

Gas phase:

We define the gas phase as a miscible mixture of $H_{2(g)}$, $CO_{2(g)}, FA_{(g)}$, $H_2O_{(g)}$ where

$$\phi_g \overset{def}{=} \phi_{FA_{(g)}} = \phi_{H_20_{(g)}} = \phi_{H_{2(g)}} = \phi_{CO_{2(g)}} \tag{3.19a}$$

$$\rho^{true}_g = \sum_k \rho^{true}_k,\ \rho^{true}_k = \frac{p_k M_k}{RT},\ k \in \{FA_{(g)}, H_20_{(g)}, H_{2(g)}, CO_{2(g)}\}. \tag{3.19b}$$

The gases are practically always considered as miscible fluids and, thus, they are supposed to share a common velocity field $\mathbf{v}_g$. The vapours of water and formic acid keep the

[5] The mass fraction denotes the ratio of the mass of α-th constituent m_α to the mass of the total mixture (liquid phase) m_l, i.e. $w_\alpha \overset{def}{=} \frac{m_\alpha}{m_l}$

azeotropic ratio and the molar concentration of hydrogen equals the molar concentration of carbon dioxide, i.e.

$$\frac{1}{1} = \frac{p_{FA_{(g)}}}{p_{H_2O_{(g)}}} \approx \frac{M_{H_2O}}{M_{FA}} R^{FA}_{H_2O}(p).$$

Consequently, the corresponding balance of mass and the mass transfers follows as

$$\partial_t(\phi_g \rho_g^{true}) + \operatorname{div}(\phi_g \rho_g^{true} \mathbf{v}_g) = \dot{m}^{gl}_{FA} + \dot{m}^{gl}_{H_2O} + \dot{m}^{gl}_{H_2} + \dot{m}^{gl}_{CO_2}$$

which, together with the previous assumptions (3.16) and (3.14), gives

$$\partial_t(\phi_g \rho_g^{true}) + \operatorname{div}(\phi_g \rho_g^{true} \mathbf{v}_g) = \left(1 + R^{FA}_{H20}\right) A_{\Sigma_{in}} \dot{m}^{in}_{H20_{(l)}} + A_{\Sigma_{ls}} \dot{m}^{ls}_{FA}. \tag{3.20}$$

Liquid phase:

We define the liquid phase within the system as the mixture of two miscible liquids $(FA_{(l)}, H_2O_{(l)})$ and the dissolved gases $(H_{2(d)}, CO_{2(d)})$, thus,

$$\phi_l \overset{def}{=} \phi_{FA_{(l)}} = \phi_{H20_{(l)}} = \phi_{FA_{(l)}} = \phi_{H20_{(l)}}. \tag{3.21a}$$

$$\tag{3.21b}$$

Unlike in case of an ideal-gases mixture, here, we cannot define the density by a simple EOS but we may use the mass fractions w_α and obtain the familiar relations

$$\rho_l^{true} \overset{def}{=} \sum_\alpha w_\alpha \rho_\alpha^{true}, \ \alpha \in \{FA_l, H_2O_l, H_{2(d)}, CO_{2(d)}\}. \tag{3.22}$$

In the next step, we employ the assumption (3.18) and the mass additivity, [6] resulting into

$$w_{H_{2(d)}} \approx w_{CO_{2(d)}} \approx 0 \quad \Rightarrow \quad w_{FA_{(l)}} + w_{H20_{(l)}} = 1. \tag{3.23}$$

Consequently, we define the material density of the liquid phase as

$$\rho_l^{true} \overset{def}{=} w_{FA_{(l)}} \rho_{FA}^{true} + w_{H20_{(l)}} \rho_{H20_{(l)}}^{true} \tag{3.24}$$

and its thermal conductivity k_l together with the volume expansion coefficient α_l as

$$\begin{aligned} \rho_l^{true} k_l &\overset{def}{=} \rho^{true}_{FA_{(l)}} w_{FA_{(l)}} k_{FA_{(l)}} + \rho^{true}_{H_2O_{(l)}} w_{H20_{(l)}} k_{H_2O_{(l)}} \\ \rho_l^{true} \alpha_l &\overset{def}{=} \rho^{true}_{FA_{(l)}} w_{FA_{(l)}} \alpha_{FA_{(l)}} + \rho_{H20_{(l)}} w_{H20_{(l)}} \alpha_{H_2O_{(l)}}. \end{aligned}$$

Since water and formic acid are miscible, both mixture-components share one velocity field $\mathbf{v}_l$. Summing the equations (3.18), we obtain:

$$\partial_t(\phi_l \rho_l^{true}) + \operatorname{div}(\phi_l \rho_l^{true} \mathbf{v}_l) = -A_{\Sigma_{gl}} \dot{m}^{gl}_l - A_{\Sigma_{ls}} \dot{m}^{ls}_l \tag{3.25a}$$

$$\overset{(3.16)}{=} -\underbrace{\left(1 + R^{FA}_{H20}\right) A_{\Sigma_{in}} \dot{m}^{in}_{H_2O_{(l)}}}_{\text{vaporization}} - \underbrace{A_{\Sigma_{ls}} \dot{m}^{ls}_{FA}}_{\text{reaction}}. \tag{3.25b}$$

[6] The mass of a mixture equals the sum of its component-masses, i.e. no mass is lost.

Solid phase:

The solid phase is represented by rigid spheres. It is considered as an ideal heterogeneous catalyst, thus, not consumed neither produced. Its conservation is expressed as

$$\partial_t(\phi_s\rho_s^{true}) + \mathrm{div}(\phi_s\rho_s^{true}\mathbf{v}_s) = 0. \tag{3.26}$$

Summing the partial mass balances (3.12), we obtain the total mass conservation and we may write the system of mass balances in the form:

$$\partial_t(\phi_l\rho_l^{true} + \phi_g\rho_g^{true} + \phi_s\rho_s^{true}) + \mathrm{div}(\phi_l\rho_l^{true}\mathbf{v}_l + \phi_g\rho_g^{true}\mathbf{v}_g + \phi_s\rho_s^{true}\mathbf{v}_s) = 0 \tag{3.27a}$$

$$\partial_t(\phi_g\rho_g^{true}) + \mathrm{div}(\phi_g\rho_g^{true}\mathbf{v}_g) = \left(1 + R^{FA}_{H_20}\right)A_{\Sigma_{in}}\dot{m}^{in}_{H_20_{(l)}} + A_{\Sigma_{gl}}\left(1 + \frac{M_{CO_2}}{M_{H_2}}\right)\dot{m}^{gl}_{H_{2(g)}} \tag{3.27b}$$

$$\partial_t(\phi_s\rho_s^{true}) + \mathrm{div}(\phi_s\rho_s^{true}\mathbf{v}_s) = 0. \tag{3.27c}$$

3.2.4 Chemical rates: Collision theory

For description of a chemical rate one usually uses the collision theory. This theory describes bimolecular reactions for ideal gases treating the atoms as a rigid spheres. Considering a closed system of a unit volume containing N^A and N^B atoms of A and B constituents with molar masses M_A, M_B. The number of collision between the molecules (the total collision frequency) corresponds to

$$Z_{AB} = N^A N^B \sigma_{AB}\sqrt{\frac{8k_BT}{\pi\mu}} = [A][B]N_A^2\sigma_{AB}\sqrt{\frac{8k_BT}{\pi\mu}} = Z[A][B]. \tag{3.28}$$

Here, the bracket $[\cdot]$ denotes molar concentration of the unit $\frac{mol}{m^3}$; $N_A \approx 6.022 \cdot 10^{23}$ is the Avogadro constant expressing the amount of atoms in one mol; $\sigma_{AB} = \pi d_{AB}^2$ is the reaction cross-section; μ is the reduced mass defined as $\frac{M_AM_B}{M_A+M_B}$; k_B is the Boltzmann's constant and Z is the collision frequency.

Consequently, the rate of an elementary [7] bimolecular chemical reaction

$$A + B \to C$$

may be expressed as

$$r_c \overset{def}{=} Z\varrho[A][B] \tag{3.29}$$

where A is the frequency factor and ϱ represents the steric factor, i.e. the experimental correction of the reaction rate [8]. Employing the temperature dependence modelled by the Arrhenius kinetics, cf. [4, 22.5], [106, 1.5], we obtain the final form of the reaction rate

$$r_c(T) = A\, e^{\frac{-E_a}{RT}}[A][B] \tag{3.30}$$

where E_a denotes the activation energy and R is the universal gas constant. [9]

[6] Commonly, $d_{AB} = r_A + r_B$ where r_A, r_B is the atomic radius of A and B, respectively.

[7] A reaction without reaction-intermediates. i.e. the reactants form directly the product. An elementary reaction is assumed to occur in a single step and to pass through a single transition state, cf. [67].

[8] The steric factor can be, alternatively, defined as a ratio of the frequency (pre-exponential) factor A and the collision frequency Z.

[9] Note that just a collision of atoms does not need to lead to the chemical reaction. Typically, the possibility of the reaction depends on the angle and the energy of collision. The relation (3.30) reflects such dependencies by the frequency factor and the activation energy.

In the case of heterogeneous chemical reactions is the situation more complicated. However, also here we can provide an analogue to the previous situation once we consider volume fractions instead of molar concentrations. Here, the frequency factor loses its original meaning, since both quantities have direct relation to the substances (atoms) but it serves as the fitting parameter. The rate of the reaction

$$FA_{(l)} + Cat_{(s)} \rightarrow H_{2(d)} + CO_{2(d)},$$

considered as a surface average of the catalytic particle can be, consequently, modelled as

$$\langle R^{\Sigma}_{sl} \rangle_{\Sigma_{sl}} = A\, e^{\frac{-E_a}{RT}} \phi_{FA_{(l)}} \phi_{Cat_{(s)}}. \tag{3.31}$$

As a consequence of the kinetic regime of the reactor, the product of the heterogeneous reaction $(H_{2(d)}, CO_{2(d)})$ is supposed to be uniformly distributed within the reactor. Therefore, the evaporation rate

$$H_{2(d)} + CO_{2(d)} \rightarrow H_{2(g)} + CO_{2(g)},$$

depends on the bubble area $A_{\Sigma_{gl}}$ and liquid saturation where the latter one in equilibrium corresponds to the volume average of the chemical rate. Together with the third assumption in (3.2.2) and (2.40), we obtain

$$\dot{m}_{gl} = \frac{\overline{A}_{\Sigma_{gl}}}{\langle \overline{A}_{\Sigma_{gl}} \rangle_{V_r}} \left(\left(1 + R^{FA}_{H_20} \right) \phi^{in}_{H_20_{(l)}} + 1 \right) \langle \langle R^{\Sigma}_{sl} \rangle_{\Sigma_{sl}} \rangle_{V_r}.$$

Finally, using the volume additivity constrain

$$\phi_l + \phi_g + \phi_s = 1, \tag{3.32}$$

together with the relation (2.19), the mass balance (3.27) adopts the form

$$\operatorname{div}(\phi_l \mathbf{v}_l + \phi_g \overline{\mathbf{v}}_g + \phi_s \mathbf{v}_s) = 0 \tag{3.33a}$$

$$\partial_t \phi_g + \operatorname{div}(\phi_g \overline{\mathbf{v}}_g) = \frac{\dot{m}_{gl}}{\rho^{true}_g} \tag{3.33b}$$

$$\partial_t \phi_s + \operatorname{div}(\phi_s \mathbf{v}_s) = \operatorname{div}\left(\frac{\rho_s}{\rho_l} \nu^{turb}_l \nabla \phi_s \right). \tag{3.33c}$$

Remarks

3.2.1 Material properties. *Material properties of pure substances are easily found in literature, e.g. [40]. However, the properties for mixtures (e.g. azeotrope) and other non-typical systems (e.g. dissolution of gases in FA) are often very scarce or impossible to find. Therefore, once the data are not measured experimentally, we estimate the material properties of mixtures by volumetric ratio of the constituents or the values are estimated by tabulated data for similar processes (e.g. Henry constant for dissolution of CO_2 and H_2 in formic-acid-azeotrope are estimated by values for water).*

3.3 Balance of momenta

3.3.1 Balance of partial momenta

The averaged partial momentum balance for liquid phase (3.10) with gl, sl-interfaces and no volumetric chemical reaction reads

$$\frac{\partial(\phi_l \rho_l^{true} \mathbf{v}_l)}{\partial t} + \operatorname{div}\left(\phi_l \rho_l^{true} \mathbf{v}_l \otimes \mathbf{v}_l\right) - \operatorname{div}\left(\phi_l(\ _l + \ ^{Re}_l)\right) = \tag{3.34}$$
$$+\phi_l \rho_l^{true} \mathbf{g} - A_{\Sigma_{gl}}\left(\dot{m}_l^{gl} \langle \mathbf{v}_l \rangle_{\Sigma_{sl}}^{\rho^{\Sigma}_{gl}} + \langle \ _g \cdot \mathbf{n} \rangle_{\Sigma_{gl}}\right) - A_{\Sigma_{sl}}\left(\dot{m}_l^{sl} \langle \mathbf{v}_l \rangle_{\Sigma_{gl}}^{\rho^{\Sigma}_{sl}} + \langle \ _s \cdot \mathbf{n} \rangle_{\Sigma_{sl}}\right).$$

In the sequel, we apply the partial mass balance for liquid (3.25a) and denote

$$\tilde{\ }_i \overset{def}{=} \frac{\ _i}{\rho_l^{true}}, \quad \tilde{\ }^{Re}_l \overset{def}{=} \frac{\ ^{Re}_l}{\rho_l^{true}}, \quad \tilde{\dot{m}}_l^{kl} \overset{def}{=} \frac{\dot{m}_l^{kl}}{\rho_l^{true}}. \tag{3.35}$$

Moreover, once the reactor operates in the steady state, the azeotrope ratio R^{FA}_{HO} may be considered as constant and the whole momentum balance may be divided by ρ_l^{true} obtaining

$$\phi_l \frac{\mathrm{d}\mathbf{v}_l}{\mathrm{d}t} - \phi_l \operatorname{div}\left(\tilde{\ }_{ls} + \tilde{\ }^{Re}_l\right) - \left(\tilde{\ }_{ls} + \tilde{\ }^{Re}_l\right) \nabla \phi_l = \phi_l \mathbf{g} \tag{3.36a}$$
$$-A_{\Sigma_{gl}} \tilde{\dot{m}}_l^{gl}\left(\langle \mathbf{v}_l \rangle_{\Sigma_{kl}}^{\rho^{\Sigma}_{gl}} - \mathbf{v}_l\right) - A_{\Sigma_{sl}} \tilde{\dot{m}}_l^{sl}\left(\langle \mathbf{v}_l \rangle_{\Sigma_{kl}}^{\rho^{\Sigma}_{sl}} - \mathbf{v}_l\right) \tag{3.36b}$$
$$-A_{\Sigma_{gl}} \langle \tilde{\ }_g \cdot \mathbf{n} \rangle_{\Sigma_{gl}} - A_{\Sigma_{sl}} \langle \tilde{\ }_s \cdot \mathbf{n} \rangle_{\Sigma_{sl}} \tag{3.36c}$$

Since our primary variables are the volume fractions, velocities and a (common) temperature, there are several terms which need to be identified, concretely, the Cauchy stress tensor $\ _l$, turbulent term $\tilde{\ }^{Re}_l$ and volume-gradient term $\left(\tilde{\ }_{ls} + \tilde{\ }^{Re}_l\right) \nabla \phi_l$; the interfacial velocity $\langle \mathbf{v}_l \rangle_{\Sigma_{kl}}^{\rho^{\Sigma}_{gl}}$; and the interfacial forces $A_{\Sigma_{gl}} \langle \tilde{\ }_g \cdot \mathbf{n} \rangle_{\Sigma_{gl}}$ and $A_{\Sigma_{sl}} \langle \tilde{\ }_s \cdot \mathbf{n} \rangle_{\Sigma_{sl}}$.

3.3.2 RANS turbulence closure & Cauchy stress tensor

RANS turbulence closure:

Although the system does not posses very large Reynolds numbers, the momentum equation is (by its averaging construction) in class of the Reynolds-averaged NavierâĂŞStokes (RANS) equations. From this reason, we need to specify the closure for the Reynolds stress tensor defined as

$$\tilde{\ }^{Re}_l \overset{def}{=} \mathbf{u}_l \otimes \mathbf{u}_l, \ \mathbf{u}_l = \langle \mathbf{v}_l \rangle - \mathbf{v}_l. \tag{3.37}$$

There is a great variety of turbulence model with a different complexity and computational demands, however, restricting on a turbulence in two-phase flow, the results are relatively sparse and most of them are adjustment of the standard $k - \varepsilon$ model proposed by Launder & Spalding, cf. [58]. The Boussinesq hypothesis, cf. [48, 5.3.5], applied on the Reynolds stress tensor, reads

$$\tilde{\ }^{Re}_l = -\mathbf{u}_l \otimes \mathbf{u}_l = 2\nu_t \ _l - \frac{2}{3} k_t \tag{3.38}$$

where ν_l denotes the turbulence eddy viscosity and $k_t = \frac{1}{2}\mathbf{u}_i\mathbf{u}_i$ the turbulence kinetic energy. The transport equations of the turbulent kinetic energy k_t and the turbulent dissipation ε_t, consequently, follows as

$$\partial_t k_t + \operatorname{div}\left(k\mathbf{v}_l - \frac{\nu_t}{\sigma_{k_t}}\nabla k_t\right) = 2\nu_t \ {}^{2}_{l} - \varepsilon_t \tag{3.39a}$$

$$\partial_t \varepsilon_t + \operatorname{div}\left(\varepsilon_t\mathbf{v}_l - \frac{\nu_t}{\sigma_\varepsilon}\nabla \varepsilon_t\right) = C_{1\varepsilon_t}\frac{\varepsilon_t}{k_t}2\nu_t \ {}^{2}_{l} - C_{2\varepsilon_t}\frac{\varepsilon_t^2}{k_t}S \tag{3.39b}$$

where the eddy viscosity is usually modelled as $\nu_t = C_{\nu_t}\frac{k_t^2}{\varepsilon_t}$ and the adjustable constants are chosen as

$$C_{\nu_t} = 0.09,\ \sigma_{k_t} = 1.00,\ \sigma_{\varepsilon_t} = 1.30,\ C_{1\varepsilon_t} = 1.44,\ C_{2\varepsilon_t} = 1.92.$$

Up to now, we have followed the standard single-phase $k-\varepsilon$ model. A generalization to a two-phase flow model was proposed by Elghobashi [29], Spalding [104], Schwarz & Turner, [89] or lately by Sokolichin [103] who proposed a single adjustment by including a term accounting the drift velocity:

$$\partial_t k_t + \operatorname{div}\left(k_t\mathbf{v}_l - \frac{\nu_t}{\sigma_{k_t}}\nabla k_t\right) = 2\nu_t \ {}^{2}_{l} - \varepsilon_t + C_{k_t}\phi_g\nabla p\,\mathbf{u}_{gl}^{slip} \tag{3.40a}$$

$$\partial_t \varepsilon_t + \operatorname{div}\left(\varepsilon_t\mathbf{v}_l - \frac{\nu_t}{\sigma_{\varepsilon_t}}\nabla \varepsilon_t\right) = C_{1\varepsilon_t}\frac{\varepsilon_t}{k_t}2\nu_t \ {}^{2}_{l} - C_{2\varepsilon_t}\frac{\varepsilon_t^2}{k_t} - C_{3\varepsilon_t}\frac{\varepsilon_t}{k_t}\phi_g\nabla p_l\,\mathbf{u}_{gl}^{slip} \tag{3.40b}$$

where $C_{k_t} = 0.505, C_{\varepsilon_t} = 0.74$ and the gas-liquid slip velocity includes the drift contribution (2.43).

Cauchy stress tensor:

To model the Cauchy stress tensor $\ {}_{l}$, we use the compressible Navier-Stokes ansatz

$$\ {}_{l} = -p_l \ + \lambda_l \operatorname{div}\mathbf{v}_l + 2\mu_l \ {}_{l}.$$

Here, $\ {}_{l}$ stays for the symmetric part of the velocity gradient, i.e. $\frac{1}{2}\left(\nabla\mathbf{v}_l + (\nabla\mathbf{v}_l)^T\right)$; λ_l denotes the bulk liquid viscosity and μ_l the dynamic liquid viscosity.

Moreover, we can employ the Stokes' hypothesis stating

$$2\mu_l + 3\lambda_l = 0$$

and reducing the Cauchy stress tensor into the form

$$\ {}_{l} = -p_l \ + \mu_l\left(2 \ {}_{l} - \frac{2}{3}\operatorname{div}\mathbf{v}_l \ \right).$$

Interpreting the influence of the solid particles by a replacement of the original liquid viscosity by packing-dependent viscosity of the suspension μ_{ls} (see (2.41)), together with the Boussinesq turbulence hypothesis (3.38), we end up with the relation

$$\ {}_{ls} + \ {}^{Re}_{l} = -p_l \ + (\mu_{ls} + \mu_t)\left(2 \ {}_{l} - \frac{2}{3}\operatorname{div}\mathbf{v}_l \ \right) - \frac{2}{3}\rho_l^{true}k_t \ . \tag{3.41}$$

3.3.3 Interfacial phenomena

Interfacial velocity The closure of the interfacial velocity will be done in several steps:

- Firstly, we recall the "stick" condition applicable in case of contaminated system (2.15)
$$\mathbf{v}_{l||} = \mathbf{v}_{gl_{||}} = \mathbf{v}_{g||} \text{ on } \Sigma_{gl}.$$
- Secondly, since the interface is considered as a very thin region with negligible mass, we may identify also normal components of liquid and gas velocity on the interface, thus,
$$\mathbf{v}_l = \mathbf{v}_g \text{ on } \Sigma_{gl}.$$
- Finally, once we neglect any internal flow within the bubble, the average over the surface equals average over volume, thus,
$$\langle \mathbf{v}_l \rangle_{\Sigma_{gl}} = \langle \mathbf{v}_g \rangle_{V_g} = \mathbf{v}_g.$$

Now, we have obtained the mass transfer force in the form

$$F_{\dot{m}} = A_{\Sigma_{gl}} \langle R^{\Sigma}_{gl} \rangle_{\Sigma_{gl}} (\mathbf{v}_l - \mathbf{v}_g).$$

Nevertheless, as we have shown in (2.4), the mass transfer force in this form may be considered as negligible in comparison with the drag force (acting in the same direction) and we omit this force in the sequel.

Solid-liquid interface:

The surface momentum balance for liquid interfaces, cf. (A.25b), (neglecting the gravitation) reads

$$\rho^{\Sigma}_{ls} \frac{\mathrm{d}^{\Sigma\Sigma} \mathbf{v}_{ls}}{\mathrm{d}t} = \mathrm{div}^{\Sigma\,\Sigma} \quad _{ls} + R^{\Sigma\Sigma}_{ls} \mathbf{v}_{ls} + [\![(\dot{\boldsymbol{m}}^{ls}_i \otimes \mathbf{v}_i + \quad _i) \cdot \mathbf{n}]\!]_{\Sigma_{ls}} \tag{3.42a}$$

$$\rho^{\Sigma}_{gl} \frac{\mathrm{d}^{\Sigma\Sigma} \mathbf{v}_{gl}}{\mathrm{d}t} = \mathrm{div}^{\Sigma\,\Sigma} \quad _{gl} + R^{\Sigma\Sigma}_{gl} \mathbf{v}_{gl} + [\![(\dot{\boldsymbol{m}}^{gl}_i \otimes \mathbf{v}_i + \quad _i) \cdot \mathbf{n}]\!]_{\Sigma_{gl}}. \tag{3.42b}$$

Since the dissolved gas is considered as a part of the liquid phase, we have no reaction neither any mass-transfer between the solid and liquid phase, i.e. $R^{\Sigma}_{ls} = 0$ and $m^{ls}_i = 0$. The no-slip condition and the fact that the *sl*-interface is a material interface reduces the equation (3.42a) into

$$[\![\quad _i \cdot \mathbf{n}]\!]_{\Sigma_{ls}} = 0. \tag{3.43}$$

Now, we focus on the interfacial forces $A_{\Sigma_{sl}} \langle \tilde{} \, _s \cdot \mathbf{n} \rangle_{\Sigma_{sl}}$ and $A_{\Sigma_{gl}} \langle \tilde{} \, _g \cdot \mathbf{n} \rangle_{\Sigma_{gl}}$. Expressed in the integral form, we firstly use the relation (3.43) and, consequently, split the stress tensor into the mean and fluctuating part. The mean part may be, furthermore, divided into averaged interfacial pressure part and averaged extra Cauchy stress part . The fluctuating part is commonly referred as the *sl*-interfacial interaction force $\mathbf{f}_{sl}$:

$$\begin{aligned} A_{\Sigma_{ls}} \langle \tilde{} \, _s \cdot \mathbf{n} \rangle_{\Sigma_{sl}} &= \frac{\Sigma_{ls}}{V} \frac{1}{\Sigma_{ls}} \int_{\Sigma_{ls}} \tilde{} \, _s \cdot \mathbf{n} \, \mathrm{dS} \overset{(3.43)}{=} \frac{1}{V} \int_{\Sigma_{ls}} \left(\langle \tilde{} \, _l \rangle_{\Sigma_{sl}} + \widehat{\tilde{} \, _l} \right) \cdot \mathbf{n} \, \mathrm{dS} \\ &= \langle \tilde{} \, _l \rangle_{\Sigma_{sl}} \frac{1}{V} \int_{\Sigma_{ls}} \mathbf{n} \, \mathrm{dS} + \mathbf{f}_{ls} = \Big(- \langle \tilde{p}_l \rangle_{\Sigma_{sl}} + \langle \tilde{} \, _l \rangle_{\Sigma_{sl}} \Big) \nabla \phi_s + \mathbf{f}_{ls}. \end{aligned}$$

Gas-liquid interface:

In case of the gas-liquid interface is the situation more complicated since the interface is non-material (due to a mass transfer). The interfacial velocity of interface ${}^{\Sigma}\mathbf{v}_{gl}$ does not need to be equal $\mathbf{v}_l$ resp. $\mathbf{v}_g$ at Σ_{gl}. However, in contaminated system the following holds

$$\langle {}^{\Sigma}\mathbf{v}_{gl}\rangle_{\Sigma_{gl}}^{\rho_{gl}^{\Sigma}} \approx \langle \mathbf{v}_g\rangle_{\Sigma_{gl}}^{\rho_{gl}^{\Sigma}}.$$

Consequently, we may reduce the equation (3.42b) into the form

$$\begin{aligned}\llbracket \quad _i \cdot \mathbf{n}\rrbracket_{\Sigma_{gl}} &= -\operatorname{div}^{\Sigma}{}^{\Sigma}{}_{gl} \\ &\overset{(A.19)}{=} \nabla^{\Sigma}\sigma_{gl} + 2H_{gl}\,\sigma_{gl}\mathbf{n}_i \approx \frac{2\sigma_{gl}}{r_g}\mathbf{n}_{gl}\end{aligned}$$

and for $\quad _g \cdot \mathbf{n} = \left(\quad _l + \frac{2\sigma_{gl}}{r_g} \right) \cdot \mathbf{n}$ we may proceed analogously to the sl-interface.

Denoting $\mathbf{f}_{gl}$ the gl-interfacial interaction force, we obtain

$$A_{\Sigma_{gl}}\langle \tilde{} _g \cdot \mathbf{n}\rangle_{\Sigma_{gl}} = \left(\langle -\tilde{p}_l\rangle_{\Sigma_{gl}} + \langle \tilde{} _l\rangle_{\Sigma_{gl}} + \langle \frac{2\tilde{\sigma}_{gl}}{r_g} \rangle_{\Sigma_{gl}}\right)\nabla\phi_g + \mathbf{f}_{gl} + \mathbf{f}_{\sigma_{gl}}$$

where

$$\mathbf{f}_{\sigma_{gl}} \overset{def}{=} \frac{1}{V}\int_{\Sigma_{gl}} \left(\frac{2\tilde{\sigma}_{gl}}{r_g} \right) \cdot \mathbf{n}\,\mathrm{dS}$$

is the Marangoni force. [10]

Volume-fraction-gradient forces:

Implementing the considerations from the previous section, we may write the momentum balance for the liquid phase in the following form:

$$\phi_l \frac{\mathrm{d}\mathbf{v}_l}{\mathrm{d}t} - \phi_l \operatorname{div}\left(\tilde{} _{ls} + \tilde{} _l^{Re}\right) = \phi_l \mathbf{g} \tag{3.44a}$$

$$-\tilde{p}_l\nabla\phi_l - \langle\tilde{p}_l\rangle_{\Sigma_{sl}}\nabla\phi_g - \langle\tilde{p}_l\rangle_{\Sigma_{gl}}\nabla\phi_s \tag{3.44b}$$

$$-\tilde{} _l\nabla\phi_l - \langle\tilde{} _l\rangle_{\Sigma_{sl}}\nabla\phi_g - \langle\tilde{} _l\rangle_{\Sigma_{gl}}\nabla\phi_s + \langle\frac{2\tilde{\sigma}_{gl}}{r_g}\rangle_{\Sigma_{gl}}\nabla\phi_g + \tilde{} _l^{Re}\nabla\phi_l. \tag{3.44c}$$

As we can see in (3.44b) and (3.44c), we have obtained terms dependent on the volume fraction gradients - usually referred as volume-fraction-gradient forces. These forces are commonly assumed to have negligible effects, however, we may proceed with a more benevolent assumption.

Let us consider an equality of the liquid pressure with the interfacial pressure in (3.44b) and we neglect the extra stress tensor, turbulent and surface tension part of the volume-fraction-gradient forces in (3.44c), i.e.

$$\tilde{p}_l \approx \langle\tilde{p}_l\rangle_{\Sigma_{sl}} \approx \langle\tilde{p}_l\rangle_{\Sigma_{gl}} \tag{3.45a}$$

$$\tilde{} _l\nabla\phi_l,\ \langle\tilde{} _l\rangle_{\Sigma_{sl}}\nabla\phi_s,\ \langle\tilde{} _l\rangle_{\Sigma_{gl}}\nabla\phi_g,\ \tilde{} _l^{Re}\nabla\phi_l,\ \langle\frac{2\tilde{\sigma}_{gl}}{r_g}\rangle_{\Sigma_{gl}}\nabla\phi_g \approx 0 \tag{3.45b}$$

Consequently, the volume-additivity constraint (3.32) implies

$$\tilde{p}_l\nabla\phi_l + \langle\tilde{p}_l\rangle_{\Sigma_{gl}}\nabla\phi_g + \langle\tilde{p}_l\rangle_{\Sigma_{sl}}\nabla\phi_s \approx -\tilde{p}_l\nabla(\overbrace{\phi_l + \phi_g + \phi_l}^{=1}) = 0. \tag{3.46}$$

[10] Due to the presence of surfactant, the Marangoni effect, caused by a surface tension gradient, occurs. However, the presence of viscous forces (significant at the small size scales) clearly surpasses this effect and we may neglect this force, i.e. $\mathbf{f}_{\sigma_{gl}} \approx 0$.

Interfacial-interaction forces:
As we have shown in section 2.3, the dominant part of $\mathbf{f}_{gl}$ and $\mathbf{f}_{ls}$ is the drag force balancing the buoyancy. Thus, we simply write

$$f_{gl} = f_{D_{gl}} + f_{B_{gl}}$$
$$f_{ls} = f_{D_{ls}} + f_{B_{ls}}.$$

Finally, we apply the Boussinesq approximation for isothermally incompressible fluids, cf. remark 2.2.1, and, together with the Krieger ansatz for viscosity of suspension, cf. (2.41), the reduced momentum balance system reads

$$\frac{\mathrm{d}\mathbf{v}_l}{\mathrm{d}t} - \operatorname{div}\left(\tilde{\ }^{dyn}_{ls} + \tilde{\ }^{Re}_{l}\right) = \alpha_l \Delta T \mathbf{g} + \frac{9}{2}\frac{\mu_{ls}}{r_s^2}\mathbf{v}_{ls}^{slip} + \frac{8}{3}\frac{C_D}{r_g}|\mathbf{v}_{gl}^{slip}|\mathbf{v}_{gl}^{slip}. \tag{3.47a}$$

3.4 Balance of energy

3.4.1 Balance of internal energy

Let us recall the local mass (A.21a) and momentum balance (A.25a) for the k-th phase:

$$\frac{\partial \rho_k}{\partial t} + \operatorname{div}(\rho_k \mathbf{v}_k) = R_k^V$$
$$\partial_t(\rho_k \mathbf{v}_k) + \operatorname{div}(\rho_k \mathbf{v}_k \otimes \mathbf{v}_k) = \operatorname{div} \quad _k + \rho_k \mathbf{b} + \rho_k R_k^V.$$

Generally, the balance of total energy of the k-th phase E_k yields

$$\partial_t(\rho_k E_k) + \operatorname{div}(\rho_k E_k \mathbf{v}_k) = \operatorname{div}(\quad _k \mathbf{v}_k + \mathbf{q}_k) + \rho_k \mathbf{b}_k \mathbf{v}_k + \rho_k r_k \tag{3.48}$$

where $\mathbf{b}_k$ stands for volume forces (gravitation in our case) and r_k is for the radiation which will be omitted in the sequel. [11]

In the next step, we split the total energy into the internal and kinetic part, i.e.

$$E_k \overset{def}{=} e_k + \frac{|\mathbf{v}_k|^2}{2}$$

and we reduce the total energy balance (3.48) by the momentum balance multiplied by $\frac{\mathbf{v}_k}{2}$. This results into the internal energy balance for k-th phase

$$\partial_t \rho_k e_k + \operatorname{div}(\rho_k \varepsilon_k \mathbf{v}_k) = \quad _k : \nabla \mathbf{v}_k + \operatorname{div} \mathbf{q}_k. \tag{3.49}$$

Now, we divide the stress tensor into the pressure and viscous part, $\quad _k \overset{def}{=} -p_k \quad + \quad _k$, obtaining

$$_k : \nabla \mathbf{v}_k = -p_k(\operatorname{div} \mathbf{v}) \quad + \quad _k : \nabla \mathbf{v}_k.$$

Nevertheless, the viscous part $\quad _k : \nabla \mathbf{v}_k$ will be omitted in the sequel.

[11] Generally speaking, the radiation is usually considerable for solid-gas interfaces only and its magnitude is commonly insignificant for surface temperatures lower than 300 °C, cf. Stephan-Boltzmann law in [60].

3.4.2 Balance of temperature

In this section we derive the balance of the common temperature. Although it is possible to derive it directly from the balance of internal energy assuming its dependency on the temperature only, we proceed the derivation via the balance of enthalpy assuming its dependency on temperature and pressure. This approach is favourable from two perspectives. Firstly, we directly obtain the heat capacity at constant pressure as $C_p \overset{def}{=} \frac{\partial h}{\partial T}$ which is more convenient (to measure) than the heat capacity at constant volume defined as $C_v \overset{def}{=} \frac{\partial e}{\partial T}$. Secondly, tabulated values of the heat of reaction correspond to the change in enthalpy rather than the change in internal energy.

Defining the enthalpy of k-th phase as

$$h_k = e_k + \frac{p_k}{\rho_k}, \tag{3.50}$$

we may write its balance, in the absence of radiation, as

$$\partial_t(\rho_k h_k) + \operatorname{div}(\rho_k h_k \mathbf{v}_k) - \frac{\mathrm{d}p_k}{\mathrm{d}t} = \operatorname{div} \mathbf{q}_k. \tag{3.51}$$

Applying the mass balance we conclude

$$\rho_k \frac{\mathrm{d}h_k}{\mathrm{d}t} = \operatorname{div} \mathbf{q}_k + R_k^V h_k + \frac{\mathrm{d}p_k}{\mathrm{d}t}. \tag{3.52}$$

Now, we consider the liquid enthalpy being function of (common) temperature and liquid pressure, i.e. $h_k = h_k(T, p_k)$. In a more general setting, one would consider also dependencies on partial densities since the liquid phase is a mixture of several constituents. However, once the azeotrope is formed, the mutual concentrations remain the same and we can omit their mutual dependencies. Thus, the total differential of the liquid enthalpy follows

$$\mathrm{d}h_l(T, p_l) = \left(\frac{\partial h_l}{\partial T}\right)_{p_k} \mathrm{d}T + \left(\frac{\partial h_l}{\partial p_l}\right)_{T} \mathrm{d}p_l \tag{3.53}$$

Recalling the second law of thermodynamic in terms of specific enthalpy, i.e.

$$\mathrm{d}h_l = \left(\frac{1}{\rho_l}\right) \mathrm{d}p_l + T\,\mathrm{d}s_l, \tag{3.54}$$

yields

$$\frac{\partial h_l}{\partial p_l} = \frac{1}{\rho_l} + T\left(\frac{\partial s_l}{\partial p_l}\right) = \frac{1}{\rho_k} - T\left(\frac{\partial \frac{1}{\rho_k}}{\partial T}\right)_{p_k,\rho_k}. \tag{3.55}$$

Here, we have used the Maxwell relations to switch second partial derivatives in the second equation, cf. [53] or [48, p. 54]. Together with (3.53), we obtain

$$\frac{\mathrm{d}h_k(T, p_k)}{\mathrm{d}t} = C_{p_k} \frac{\mathrm{d}T_k}{\mathrm{d}t} + \left(\frac{1}{\rho_k} - T\left(\frac{\partial \frac{1}{\rho_k}}{\partial T}\right)_{p_k,\rho_k}\right) \frac{\mathrm{d}p_k}{\mathrm{d}t}.$$

Employing this relation into the enthalpy balance results into

$$\rho_k C_{p_k} \frac{\mathrm{d}T_k}{\mathrm{d}t} = \operatorname{div} \mathbf{q}_k - \frac{T_k}{\rho_k}\left(\frac{\partial \rho_k}{\partial T_k}\right)_{p_k,\rho_k} \frac{\mathrm{d}p_k}{\mathrm{d}t}.$$

Furthermore, since the Boussinesq approximation for isothermally incompressible fluids is used, we neglect the thermal expansion contribution $\frac{\partial \rho_k}{\partial T_k}$ in the sequel.

By the averaging of the equation assuming a constant liquid density ρ_l^{true} and heat capacity C_{p_l}, we obtain

$$\phi_l \rho_l^{true} C_{p_l} \left(\frac{\mathrm{d}\langle T_l \rangle_{V_l}}{\mathrm{d}t} + \langle \widehat{\mathbf{v}}_l \cdot \nabla \widehat{T}_l \rangle_{V_k} \right) = \phi_l \operatorname{div} \langle \mathbf{q}_l \rangle_{V_l} + \langle \mathbf{q}_l \rangle_{V_l} \nabla \phi_l - A_{\Sigma_{gl}} \langle \dot{m}_l^{gl} h_l^{gl} + \mathbf{q}_l \cdot \mathbf{n} \rangle_{\Sigma_{gl}} - A_{\Sigma_{sl}} \langle \dot{m}_l^{sl} h_l^{sl} + \mathbf{q}_l \cdot \mathbf{n} \rangle_{\Sigma_{sl}} \tag{3.56}$$

where $\dot{h}_l^{gl}$ stands for enthalpy exchange via kl-interface.

Unlike in the momentum balance where the liquid species share one velocity field $\mathbf{v}_l$ and the gaseous species $\mathbf{v}_g$, here, we can not use similar argumentation for partial enthalpies. Therefore, we prefer to write the liquid enthalpy change on the gas-liquid and solid-liquid interface in the general form as

$$\dot{h}_l^{gl} = \sum_i \dot{m}_i^{gl} h_i, \ i \in \{FA, H_2O, H_2, CO_2\}$$
$$\dot{h}_l^{sl} = \sum_i \dot{m}_i^{sl} h_i, \ i \in \{FA, H_2, CO_2\}.$$

As the next step, we neglect the temperature deviation within the averaging volume, i.e. $\widehat{T}_l \approx 0$, [12] and we model the heat flux by standard Fourrier's constitutive relation [48, 5.3.4] :

$$\mathbf{q}_l \approx -\rho_l^{true} k_l \nabla T_l \tag{3.57}$$

where $k_l[\frac{\mathrm{W}}{\mathrm{m \cdot K}}]$ is the conductivity of the liquid phase. As a consequence, the heat fluxes via the interfaces are zero, i.e. $\langle \mathbf{q}_l \cdot \mathbf{n} \rangle_{\Sigma_{gl}} = \langle \mathbf{q}_l \cdot \mathbf{n} \rangle_{\Sigma_{sl}} = 0$.

Furthermore, we consider the composition (molar concentration) of the phases being constant, cf. assumption (3.2.2), and we may identify the jump in the enthalpy of reaction with the enthalpy of the mass-transfer:

$$\langle \dot{m}_l^{ls} h_l \rangle_{\Sigma_{sl}} \approx \langle R_{sl}^{\Sigma} \rangle_{\Sigma_{sl}} \Delta h_r$$
$$\langle \dot{m}_l^{gl} h_l \rangle_{\Sigma_{gl}} \approx \dot{m}_{gl} \Big(\underbrace{\left(h_{H_2O}^{vap} + R_{H_20}^{FA} h_{FA}^{vap} \right) \phi_{H_2 0_{(l)}}^{in} + \left(1 + \tfrac{M_{CO_2}}{M_{H_2}} \right) h_{H_2}^{sln}}_{h^{vap}} \Big).$$

Here, we denoted $\Delta h_r[\frac{\mathrm{kJ}}{\mathrm{kg}}] = \frac{H_f}{M_{FA}}$ the enthalpy of reaction; $h_{vap}[\frac{\mathrm{kJ}}{\mathrm{kg}}]$ the enthalpy of vaporization; $h_{sln}[\frac{\mathrm{kJ}}{\mathrm{kg}}]$ the enthalpy of solution; and $\langle R_{sl}^{\Sigma} \rangle_{\Sigma_{sl}}[\frac{\mathrm{kJ}}{\mathrm{kg}}] = \rho_l^{true} A \, e^{\frac{-E_a}{RT}} R_{H_20}^{FA} \phi_l \phi_s$ represents the reaction rate. Consequently, we may write the heat balance of the liquid phase in the form

$$C_{p_l} \frac{\mathrm{d}T_l}{\mathrm{d}t} - \operatorname{div}\left(k_l \nabla T_l \right) = \dot{m}_{gl} h_{vap} + \langle R_{sl}^{\Sigma} \rangle_{\Sigma_{sl}} \Delta h_r. \tag{3.58}$$

Remarks

3.4.1 Enthalpy of solution. *Since the reaction and mass transfer between the phases occurs at different places, we need to distinguish also the corresponding enthalpies. To*

[12] Let us mention, that employing of the temperature deviation within the control volume would lead to requirement of an additional closure for the term $\langle \widehat{\mathbf{v}}_l \cdot \nabla \widehat{T}_l \rangle_{V_k}$, i.e. a temperature-turbulent model, cf. [57].

understand the mechanism properly, we recall the decarboxylation of formic acid in the following general form

$$\underbrace{HCOOH_{(l)} \xrightarrow{\Delta H_{ad}} HCOOH^{*}}_{adsorption} \overbrace{\xrightarrow{\Delta H_r} \underbrace{H_2^{*} + CO_2^{*} \xrightarrow{\Delta H_{de}} H_{2(d)} + CO_{2(d)}}_{desorption}}^{chemical\ reaction} \overbrace{\xrightarrow{\Delta H_{sln}} H_{2(g)} + CO_{2(g)}}^{solution}$$

where we denote ΔH_{ad} the enthalpy of adsorption; ΔH_r the enthalpy of reaction; ΔH_{ad} the enthalpy of desorption; and ΔH_{sln} the enthalpy of solution. The change in the enthalpy of formation, consequently, equals

$$\Delta H_f = \Delta H_{ad} + \Delta H_r + \Delta H_{de} + \Delta H_{sln}.$$

First three transformations (adsorption, reaction, desorption) take a place on the surface of solid particles and may be WLOG substitute by a single transformation process, however, the last one proceeds on the bubble interfaces and need to the treated independently.

To estimate the enthalpy of solution, we employ the results of Carrol et al. [16] approximating the enthalpy of solution via the Henry constant. For the enthalpy of solution of carbon dioxide dissolved in water, they induce the relation

$$\Delta H_{sln}(T)[kJ/mol] \approx 106.56 - 6.2634 \cdot 10^4/T + 7.475 \cdot 10^6/T^2.$$

Expressing the enthalpy of solution graphically, cf. fig. (3.2)*, we may see, that its magnitude tends towards the zero-value at the temperature* $\sim 148\,^{\circ}\mathrm{C}$.

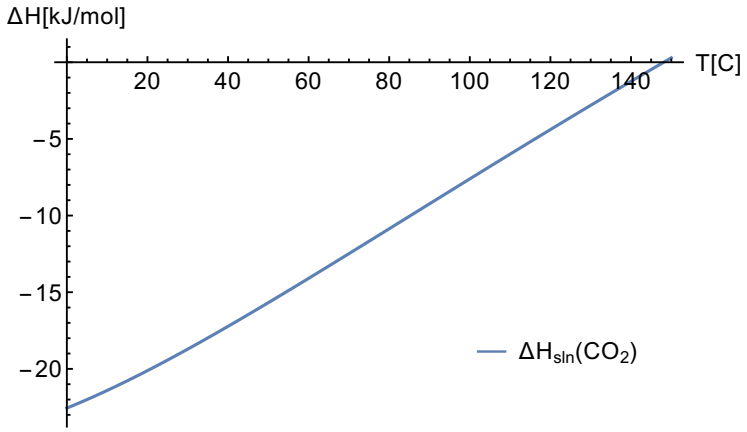

Figure 3.2: Enthalpy of dissolution for carbon dioxide.

Unfortunately, as far as the author knows, similar data are publicly not available for hydrogen solution. However, since the reactor operates at the temperature around 100 *℃, we neglect the enthalpy of solution for carbon dioxide as well as for hydrogen and identify the enthalpy of reaction with the change in enthalpy of formation, i.e.*

$$\Delta H_{sln} \approx 0 \quad \& \quad \Delta H_r \overset{def}{=} \Delta H_f \approx 32.9\,\mathrm{kJ/mol}$$

3.5 Summary of the model

Let us recall a summary of the model of three-phase flow fluidized bed reactor. We search for volume fractions ϕ_l, ϕ_g, ϕ_s; partial (averaged) velocities $\mathbf{v}_l, \mathbf{v}_g, \mathbf{v}_s$; common (averaged) dynamic pressure p_l^{dyn}; liquid temperature T_l and turbulent variables k_t and ε_t such that

$$\operatorname{div}(\phi_l \mathbf{v}_l + \phi_g \overline{\mathbf{v}}_g + \phi_s \mathbf{v}_s) = 0 \tag{3.59a}$$

$$\partial_t \phi_g + \operatorname{div}(\phi_g \overline{\mathbf{v}}_g) = \frac{\dot{m}_{gl}}{\rho_{FA}^{true}} \tag{3.59b}$$

$$\partial_t \phi_s + \operatorname{div}(\phi_s \mathbf{v}_s) = \operatorname{div}\left(\frac{\rho_s^{true}}{\rho_l^{true}} \mu_l^t \nabla \phi_s\right) \tag{3.59c}$$

$$\phi_l \frac{\mathrm{d}\mathbf{v}_l}{\mathrm{d}t} - \phi_l \operatorname{div}\left(\tilde{}_{ls}^{dyn} + \tilde{}_{l}^{Re}\right) = \phi_l \alpha_l \Delta T\, \mathbf{g} + \phi_s \frac{\rho_l - \rho_s}{\rho_l} + \phi_g \mathbf{g} \tag{3.59d}$$

$$\frac{3}{8} C_D \frac{|\mathbf{v}_{gl}^{slip}|}{r_g} \mathbf{v}_{gl}^{slip} = -\mathbf{g} \tag{3.59e}$$

$$\frac{9}{2} \frac{\nu_l}{r_s^2} \mathbf{v}_{ls}^{slip} = -\frac{\rho_l^{true} - \rho_s^{true}}{\rho_l^{true}} \mathbf{g} \tag{3.59f}$$

$$\partial_t(\rho_l^{true} k_t) + \operatorname{div}\left(\rho_l^{true} k \mathbf{v}_l - \frac{\mu_t}{\sigma_{k_t}} \nabla k_t\right) = 2\mu_t \; {}_l^2 - \rho_l^{true} \varepsilon_t + C_{k_t} \phi_g \nabla p_l^{dyn}\, \mathbf{u}_{gl}^{slip} \tag{3.59g}$$

$$\partial_t(\rho_l^{true} \varepsilon_t) + \operatorname{div}\left(\rho_l^{true} \varepsilon_t \mathbf{v}_l - \frac{\mu_t}{\sigma_\varepsilon} \nabla \varepsilon_t\right) = C_{1\varepsilon_t} \frac{\varepsilon_t}{k_t} 2\mu_t \; {}_l^2 - C_{2\varepsilon_t} \rho_l^{true} \frac{\varepsilon_t^2}{k_t} \tag{3.59h}$$

$$- C_{3\varepsilon_t} \frac{\varepsilon_t}{k_t} \phi_g \nabla p_l^{dyn}\, \mathbf{u}_{gl}^{slip} \tag{3.59i}$$

$$C_{p_l} \frac{\mathrm{d}T_l}{\mathrm{d}t} - \operatorname{div}(k_l \nabla T_l) = \dot{m}_{gl} h_{vap} + \langle R_{sl}^{\Sigma} \rangle_{\Sigma_{sl}} \Delta h_r. \tag{3.59j}$$

where $\mathbf{v}_{gl}^{slip} = \mathbf{v}_g - \mathbf{v}_l$, $\mathbf{v}_{ls}^{slip} = \mathbf{v}_s - \mathbf{v}_l$, $\overline{\mathbf{v}}_g = \overline{\mathbf{v}}_{gl}^{slip} + \mathbf{v}_l$, $\mathbf{u}_{gl}^{slip} = \langle \mathbf{v}_{gl}^{slip} \rangle - \mathbf{v}_{gl}^{slip}$ and

$$1 = \phi_l + \phi_g + \phi_s$$

$$\dot{m}_{gl} = \frac{\bar{A}_{\Sigma_{gl}}}{\langle \bar{A}_{\Sigma_{gl}} \rangle_{V_r}} \left(\left(1 + R_{H_20}^{FA}\right) \phi_{H_20_{(l)}}^{in} + 1\right) \langle \langle R_{sl}^{\Sigma} \rangle_{\Sigma_{sl}} \rangle_{V_r}$$

$$A_{\Sigma_{gl}} = 4\pi r_g^2(\tau),\; r_g(\tau) = k_{gl}^{\rho_g} \tau + r_0,\; \bar{f} = \frac{1}{|t_r|} \int_0^t f \,\mathrm{d}\tau,\; \langle f \rangle_{V_r} = \frac{1}{|V_r|} \int_{V_r} f \,\mathrm{d}V$$

$$\tilde{}_{ls}^{dyn} + \tilde{}_{l}^{Re} = -p_l^{dyn} \; + (\nu_{ls} + \nu_t) \left(2 \; {}_l - \frac{2}{3} \operatorname{div} \mathbf{v}_l \right) - \frac{2}{3} k_t$$

$$\nu_{ls} = \nu_l \left(1 - \frac{\phi_s/(\phi_l + \phi_s)}{\phi_{max}}\right)^{-2.5\phi_{max}},\; \phi_{max} = 0.64;\; \nu_l(T) = \nu_l^0 e^{\frac{E_a^\nu}{RT}}$$

$$C_D = \max\left\{\frac{24}{Re_p}\left(1 + 0.15 Re_p^{0.687}\right), \frac{8}{3} \frac{E\ddot{o}}{E\ddot{o} + 4}\right\}$$

$$\langle R_{sl}^{\Sigma} \rangle_{\Sigma_{sl}} = \rho_l^{true} A\, e^{\frac{-E_a}{RT}} R_{H_20}^{FA} \phi_l \phi_s,\; h_{vap} = \left(h_{vap}^{H_2O} + R_{H_20}^{FA} h_{vap}^{FA}\right) \phi_{H_20_{(l)}}^{in},$$

$$C_{\mu_t} = 0.09,\; C_{1\varepsilon_t} = 1.44,\; C_{2\varepsilon_t} = 1.92,\; C_{k_t} = 0.505,\; C_{\varepsilon_t} = 0.74,\; \sigma_{k_t} = 1.00,\; \sigma_{\varepsilon_t} = 1.30.$$

4. CFD simulation and analysis

In the last chapter of the first part the basic features of the numerical implementation, results and their analysis is given. After a brief introduction of the used numerical software and parameter fitting, a test simulation on a 2D-axially symmetric geometry is provided together with basic mesh and time stepping sensitivity. Furthermore, results of the lab-scale reactor, its verification and, finally, a suggestion for possible optimization and up-scale of the reactor are discussed.

4.1 Numerics

4.1.1 Software

Wolfram Mathematica:
In the case of BBO equation (2.5), we investigate the acting forces on a single particle in still liquid with later employment of the collective effects. As a consequence, the equations of motion reduce form PDEs to ODEs which can be conveniently solved (numerically or symbolically) in Wolfram Mathematica software. The numerical solution is obtained by a default method which is of 5^{th} order explicit Runge-Kutta method (Bogacki and Shampine 5(4) pair), see [9].

Comsol Multiphysics:
The final model (3.59) was implemented in Comsol Multiphysics software. It is a complex commercial software for solving multi-physics problem using finite element method (FEM) discretization. It includes automatized pre-processing (meshing) as well as fine post-processing. The main advantage of the software is simple user-friendly GUI with many predefined "physics interfaces". These are GUIs oriented on the particular problems (e.g. Fluid Flow, Heat Transfer, AC/DC, ...) which significantly simplify the model implementation.

Despite the fact that Comsol Multiphysics is commercial software, it allows to implement the weak formulation of PDE, thus, the robustness in solving variety of different problems is ensured.

4.1.2 Integro-differential equations

In the system (3.59), we need to treat integro-differential equations in the case of mass balance (integral term m_{gl}) and momentum balance (integral term $\mathbf{v}_{gl}^{slip}$). However, solving such a problem numerically is very complicated and we would like to avoid it by suitable approximations of the integrals.

The gas-liquid slip velocity $\mathbf{v}_{gl}^{slip}$ has the vertical component only, thus, we may approximate it by a z-variable function. Choosing the basis of the approximation-function as $\{1, \sqrt{z}, z\}$, we obtain the result

$$\mathbf{v}_{gl}^{slip} = \frac{1}{|t_r|}\int_0^t \sqrt{\frac{8}{3}\frac{r_g(\tau)|\mathbf{g}|}{C_D(\tau)}}\,\mathrm{d}\tau\,\mathbf{e}_z \approx (0.0117 + 0.446\sqrt{z} - 0.195z)\,\mathbf{e}_z \tag{4.1}$$

The results of the approximation are depicted in the Figure (4.1).

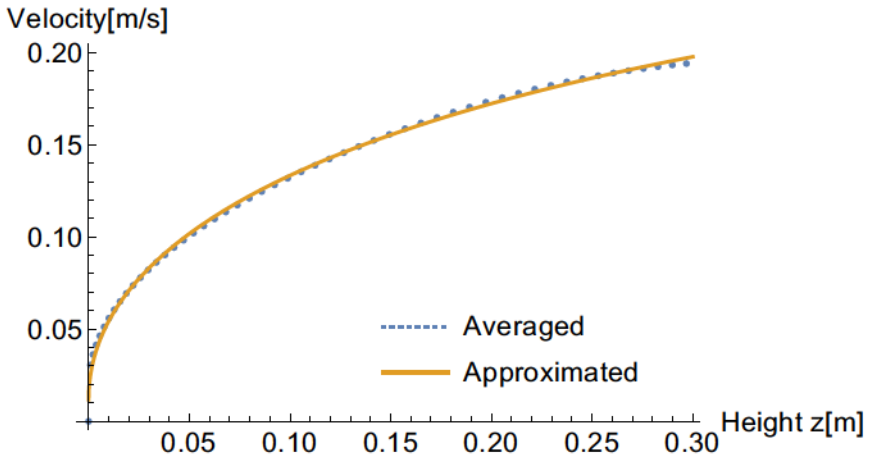

Figure 4.1: The approximation of the gas-liquid slip velocity.

Similarly to the previous, we treat also the bubble interfacial area $\bar{A}_{\Sigma_{gl}}$. Here, we again exploit the fact that the area is changing in the vertical direction only. Choosing the basis of the approximation-function as $\{1, z, z^2\}$ we obtain

$$\bar{A}_{\Sigma_{gl}} = \frac{1}{|t_r|}\int_0^t 4\pi r_g^2(\tau)\,\mathrm{d}\tau,\ r_g(\tau) = k_{gl}^{\rho_g}\,\tau + r_0 \approx (3.15z + 2.44z^2)\cdot 10^{-5}\,\mathbf{e}_z\,[\mathrm{m}^2]$$

or, expressed graphically in fig. (4.2):

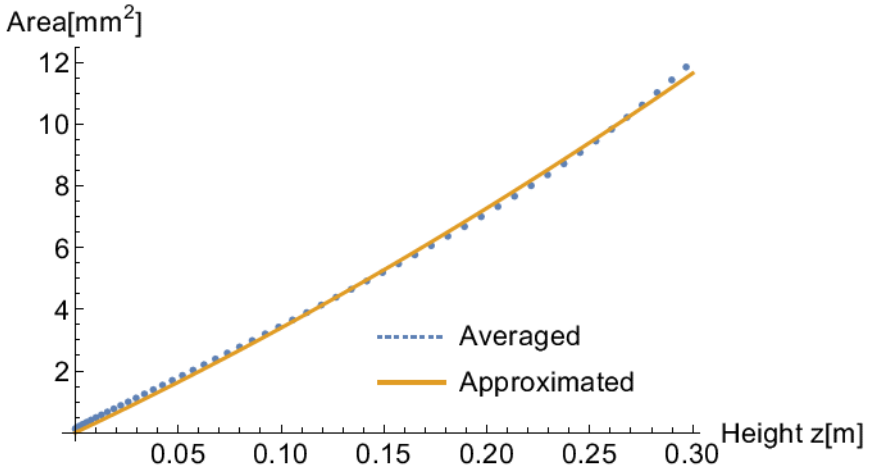

Figure 4.2: The Approximation of the gas-liquid interfacial area.

4.1.3 Fitting of the kinetic parameters

One of the most important parameters of the model are the chemical-kinetic parameters, namely the frequency factor A and the activation energy E_a. Generally speaking, these data are specific for each application and practically impossible to find in the literature for none but the ideal-gas setting.

Since the temperature in the reactor is not uniform and the reaction rate changes rapidly following the Arrhenius kinetics (3.30), we need to approximate the averaged [1]

[1] Averaged with respect to the exponential dependency.

temperature as accurate as possible. To do so, we may use the measured temperature in the middle of the reactor T_r^{meas} and the overall reactor production.

In the first step, we simply calculate the kinetic parameters from the measured temperature and the reactor production (assuming the steady state and the uniform temperature profile). In the second step, we proceed the simulation of the reactor with the derived kinetic parameters and we fit the reactor boundary conditions [2] in such a way that the modelled reactor production corresponds to the measured production. Consequently, we can calculate the weighted temperature average T_{av} from which we derive the corrected kinetic parameters.

The whole procedure is an iterative process and can be repeated. However, the difference between the zeroth iteration (measured values) and the first iteration (corrected values) is less than 10 % for $T_r < 105\,^{\circ}\mathrm{C}$ and, with respect to the measurement error, we take the first iteration as the sufficient approximation (Figure (4.3) and Table (4.1).

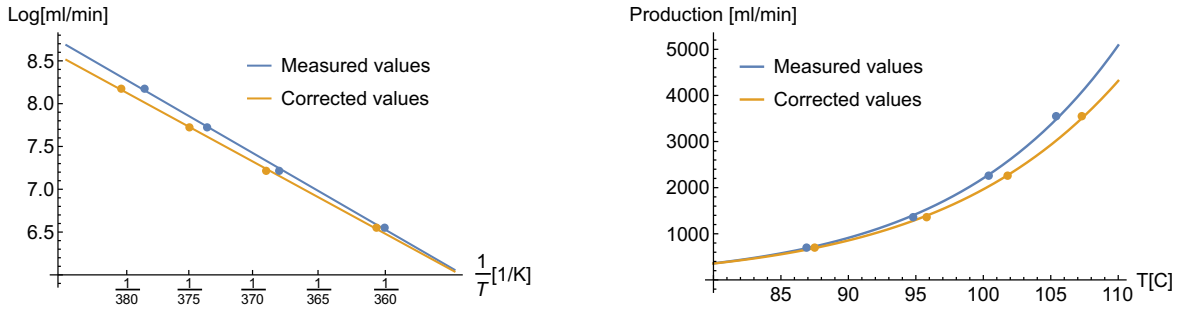

Figure 4.3: The measured and corrected kinetic parameters comparison. Left: the logarithmic Arrhenius plot. Right: The Arrhenius exponential response of the reaction rate on the temperature.

Iteration	$A\,[1/\mathrm{s}]$	$E_a\,[\mathrm{kJ/mol}]$
0-th:	$9.05 \cdot 10^{10}$	99.4
1-st:	$1.25 \cdot 10^{10}$	93.6

Table 4.1: The estimated kinetic parameters for the zero-th first approximation.

Remarks

4.1.1 Long-time solution. *The reactor is supposed to supply a relatively constant amount of hydrogen after an intermediate start-up (several minutes). This condition mostly determines the sought solution which we designate as the long-time solution. Once the system is stable and posses a unique steady solution, the long-time solution tends to it. In our case, the long-time solution is characterised by the following restrictions:*

The hydrogen production is stable over sufficiently long period (e.g. deviation less that 5% *within last* 100 s*) as well as the temperature profile (deviation of the averaged reactor temperature is less than* 0.1℃ *within the last* 100 s*).*

[2] Here, we have used a simplified assumption of uniform boundary-temperature.

4.2 Test simulation

4.2.1 The setting

To verify the consistency of the numerical simulations, we firstly proceed the simulation on a simple (2D axial) geometry, see the Figure (4.4), with consequent analysis of the mesh-convergence, time-stepping and discretization.

The axially symmetric geometry consists of a cylinder with radius 35 mm and height 300 mm. The inlet of the liquid is in the middle of the bottom-plate (a tube with radius 2 mm) and the gaseous outlet is situated on the top of the reactor. The reactor (heated) walls are assumed to have a constant temperature.

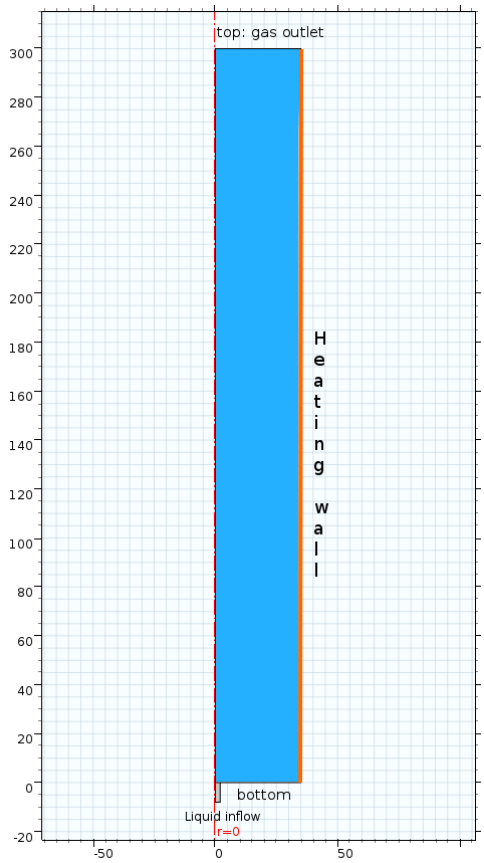

Figure 4.4: The geometry of the 2D-axially symmetric reactor [mm].

4.2.2 Numerical setting

Mesh:
The meshing algorithm of Comsol Multiphysics is based on the Delaunay triangulation [59] and recently also on its advancing front version [61]. It uses triangle/tetrahedral elements together with optional boundary quadrilateral/hexahedral elements. Comsol Multiphysics allows several possible mesh-adaptivity algorithms. In our case, we use a simple a priory adaptivity method based on the mathematical nature of the equation system. It creates a triangle mesh inside of the domain and a boundary layer consists of several layers of narrow quadrilateral/hexahedral elements near the boundary. The use of boundary layer,

Mesh	DOF	CPU [s]	[kg/s]·10^{-4}	In/Out error [%]
UN40	52 979	1 065	1.219	1.23
UN80	359 760	11 606	1.226	0.98
UN120	850 080	31 915	1.227	0.81
S80	1 252 253	52 144	1.116	7.53
S120	3 459 079	146 422	1.224	0.98

Table 4.2: The table of the corresponding DOFs (degrees of freedom), CPU time, reactor production and relative error between inflow and outflow for different mesh-setting.

cf. fig. (4.5) is very favourable to the problems with significant (e.g. velocity or temperature) gradients near the boundary and it is convenient also for the proper simulation of a turbulent flow which use a boundary wall-function requiring very fine mesh-resolution in perpendicular-to-boundary direction.

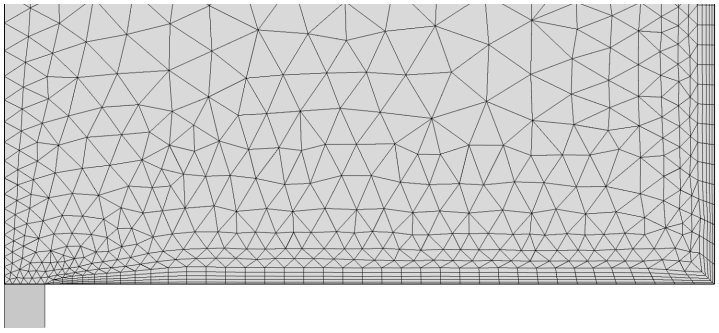

Figure 4.5: Detail of the adaptive mesh (UN1) with a boundary layer. Axially symmetric geometry - bottom with the liquid inflow (left).

To investigate the quality of the mesh and its convergence (resp. mesh-size independence), we have chosen several meshes with various refinements. As the decisive value we take the reactor production and inflow/outflow mass flow error ($t_{fin} = 1000\,\mathrm{s}$).

This was tested on several structured (Sx) and unstructured (UNx) meshes distinguished according to number of elements on the bottom plate of the geometry. The results, depicted in table (4.2), reflect the requirements of very fine mesh resolution or use of boundary layer. The structured meshes need very fine resolution (S120) to obtain a results with error less than 1 % leading to significant CPU demands. On the other hand, unstructured mesh refined on the boundary leads to enough precise solution with relatively coarse refinement (UN80) and small CPU demands.

Taking into account relatively significant error of the model parameters, we consider as the sufficiently good mesh results the UN80 mesh-setting which will serve as the decisive setting for further investigation.

Choice of the FEM elements and solvers:
All computations were proceed with the default Comsol combination of the FEM elements, namely linear P1 elements for pressure and velocity of the liquid, P1 elements for temperature and P1 elements for solid-particle concentrations. Although the P1/P1 combination of velocity/pressure elements to solve the NS equation does not a priori satisfy the Babuška-Brezzi inf-sub condition, Comsol uses streamline stabilization (diffusion) to circumvent the

condition and provide fast solution of the problem. For more details we refer to [44]. To validate the correctness of P1/P1 elements we performed also the computation using P2/P1 elements as well - obtaining very similar results but with much higher CPU demands.

The (non-symmetric) matrix system obtained by the FEM-discretization is consequently solved by segregated combination of three MUMPS solvers for velocity (coupled) with pressure, temperature, solid concentration and two PARDISO solvers for gas concentration and turbulent variables (energy dissipation and rate of the dissipation). Both MUMPS and PARDISO implement direct solvers for general sparse matrices. Optional Krylov subspace methods (CG, BiCG) are available as well. For more details, we refer to [2] and [87].

Adaptive time stepping
Comsol Multiphysics uses backward differential formula of the first and second order (BDF1 and BDF2). The step-size is adaptive by default using as the decisive criteria a magnitude of the CFL and Von Neumann number, cf. [47]. We have proceed several tests regarding the accuracy of the time-stepping (with limited or uniform time stepping) with negligible deviance from the default (fast) adaptive setting. Therefore, we remain the default adaptive time-stepping also in the further computations.

4.2.3 Comsol implementation specifications

The implementation of the problem in COMSOL Multiphysics is not so straightforward and, therefore, we present the essential setting options necessary for successful computation. To begin with, additionally to the streamline diffusion, we need to incorporate also an isotropic diffusion for the NS-equation. Depending on the magnitude of convective field $\|\mathbf{v}_l\|$ and the mesh-element size h, both of the stabilizations add the additional artificial diffusion expressed by the diffusion coefficient $c_{art} = (\delta_{is} + \delta_{st})h\|\mathbf{v}_l\|$.

As we can see, the magnitude of these stabilizations depends on the mesh size and in the case of isotropic diffusion it may be even omitted once we sufficiently increase the mesh resolution. Nevertheless, in the case of 3D computation, a finer mesh resolution may easily lead to unaffordable numerical requirements.

Beside the stabilizations, we need to use also a start-up (ramp) function for better convergence. These functions are typically a ramp function defined as

$$rm(t) = \begin{cases} 0, \ t \leq 0 \\ \frac{t}{\alpha}, \ t \in (0, \alpha) \\ 1, \ t \geq \alpha \end{cases}$$

and we use them to start-up the mass transfer term m_{gl}, reaction rate term R_{sl}^{Σ} and boundary conditions for temperature.

4.2.4 Test reactor results

In this section, we present the result of the final equation-system (3.59) together with the BC and IC conditions from section 4.2.1. Investigating four profiles (velocity, temperature, volume fraction of the gas and volume fraction of the catalytic particles), we illustrate the result in the revolved 2D geometry in the Figure (4.6)

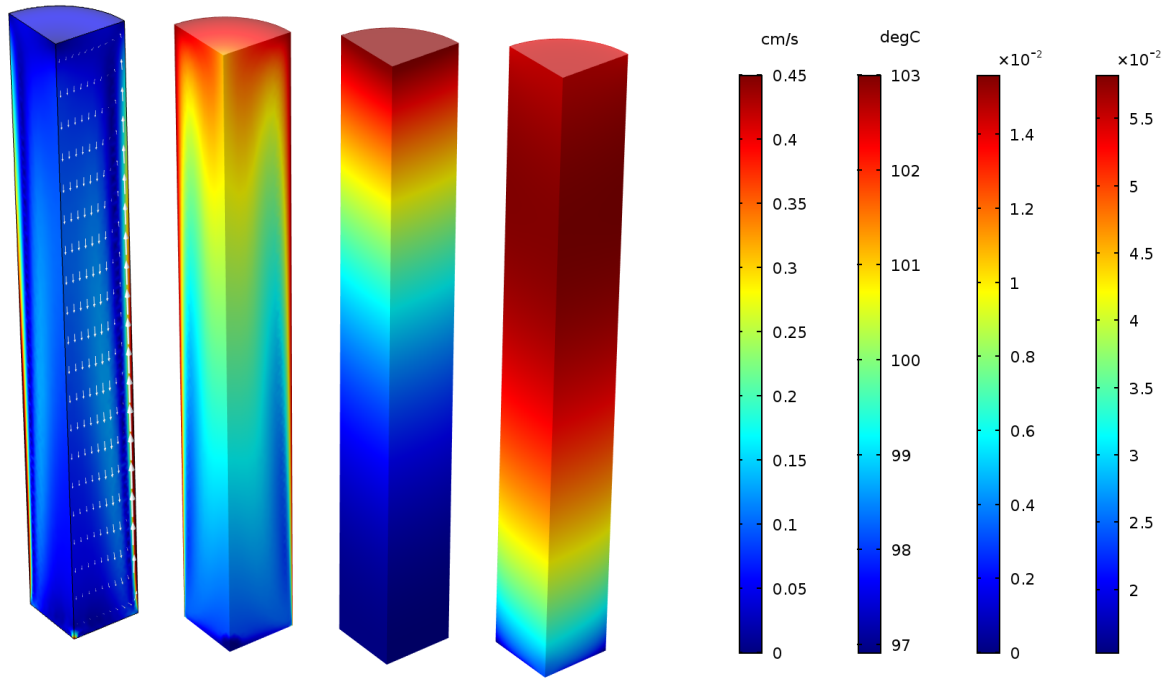

Figure 4.6: From left: velocity magnitude profile $\|\mathbf{v}\|$[cm/s] with velocity arrow field; temperature profile T[℃]; gas volume fraction ϕ_g[1] and solid volume fraction ϕ_s[1].

As we can see on the first (from left) profile, the flow is driven by the thermal convection when the hotter (lighter) fluid ascents around the heated wall with the velocity magnitude around 0.4 cm/s. Once it cools down, it descents via the middle of the reactor with a slightly lower magnitude around 0.1 cm/s.

The second picture depicts the temperature profile. It posses the maximum temperature on the heated wall (103 ℃) and the top of the reactor (101 ℃). The colder spots of the reactor lies in the lower half of the reactor and at the flow-stagnation-regions placed cca 1 cm from the wall where the ascending and descending forces cancel-out each other which results in a zero-velocity field.

The next profile describes the volume fraction of the gas. As one would expect, it has increasing tendency with the heigh of the reactor and the maximum value (around 1.5 %) on the top of the reactor. Let us mention that somehow higher gas hold-up would lead to two unwanted effects. Firstly, the whole volume of the gas-liquid-solid mixture would expand due to the higher gas concentration resulting into volumetrically less efficient system. Secondly, we may experience a formation of slug flow in the higher parts of the reactor which may cause unwanted spitting (splashing) of the liquid and pressure oscillation.

Finally, in the last (fourth) picture we can see the concentration of the solid (catalytic) particles. In this regime, the particles flow more or less in well mixed regime without any unwanted aggregation of the particles. The a priori density of the solid catalytic particles is chosen 10 $\frac{\text{kg}}{\text{m}^3}$ lighter than the surrounding fluid, however, the buoyancy in the upper part is lower due to the presence of bubbles. This fact restrict the particles from aggregation near the top of the reactor and support a fluctuation in the whole body of the reactor. We can observe the maximum value 6 % approximately at 3/4 of the reactor height and minimum value circa 1 % on the bottom of the reactor. The solid-concentration-profile is

strongly influenced by the bubble induced turbulence which is strongest on the top of the reactor causing more flatter profile in this parts than in the bottom.

4.3 The lab-scale reactor

4.3.1 Setting

Let us recall the geometry of the lab-scale prototype which is heated by a heating oil circulating within a system of internal hollow tubes (Figure (4.7)).

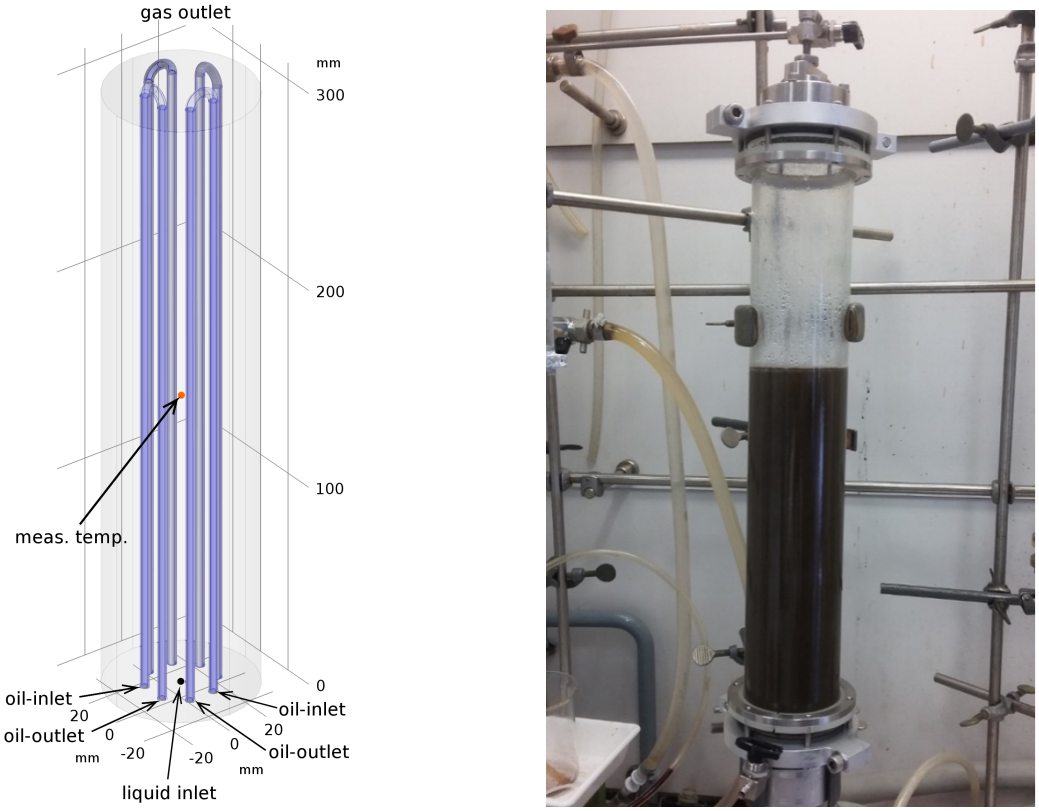

Figure 4.7: Reactor interior [mm] with heating tubes (left) and the lab installation.

Contrary to the test reactor, here, we can not use an uniform Dirichlet boundary condition for the surface temperature of the heating tubes ($T_{wall} = const.$) but we need to model the heat transfer within the tubes based on the inflow/outflow boundary conditions only. Therefore, we need to employ an additional NS-equation and heat transfer equation for the oil inside of the hollow tubes plus the heat transfer through the steel wall of the tubes.

Since we treat a full 3D geometry and the internal tubes has much lower thickness than the whole reactor, we need to simplify the model in order to receive numerically feasible computations. This will be done in the following manner:

1. We exploit the fact, that the heating system is composed of four U-shaped tubes which are symmetrically placed around the centre of the reactor. These divide the

reactor into four symmetrical parts. Without big loss of accuracy, we may consider even those parts symmetrical and take as a representative part one eighth of the reactor (Figure (4.8)):

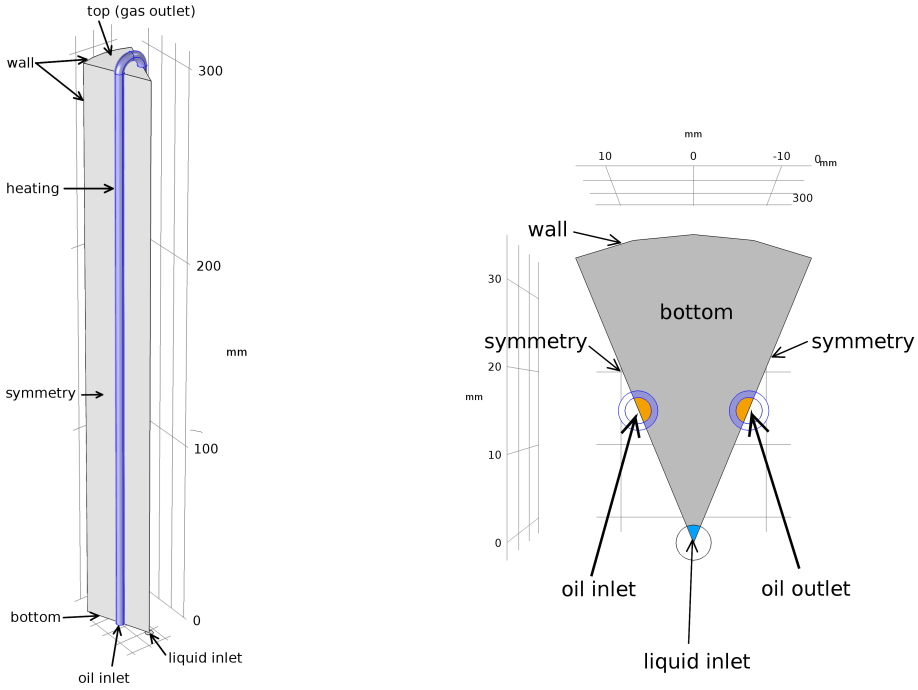

Figure 4.8: An illustration of the computational domain. Left: 1/8 of the reactor with highlighted U-shaped heating tube; Right: The bottom view with highlighted heating tube.

2. Another significant simplification lies in the a priori computed flow pattern inside of the internal tubes. This is done with guessed values of the temperature (usually little lower than T_{set}) and corresponding dependent quantities, e.g. viscosity (Figure (4.9)). The obtained (steady) velocity profile is, consequently, used in the overall equation-system.

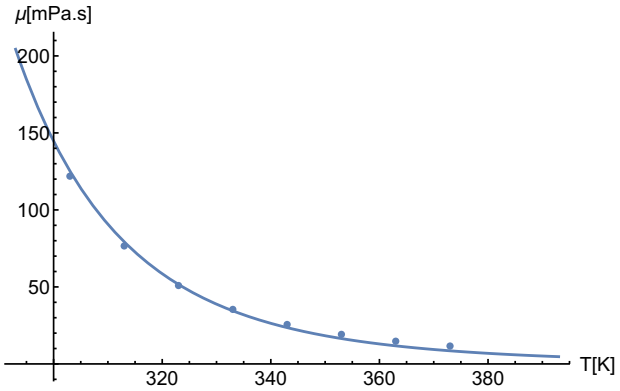

Figure 4.9: The estimated value of the viscosity of heating oil SAE 5W-40. The value used in the simulation correspond to $\mu_{oil}(110\,℃) \approx 8$ mPa $\cdot$ s.

4.3.2 The model

To distinguish the computational domains, we denote the hollow interior of the heating tubes as Ω_{ht}^{oil}, the steel heating tubes Ω_{ht}^{steel} and the rest of reactor body as Ω_r (Figure (4.8)). Moreover, we denote the boundaries of Ω_{ht}^{oil} as Γ_{in}^{oil} for the oil inlet; Γ_{out}^{oil} for the oil outlet; and Γ_{steel}^{oil} for oil/steel boundary. For the heating tubes, we furthermore denote Γ_{steel} the boundary near oil inlet/outlet and Γ_{steel}^{liquid} for the liquid/steel boundary. Finally, for Ω_r, we denote Γ_{in}^{liquid} the liquid inlet, Γ_{top}^{liquid} the liquid surface and Γ_{wall}^{liquid} the rest.

The resulting equation system is the following:

$$(\mathbf{v}_{oil} \cdot \nabla)\mathbf{v}_{oil} = -\nabla p_{oil} + \nu_{oil}\Delta \mathbf{v}_{oil} \qquad \text{in } \Omega_{ht}^{oil} \quad (4.2a)$$

$$\operatorname{div} \mathbf{v}_{oil} = 0 \qquad \text{in } \Omega_{ht}^{oil} \quad (4.2b)$$

$$\rho_{oil} C_p^{oil} \frac{\mathrm{d}T_{oil}}{\mathrm{d}t} = k_{oil}\Delta T_{oil} \qquad \text{in } \Omega_{ht}^{oil} \quad (4.2c)$$

$$\rho_{steel} C_p^{steel} \partial_t T_{steel} = k_{steel}\Delta T_{steel} \qquad \text{in } \Omega_{ht}^{steel} \quad (4.2d)$$

$$\operatorname{div}(\phi_l \mathbf{v}_l + \phi_g \overline{\mathbf{v}}_g + \phi_s \mathbf{v}_s) = 0 \qquad \text{in } \Omega_r \quad (4.2e)$$

$$\partial_t \phi_g + \operatorname{div}(\phi_g \overline{\mathbf{v}}_g) = \frac{\dot{m}_{gl}}{\rho_g^{true}} \qquad \text{in } \Omega_r \quad (4.2f)$$

$$\partial_t \phi_s + \operatorname{div}(\phi_s \mathbf{v}_s) = \operatorname{div}\left(\frac{\rho_s^{true}}{\rho_l^{true}} \mu_l^t \nabla \phi_s\right) \qquad \text{in } \Omega_r \quad (4.2g)$$

$$\phi_l \frac{\mathrm{d}\mathbf{v}_l}{\mathrm{d}t} - \phi_l \operatorname{div}\left(\tilde{}_{ls}^{dyn} + \tilde{}_{l}^{Re}\right) = \phi_l \alpha_l \Delta T\, \mathbf{g} + \phi_s \frac{\rho_l - \rho_s}{\rho_l} + \phi_g \mathbf{g} \qquad \text{in } \Omega_r \quad (4.2h)$$

$$\frac{3}{8} C_D \frac{|\mathbf{v}_{gl}^{slip}|}{r_g} \mathbf{v}_{gl}^{slip} = -\mathbf{g} \qquad \text{in } \Omega_r \quad (4.2i)$$

$$\frac{9}{2} \frac{\nu_l}{r_s^2} \mathbf{v}_{ls}^{slip} = -\frac{\rho_l^{true} - \rho_s^{true}}{\rho_l^{true}} \mathbf{g} \qquad \text{in } \Omega_r \quad (4.2j)$$

$$\begin{aligned} \partial_t(\rho_l^{true} k_t) + \operatorname{div}\left(\rho_l^{true} k \mathbf{v}_l - \frac{\mu_t}{\sigma_{k_t}} \nabla k_t\right) &= 2\mu_t \ {}_l^2 - \rho_l^{true} \varepsilon_t \\ &\quad + C_{k_t} \phi_g \nabla p_l^{dyn}\, \mathbf{u}_{gl}^{slip} \qquad \text{in } \Omega_r \quad (4.2k) \\ \partial_t(\rho_l^{true} \varepsilon_t) + \operatorname{div}\left(\rho_l^{true} \varepsilon_t \mathbf{v}_l - \frac{\mu_t}{\sigma_\varepsilon} \nabla \varepsilon_t\right) &= C_{1\varepsilon_t} \frac{\varepsilon_t}{k_t} 2\mu_t \ {}_l^2 - C_{2\varepsilon_t} \rho_l^{true} \frac{\varepsilon_t^2}{k_t} \\ &\quad - C_{3\varepsilon_t} \frac{\varepsilon_t}{k_t} \phi_g \nabla p_l^{dyn}\, \mathbf{u}_{gl}^{slip} \qquad \text{in } \Omega_r \quad (4.2l) \end{aligned}$$

$$\rho_l C_{p_l} \frac{\mathrm{d}T_l}{\mathrm{d}t} - \operatorname{div}(k_l \nabla T_l) = \dot{m}_{gl} h_{vap} + R_{sl}^{\Sigma} \Delta h_r \qquad \text{in } \Omega_r. \quad (4.2m)$$

where $\mathbf{v}_{gl}^{slip} = \mathbf{v}_g - \mathbf{v}_l$, $\mathbf{v}_{ls}^{slip} = \mathbf{v}_s - \mathbf{v}_l$, $\overline{\mathbf{v}}_g = \overline{\mathbf{v}}_{gl}^{slip} + \mathbf{v}_l$, $\mathbf{u}_{gl}^{slip} = \langle \mathbf{v}_{gl}^{slip} \rangle - \mathbf{v}_{gl}^{slip}$ and

$$
\begin{aligned}
1 &= \phi_l + \phi_g + \phi_s \\
\dot{m}_{gl} &= \frac{\bar{A}_{\Sigma_{gl}}}{\langle \bar{A}_{\Sigma_{gl}} \rangle_{V_r}} \left\langle \left(\left(1 + R_{H20}^{FA}\right) \phi_{H20_{(l)}}^{in} + 1 \right) A\, e^{\frac{-E_a}{RT}} R_{H20}^{FA} \phi_l \phi_s \right\rangle_{V_r} \\
\frac{\bar{A}_{\Sigma_{gl}}}{\langle \bar{A}_{\Sigma_{gl}} \rangle_{V_r}} &= 6.1(3.15z + 2.44z^2) \\
\overline{\mathbf{v}}_{gl}^{slip} &= (0.0117 + 0.446\sqrt{z} - 0.195z)\, \mathbf{e}_z \\
{}^{\sim}{}_{ls}^{dyn} + {}^{\sim}{}_{l}^{Re} &= -p_l^{dyn}\ + (\nu_{ls} + \nu_{turb}) \left(2\ {}_{l} - \frac{2}{3} \operatorname{div} \mathbf{v}_l \right) - \frac{2}{3} k_t \\
\nu_{ls} &= \nu_l \left(1 - \frac{\phi_s/(\phi_l + \phi_s)}{\phi_{max}} \right)^{-2.5\phi_{max}}, \ \phi_{max} = 0.64;\ \nu_l(T) = \nu_l^0 e^{\frac{E^\nu}{RT}} \\
C_D &= \max \left\{ \frac{24}{Re_p} \left(1 + 0.15 Re_p^{0.687} \right), \frac{8}{3} \frac{E\ddot{o}}{E\ddot{o} + 4} \right\} \\
h_{vap} &= \left(h_{vap}^{H_2O} + R_{H20}^{FA} h_{vap}^{FA} \right) \phi_{H20_{(l)}}^{in} \\
\langle R_{sl}^{\Sigma} \rangle_{\Sigma_{sl}} &= \rho_l^{true} A\, e^{\frac{-E_a}{RT}} R_{H20}^{FA} \phi_l \phi_s \\
C_{\mu_t} &= 0.09,\ C_{1\varepsilon_t} = 1.44,\ C_{2\varepsilon_t} = 1.92,\ C_{k_t} = 0.505,\ C_{\varepsilon_t} = 0.74 \\
\sigma_{k_t} &= 1.00,\ \sigma_{\varepsilon_t} = 1.30.
\end{aligned}
$$

The initial conditions read:

$$T_l = T_{oil} = T_{steel} = T_{in}, \mathbf{v}_l = \mathbf{v}_{oil} = 0, p = 3\,\text{atm}, k_t = 0, \varepsilon_t = 0, \phi_s = 0.05, \phi_g = 0$$

and boundary conditions yield:

$$
\begin{aligned}
Oil: & T_{oil} = T_{in} \text{ at } \Omega_{in}^{oil},\ \nabla T_{oil} \cdot \mathbf{n} = 0 \text{ at } \Gamma_{out}^{oil},\ T_{oil} = T_{steel} \text{ at } \Gamma_{steel}^{oil},\ \mathbf{v}_{oil} \text{ is given } [3] \\
Steel: & T_{oil} = T_{steel} \text{ at } \Gamma_{steel}^{oil},\ \nabla T_{steel} \cdot \mathbf{n} = 0 \text{ at } \Gamma_{steel},\ T_{steel} = T_l \text{ at } \Gamma_{steel}^{liquid} \\
Liquid: & T_{steel} = T_l \text{ at } \Gamma_{steel}^{liquid},\ \nabla T_l \cdot \mathbf{n} = 0 \text{ at } \Gamma_{top}^{liquid} \cup \Gamma_{wall}^{liquid} \cup \Gamma_{in}^{liquid} \\
& \mathbf{v}_l = 0,\ \nabla k_t \cdot \mathbf{n} = 0,\ \nabla \varepsilon_t \cdot \mathbf{n} = 0 \text{ at } \Gamma_{wall}^{liquid} \\
& \mathbf{v}_l \cdot \mathbf{n} = 0,\ p = 3\,\text{atm},\ {}_{ls}^{Re} - (\ {}_{ls}^{Re} \cdot \mathbf{n})\mathbf{n} = 0,\ \nabla k_t \cdot \mathbf{n} = 0,\ \nabla \varepsilon_t \cdot \mathbf{n} = 0 \text{ at } \Gamma_{top}^{liquid} \\
& \nabla T \cdot \mathbf{n} = 0,\ \mathbf{v}_l - (\mathbf{v}_l \cdot \mathbf{n})\mathbf{n} = 0,\ p = 0.3\rho_l |\mathbf{g}| + 3\,\text{atm},\ \ \cdot \mathbf{n} = 0, \\
& k_t = 0,\ \varepsilon_t = 0,\ \phi_s = 0,\ \phi_g = 0 \text{ at } \Gamma_{in}^{liquid}
\end{aligned}
$$

4.3.3 Lab-scale reactor results

As an illustrative example of the computations, we present the results simulating the behaviour of the reactor at $T_{set} = 110\,°\text{C}$ ($T_{in} \approx 108.1°\text{C}$) and initial loading $\phi_{Cat} = 0.05$. The presented result corresponds to a long-time solution ($t = 1000\,\text{s}$) when the main model characteristics (gaseous production, temperature profile, gas hold-up profile etc.) posses nearly steady behaviour. Concretelly, within the last 100 s the gaseous production changes 0.61 %, temperature in the middle 0.03 °C and averaged gas hold-up 0.24 %.

Analogously to the test-reactor results, also here, we demonstrate the long-time behaviour on four profiles (liquid velocity, temperature, volume fraction of the gas and volume fraction of the solid particles), cf. Figure (4.10) and (4.11).

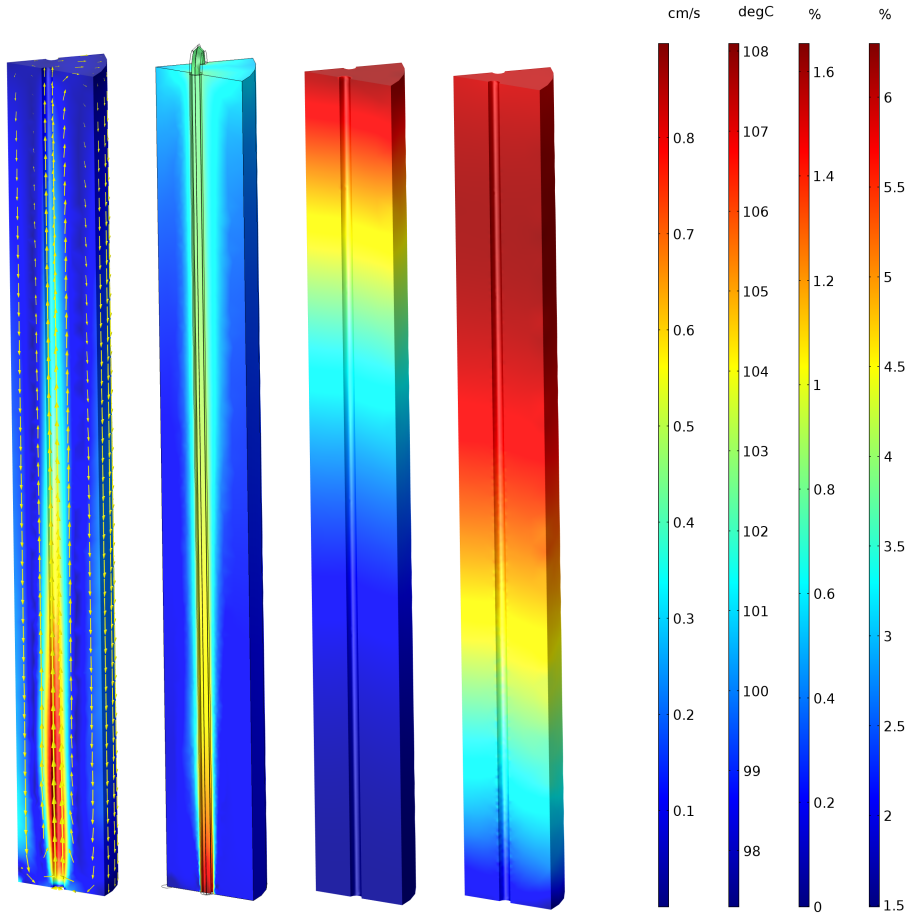

Figure 4.10: Setting $T_{set} = 110\,℃$, $\phi_s^{init} = 0.05$. From left: velocity magnitude $\mathbf{v}_l$ [cm/s] with arrow velocity field, temperature T [℃], gas hold-up ϕ_g [%]; solid concentration ϕ_s [%].

The production of the reactor is approximately 1810 $\frac{\text{mL}}{\text{min}}$ of $H_2 : CO_2$ gaseous mixture at molar ratio 1 : 1. This correspond to 186 W of the hydrogen chemical energy from which we may theoretically exploit 83 % via PEMFC, cf. [69], i.e. 154 W.

From qualitative perspective, we have obtained a similar behaviour to the test-reactor. The dominant effect is again the thermal convection when the hotter fluid ascents near the heated tubes, cools down due to the endothermic reaction and descents near the colder wall, resp. in the middle of the reactor. Unlike in the test reactor, here, we can observe slightly higher velocity magnitude (up to 0.8 cm/s) due to the higher temperature of the heating tubes.

The temperature profile posses similar course as in the test reactor with the hottest region on the top of the reactor (cca 102 ℃) and near the heating flow inlet (approx. 108 ℃). The regions of the lowest temperature lies near the bottom (around 98 ℃) and in the lower centre of the reactor (circa 99 ℃). Since the velocity profile is not so stable as in the case of the test reactor (it slightly fluctuates), the flow-stagnation-regions with local

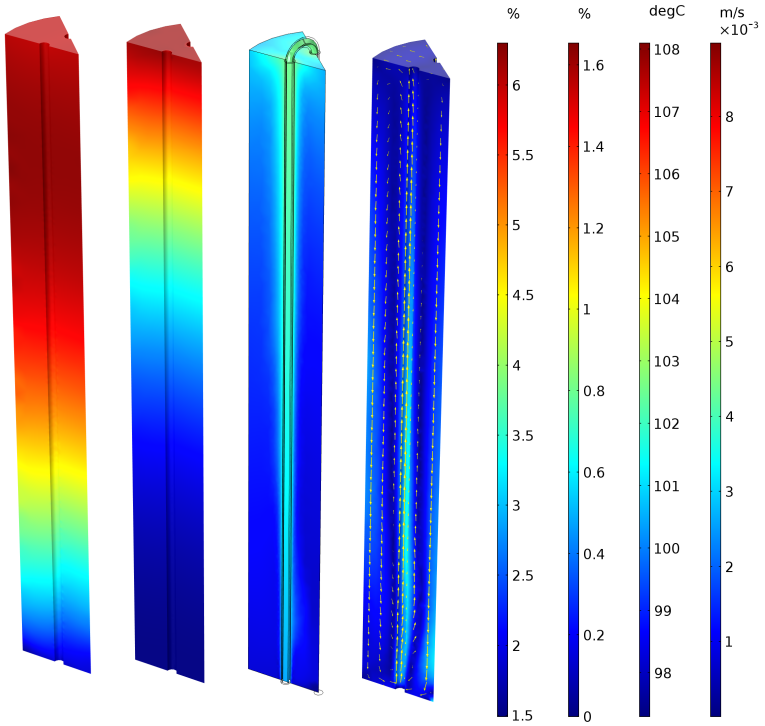

Figure 4.11: The opposite view to fig. (4.10) for $T_{set} = 110\,^{\circ}\mathrm{C}$. From left: solid concentration ϕ_s [%]; gas hold-up ϕ_g [%]; temperature T [°C]; velocity field magnitude $\mathbf{v}_l$ [cm/s].

temperature-minima do not occur in this case.

The gas hold-up profile is practically identical to the test reactor which is about to be expected - resulting in the similar slip velocity and temperature profiles in both test and lab cases. Finally, as an consequence of the previous observations, the solid concentration profile practically coincides with the test-reactor case.

Choosing the second simulation temperature as $T_{set} = 120\,^{\circ}\mathrm{C}$, which corresponds to the inlet temperature $T_{in} = 117.3\,^{\circ}\mathrm{C}$, we obtain the results depicted in fig. (4.12) As we would expect, there is practically no qualitative change but the quantitative only. For $T_{set} = 120\,^{\circ}\mathrm{C}$ we may observe the production rate 2741 $\frac{\mathrm{mL}}{\mathrm{min}}$; slightly higher maximum velocity magnitude (up to 1.2 cm/s) and higher gas hold-up (up to 2.4 % on the top).

4.4 Reactor verification

The verification of such a complicated multi-phase reactor when ideal conditions are hardly achieved is rather delicate task. The available data for the particular reactor are very sparse since the high acidity, temperature and pressure of the reactor environment complicates the measurements.

Catalytic deactivation:
One of the typical example of such a complicated measurements is the catalyst deactivation. The fresh load of catalyst has usually a higher activity than the repeatedly used one. [4]

[4]The reactor is cooled down to room temperature and, consequently, heated up again.

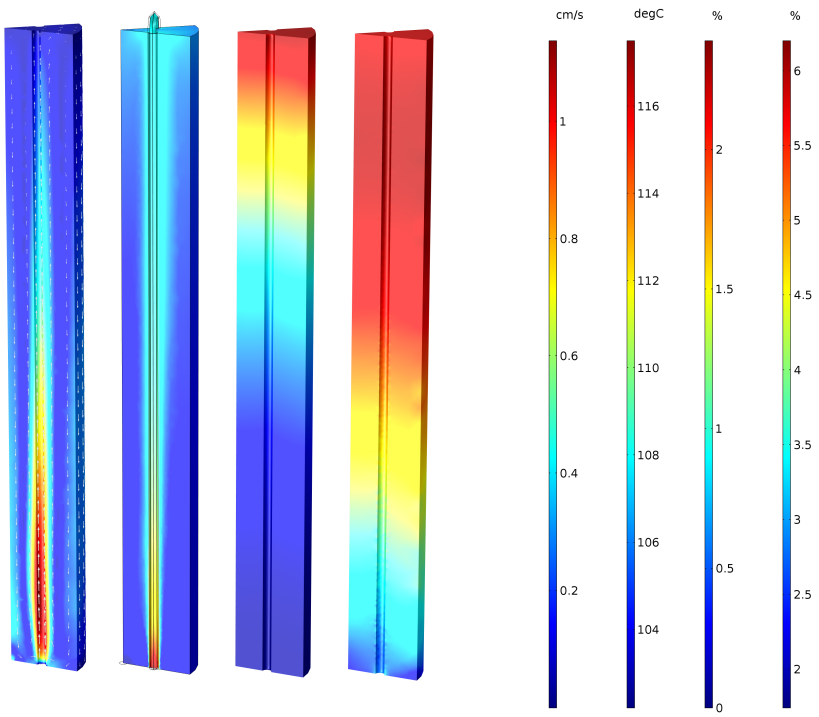

Figure 4.12: Setting $T_{set} = 120\,^{\circ}\text{C}$, $\phi_s^{init} = 0.05$. From left: velocity magnitude $\mathbf{v}_l$ [cm/s] with arrow velocity field, temperature T [°C], gas hold-up ϕ_g [%]; solid concentration ϕ_s [%].

However, we assume that the performance of the catalyst is relatively stable after several (~ 3) runs (Figure (4.13)).

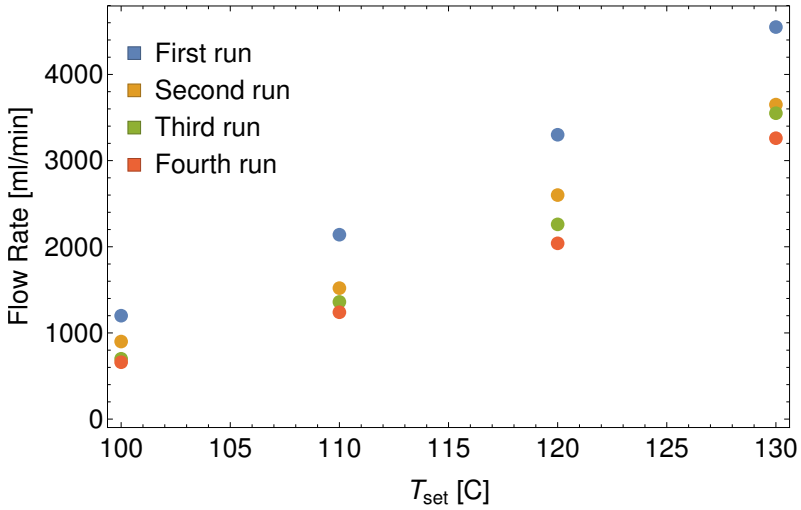

Figure 4.13: Drop in the catalyst performance within the first runs.

Temperature dependence:
For a verification of the reactor performance dependence in the temperature we have used a comparison of the measured and modelled temperature in the middle of reactor T_r.

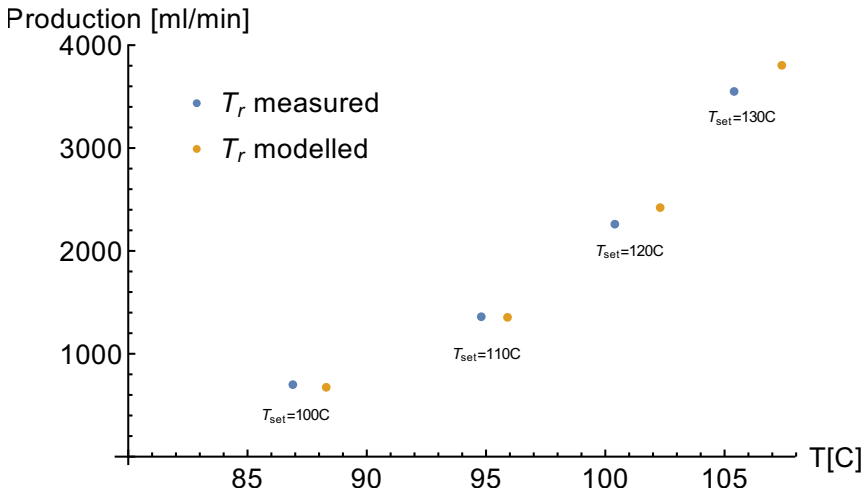

Figure 4.14: Verification of the measured and modelled reactor temperature T_r for the thermostat-temperature $T_{set} = 100 - 130\,℃$.

. As we can see in fig. (4.14), the model closely fit the trend of the dependency having the deviance within the temperature range 2 ℃ for $T_{set} = 100 - 130\,℃$ and 5% of the hydrogen and carbon dioxide production.

Amount of condensate:
The amount of condensate in the out-coming gas, i.e. the vapour of liquid ($FA_{(l)}$ and $H_2O_{(l)}$) depends on many factors and it is delicate task to estimate its value. Roughly speaking, the aqueous solution of formic acid contains approx. 2 %[wt.] of water which need to be evaporated. Keeping the azeotropic ratio $R^{FA}_{H_20}$ of the liquid vapour, we may expect around $7 - 13\,\%$[wt.] of the $FA_{(g)}$ on the outcome.

Since the reactor is held out of the equilibrium, we may expect little bit less of $FA_{(g)}$ within the outcomming gas. However, the amount of condensate around 10 %[wt.] is to be expected within the pressure range $3 - 5\,\text{atm}$. The enthalpy of vaporization for liquid vapour at ratio $\frac{2}{8}$ [wt.] $= \frac{2}{23}$ [mol] corresponds approximately to $24.5\,\frac{\text{kJ}}{\text{mol}}$.

Pressure dependence:
Considering the reaction rate, there should be no significant pressure dependence. However, there is an indirect influence of the pressure caused by change of interfacial area, thus, change of rate of evaporation for liquid. The rate of vaporization of dissolved gas, on the other hand, stays practically the same due to the very quick increase of dissolved gas concentration to equilibrate the chemical reaction rate.

As a consequence of lower evaporation rate, the temperature slightly rises and subsequently the reaction rate somehow rises as well. The change is not radical, but we can gain about 10 % more production by increasing the pressure from 2.5 to 5 atm, hence, reducing the interfacial area by 37 %. If the liquid vapour consumes around 8 % of the overall energy consumption, it reduces to 5 % increasing the reaction rate by 3 %. Therefore, we consider the pressure dependency as negligible.

Based on the presented results, we conclude that the model is able to catch qualitative and quantitative behaviour of the reactor within 5 % production and 2 ℃ temperature error for $T_{set} = 100 - 130\,℃$ and $P = 1.5 - 4\,\text{atm}$.

4.5 CFD Analysis

4.5.1 System bottleneck

One of the important output of the CFD analysis is the determination of system bottlenecks. From the simulation of the whole reactor system including the heating tubes, we may observe a significant temperature drop during the oil flow through the pipe. The temperature was measured on the inflow (T_{in}) and outflow (T_{out}) of the reactor with a drop between 6 ℃ for the thermostat $T_{set} = 100$ ℃ and 10 ℃ for $T_{set} = 130$ ℃.

T_{set}[℃]	T_{in}[℃]	T_{out}[℃]	T_r[℃]	Prod. [ml/min]	T_{in}/T_{out} drop
100	98.5	92.1	87.7	660	41 %
110	108.1	100.4	94.7	1240	45 %
120	117.3	109.5	101.2	2040	45 %
130	127.2	117.5	106.2	3260	50 %

Table 4.3: Measured temperatures with corresponding productions and temperature-drops.

To verify the conjecture, we made a measurement for different rotation of the pump compressor, i.e. different pump pressure, namely $2000, 3000$ (default) and 4000 rpm. The results are shown in the table (4.4):

T_{set}[°C]	rpm [Hz]	T_r[°C]	Gas flow[ml/min]
100	2000	79.3	190
100	3000	86.7	420
100	4000	90.2	560
120	2000	95.7	1060
120	3000	102.5	2050
120	4000	115.6	2600

Table 4.4: Different pump rpm for $T_{set} = 100, 120$ ℃ and corresponding change in measured temperature T_r and reactor production.

To obtain the corresponding flow rate within the heating tube, we modelled the situation with the prescribed inlet temperature T_{in} trying to obtain the measured outlet temperature T_{out}. The situation is illustrated at the Figure (4.15):

From the measurements and the modelling results, we can clearly see that the weakest point of the whole reactor is the heating system which, due to the significant temperature drop, is not able to transfer enough heat into the system. This is caused by an insufficient flow-rate (big pressure drop), thus, low heat supply.

Some improvements can be made by increase of the reactor pump-pressure, however, commonly available heating liquids posses relatively high viscosity (causing the pressure drop) and the maximum pressure provided by the pump is the limiting factor. Another possibility to increase the flow rate is the enlarging of the inner heating tubes cross-section, thus, reduce the pressure drop and increasing the flow rate.

The possible improvement-potential in the reactor performance for a uniform temperature profile, an ideal heating (Dirichlet BC) and the real BC are illustrated in the fig. (4.16).

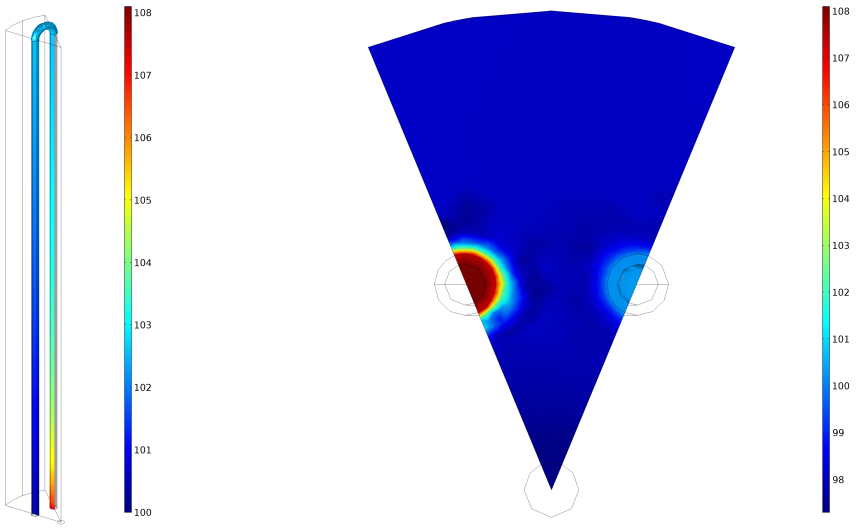

Figure 4.15: Modelling fitting for situation $T_{in} = 108.1\,℃$ and $T_{out} = 100.4\,℃$ - corresponding to $T_{set} = 110\,℃$ and 3000 rpm.

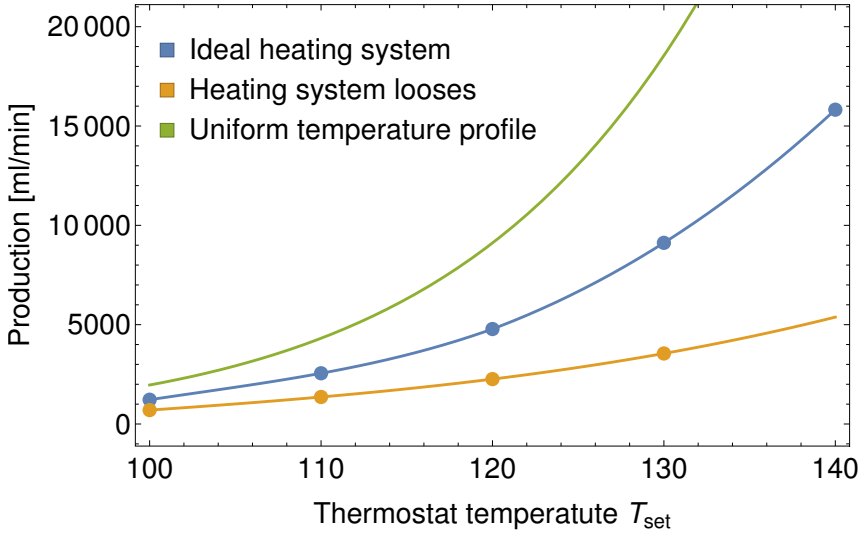

Figure 4.16: Heating system loses and modelled reactor temperature T_r for thermostat temperature $T_{set} = 100 - 130\,℃$.

4.5.2 System improvement and up-scale

Since the bottleneck of the system lies in the capability of the heating system to transfer enough heat inside the reactor, the change of the heating tubes design or change of operational conditions is just partial solution. To solve the problem properly, we propose the following: The heating system should not be based on the heating oil circulation but on a different type of heating providing more uniform temperature profile. The suggested solution is the electrical heating system.

The biggest disadvantage of the electrical heating is the impossibility of direct temperature control and possibility of unwanted hot spots. However, this problem may be solved by convenient placement of the heating providing sufficient circulation. Similar situation

is for example the placement of the heating body inside of a jug kettle where we can find an inspiration for the desired effective design.

Once we place the heating body on the bottom of the reactor, the thermal convection becomes strong enough to sufficiently distribute the heat along the reactor and the magnitude of hot spots is rapidly reduced.

We present the following up-scale design of the reactor to obtain desired net-power 5 kW: the reactor has a simple cylindrical shape with radius 75 mm and height 192 mm, i.e. the volume is 3350 ml. The heating body formed by 7-mm radius wire of length 656 mm is based on the bottom. It has resistance 89 Ω at current 2.58A A and 230 V (DC). The electric power of the heating wire is 593 W.

For simulation we have used 80 g, i.e. cca 3 %[vol], of the solid catalyst which is, actually, less percentage than at the lab-scale prototype. However, the new reactor design and electrical heating allows to improve the performance easily by increasing its amount. The operating pressure for the reactor is assumed to be 5 atm. Since the formic acid forms with water a negative azeotrope, its boiling point lies above boiling point of both of its constituents. [5]

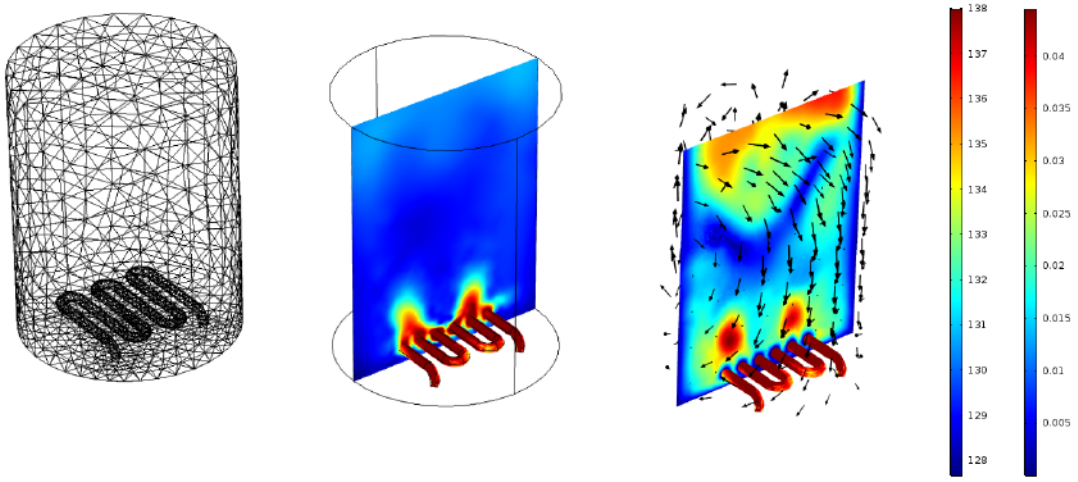

Figure 4.17: Mesh, temperature [°C] and velocity profile [m/s] of the up-scaled reactor.

As we can see in the Figure (4.17), the operating temperature is about 20 °C higher that in case of lab-scale prototype and the liquid circulate in higher rate (max. 4.5 cm/s, av. 1.8 cm/s). The average temperature of the heating is 142 °C and maximum is 148 °C, thus, the heating posses relatively uniform temperature profile and we did not observed any significant hot-spots.

The reactor produces approximately 50 L/min of the H_2/CO_2 gas at molar ratio 1 : 1 which corresponds to 5 kW of theoretical chemical power of produced hydrogen. Using PEMFC, the (realistic) efficiency drop to $50 - 60$ % or, with the recirculation of the exhausted gas and heat recapture, we can move towards the theoretical maximum efficiency 83 %. From this reason, although the chemical energy of the up-scale system is about 5 kW, we should expect the real power, reduced by the heating system consumption, around 2 kW.

[5] The boiling point at 5 atm is approx. 152 °C for water and 205 °C for formic acid.

Appendices

Appendix A

In the following sections some standard results on the averaging procedure for multi-fluid models are presented. After a formal introduction of an interface as a dividing surface, surfacial variables such as the surface density and velocity are discussed. Furthermore, the transport and balance equations of the systems containing possibly non-material interfaces are derived.

The beginning of the multi-fluid volume-averaged theory is dated from early 60's by Scriven [90] and Stattery [99]. Especially, the latter one can be considered as the pioneer in the field with many subsequent publications, e.g. [100], [96], [102], [98]. For other resources we refer to fundamental work of Batchelor [6] or Truesdell [111] and other authors of the multi-fluid theory as Deemer [24], Ranson [82] or Jakobsen [48].

A.1 Interface as a dividing surface

A.1.1 Phase interface

The concept of phase interface is not unified within the scientific community. Generally speaking, a phase interface is a region separating two phases in which the properties or behaviour differ from those of the adjoining phases. The region can be described by molecular or continuum models. Working in a framework of the latter one, we further distinguish a model of thin 3D region or 2D dividing surface.

The interpretation of phase interface as a 2D dividing surface was originally proposed by Gibbs [34, p. 219] and it is widely accepted in scope of continuum mechanics as well as in this work. Quoting Jakobsen [48]:

Although it is appealing from a scientific point of view to regard the interface as a 3D region of finite thickness, the computational difficulties involved considering the implicit numerical grid resolution requirements make the application of this concept infeasible.

From a practical viewpoint instrumentation size limitations enable only indirect observations of the interfacial properties through their influence upon the surrounding bulk phases. Therefore, in engineering applications an interface has traditionally been viewed as a singular 2D dividing surface separating two immiscible homogeneous bulk phases.

In the 80s, Slattery [101] introduced a mathematical concept allowing expression of a 3D interface model in terms of a 2D dividing surface model and vice versa by a suitable definition of interfacial quantities. In this work, we adopt this concept exploiting the fact that both (2D/3D) approaches introduce a different perspective important for the proper understanding.

A.1.2 Mathematical description of dividing surface

Let us consider a *material particle* ζ of a body B. A one-to-one continuous mapping of the control volume V and a 3D subset of Euclidean space ^{3}, is called *configuration*:

$$\mathbf{z} = \chi(\zeta)$$
$$\zeta = \chi^{-1}(\mathbf{z}).$$

A motion of the body is one-parameter family of configurations; the parameter is time and we may write

$$\begin{aligned}\mathbf{z} &= \chi(\zeta, t)\\ \zeta &= \chi^{-1}(\mathbf{z}, t).\end{aligned}$$

The *material derivative* of a (bulk) quantity A, where we track the motion of the particle, is defined as

$$\frac{\mathrm{d}A(\mathbf{z})}{\mathrm{d}t} = \left(\frac{\partial A(\zeta, t)}{\partial t}\right)_{\zeta}.$$

The *material velocity* is, consequently, defined in the standard way as the rate of change of the particle motion:

$$\mathbf{v}(\mathbf{z}) := \left(\frac{\partial \chi(\zeta, t)}{\partial t}\right)_{\zeta} = \frac{\mathrm{d}\mathbf{z}}{\mathrm{d}t}.$$

Now, we identify the material particle ζ by their position $\mathbf{z}$ in some particular configuration. This configuration is called the reference configuration χ_κ, hence,

$$\begin{aligned}\mathbf{z}_\kappa &= \kappa(\zeta)\\ \zeta &= \kappa^{-1}(\mathbf{z}_\kappa).\end{aligned}$$

If χ is a motion of the body, we obtain

$$\begin{aligned}\mathbf{z} &= \chi_\kappa(\mathbf{z}_\kappa, t) := \chi(\kappa^{-1}(\mathbf{z}_\kappa, t))\\ \mathbf{z}_\kappa &= \chi_\kappa^{-1}(\mathbf{z}, t) := \kappa(\chi^{-1}(\mathbf{z}, t)).\end{aligned}$$

and, consequently,

$$\begin{aligned}\frac{\mathrm{d}A(\mathbf{z})}{\mathrm{d}t} &= \left(\frac{\partial A(\mathbf{z}_\kappa, t)}{\partial t}\right)_{\mathbf{z}_\kappa}\\ \mathbf{v}(\mathbf{z}) := \left(\frac{\partial \chi_\kappa(\mathbf{z}_\kappa, t)}{\partial t}\right)_{\mathbf{z}_\kappa} &= \frac{\mathrm{d}\mathbf{z}}{\mathrm{d}t}.\end{aligned}$$

In case of an interface, treated as 2D dividing surface, is the situation a bit complicated and we adopt the definition of Slaterry [98]: a moving dividing surface $\Sigma(t)$ in the Euclidean space is the locus of a point whose position is a function of two spatial parameters y^1, y^2 and time t, i.e.

$$\mathbf{z} = P(y^1, y^2, t), \mathbf{z} \in \Sigma(t).$$

The two surface coordinates uniquely determine the point on the surface at any time and the function P is assumed to be differentiable with respect to both space and time coordinates. The interface is generally non-material and the mapping $\chi_{|\Sigma}$ does not have an inverse, i.e although there is a position in space corresponding to every surface particle, the converse is not true. This situation is common for interfaces mediating a mass transfer between phases.

In the next, we identify the surface particle ζ^Σ by its *reference intrinsic configuration* in the reference dividing surface:

$$\begin{aligned}\mathbf{y}_\kappa &= {}^\Sigma\kappa(\zeta^\Sigma) \text{ , resp. } y^\alpha_\kappa = {}^\Sigma\kappa^\alpha(\zeta^\Sigma), \alpha = 1, 2.\\ \zeta^\Sigma &= {}^\Sigma\kappa^{-1}(\mathbf{y}_\kappa) = \left(({}^\Sigma\kappa^1)^{-1}(\zeta^\Sigma), ({}^\Sigma\kappa^2)^{-1}(\zeta^\Sigma)\right).\end{aligned}$$

If χ^Σ is a motion on the dividing surface, then

$$\begin{aligned}\mathbf{y} = \chi_{\Sigma_\kappa}(\mathbf{y}_\kappa, t) &:= \chi^\Sigma({}^\Sigma\kappa^{-1}(\mathbf{y}_\kappa), t)\\ \mathbf{y}_\kappa = \chi^{-1}_{\Sigma_\kappa}(\mathbf{y}, t) &:= {}^\Sigma\kappa\left(\chi^{\Sigma\,-1}(\mathbf{y}, t)\right)\end{aligned}$$

and

$$\begin{aligned}\frac{\mathrm{d}^\Sigma A(\mathbf{y}, t)}{\mathrm{d}t} :=& \left(\frac{\partial A(\mathbf{y}_\kappa, t)}{\partial t}\right)_{\mathbf{y}_\kappa}\\ =& \frac{\partial A(y^1, y^2, t)}{\partial t} + \sum_{\alpha=1}^{2} \frac{A(y^1, y^2, t)}{\partial y^\alpha} \frac{\chi^\alpha_\kappa(y^1_\kappa, y^2_\kappa, t)}{\partial t}\\ =& \frac{\partial A(\mathbf{y}, t)}{\partial t} + \nabla^\Sigma A(\mathbf{y}, t) \cdot \dot{\mathbf{y}}\end{aligned}$$

where $\dot{\mathbf{y}}$ denotes the *intrinsic surface velocity* which is, basically, an analogy to the velocity in ^{2}.

Once the surface is non-material, its useful to describe the motion of a surface particle using its *reference extrinsic configuration* in ^{3} defined as:

$$\mathbf{z}_\kappa = \kappa(\zeta^\Sigma) = \kappa\left({}^\Sigma\kappa^{-1}(\mathbf{y}, t))\right).$$

If χ is a motion of the dividing surface in ^{3}, then

$$\begin{aligned}\mathbf{z} = \chi_\kappa(\mathbf{z}_\kappa, t) &:= \chi\left(\kappa\left({}^\Sigma\kappa^{-1}(\mathbf{y})\right), t\right)\\ \mathbf{z}_\kappa = \chi^{-1}_{\Sigma_\kappa}(\mathbf{z}, t) &:= \kappa\left(\chi^{\Sigma\,-1}(\mathbf{y}, t)\right).\end{aligned}$$

Consequently, we may define also the *extrinsic surface velocity* - the time rate of change of spatial (reference) position following the surface particle:

$$\begin{aligned}\mathbf{v}(\mathbf{z}) :=& \left(\frac{\partial \chi_\kappa(\mathbf{z}, t)}{\partial t}\right)_{\mathbf{z}_\kappa} = \frac{\mathrm{d}^\Sigma \mathbf{z}}{\mathrm{d}t} = \frac{\mathrm{d}^\Sigma \mathbf{P}(y^1, y^2, t)}{\mathrm{d}t}\\ =& \frac{\partial \mathbf{P}(y^1, y^2, t)}{\partial t} + \nabla^\Sigma \mathbf{P}(y^1, y^2, t) \cdot \dot{\mathbf{y}}\\ =& \mathbf{u} + \dot{\mathbf{y}}.\end{aligned}$$

Here, we introduced the rate of change of spatial position in ^{3} following a surface point (y^1, y^2) as

$$\mathbf{u} = (u^1, u^2, u^3) := \frac{\partial \mathbf{P}(y^1, y^2, t)}{\partial t}.$$

Note that $\dot{\mathbf{y}}$ has the tangential component only but $\mathbf{u}$ has generally both. Therefore, for $\mathbf{n}$ being a vector normal to the interface Σ we have

$$\begin{aligned}\dot{\mathbf{y}} \cdot \mathbf{n} &= 0\\ {}^\Sigma\mathbf{v} \cdot \mathbf{n}^\Sigma &= \mathbf{u} \cdot \mathbf{n} =: v^\Sigma_{\mathbf{n}}.\end{aligned}$$

We refer to $v^\Sigma_{\mathbf{n}}$ as the *speed of displacement* of the surface and we conclude

$${}^\Sigma\mathbf{v} := \sum_{\alpha=1}^{3} u_\alpha \mathbf{e}_\alpha + v^\Sigma_{\mathbf{n}} \cdot \mathbf{n}$$

where $\mathbf{e}_\alpha, \alpha = 1,2,3$ denotes the Cartesian base vectors in ^{3}. Consequently, considering a quantity f on a moving and deforming dividing surface Σ, we express its conservation by the relation

$$\frac{\partial f}{\partial t} + \nabla f \cdot \mathbf{u} = 0.$$

A.1.3 Surface sensity

Let us start with the conservation equation of mass. The statement that the mass M of a body B occupying volume V is independent of time is mathematically expressed as

$$\frac{\mathrm{d}}{\mathrm{d}t} M(B) = \frac{\mathrm{d}}{\mathrm{d}t} \int_V \mathrm{d}m = 0$$

where $\frac{\mathrm{d}}{\mathrm{d}t}$ is a material derivative and m is a non-negative, time-independent, scalar measure. Assuming the absolute continuity of the measure m to the three dimensional Lebesque measure, we get the existence of a function called density such that

$$M(B) = \int_V \rho \,\mathrm{dV}.$$

This is the standard approach for one phase or continuous mixture body but the absolute continuity fails in the interfacial region (considered as a 2D dividing surface). For that case, we follow the approach of Slattery [98] or, resp. one of the possible viewpoint of the balance equation consisting dividing surface.

Let us have a body consist of two phases occupying region V_1 and V_2, and its mass density ρ_1 and ρ_2. The densities are assumed to be a continuous functions of position within the phase region. Let us, therefore, consider a 2D dividing surface $\Sigma \subset B : \Sigma \cap V_1 = \emptyset = \Sigma \cap V_2$, and the corresponding surface density ρ^Σ being a continuous function of position on Σ. The mass conservation of the body, consequently, follows

$$M(B) = \int_{V_1} \rho_1 \,\mathrm{dV} + \int_{V_2} \rho_2 \,\mathrm{dV} + \int_\Sigma \rho^\Sigma \,\mathrm{dS}.$$

On the other hand, we may treat the interface as a three-dimensional region V_I between the volumes V_1 and V_2 of finite thickness having its own material behaviour (Figure A.18).

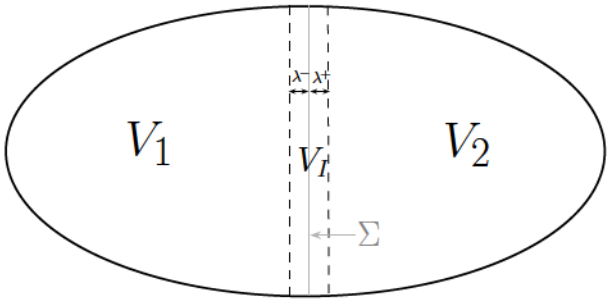

Figure A.18: Interface.

Decomposing the body domain $V = V_1 \cup V_I \cup V_2$, we express the mass conservation as

$$\frac{\mathrm{d}}{\mathrm{d}t} \int_V \rho \,\mathrm{dV} = \frac{\mathrm{d}}{\mathrm{d}t} \left[\int_{(V_1 \cup V_2) \setminus V_I} \rho \,\mathrm{dV} + \int_{V_I} \rho_I \,\mathrm{dV} \right] = \frac{\mathrm{d}}{\mathrm{d}t} \left[\int_{V_1 \cup V_2} \rho \,\mathrm{dV} + \int_{V_I} (\rho_I - \rho) \,\mathrm{dV} \right].$$

where $\rho_I = \rho$ outside of V_I. The proper mathematical definition of the surface density ρ^Σ is not an easy task and for more details we refer the readers to Slattery [98, 1.3].

Restricting ourself to very simple example of straight interface $V_I = \Sigma \times [\lambda^-, \lambda^+]$, we may identify [6]

$$\int_{V_I} (\rho_I - \rho)\,\mathrm{dV} = \int_\Sigma \int_{\lambda^-}^{\lambda^+} (\rho_I - \rho)\,\mathrm{d}\lambda\,\mathrm{dS} = \int_\Sigma \rho^\Sigma\,\mathrm{dS}.$$

Consequently, we obtain the mass conservation in the standard form

$$\frac{\mathrm{d}}{\mathrm{d}t} M = \frac{\mathrm{d}}{\mathrm{d}t} \int_V \rho\,\mathrm{dV} = \frac{\mathrm{d}}{\mathrm{d}t} \left[\int_{V_1 \cup V_2} \rho\,\mathrm{dV} + \int_\Sigma \rho^\Sigma\,\mathrm{dS} \right] = 0. \tag{A.3}$$

The material derivative $\frac{\mathrm{d}}{\mathrm{d}t}$ describes the time rate of change of a physical quantity subjected to a macroscopic velocity field $\mathbf{v}$. Treating an interface with its own material velocity ${}^\Sigma\mathbf{v}$, we identify the material derivatives $\frac{\mathrm{d}}{\mathrm{d}t}$ as

$$\left(\frac{\mathrm{d}\rho}{\mathrm{d}t} \right)_{|_{V_1 \cup V_2}} = \frac{\partial \rho}{\partial t} + \mathbf{v} \cdot \nabla \rho$$

and

$$\frac{\mathrm{d}^\Sigma \rho^\Sigma}{\mathrm{d}t} := \frac{\mathrm{d}\rho^\Sigma}{\mathrm{d}t} = \frac{\partial \rho^\Sigma}{\partial t} + \dot{\mathbf{y}} \cdot \nabla^\Sigma \rho^\Sigma = \frac{\partial \rho^\Sigma}{\partial t} + ({}^\Sigma\mathbf{v} - \mathbf{u}) \cdot \nabla^\Sigma \rho^\Sigma.$$

The previous considerations can be easily generalized for a body consisting of m phases once we restrict to the situation of non-intersecting interfaces. Let Σ_{ij} be the dividing surface separating the phases i, j and ρ^Σ_{ij} its density. The mass of the body (summing over all possible interfaces) equals:

$$M = \sum_{i=1}^{m} \int_{V_i} \rho_i\,\mathrm{dV} + \sum_{i=1}^{m-1} \sum_{j=j+1}^{m} \int_{\Sigma_{ij}} \rho^\Sigma_{ij}\,\mathrm{dS}.$$

Introducing a less formidable notation assuming integrability of the function ρ such that $\rho = \rho_i$ in phase i, we may write

$$\int_V \rho\,\mathrm{dV} \equiv \sum_{i=1}^{m} \int_{V_i} \rho_i\,\mathrm{dV}$$

where $V := \bigcup_{i=1}^m V_i$. Analogously:

$$\int_\Sigma \rho^\Sigma\,\mathrm{dS} \equiv \sum_{i=1}^{m-1} \sum_{j=i+1}^{m} \int_{\Sigma_{ij}} \rho^\Sigma_{ij}\,\mathrm{dS}$$

where $\Sigma := \bigcup_{i=1}^{m-1} \bigcup_{j=i+1}^{m} \Sigma_{ij}$.

Remarks:

A.1.1 Surface coverage. *One of the heuristic descriptions of the surface density on the fluid-solid interface offer a uniformly thick plague formed on the solid surface. The surface density is simply proportional to the surface coverage.*

[6] In the sequel, we will understand definitions of other surface quantities (e.g. the surface velocity ${}^\Sigma\mathbf{v}$) in the same sense.

A.1.2 Excess quantity. *Let us mention that we might consider also an excess line quantity associated with the common line, i.e. with* $C^{cl} = \partial\Sigma \cap \partial V$*. In this case, the (mass) conservation would be expressed by*

$$\frac{\mathrm{d}}{\mathrm{d}t}\int_V \rho\,\mathrm{dV} = \frac{\mathrm{d}}{\mathrm{d}t}\left(\int_{V_1\cup V_2}\rho\,\mathrm{dV} + \int_\Sigma \rho^\Sigma\,\mathrm{dS} + \int_{C^{cl}} {}^{cl}\rho\,\mathrm{dl}\right) = 0.$$

Nevertheless, we do not consider any excess line quantity in our case and we will drop the term in the sequel.

A.2 Multi-fluid balances in bulk and on dividing surfaces

In this section we introduce balance equations of mass, momentum and energy for a multi-fluid body. We restrict ourself to a simplified example of a multiphase body consist of m phases with non-intersecting interfaces. For more general case and proofs of the statements, we refer to the literature, e.g. Slaterry [98, 1.3] and Jakobsen [48, 3.3].

A.2.1 Transport theorems

Let us consider an illustrative multi-phase body with non-intersecting interfaces, see e.g. the Figure (A.19)

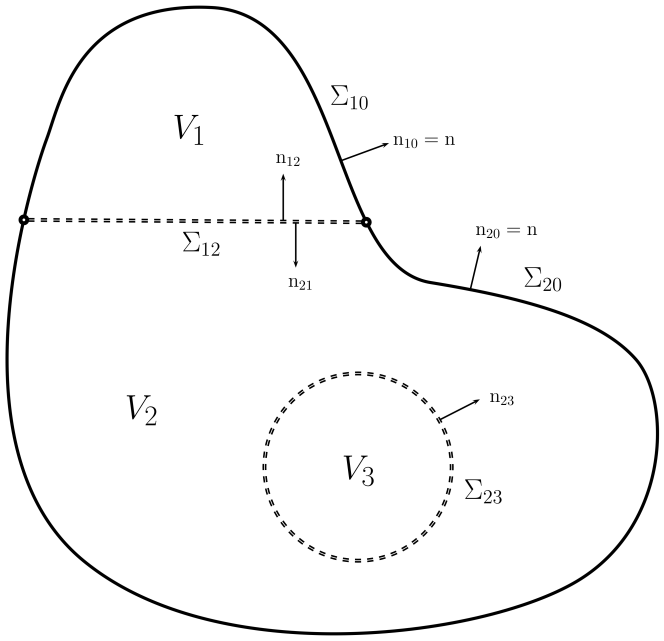

Figure A.19: Multi-phase system

The surfaces with subscript containing "0" mark parts of the outer physical (material) boundary of the body and $\partial V = \bigcup_{i=1}^{m}\Sigma_{i0} = \Sigma_{10}\cup\Sigma_{20}$. Furthermore, we denote $V =$

$V_1 \cup V_2 \cup V_3$ and $\Sigma = \Sigma_{12} \cup \Sigma_{23}$. Investigating the mass of the body, we are interested in the expression

$$\frac{\mathrm{d}}{\mathrm{d}t}\left(\int_V \psi \,\mathrm{dV} + \int_\Sigma \psi^\Sigma \,\mathrm{dS}\right).$$

Transport theorem for bulk quantities: We introduce the *transport theorem for the whole body* (neglecting the excess quantity on the common lines) as

$$\frac{\mathrm{d}}{\mathrm{d}t}\left(\int_V \psi \,\mathrm{dV}\right) = \int_V \frac{\partial \psi}{\partial t}\,\mathrm{dV} + \int_{\partial V} \psi \mathbf{v}\cdot\mathbf{n}\,\mathrm{dS}.$$

The *generalized transport theorem for the phase k occupying volume V_k* with boundary $\partial V = \sum_{l=0}^{m} \Sigma_{kl}$ follows

$$\begin{aligned}\frac{\mathrm{d}}{\mathrm{d}t}\int_{V_k} \psi_k \,\mathrm{dV} &= \int_{V_k} \frac{\partial \psi_k}{\partial t}\,\mathrm{dV} + \int_{\partial V_i} \psi_k \mathbf{v}_k\cdot\mathbf{n}_k\,\mathrm{dS} \\ &= \int_{V_k} \frac{\partial \psi_k}{\partial t}\,\mathrm{dV} + \int_{\Sigma_{k0}} \psi_k \mathbf{v}_k\cdot\mathbf{n}\,\mathrm{dS} + \sum_{\substack{l=1\\ l\neq k}}^{m} \int_{\Sigma_{kl}\cap V_k} \psi_k{}^{\Sigma}\mathbf{v}_{kl}\mathbf{n}_{kl}\,\mathrm{dS}.\end{aligned}$$

Summing the relations through all the bulk phases, we obtain

$$\begin{aligned}\frac{\mathrm{d}}{\mathrm{d}t}\int_V \psi \,\mathrm{dV} &= \frac{\mathrm{d}}{\mathrm{d}t}\sum_{k=1}^{m}\int_{V_k} \psi_k \,\mathrm{dV} \\ &= \sum_{k=1}^{m}\int_{V_k} \frac{\partial \psi_k}{\partial t}\,\mathrm{dV} + \sum_{k=1}^{m}\int_{\Sigma_{k0}} \psi_k \mathbf{v}_k\cdot\mathbf{n}\,\mathrm{dS} \\ &\quad - \sum_{k=1}^{m}\sum_{\substack{l=1\\ l\neq k}}^{m}\int_{\Sigma_{kl}\cap V_k} \psi_k{}^{\Sigma}\mathbf{v}_{kl}\cdot\mathbf{n}_{kl}.\,\mathrm{dS}\end{aligned} \tag{A.4}$$

Note, that ${}^{\Sigma}\mathbf{v}_{l0} = \mathbf{v}_k$ and $\mathbf{n}_{k0} = \mathbf{n}$ since Σ_{k0} are material boundaries. On the other hand, we have $\Sigma_{kl} = \Sigma_{lk}$ and $\mathbf{n}_{kl} = -\mathbf{n}_{lk}$, hence, the last term at the RHS of the equation (A.4) can be reduced to

$$\sum_{k=1}^{m}\sum_{\substack{l=1\\ l\neq k}}^{m}\int_{\Sigma_{kl}\cap V_k} \psi_k{}^{\Sigma}\mathbf{v}_{kl}\cdot\mathbf{n}_{kl}\,\mathrm{dS} = \sum_{k=1}^{m-1}\sum_{l=k+1}^{m}\int_{\Sigma_{kl}\cap(V_k\cup V_l)} (\psi_k - \psi_l)^{\Sigma}\mathbf{v}_{kl}\cdot\mathbf{n}_{kl}\,\mathrm{dS}.$$

The quantity ψ is considered as a piecewise continuous function with (continuous) values ϕ_k at V_k, thus, we define the difference $\psi_k - \psi_l$ at $x \in \Sigma_{kl}$ as the jump bracket:

$$[\![\psi(x)]\!]_l^k := (\psi_k^+ - \psi_l^-)_{|x\in\Sigma_{kl}} = \lim_{\lambda\to 0^+}(\psi_k(x+\lambda\mathbf{n}_{kl}(x)) - \psi_l(x+\lambda\mathbf{n}_{lk}(x))). \tag{A.5}$$

Consequently, the transport theorem (A.4) may be written as

$$\begin{aligned}\frac{\mathrm{d}}{\mathrm{d}t}\int_V \psi \,\mathrm{dV} &= \int_V \frac{\partial \psi}{\partial t}\,\mathrm{dV} + \int_{\partial V} \psi\mathbf{v}\cdot\mathbf{n}\,\mathrm{dS} - \int_\Sigma [\![\psi]\!]^{\Sigma}\mathbf{v}\cdot\mathbf{n} \\ &= \sum_{k=1}^{m}\int_{V_k} \frac{\partial \psi_k}{\partial t}\,\mathrm{dV} + \sum_{k=1}^{m}\int_{\Sigma_{k0}} \psi_k\mathbf{v}_k\cdot\mathbf{n}\,\mathrm{dS} - \sum_{k=1}^{m-1}\sum_{l=k+1}^{m}\int_{\Sigma_{kl}} [\![\psi]\!]_l^{k\Sigma}\mathbf{v}_{kl}\cdot\mathbf{n}.\end{aligned} \tag{A.6}$$

The version for the k-th phase, denoting the interface area of the k-th phase $\Sigma_k := \sum_{\substack{l=1\\ l\neq k}}^{m} \Sigma_{kl}\cap V_k$, follows

$$\frac{\mathrm{d}}{\mathrm{d}t}\int_{V_k} \psi_k \,\mathrm{dV} = \int_{V_k} \frac{\partial \psi_k}{\partial t}\,\mathrm{dV} + \int_{\Sigma_{k0}} \psi_k\mathbf{v}_k\cdot\mathbf{n}\,\mathrm{dS} - \int_{\Sigma_k} \psi_k{}^{\Sigma}\mathbf{v}\cdot\mathbf{n}. \tag{A.7}$$

Transport theorem for surface quantities: We introduce the *generalized transport theorem for a surface* as:

$$\frac{\mathrm{d}^\Sigma}{\mathrm{d}t}\int_{\Sigma(t)}\rho^\Sigma\psi^\Sigma\,\mathrm{dS} = \int_{\Sigma(t)}\frac{\mathrm{d}^\Sigma\rho^\Sigma\psi^\Sigma}{\mathrm{d}t} + \rho^\Sigma\psi^\Sigma\,\mathrm{div}^\Sigma\,{}^\Sigma\mathbf{v}\,\mathrm{dS} \tag{A.8a}$$

$$= \int_{\Sigma(t)}\frac{\partial\rho^\Sigma\psi^\Sigma}{\partial t} - \nabla^\Sigma\rho^\Sigma\psi^\Sigma\cdot\mathbf{u} + \mathrm{div}^\Sigma(\rho^\Sigma\psi^{\Sigma\Sigma}\mathbf{v})\,\mathrm{dS}$$

$$= \int_{\Sigma(t)}\frac{\partial\rho^\Sigma\psi^\Sigma}{\partial t} - \nabla^\Sigma\rho^\Sigma\psi^\Sigma\cdot\mathbf{u} - 2H\rho^\Sigma\psi^{\Sigma\Sigma}\mathbf{v}\cdot\mathbf{n}\,\mathrm{dS} + \int_{C^{cl}}\rho^\Sigma\psi^\Sigma\mathbf{u}\cdot\mathbf{n}^\Sigma\,\mathrm{dl}. \tag{A.8a*}$$

Here, we exploit the *surface divergence theorem*, cf. Slaterry 2007 [98, A.6.3]

$$\int_\Sigma\mathrm{div}^\Sigma(\rho^\Sigma\psi^{\Sigma\Sigma}\mathbf{v}) = \int_{C^{cl}}\rho^\Sigma\psi^\Sigma\mathbf{u}\cdot\mathbf{n}^\Sigma\,\mathrm{dl} - \int_\Sigma 2H\rho^\Sigma\psi^{\Sigma\Sigma}\mathbf{v}\cdot\mathbf{n}\,\mathrm{dS} \tag{A.9}$$

which uses the velocity decomposition (A.1.2) and the relation for the mean curvature H in [3]

$$\mathrm{div}^\Sigma\,\mathbf{n}^\Sigma = -2H.$$

For a general flux $\mathbf{J}$ (possibly both convective and diffusive), we introduce the *Gauss rule*, (divergence theorem for a control volume containing an interface) as:

$$\int_{V(t)}\mathrm{div}\,\mathbf{J}\,\mathrm{dV} = \int_{\partial V(t)}\mathbf{J}\cdot\mathbf{n}\,\mathrm{dS} + \int_\Sigma\mathbf{J}\cdot\mathbf{n}\,\mathrm{dS}. \tag{A.10}$$

Treating immiscible phases, we can choose the control volume $V(t)$ such that it consists none but one single phase, hence, the interface Σ becomes a part of the boundary $\partial V(t)$. Combining the Leibnitz theorem and Gauss rule (for $\mathbf{J}\equiv\rho\psi\mathbf{v}$), we arrive to the *transport theorem for a region where the closing control volume surface partly consists of a non-material phase interface* in the form:

$$\frac{\mathrm{d}}{\mathrm{d}t}\int_{V(t)}\rho\psi\,\mathrm{dV} = \int_{V(t)}\left(\frac{\partial\rho\psi}{\partial t} + \mathrm{div}\,\rho\psi\mathbf{v}\right)\mathrm{dV} + \int_{\Sigma(t)}\rho\psi({}^\Sigma\mathbf{v}-\mathbf{v})\cdot\mathbf{n}\,\mathrm{dS}. \tag{A.11}$$

A.2.2 Generic balance equations

Integral balances: Let us consider an intensive quantity ψ with the density ρ, its (non-convective) flux $\mathbf{J}$ and the source terms R with density ρ_R. The *governing balance equation in the generic form* for a time dependent control volume $V(t)$ read as

$$\frac{\mathrm{d}}{\mathrm{d}t}\int_{V(t)}\rho\psi\,\mathrm{dV} = -\int_{\partial V(t)}\mathbf{J}\cdot\mathbf{n}\,\mathrm{dS} + \int_{V(t)}R\,\mathrm{dV}. \tag{A.12}$$

Considering a multi-phase body with the (non-material) 2D dividing surfaces as in fig. (A.18), we may write

$$\frac{\mathrm{d}}{\mathrm{d}t}\int_{V(t)}\rho\psi\,\mathrm{dV} = \frac{\mathrm{d}}{\mathrm{d}t}\int_{V(t)}\rho\psi\,\mathrm{dV} + \frac{\mathrm{d}^\Sigma}{\mathrm{d}t}\int_{\Sigma(t)}\rho^\Sigma\psi^\Sigma\,\mathrm{dS} \tag{A.13a}$$

$$-\int_{\partial V(t)}\mathbf{J}\cdot\mathbf{n}\,\mathrm{dS} = -\int_{\partial V(t)}\mathbf{J}\cdot\mathbf{n}\,\mathrm{dS} - \int_{C^{cl}(t)}\mathbf{J}^\Sigma\cdot\mathbf{n}^\Sigma\,\mathrm{dl} \tag{A.13b}$$

$$\int_{V(t)}R\,\mathrm{dV} = \int_{V(t)}R^V\,\mathrm{dV} + \int_{\Sigma(t)}R^\Sigma\,\mathrm{dS} \tag{A.13c}$$

where $\mathbf{n}^\Sigma$ is a normal vector to the common line C^{cl} and tangential to Σ and $\mathbf{J}^\Sigma$ is the interfacial flux. Consequently, the balance equation for multi-phase body containing dividing surface (A.12) adopts the form

$$\frac{\mathrm{d}}{\mathrm{d}t}\int_{V(t)}\rho\psi\,\mathrm{dV}+\frac{\mathrm{d}^\Sigma}{\mathrm{d}t}\int_{\Sigma(t)}\rho^\Sigma\psi^\Sigma\,\mathrm{dS}=-\int_{\partial V(t)}\mathbf{J}\cdot\mathbf{n}\,\mathrm{dS}-\int_{C^{cl}(t)}\mathbf{J}^\Sigma\cdot\mathbf{n}^\Sigma\,\mathrm{dl}\\+\int_{V(t)}R^V\,\mathrm{dV}+\int_{\Sigma(t)}R^\Sigma\,\mathrm{dS}. \tag{A.14}$$

In the next step, we split the interfacial flux $\mathbf{J}^\Sigma$ into isotropic part ς and the rest representing a vector flux:

$$\mathbf{J}^\Sigma=\varsigma\ +\boldsymbol{\zeta}.$$

Consequently, applying two different surface divergence theorems, cf. [28, 3.4] we obtain

$$\begin{aligned}\int_{C^{cl}(t)}\mathbf{J}^\Sigma\cdot\mathbf{n}^\Sigma\,\mathrm{dl}&=\int_{C^{cl}(t)}(\varsigma\ \cdot\mathbf{n}^\Sigma+\boldsymbol{\zeta}\cdot\mathbf{n}^\Sigma)\,\mathrm{dl}\\&=\int_{\Sigma(t)}\underbrace{(\nabla^\Sigma\varsigma+2H\varsigma\mathbf{n})+\mathrm{div}^\Sigma\boldsymbol{\zeta}}_{\mathrm{div}^\Sigma\mathbf{J}^\Sigma}\,\mathrm{dS}.\end{aligned} \tag{A.15}$$

Finally, using the transport theorems (A.11) and (A.8a) on the multi-phase balance equation (A.14) yields

$$\int_{V(t)}\left(\frac{\partial\rho\psi}{\partial t}+\mathrm{div}(\rho\psi\mathbf{v})+\mathrm{div}\,\mathbf{J}-R^V\right)\mathrm{dV} \tag{A.16}$$
$$+\int_{\Sigma(t)}\left(\frac{\mathrm{d}^\Sigma\rho^\Sigma\psi^\Sigma}{\mathrm{d}t}+\rho^\Sigma\psi^\Sigma\nabla^{\Sigma\Sigma}\mathbf{v}+\mathrm{div}^\Sigma\mathbf{J}^\Sigma-R^\Sigma-[\![(\psi\rho(\mathbf{v}-{}^\Sigma\mathbf{v})+\mathbf{J})\cdot\mathbf{n}]\!]\right)\mathrm{dS}=0.$$

We refer to (A.16) as the *integral balance for multi-phase body containing (non-intersecting) dividing surfaces.*

Local balances: Let us mention that the local version of the bulk and surface balance equation follows directly from the fact that the equation (A.2.2) holds for an arbitrary volume of the body. Therefore, we may introduce also the *integral balance for k^{th}-phase containing (non-intersecting) dividing surfaces*:

$$0=\int_{V_k(t)}\frac{\partial\rho_k\psi_k}{\partial t}+\mathrm{div}(\rho_k\psi_k\mathbf{v}_k)+\mathrm{div}\,\mathbf{J}_k-R_k^V\,\mathrm{dV} \tag{A.17a}$$
$$+\sum_{\substack{l=1\\l\neq k}}^{m}\int_{\Sigma_{kl}(t)}\frac{\mathrm{d}^\Sigma\rho_{kl}^\Sigma\psi_{kl}^\Sigma}{\mathrm{d}t}+\rho_{kl}^\Sigma\psi_{kl}^\Sigma\nabla^{\Sigma\Sigma}\mathbf{v}_{kl}+\mathrm{div}^\Sigma\mathbf{J}_{kl}^\Sigma-R_{kl}^\Sigma-[\![(\psi_i\rho_i(\mathbf{v}_i-{}^\Sigma\mathbf{v}_{kl})+\mathbf{J}_i)\cdot\mathbf{n}_i]\!]_l^k\,\mathrm{dS}.$$

The conservation of the quantities is, consequently, expressed in the following *local version of balance equations for k^{th}-phase containing (non-intersecting) dividing surfaces*:

$$\frac{\partial\rho_k\psi_k}{\partial t}+\mathrm{div}(\rho_k\psi_k\mathbf{v}_k)+\mathrm{div}\,\mathbf{J}_k=R_k^V\qquad\text{in } V_k \tag{A.18a}$$
$$\frac{\mathrm{d}^\Sigma\rho_{kl}^\Sigma\psi_{kl}^\Sigma}{\mathrm{d}t}+\rho_{kl}^\Sigma\psi_{kl}^\Sigma\,\mathrm{div}^\Sigma{}^\Sigma\mathbf{v}_{kl}+\mathrm{div}^\Sigma\mathbf{J}_{kl}^\Sigma=R_{kl}^\Sigma+[\![\dot{\boldsymbol{m}}_i^{kl}\psi_i+\mathbf{J}_i\cdot\mathbf{n}_i]\!]_l^k,\forall l\neq k\qquad\text{on }\Sigma \tag{A.18b}$$

where we denoted the specific mass transfer over the interface $\dot{\boldsymbol{m}}_i^{kl}=\rho_i(\mathbf{v}_i-{}^\Sigma\mathbf{v}_{kl})\cdot\mathbf{n}$.

Remarks:

A.2.1 Surface Tension. *In the momentum equation for a fluid/fluid interface, the molecular flux represents the interfacial stress force* ${}^{\Sigma}_{kl}$ *and the scalar* $\varsigma_{kl} = \sigma_{kl}$ *represents the surface tension of the interface between i-th and k-th phase. The application of the surface divergence theorem* (A.9) *gives the familiar result*

$$\int_{C^{cl}_{kl}} \mathbf{J}^{\Sigma}_{kl} \cdot \mathbf{n}^{\Sigma} \,\mathrm{dl} = \int_{C^{cl}_{kl}} {}^{\Sigma}_{kl} \cdot \mathbf{n}^{\Sigma} \,\mathrm{dl} = \int_{\Sigma_{kl}} (\nabla^{\Sigma}\sigma_{kl} + 2H_{kl}\,\sigma_{kl}\mathbf{n}) \,\mathrm{dS}. \tag{A.19}$$

A.2.3 Mass balance

The mass of a k-th phase occupying control volume V, where the boundary ∂V partly consists of an interface Σ, depends on a flux through the boundary and volumetric source terms:

$$\frac{\mathrm{d}}{\mathrm{d}t}\int_{V(t)} \rho_k \,\mathrm{dV} = -\int_{\partial V(t)} \mathbf{J}_k \cdot \mathbf{n} \,\mathrm{dS} + \int_{V(t)} R_k \,\mathrm{dV}. \tag{A.20}$$

The non-convective (diffusive) flux term $\mathbf{J}_k$ stands for molecular flux and the source term R_k represents chemical transformations contribution to the mass of k-th phase, e.g. chemical reactions and phase changes.

Speaking about chemical reactions, we usually distinguish homogeneous (in a bulk) and heterogeneous one (on a surface). Similarly, the phase change will be typically considered in the form of heterogeneous (R^{Σ}_k) or homogeneous (R^{V}_k) nucleation. Using previously derived theorem (A.18) substituting $\psi_k = 1, \psi^{\Sigma}_{kl} = 1$ and neglecting the molecular fluxes $\mathbf{J}_i$ and $\mathbf{J}^{\Sigma}_i$, we arrive to the following mass balance expression:

$$\frac{\partial \rho_k}{\partial t} + \mathrm{div}(\rho_k \mathbf{v}_k) = R^{V}_k \tag{A.21a}$$

$$\frac{\mathrm{d}^{\Sigma}\rho^{\Sigma}_{kl}}{\mathrm{d}t} + \rho^{\Sigma}_{kl}\,\mathrm{div}^{\Sigma}\,{}^{\Sigma}\mathbf{v}_{kl} = R^{\Sigma}_{kl} + [\![\dot{\boldsymbol{m}}^{kl}_i \cdot \mathbf{n}]\!]^k_l \qquad ,\forall l \neq k. \tag{A.21b}$$

A.2.4 Momentum balance

Total balance: According to the second Newton's law, the momentum of a body changes due to the acting forces which may be separated into two classes: *body forces* F^V and *contact forces* F^S:

$$\frac{\mathrm{d}}{\mathrm{d}t}\int_V \rho\mathbf{v} \,\mathrm{dV} = F^S + F^V.$$

The body forces act directly on each material particle. Defining $\mathbf{b}$ the density of body forces and ${}^{\Sigma}\mathbf{b}$ the density of surface forces, we express the body force action as

$$F^V = \int_V \rho\mathbf{b} \,\mathrm{dV} + \int_{\Sigma} \rho^{\Sigma\Sigma}\mathbf{b} \,\mathrm{dS}.$$

Within the particular application, we do not consider any electric or magnetic forces but the gravitation force and the momentum transfer force due to the mass production (e.g. chemical transformations). Consequently, we write

$$\mathbf{b}(\mathbf{z},t) = \mathbf{g} + R^{V}\mathbf{v}, \;\; {}^{\Sigma}\mathbf{b}(\mathbf{z},t) = \mathbf{g} + R^{\Sigma\Sigma}\mathbf{v}.$$

Contact forces, on the other hand, are those that appear to be exerted on one body or another through their common surface contact. Using the *Cauchy's stress principle*, we

identify the stress vector $\mathbf{t}(\mathbf{z}, S), S \in \Sigma$ with the vector valued function $\mathbf{t}(\mathbf{z}, \mathbf{n})$. This can be expressed as the transformation of the outer unit vector $\mathbf{n}$ by the stress tensor , cf. [102, p. 32]. Analogously, we proceed on the surface resulting into the common relation

$$F^S = \int_{\partial V} \cdot \mathbf{n} \, \mathrm{dS} + \int_{C^{cl}} {}^{\Sigma} \cdot \mathbf{n}^{\Sigma} \, \mathrm{dl}.$$

The *total momentum balance* (A.2.4), consequently, reads

$$\frac{\mathrm{d}}{\mathrm{d}t} \int_V \rho \mathbf{v} \, \mathrm{dV} = \int_{\partial V} \cdot \mathbf{n} \, \mathrm{dS} + \int_{C^{cl}} {}^{\Sigma} \cdot \mathbf{n}^{\Sigma} \, \mathrm{dl} + \int_V \rho \mathbf{b} \, \mathrm{dV} + \int_{\Sigma} \rho^{\Sigma\Sigma} \mathbf{b} \, \mathrm{dS}. \tag{A.22}$$

Partial balances: Additionally to the situation for a single phase, in the case of a multi-phase body one need to consider also momentum of a matter produced by chemical transformations. These contributions correspond to the term $R_k^V \mathbf{v}_k$ in the bulk or $R_{ij}^{\Sigma\Sigma} \mathbf{v}_i$ on the interface resulting in the overall momentum balance:

$$\begin{aligned} \frac{\mathrm{d}}{\mathrm{d}t} \int_V \rho \mathbf{v} \, \mathrm{dV} + \frac{\mathrm{d}^{\Sigma}}{\mathrm{d}t} \int_{\Sigma} \rho^{\Sigma\Sigma} \mathbf{v} \, \mathrm{dS} = \int_{\partial V} \cdot \mathbf{n} \, \mathrm{dS} + \int_{C^{cl}(t)} {}^{\Sigma} \cdot \mathbf{n}^{\Sigma} \, \mathrm{dl} \\ + \int_V \rho \mathbf{b} + R^V \mathbf{v} \, \mathrm{dV} + \int_{\Sigma} \rho^{\Sigma\Sigma} \mathbf{b} + R^{\Sigma\Sigma} \mathbf{v} \, \mathrm{dS}. \end{aligned} \tag{A.23}$$

In the next step, we apply the transport theorems (A.11) and (A.8a) obtaining the *multi-phase momentum balance*:

$$\begin{aligned} &\int_V \partial_t(\rho \mathbf{v}) + \mathrm{div}(\rho \mathbf{v} \otimes \mathbf{v}) \, \mathrm{dV} + \int_{\Sigma} \partial_t(\rho^{\Sigma\Sigma} \mathbf{v}) + \mathrm{div}^{\Sigma}(\rho^{\Sigma\Sigma} \mathbf{v} \otimes {}^{\Sigma}\mathbf{v}) \, \mathrm{dS} = \\ &\int_V \mathrm{div} \quad + \rho \mathbf{b} + R^V \mathbf{v} \, \mathrm{dV} + \int_{\Sigma} \mathrm{div}^{\Sigma} {}^{\Sigma} \quad + \rho^{\Sigma\Sigma} \mathbf{b} + R^{\Sigma\Sigma} \mathbf{v} + [\![\dot{\boldsymbol{m}} \otimes \mathbf{v} \cdot \mathbf{n}]\!] \, \mathrm{dS} \end{aligned} \tag{A.24}$$

where the outer product of vectors $a = (a_1, a_2, a_3)^T, b = (b_1, b_2, b_3)^T$ is defined as the matrix $a \otimes b = (a_i b_j)^{ij}$. Using the Green's transformations [102, p. 680]

$$\int_{\partial V} \cdot \mathbf{n} \, \mathrm{dS} = \int_V \mathrm{div} \quad \mathrm{dV} + \int_{\Sigma} [\![\cdot \mathbf{n}]\!],$$

we obtain for an arbitrary volume the *local multi-phase momentum balance* in the form:

$$\partial_t(\rho_k \mathbf{v}_k) + \mathrm{div}(\rho_k \mathbf{v}_k \otimes \mathbf{v}_k) = \mathrm{div} \quad {}_k + \rho_k \mathbf{b} + R_k^V \mathbf{v}_k \tag{A.25a}$$

$$\begin{aligned} \partial_t(\rho_{kl}^{\Sigma\Sigma} \mathbf{v}_{kl}) + \mathrm{div}^{\Sigma}(\rho_{kl}^{\Sigma\Sigma} \mathbf{v}_{kl} \otimes {}^{\Sigma}\mathbf{v}_{kl}) = \mathrm{div}^{\Sigma} {}^{\Sigma} \quad {}_{kl} + \rho_{kl}^{\Sigma\Sigma} \mathbf{b} + R_{kl}^{\Sigma\Sigma} \mathbf{v}_{kl} \\ + [\![\left(\dot{\boldsymbol{m}}_i^{kl} \otimes \mathbf{v}_i + \quad {}_i \right) \cdot \mathbf{n}_i]\!]_l^k. \end{aligned} \tag{A.25b}$$

Angular momentum balance: In this work, we restrict ourself to non-polar multi-fluid systems which we assumed to be irrotational. Then, we obtain the standard symmetric relation

$$\begin{aligned} {}_k &= (\quad {}_k)^T, \ \forall k \\ {}^{\Sigma} \quad {}_{kl} &= ({}^{\Sigma} \quad {}_{kl})^T, \ \forall i \neq k. \end{aligned}$$

A.3 Averaging procedure

In this section we recall some basic volume averaging theorems which are essential for derivation of transport equation for the multi-phase body. For more details see refer to [98, 1.3] or [48, 3.4].

A.3.1 Leignitz and Gauss rule

To average a time derivative, the Leibniz rule which can be understand as a transport equation for an averaged quantity ψ_k and its density ρ_k follows

$$\begin{aligned}\frac{1}{V}\int_V \frac{\partial \rho\psi}{\partial t}\,\mathrm{dV} &= \sum_k \left(\frac{1}{V}\int_{V_k}\frac{\partial \rho_k\psi_k}{\partial t}\,\mathrm{dV}\right)\\ &= \sum_k\left(\frac{\partial}{\partial t}\left(\frac{1}{V}\int_{V_k}\rho_k\psi_k\,\mathrm{dV}\right)\right) - A_{\Sigma_k l}\frac{1}{\Sigma_{kl}}\int_{\Sigma_{kl}}[\![\rho_i\psi_i{}^{\Sigma}\mathbf{v}_{kl}\cdot\mathbf{n}_i]\!]_l^k\,\mathrm{dS}.\end{aligned} \tag{A.26}$$

Now, we identify the interfacial area density $A_{\Sigma_{kl}} = \Sigma_{kl}/V$ and as an analogy to the volume averiging, we may define the interface averaging as

$$\langle\psi_{kl}^{\Sigma}\rangle_{\Sigma_{kl}} \overset{def}{=} \frac{1}{\Sigma_{kl}}\int_{\Sigma_{kl}}\psi_{kl}^{\Sigma}\,\mathrm{dS}. \tag{A.27}$$

Since the averaging volume is arbitrary, we can choose a volume containing a single phase only, i.e.

$$V = V_k,\ \partial V_k = \Sigma_k = \sum_{l=1,l\neq k}^{m}\Sigma_{kl}\cap V_k$$

and the Leibnitz rule gives

$$\left\langle\frac{\partial\rho_k\psi_k}{\partial t}\right\rangle_V = \frac{\partial}{\partial t}\langle\rho_k\psi_k\rangle_V - A_{\Sigma_k}\langle\rho_k\psi_k{}^{\Sigma}\mathbf{v}_{kl}\cdot\mathbf{n}_k\rangle_{\Sigma_{kl}}. \tag{A.28}$$

In the next, we introduce the *Gauss rule for volume averaging* as

$$\langle\nabla(\rho_k\psi_k)\rangle_V = \nabla\langle\rho_k\psi_k\rangle_V + \frac{1}{V}\int_{\Sigma_k}\rho_k\psi_k\mathbf{n}_k\,\mathrm{dS}.$$

Applied on the divergence operator, we obtain

$$\langle\mathrm{div}(\rho_k\psi_k\mathbf{v}_k)\rangle_V = \mathrm{div}\langle\rho_k\psi_k\mathbf{v}_k\rangle_V + \frac{1}{V}\int_{\Sigma_k}\rho_k\psi_k\mathbf{v}_k\cdot\mathbf{n}_k\,\mathrm{dS}.$$

The direct consequence of the two rules acting on the volume fraction ϕ_k reads

$$0 = \frac{\partial\phi_k}{\partial t} - \frac{1}{V}\int_{\Sigma_k}{}^{\Sigma}\mathbf{v}_{kl}\cdot\mathbf{n}_k\,\mathrm{dS}. \tag{A.29a}$$

$$0 = \nabla\phi_k + \frac{1}{V}\int_{\Sigma_k}\mathbf{n}_k\,\mathrm{dS}. \tag{A.29b}$$

A.3.2 Transport equation for an averaged quantity

Using the notation $\dot{\boldsymbol{m}}_i^{kl} \overset{def}{=} \rho_i({}^{\Sigma}\mathbf{v}_{kl} - \mathbf{v}_i)$, the transport theorem (A.11) for an averaged quantity follows

$$\left\langle \frac{\mathrm{D}(\rho_k\psi_k)}{\mathrm{D}t} \right\rangle_V = \frac{\mathrm{D}}{\mathrm{D}t}\langle\rho_k\psi_k\rangle_V + \sum_{\substack{l=1\\l\neq k}}^{m} A_{\Sigma_{kl}}\langle\dot{\boldsymbol{m}}_k^{kl}\psi_k\cdot\mathbf{n}\rangle_{\Sigma_{kl}}.$$

Applying the averaging to the local version of generic equation in bulk (A.18a), we obtain

$$\frac{\partial\langle\rho_k\psi_k\rangle_V}{\partial t} + \operatorname{div}\left(\langle\rho_k\psi_k\mathbf{v}_k\rho_k\psi_k\rangle_V\right) + \langle\operatorname{div}\mathbf{J}_k\rangle_V = \langle R_k\rangle_V - \sum_{\substack{l=1\\l\neq k}}^{m} A_{\Sigma_{kl}}\langle(\dot{\boldsymbol{m}}_k^{kl}\psi_k + \mathbf{J}_k)\cdot\mathbf{n}\rangle_{\Sigma_{kl}}$$

and, using the concept of volume fraction together the relations (A.29a) and (A.29b), we, finally receive the *transport equation for the k^{th}-phase* as

$$\begin{aligned}\frac{\partial(\phi_k\langle\rho_k\psi_k\rangle_{V_k})}{\partial t} &+ \operatorname{div}(\phi_k\langle\rho_k\mathbf{v}_k\psi_k\rangle_{V_k}) + \operatorname{div}(\phi_k\langle\mathbf{J}_k\rangle_{V_k})\\ &= \phi_k\langle R_k\rangle_{V_k} - \sum_{\substack{l=1\\l\neq k}}^{m} A_{\Sigma_{kl}}\langle(\dot{\boldsymbol{m}}_k^{kl}\psi_k + \mathbf{J}_k)\cdot\mathbf{n}\rangle_{\Sigma_{kl}}.\end{aligned} \tag{A.30}$$

Let us introduce also a version for vectorial quantity $\boldsymbol{\psi}_k$, where $\mathbf{J}_k$ denotes a (diffusive flux) tensor:

$$\begin{aligned}\frac{\partial(\phi_k\langle\rho_k\boldsymbol{\psi}_k\rangle_{V_k})}{\partial t} &+ \operatorname{div}(\phi_k\langle\rho_k\mathbf{v}_k\otimes\boldsymbol{\psi}_k\rangle_{V_k}) + \operatorname{div}(\phi_k\langle\mathbf{J}_k\rangle_{V_k})\\ &= \phi_k\langle R_k\rangle_{V_k} - \sum_{\substack{l=1\\l\neq k}}^{m} A_{\Sigma_{kl}}\langle(\dot{\boldsymbol{m}}_k^{kl}\otimes\boldsymbol{\psi}_k + \mathbf{J}_k)\cdot\mathbf{n}\rangle_{\Sigma_{kl}}.\end{aligned} \tag{A.31}$$

Part II

A continuum model of heterogeneous catalysis: thermodynamic framework for multicomponent bulk and surface phenomena coupled by sorption

5. Introduction

The second part of the thesis is a preprint of the same name article by O. Souček, V.O., J. Málek and D. Bothe which is under review in the International Journal of Engineering Science.

5.1 Active surfaces

5.1.1 Heterogeneous catalysis on active surfaces

Catalysis stands for the increase in the rate of chemical reactions caused by presence of an additional agent called catalyst. As such, catalysis plays a critical role in physical and biological sciences, chemical technology and industry. Some of the most important applications can be found for example in reduction of atmospheric pollution, in laboratory chemical syntheses, in petrochemistry, in the development of new ways of energy generation and storage such as chemical conversion of hydrocarbons, and in a plethora of other areas. A *heterogeneous* catalysis is a form of catalysis when the phases of the reactants and the catalyst differ - a prototypical example is a mixture of a gaseous or fluid substances (reactants) adsorbing onto a solid surface (catalyst). There, thanks to a reduction of the energetic barriers by the presence of the catalyst, reactions among the reactants take place much faster than elsewhere. The description and macroscopic modelling of the process of heterogeneous catalysis is an interdisciplinary task combining surface solid-state physics, physical chemistry, material science and, by interaction of the surface with the bulk, also all the field of continuum thermodynamics.

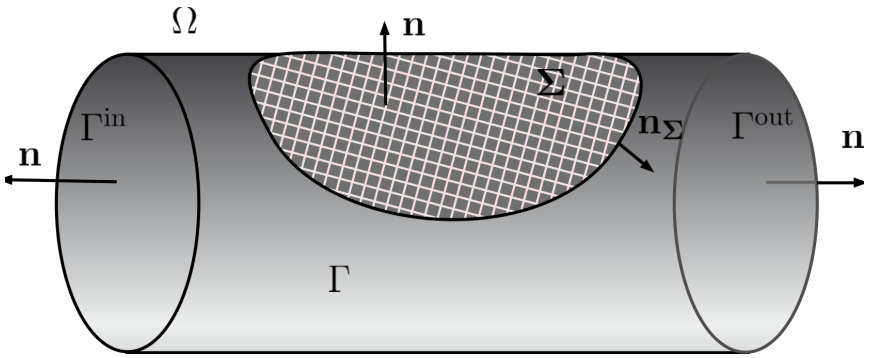

Figure 5.1: Sketch of the typical problem geometry depicting the bulk region of the mixture Ω with a boundary $\partial\Omega = \Sigma \cup \Gamma \cup \Gamma^{\text{in}} \cup \Gamma^{\text{out}}$, where Γ^{in} denotes the inflow part of the boundary, Γ^{out} denotes the outflow part of the boundary and Σ is the active surface at which sorption, surface chemical reactions and transport phenomena take place.

The aim of this paper is to formulate a continuum thermodynamical model describing heterogeneous catalysis of a gas/liquid mixture on a (solid) active surface. On such a surface the catalyzed chemical reactions together with other transport phenomena, such as diffusion of species, may occur. The model is formulated in the framework of phenomenological multi-component continuum thermodynamics applied to both bulk and surface processes and includes their mutual coupling. The prototypical geometry of the problem, relevant

for practical applications of heterogeneous catalysis, is sketched in Fig. 5.1. The domain contains a bulk region Ω with boundary $\partial\Omega$ containing an active (catalytic) subregion Σ.

Our modelling approach benefits from a simplified framework of the theory of interacting continua (theory of mixtures) in which the individual constituents of the mixture are distinguished only at the level of mass balances while the balance equations for linear and angular momentum, energy and entropy are considered for the mixture as a whole[1]. The essential physical processes captured by the model are (i) surface and bulk flow dynamics, (ii) surface and bulk energy transfer, (iii) energy transfer between the active surface and the bulk, (iv) surface and bulk chemical reactions, (v) sorption, that is transfer of mass between the active surface and the bulk, and (vi) surface and bulk diffusion. For all the surface quantities, we implicitly follow the notion of surface excess introduced by [33]; in this respect we follow the long-list of standard references in the field of continuum mechanics and thermodynamics of coupled interfacial and bulk phenomena, such as [7, 27, 80, 32, 97].

The constitutive theory for bulk and surface dissipative processes is obtained through the following thermodynamic procedure: (i) we postulate constitutive equations for bulk and surface free energies, (ii) we identify the entropy-producing mechanisms and (iii) we propose the constitutive relations which enforce the fulfilment of the second law of thermodynamics. For most entropy-producing processes, we confine ourselves to linear constitutive relations [i.e. we incorporate the framework of the classical irreversible thermodynamics - CIT - 23] with the exception of chemical reactions and sorption. For these processes non-linear logarithmic constitutive relations are postulated, which lead to standard chemical and sorption kinetics. For simplicity the Helmholtz potential in the bulk is considered in ideal-mixture form and the thermodynamic description of the surface corresponds to a simple lattice gas model. This gives rise to a Langmuir-type sorption kinetics [56], however, the developed framework allows a straightforward extension for much more involved sorption phenomena that have been studied in the past decades and involve multi-site adsorption and nearest neighbour interactions of the adsorbed species, among other features. See for example [85, 25, 64, 1] and references therein for an overview.

From this point of view, the framework should serve as a guideline for researchers interested in application of the rich and still rapidly developing field of statistical mechanics of adsorption to continuum mechanics and thermodynamic framework that is suitable for mathematical analysis and numerical implementation for practical calculations.

The structure of the paper is as follows. In Section 2, we introduce the notation and postulate the balance equations in the bulk and on the active surface. In Sections 3 and 4, the corresponding constitutive relations are proposed by means of irreversible thermodynamics. In Section 5, we summarize the derived model in the form that may serve as a starting point either for numerical implementation or mathematical analysis.

5.1.2 Notation and basic definitions

Our model comprises a fluid mixture consisting of N-1 chemical constituents reacting (or interacting) in a solvent (N-th constituent), i.e. we distinguish

- the constituents A_α in Ω, $\alpha \in \{1, \dots, N\} \stackrel{\text{def}}{=} K$, (bulk constituents)
- the constituents ${}^{\Sigma}\mathrm{A}_\alpha$ on Σ, $\alpha \in \{0, 1, \dots, N\} \stackrel{\text{def}}{=} K_0$, (surface constituents)

[1] If we use the terminology introduced in [45], we could call this framework Class-I mixture.

where the constituents A_N and ${}^{\Sigma}\mathrm{A}_N$ denote the solvent constituent and the formally added constituent ${}^{\Sigma}\mathrm{A}_0$ (introduced only on the surface Σ) represents the empty adsorption sites (vacancies). Note that ${}^{\Sigma}\mathrm{A}_0$ is by definition massless, but it can be sensibly assigned a molar number and all other molar-based quantities such as molar concentration, molar fraction, molar energy, etc. While we apriori assume that all bulk molecules can adsorb (i.e. all bulk constituents have their surface counterparts), we later provide a mechanism how to distinguish between adsorbing and non-adsorbing species, see a remark in the part on sorption in Section 7.2.3.

Let us consider a volume element of the mixture with the volume V and a surface element with the surface area S. We introduce the following measures: $N_\alpha(V)$ - denoting the number of moles of the constituent A_α in the given volume element V; and ${}^{\Sigma}N_\alpha(S)$ - the number of moles of the constituent ${}^{\Sigma}\mathrm{A}_\alpha$ on the surface element S, respectively. Assuming absolute continuity of these measures with respect to the corresponding volume and surface measures, we obtain the bulk and surface molar concentrations c_α^{M}, ${}^{\Sigma}c_\alpha^{\mathrm{M}}$, as follows:

$$N_\alpha(V) \stackrel{\mathrm{def}}{=} \int_V c_\alpha^{\mathrm{M}} dx \ , \qquad \alpha \in K \ , \tag{5.1a}$$

$${}^{\Sigma}N_\alpha(S) \stackrel{\mathrm{def}}{=} \int_S {}^{\Sigma}c_\alpha^{\mathrm{M}} dS \ , \qquad \alpha \in K_0 \ . \tag{5.1b}$$

The bulk molar concentration c^{M} of the mixture as a whole and its surface counterpart[2] ${}^{\Sigma}c^{\mathrm{M}}$ are, consequently, defined by

$$c^{\mathrm{M}} \stackrel{\mathrm{def}}{=} \sum_{\alpha \in K} c_\alpha^{\mathrm{M}} \ , \qquad {}^{\Sigma}c^{\mathrm{M}} \stackrel{\mathrm{def}}{=} \sum_{\alpha \in K_0} {}^{\Sigma}c_\alpha^{\mathrm{M}} \ . \tag{5.2}$$

This allows us to introduce the bulk and surface molar fractions x_α, ${}^{\Sigma}x_\alpha$ by

$$x_\alpha \stackrel{\mathrm{def}}{=} \frac{c_\alpha^{\mathrm{M}}}{c^{\mathrm{M}}} \ , \qquad \alpha \in K \ , \qquad {}^{\Sigma}x_\alpha \stackrel{\mathrm{def}}{=} \frac{{}^{\Sigma}c_\alpha^{\mathrm{M}}}{{}^{\Sigma}c^{\mathrm{M}}} \ , \qquad \alpha \in K_0 \ . \tag{5.3}$$

Introducing the molar mass M_α of the αth constituent (the same for both bulk and surface molecules), and postulating for the vacancies $M_0 \stackrel{\mathrm{def}}{=} 0$, we define the bulk and surface densities ρ_α and ρ_α^Σ as follows

$$\rho_\alpha \stackrel{\mathrm{def}}{=} c_\alpha^{\mathrm{M}} M_\alpha \ , \qquad \alpha \in K \ , \tag{5.4a}$$

$$\rho_\alpha^\Sigma \stackrel{\mathrm{def}}{=} {}^{\Sigma}c_\alpha^{\mathrm{M}} M_\alpha \ , \qquad \alpha \in K_0 \ . \tag{5.4b}$$

The bulk and surface mixture densities of the mixture as a whole are defined as follows

$$\rho \stackrel{\mathrm{def}}{=} \sum_{\alpha \in K} \rho_\alpha \ , \qquad \rho^\Sigma \stackrel{\mathrm{def}}{=} \sum_{\alpha \in K_0} \rho_\alpha^\Sigma \ , \tag{5.5}$$

and the mass fractions (concentrations) c_α, ${}^{\Sigma}c_\alpha$ are defined by

$$c_\alpha \stackrel{\mathrm{def}}{=} \frac{\rho_\alpha}{\rho} \ , \qquad \alpha \in K, \qquad {}^{\Sigma}c_\alpha \stackrel{\mathrm{def}}{=} \frac{\rho_\alpha^\Sigma}{\rho^\Sigma} \ , \qquad \alpha \in K_0 \ . \tag{5.6}$$

To each constituent we assign their bulk and surface velocities $\mathbf{v}_\alpha$ and ${}^{\Sigma}\mathbf{v}_\alpha$, respectively. The mixture bulk and surface velocities $\mathbf{v}$ and ${}^{\Sigma}\mathbf{v}$ are defined here as the corresponding barycentric velocities

$$\rho \mathbf{v} \stackrel{\mathrm{def}}{=} \sum_{\alpha \in K} \rho_\alpha \mathbf{v}_\alpha \ , \qquad \rho^{\Sigma\Sigma}\mathbf{v} \stackrel{\mathrm{def}}{=} \sum_{\alpha \in K_0} \rho_\alpha^{\Sigma\Sigma} \mathbf{v}_\alpha \ . \tag{5.7}$$

[2]The quantity ${}^{\Sigma}c^{\mathrm{M}}$ represents in fact the surface molar concentration of adsorption sites, see B.142.

We proceed by formulating balance equations - balances of mass, linear and angular momentum, energy and entropy - both in the bulk Ω and on the active surface Σ.

In this study, we distinguish the individual constituents of the mixture only at the level of mass balances. Concerning the balances of momentum, angular momentum, energy and entropy, the mixture is treated as a standard single-component continuum.

6. Balance equations

6.1 Balance of mass

6.1.1 Balances of partial masses

Bulk:

The mass balance of the α-th constituent inside the domain Ω reads as follows

$$\frac{\partial \rho_\alpha}{\partial t} + \operatorname{div}\left(\rho_\alpha \mathbf{v} + \mathbf{J}_\alpha^{\text{diff}}\right) = r_\alpha \ , \qquad \alpha \in K \ , \tag{6.1}$$

where r_α is the chemical production rate of the αth constituent and $\mathbf{J}_\alpha^{\text{diff}}$ is the diffusive flux of the αth constituent defined as $\mathbf{J}_\alpha^{\text{diff}} \overset{\text{def}}{=} \rho_\alpha(\mathbf{v}_\alpha - \mathbf{v})$, but modelled via a constitutive relation since, in this study, the individual velocities of the species are not distinguished in the balance equations. The above definition however leads to the following constraint (due to (5.5) and (5.7)):

$$\sum_{\alpha \in K} \mathbf{J}_\alpha^{\text{diff}} = \mathbf{0} \ . \tag{6.2}$$

Conservation of mass in the chemical reactions dictates the following constraint on the reaction rates:

$$\sum_{\alpha \in K} r_\alpha = 0 \iff \frac{\partial \rho}{\partial t} + \operatorname{div}(\rho \mathbf{v}) = 0 \iff \dot{\rho} = -\rho \operatorname{div} \mathbf{v} \ , \tag{6.3}$$

where we used the definitions (5.5) and (5.7) and the constraint (6.2), yielding the mass balance for the mixture as a whole. In the last form of the mass balance, we introduced the dot operator denoting the material time derivative with respect to the barycentric velocity $\dot{(\,)} \overset{\text{def}}{=} \frac{\partial (\,)}{\partial t} + \mathbf{v} \cdot \nabla(\,)$.

Surface:

The boundary of Ω and thus also the active surface Σ are assumed to be static in our application, in particular we assume that ${}^{\Sigma}\mathbf{v} \cdot \mathbf{n} = 0$. The surface velocities ${}^{\Sigma}\mathbf{v}_\alpha$ are therefore assumed to be tangential, i.e. ${}^{\Sigma}\mathbf{v}_\alpha \cdot \mathbf{n} = 0$, $\alpha \in K$. It should be noted that everywhere in the text where terms $\mathbf{v} \cdot \mathbf{n}$ or $\mathbf{v}_\alpha \cdot \mathbf{n}$ appear, they in fact stand for $(\mathbf{v} - {}^{\Sigma}\mathbf{v}) \cdot \mathbf{n}$ and $(\mathbf{v}_\alpha - {}^{\Sigma}\mathbf{v}) \cdot \mathbf{n}$, which are frame-indifferent expressions. Under such an assumption[1], the surface balance of mass on Σ can be postulated as follows [97, Section 1.3.5]:

$$\frac{\partial \rho_\alpha^\Sigma}{\partial t} + \operatorname{div}^\Sigma\left(\rho_\alpha^\Sigma {}^{\Sigma}\mathbf{v} + {}^{\Sigma}\mathbf{J}_\alpha^{\text{diff}}\right) + [\![\rho_\alpha \mathbf{v}_\alpha]\!] \cdot \mathbf{n} = {}^{\Sigma}r_\alpha \ , \qquad \alpha \in K \ , \tag{6.4}$$

where $\operatorname{div}^\Sigma()$ is the surface divergence operator, the term ${}^{\Sigma}r_\alpha$ describes the chemical reaction production rate for the α-th constituent ${}^{\Sigma}\mathrm{A}_\alpha$, and ${}^{\Sigma}\mathbf{J}_\alpha^{\text{diff}} \overset{\text{def}}{=} \rho_\alpha^\Sigma({}^{\Sigma}\mathbf{v}_\alpha - {}^{\Sigma}\mathbf{v})$ are the surface diffusive fluxes (again modelled via a constitutive relation). The brackets $[\![\cdot]\!]$ denote the jump of the quantity (in the sense of traces) across Σ: $[\![\phi]\!] \overset{\text{def}}{=} {}^{+}\phi - {}^{-}\phi$, where the orientation is given by the (outer) unit normal $\mathbf{n}$ to the surface Σ, i.e. pointing "outside" from Ω, see

[1] This assumption allows to fix the spatial coordinate system y_α, and identify the *intrinsic* surface velocity with the surface velocity - see Section 1.2.7. in [97].

Fig. 5.1. The definitions (5.5) and (5.7) imply that the diffusive fluxes sum up to zero, i.e.

$$\sum_{\alpha\in K} {}^{\Sigma}\mathbf{J}_{\alpha}^{\mathrm{diff}} = \mathbf{0}\ , \tag{6.5}$$

and conservation of mass in the surface chemical reactions implies the constraint

$$\sum_{\alpha\in K} {}^{\Sigma}r_{\alpha} = 0 \iff \frac{\partial\,\rho^{\Sigma}}{\partial t} + \mathrm{div}^{\Sigma}\,(\rho^{\Sigma}\,{}^{\Sigma}\mathbf{v}) = -\,[\![\rho\mathbf{v}]\!]\cdot\mathbf{n} \iff \dot{\rho^{\Sigma}} = -\rho^{\Sigma}\,\mathrm{div}^{\Sigma}\,{}^{\Sigma}\mathbf{v} - [\![\rho\mathbf{v}]\!]\cdot\mathbf{n}\ , \tag{6.6}$$

where we used (5.5) and (5.7) to obtain the surface mass balance of the mixture as a whole. The operator $\dot{()}$ denotes the material time derivative with respect to the surface barycentric velocity $\dot{()} \overset{\mathrm{def}}{=} \frac{\partial()}{\partial t} + {}^{\Sigma}\mathbf{v}\cdot\nabla^{\Sigma}()$.

The bracketed term in eq. (6.4) corresponds to the mass flux of the αth constituent from the bulk to the surface Σ (or vice-versa), and thus describes the corresponding adsorption/desorption rates ${}^{\Sigma}s_{\alpha}$ defined as

$${}^{\pm}({}^{\Sigma}s_{\alpha}) \overset{\mathrm{def}}{=} \mp {}^{\pm}\rho_{\alpha}\,{}^{\pm}\mathbf{v}_{\alpha}\cdot\mathbf{n}\ , \qquad \alpha\in K\ . \tag{6.7}$$

The total sorption rate, which measures the total gain or loss of mass of the αth constituent is defined as

$${}^{\Sigma}s_{\alpha} \overset{\mathrm{def}}{=} {}^{-}({}^{\Sigma}s_{\alpha}) + {}^{+}({}^{\Sigma}s_{\alpha}) = -\,[\![\rho_{\alpha}\mathbf{v}_{\alpha}]\!]\cdot\mathbf{n}\ . \tag{6.8}$$

With this notation, the surface mass balance (6.4) takes the form

$$\frac{\partial\,\rho_{\alpha}^{\Sigma}}{\partial t} + \mathrm{div}^{\Sigma}\,(\rho_{\alpha}^{\Sigma}\,{}^{\Sigma}\mathbf{v} + {}^{\Sigma}\mathbf{J}_{\alpha}^{\mathrm{diff}}) = {}^{\Sigma}r_{\alpha} + {}^{\Sigma}s_{\alpha}\ , \qquad \alpha\in K\ . \tag{6.9}$$

Let us note that the structure of equation (6.4) corresponds to the structure of a general balance equation at a singular surface embedded in a bulk domain [see, for example 70, 97]. In our application, we need to treat all the jump terms with certain caution, especially whenever interpreting the terms with the "+" sign, which denote contributions from the outer side of the interface. In our model, the interface Σ of interest is in fact a subset of the outer boundary $\partial\Omega$, all the outward fluxes must therefore be specified in the form of boundary conditions. This is done is Section 6.4.

6.1.2 Molar balances

Using the relations (5.4), we can rewrite the bulk and surface mass balances (6.1) and (6.9) in terms of molar concentrations as follows:

Bulk:

$$\frac{\partial c_{\alpha}^{\mathrm{M}}}{\partial t} + \mathrm{div}\,(c_{\alpha}^{\mathrm{M}}\,\mathbf{v}) + \mathrm{div}\,\mathbf{J}_{\alpha}^{\mathrm{M,diff}} = r_{\alpha}^{\mathrm{M}} \iff \dot{c_{\alpha}^{\mathrm{M}}} = -c_{\alpha}^{\mathrm{M}}\,\mathrm{div}\,\mathbf{v} - \mathrm{div}\,\mathbf{J}_{\alpha}^{\mathrm{M,diff}} + r_{\alpha}^{\mathrm{M}}\ , \qquad \alpha\in K\ , \tag{6.10}$$

where the molar diffusive fluxes $\mathbf{J}_{\alpha}^{\mathrm{M,diff}}$ and molar reaction rates r_{α}^{M} are introduced in the following way

$$\mathbf{J}_{\alpha}^{\mathrm{M,diff}} \overset{\mathrm{def}}{=} \mathbf{J}_{\alpha}^{\mathrm{diff}} M_{\alpha}^{-1}\ , \qquad r_{\alpha}^{\mathrm{M}} \overset{\mathrm{def}}{=} r_{\alpha} M_{\alpha}^{-1}, \qquad \alpha\in K\ . \tag{6.11}$$

The constraints (6.2) and (6.3) can then be rewritten as

$$\sum_{\alpha\in K} M_{\alpha}\mathbf{J}_{\alpha}^{\mathrm{M,diff}} = \mathbf{0}\ , \qquad \text{and} \qquad \sum_{\alpha\in K} M_{\alpha} r_{\alpha}^{\mathrm{M}} = 0\ . \tag{6.12}$$

Surface:

$$\frac{\partial {}^{\Sigma}c_{\alpha}^{\mathrm{M}}}{\partial t} + \mathrm{div}^{\Sigma}\left({}^{\Sigma}c_{\alpha}^{\mathrm{M}}\,{}^{\Sigma}\mathbf{v}\right) + \mathrm{div}^{\Sigma}\,{}^{\Sigma}\mathbf{J}_{\alpha}^{\mathrm{M,diff}} = {}^{\Sigma}r_{\alpha}^{\mathrm{M}} + {}^{\Sigma}s_{\alpha}^{\mathrm{M}} \iff$$
$${}^{\Sigma}\dot{c}_{\alpha}^{\mathrm{M}} = -{}^{\Sigma}c_{\alpha}^{\mathrm{M}}\,\mathrm{div}^{\Sigma}\,{}^{\Sigma}\mathbf{v} - \mathrm{div}^{\Sigma}\,{}^{\Sigma}\mathbf{J}_{\alpha}^{\mathrm{M,diff}} + {}^{\Sigma}r_{\alpha}^{\mathrm{M}} + {}^{\Sigma}s_{\alpha}^{\mathrm{M}}\,, \qquad \alpha\in K\,, \tag{6.13}$$

where the surface molar diffusive fluxes ${}^{\Sigma}\mathbf{J}_{\alpha}^{\mathrm{M,diff}}$, molar sorption rates ${}^{\Sigma}s_{\alpha}^{\mathrm{M}}$ and molar production rates ${}^{\Sigma}r_{\alpha}^{\mathrm{M}}$ are defined as

$${}^{\Sigma}\mathbf{J}_{\alpha}^{\mathrm{M,diff}} \stackrel{\mathrm{def}}{=} {}^{\Sigma}\mathbf{J}_{\alpha}^{\mathrm{diff}} M_{\alpha}^{-1}\,, \qquad {}^{\Sigma}s_{\alpha}^{\mathrm{M}} \stackrel{\mathrm{def}}{=} {}^{\Sigma}s_{\alpha} M_{\alpha}^{-1}, \qquad {}^{\Sigma}r_{\alpha}^{\mathrm{M}} \stackrel{\mathrm{def}}{=} {}^{\Sigma}r_{\alpha} M_{\alpha}^{-1}\,, \qquad \alpha\in K\,. \tag{6.14}$$

The constraints (6.5) and (6.6) then read

$$\sum_{\alpha\in K} M_{\alpha}\,{}^{\Sigma}\mathbf{J}_{\alpha}^{\mathrm{M,diff}} = \mathbf{0}\,, \qquad \text{and} \qquad \sum_{\alpha\in K} M_{\alpha}\,{}^{\Sigma}r_{\alpha}^{\mathrm{M}} = 0\,. \tag{6.15}$$

Finally, note that the definitions (6.8) and (6.14), together with (5.7) imply that

$$\sum_{\alpha\in K} M_{\alpha}\,{}^{\Sigma}s_{\alpha}^{\mathrm{M}} = -\left[\!\left[\rho\mathbf{v}\right]\!\right]\cdot\mathbf{n}\,. \tag{6.16}$$

We extend the molar-based description of the surface processes to account also for the vacancies assuming that *neither diffusion nor chemical reactions/sorption affect the number of surface sites.* We postulate (compare with eq. (6.1.2)):

$$\frac{\partial {}^{\Sigma}c_{0}^{\mathrm{M}}}{\partial t} + \mathrm{div}^{\Sigma}\left({}^{\Sigma}c_{0}^{\mathrm{M}}\,{}^{\Sigma}\mathbf{v}\right) + \mathrm{div}^{\Sigma}\,{}^{\Sigma}\mathbf{J}_{0}^{\mathrm{M,diff}} = {}^{\Sigma}r_{0}^{\mathrm{M}} + {}^{\Sigma}s_{0}^{\mathrm{M}}\,, \tag{6.17}$$

defining ${}^{\Sigma}\mathbf{J}_{0}^{\mathrm{M,diff}}$, ${}^{\Sigma}r_{0}^{\mathrm{M}}$ and ${}^{\Sigma}s_{0}^{\mathrm{M}}$ through the following additional constraints:

$$\sum_{\alpha\in K_0} {}^{\Sigma}\mathbf{J}_{\alpha}^{\mathrm{M,diff}} = -{}^{\Sigma}c^{\mathrm{M}}\mathbf{v}^{\Sigma}\,, \qquad \sum_{\alpha\in K_0} {}^{\Sigma}s_{\alpha}^{\mathrm{M}} = 0\,, \qquad \sum_{\alpha\in K_0} {}^{\Sigma}r_{\alpha}^{\mathrm{M}} = 0\,, \tag{6.18}$$

where ${}^{\Sigma}c^{\mathrm{M}}$ is defined in (5.2). Adding the sum of (6.1.2) over $\alpha\in K$, to eq. (6.17), the above relations imply the following form of the balance of adsorption sites

$$\frac{\partial\,{}^{\Sigma}c^{\mathrm{M}}}{\partial t} = 0\,, \tag{6.19}$$

which implies that ${}^{\Sigma}c^{\mathrm{M}}({}^{\Sigma}\mathbf{x},t) = {}^{\Sigma}c^{\mathrm{M}}({}^{\Sigma}\mathbf{x},0) = {}^{\Sigma}c_{\mathrm{ini}}^{\mathrm{M}}({}^{\Sigma}\mathbf{x})$, for all $t\geq 0$ and for all ${}^{\Sigma}\mathbf{x}\in\Sigma$. In particular, assuming the initial distribution of adsorption sites to be uniform, i.e. asserting ${}^{\Sigma}c_{\mathrm{ini}}^{\mathrm{M}} = \text{constant} > 0$, we get

$${}^{\Sigma}c^{\mathrm{M}}({}^{\Sigma}\mathbf{x},t) = {}^{\Sigma}c_{\mathrm{ini}}^{\mathrm{M}} \in \mathbb{R}^{+}\,, \qquad \text{for all } t\geq 0, \text{and for all } {}^{\Sigma}\mathbf{x}\in\Sigma\,. \tag{6.20}$$

We relax this condition in the derivation of surface energetics in Section 7.2.1, allowing certain small compressibility in order to obtain sensible notions of quantities such as surface tension.

6.2 Balance of momentum

6.2.1 Balance of linear momentum

Bulk: Balance of linear momentum for the mixture as a whole is postulated in the standard form

$$\frac{\partial(\rho\mathbf{v})}{\partial t} + \operatorname{div}(\rho\mathbf{v}\otimes\mathbf{v}) = \operatorname{div}\mathbb{T} + \rho\mathbf{b}\ , \tag{6.21}$$

where $\mathbb{T}$ denotes the Cauchy stress tensor (specified by a constitutive relation) and $\mathbf{b}$ is the specific body force defined by

$$\rho\mathbf{b} \stackrel{\text{def}}{=} \sum_{\alpha\in K}\rho_\alpha\mathbf{b}_\alpha\ , \tag{6.22}$$

where $\mathbf{b}_\alpha$, $\alpha\in K$, are the specific body forces acting on individual bulk constituents. We decompose the Cauchy stress into a spherical part P (mean normal stress) and a traceless part $\mathbb{S}$

$$\mathrm{P} \stackrel{\text{def}}{=} \frac{1}{3}\operatorname{Tr}\mathbb{T}\ , \qquad \mathbb{S} \stackrel{\text{def}}{=} \mathbb{T} - \mathrm{P}\mathbb{I}\ , \tag{6.23}$$

where $\operatorname{Tr}\mathbb{A} \stackrel{\text{def}}{=} \sum_{k=1}^{3}\mathbb{A}_{kk}$ denotes the trace of a tensor $\mathbb{A}$.

Surface: The surface linear momentum balance on the active surface Σ (fixed in the sense ${}^{\Sigma}\mathbf{v}\cdot\mathbf{n}=0$) is postulated [97, Section 2.1.6] as follows

$$\frac{\partial(\rho^{\Sigma\Sigma}\mathbf{v})}{\partial t} + \operatorname{div}^{\Sigma}(\rho^{\Sigma\Sigma}\mathbf{v}\otimes{}^{\Sigma}\mathbf{v}) + [\![\rho\mathbf{v}\otimes\mathbf{v} - \mathbb{T}]\!]\,\mathbf{n} = \operatorname{div}^{\Sigma}{}^{\Sigma}\mathbb{T} + \rho^{\Sigma\Sigma}\mathbf{b}\ . \tag{6.24}$$

Here ${}^{\Sigma}\mathbb{T}$ denotes the surface Cauchy stress tensor, which we again decompose into its spherical and traceless parts

$${}^{\Sigma}\mathrm{P} \stackrel{\text{def}}{=} \frac{1}{2}\operatorname{Tr}{}^{\Sigma}\mathbb{T}\ , \qquad {}^{\Sigma}\mathbb{S} \stackrel{\text{def}}{=} {}^{\Sigma}\mathbb{T} - {}^{\Sigma}\mathrm{P}\,{}^{\Sigma}\mathbb{I}\ , \qquad {}^{\Sigma}\mathbb{I} \stackrel{\text{def}}{=} \mathbb{I} - \mathbf{n}\otimes\mathbf{n}\ , \tag{6.25}$$

and ${}^{\Sigma}\mathbf{b}$ is the specific density of surface forces defined by

$$\rho^{\Sigma\Sigma}\mathbf{b} \stackrel{\text{def}}{=} \sum_{\alpha\in K}\rho_\alpha^{\Sigma\Sigma}\mathbf{b}_\alpha\ , \tag{6.26}$$

where ${}^{\Sigma}\mathbf{b}_\alpha, \alpha\in K$, are the specific surface forces acting on individual surface constituents. Note that both the convective momentum flux and the Cauchy stress from outside the domain Ω must be specified as parts of the model boundary conditions, see Section 6.4.

6.2.2 Balance of angular momentum

We assume the mixture to be non-polar as a whole, consequently, the balance of angular momentum for the mixture as a whole reduces to the assumption of symmetry of the mixture Cauchy stress tensors [see 64, Section 4.5.3, for the surface angular momentum balance]:

$$\mathbb{T} = \mathbb{T}^{\mathrm{T}}\ , \qquad {}^{\Sigma}\mathbb{T} = {}^{\Sigma}\mathbb{T}^{\mathrm{T}}\ , \tag{6.27}$$

where the superscript ${}^{\mathrm{T}}$ denotes the transpose of a tensor.

6.3 Balance of energy

6.3.1 Balance of internal energy

Bulk: The balance of the total energy of the mixture as a whole is postulated in the standard single-component form extended for the power of body forces acting on the individual constituents of the mixture [e.g. 23, 64, Section 4.6.4]

$$\frac{\partial}{\partial t}\left(\rho(e+\frac{1}{2}|\mathbf{v}|^2)\right)+\operatorname{div}\left(\rho(e+\frac{1}{2}|\mathbf{v}|^2)\mathbf{v}\right)=-\operatorname{div}\mathbf{J}_e+\operatorname{div}(\mathbb{T}\mathbf{v})+\rho\mathbf{b}\cdot\mathbf{v}+\sum_{\alpha\in K}\mathbf{J}_\alpha^{\mathrm{M,diff}}\cdot\mathbf{b}_\alpha^{\mathrm{M}}+\mathrm{s}_e\ , \tag{6.28}$$

where e denotes the specific internal energy of the mixture, $\mathbf{J}_e$ denotes the bulk energy flux, $\mathbf{b}_\alpha^{\mathrm{M}}$ are defined as

$$\mathbf{b}_\alpha^{\mathrm{M}}\overset{\mathrm{def}}{=}M_\alpha\mathbf{b}_\alpha\ ,\qquad \alpha\in K\ , \tag{6.29}$$

and s_e represents the energy sources (e.g. due to radiation), which we set to zero for simplicity, i.e. we take $\mathrm{s}_e\equiv 0$. Note that if $\mathbf{b}_\alpha=\mathbf{b}$, $\alpha\in K$, then the term $\sum_{\alpha\in K}\mathbf{J}_\alpha^{\mathrm{diff}}\cdot\mathbf{b}_\alpha$ vanishes due to (6.2). With the use of (6.21), we can rewrite (6.28) in the reduced form of the internal energy balance

$$\rho\dot{e}=\mathbb{T}:\mathbb{D}-\operatorname{div}\mathbf{J}_e+\sum_{\alpha\in K}\mathbf{J}_\alpha^{\mathrm{diff}}\cdot\mathbf{b}_\alpha\ , \tag{6.30}$$

where $\mathbb{D}\overset{\mathrm{def}}{=}\frac{1}{2}(\nabla\mathbf{v}+(\nabla\mathbf{v})^{\mathrm{T}})$ denotes the symmetric part of the velocity gradient. Both the internal energy e and the energy flux $\mathbf{J}_e$ as well as $\mathbf{J}_\alpha^{\mathrm{diff}}$ are specified later by the constitutive relations.

Surface: The balance of total surface energy is postulated [97, Section 4.6.4] as follows

$$\begin{aligned}&\frac{\partial\left(\rho^\Sigma({}^\Sigma e+\frac{1}{2}|{}^\Sigma\mathbf{v}|^2)\right)}{\partial t}+\operatorname{div}^\Sigma\left(\rho^\Sigma({}^\Sigma e+\frac{1}{2}|{}^\Sigma\mathbf{v}|^2){}^\Sigma\mathbf{v}\right)-\operatorname{div}^\Sigma({}^\Sigma\mathbb{T}{}^\Sigma\mathbf{v})-\rho^{\Sigma\Sigma}\mathbf{v}\cdot{}^\Sigma\mathbf{b}\\&-\sum_{\alpha\in K}{}^\Sigma\mathbf{J}_\alpha^{\mathrm{M,diff}}\cdot{}^\Sigma\mathbf{b}_\alpha^{\mathrm{M}}+\operatorname{div}^\Sigma{}^\Sigma\mathbf{J}_e-{}^\Sigma\mathrm{s}_e+\left[\!\!\left[\rho(e+\frac{1}{2}|\mathbf{v}|^2)\mathbf{v}-\mathbf{v}\cdot\mathbb{T}+\mathbf{J}_e\right]\!\!\right]\cdot\mathbf{n}=0\ ,\end{aligned} \tag{6.31}$$

where ${}^\Sigma e$ denotes the surface specific internal energy, ${}^\Sigma\mathbf{J}_e$ is the surface energy flux, ${}^\Sigma\mathrm{s}_e$ are the energy sources and we introduced

$${}^\Sigma\mathbf{b}_\alpha^{\mathrm{M}}\overset{\mathrm{def}}{=}M_\alpha{}^\Sigma\mathbf{b}_\alpha\ ,\qquad \alpha\in K\ . \tag{6.32}$$

As in the bulk, we also set the energy sources equal to zero, i.e. ${}^\Sigma\mathrm{s}_e\equiv 0$. The reduced form (internal energy balance) can be derived from (6.31) by subtracting the kinetic energy balance (obtained from (6.24) by employing the mass balance (6.4) and multiplying by ${}^\Sigma\mathbf{v}$) leading to [97, Section 4.6.4]:

$$\begin{aligned}\rho^{\Sigma}\dot{{}^\Sigma e}=&\ {}^\Sigma\mathbb{T}:\nabla^{\Sigma\Sigma}\mathbf{v}+\sum_{\alpha\in K}{}^\Sigma\mathbf{J}_\alpha^{\mathrm{M,diff}}\cdot{}^\Sigma\mathbf{b}_\alpha^{\mathrm{M}}-\operatorname{div}^\Sigma{}^\Sigma\mathbf{J}_e\\&-\left[\!\!\left[\rho\left(e-{}^\Sigma e+\frac{1}{2}|\mathbf{v}-{}^\Sigma\mathbf{v}|^2\right)\mathbf{v}\right]\!\!\right]\cdot\mathbf{n}+[\![(\mathbf{v}-{}^\Sigma\mathbf{v})\cdot\mathbb{T}]\!]\,\mathbf{n}-[\![\mathbf{J}_e]\!]\cdot\mathbf{n}\ .\end{aligned} \tag{6.33}$$

6.3.2 Balance of entropy

Bulk: Balance of entropy for the mixture as a whole is postulated in the following standard single-component form [64, 4.7.3]:

$$\rho\dot{\eta} + \operatorname{div}\mathbf{J}_\eta - \mathrm{s}_\eta = \Pi_\eta \ \geq 0 \ , \tag{6.34}$$

where η denotes the specific bulk entropy, $\mathbf{J}_\eta$ denotes the entropy flux, s_η is the external entropy source and Π_η is the bulk entropy production, which is required to be non-negative in order to fulfil the second law of thermodynamics. The functional form of the entropy follows from the choice of the free energy, the constitutive procedure requires the identification of the entropy production and the entropy flux, see Section 7.1. Consistently with the assumption of zero energy sources used in the balance of energy, we omit in the following the external entropy sources in eq. (6.34) by setting $\mathrm{s}_\eta \equiv 0$.

Surface: The surface entropy balance is postulated [64, Section 4.7.3] as follows:

$$\rho^\Sigma \overset{\cdot}{{}^\Sigma\eta} + \operatorname{div}^\Sigma {}^\Sigma\mathbf{J}_\eta - {}^\Sigma\mathrm{s}_\eta + [\![\rho(\eta - {}^\Sigma\eta)\mathbf{v} + \mathbf{J}_\eta]\!] \cdot \mathbf{n} = {}^\Sigma\Pi_\eta \geq 0 \ , \tag{6.35}$$

where ${}^\Sigma\eta$ is the surface specific entropy, ${}^\Sigma\mathbf{J}_\eta$ is the surface entropy flux, ${}^\Sigma\mathrm{s}_\eta$ is the surface external entropy source (set to zero by an assumption ${}^\Sigma\mathrm{s}_\eta \equiv 0$) and ${}^\Sigma\Pi_\eta$ is the surface entropy production – non-negative in order to satisfy the second law of thermodynamics.

6.4 Boundary conditions

The system of balance equations in the bulk and at the active surface must be supplemented by suitable boundary conditions. In particular, we need to address the following boundaries: $\partial\Omega = \Sigma \cup \Gamma \cup \Gamma^{\mathrm{in}} \cup \Gamma^{\mathrm{out}}$, and the boundary of the active surface $\partial\Sigma$. For the considered problem with inflow and outflow boundary (see Fig. 5.1), we may consider the following boundary conditions.

- **Inflow boundary Γ^{in}:** At the inflow boundary, we specify the inflow mixture velocity and temperature and the molar diffusive fluxes and molar concentrations for all the species:

$$\mathbf{v} = \mathbf{v}^{\mathrm{in}} \ , \tag{6.36a}$$
$$\mathbf{J}_\alpha^{\mathrm{M,diff}} = (\mathbf{J}_\alpha^{\mathrm{M,diff}})^{\mathrm{in}} \ , \qquad \alpha \in K \ , \tag{6.36b}$$
$$c_\alpha^{\mathrm{M}} = (c_\alpha^{\mathrm{M}})^{\mathrm{in}} \ , \qquad \alpha \in K \ , \tag{6.36c}$$
$$\vartheta = \vartheta^{\mathrm{in}} \ . \tag{6.36d}$$

- **Outflow boundary Γ^{out}:** At the outflow boundary, we prescribe normal outflow, normal traction given by uniform outer pressure field and zero normal diffusive fluxes of mass and energy:

$$\mathbf{v}_\tau = \mathbf{0} \ , \tag{6.37a}$$
$$\mathbf{n} \cdot \mathbb{T}\mathbf{n} = -P^{\mathrm{out}} \ , \tag{6.37b}$$
$$\mathbf{J}_\alpha^{\mathrm{M,diff}} \cdot \mathbf{n} = 0 \ , \qquad \alpha \in K \ , \tag{6.37c}$$
$$\mathbf{J}_e \cdot \mathbf{n} = 0 \ . \tag{6.37d}$$

- **Active surface Σ:**
  On the active surface we need to specify the outer fluxes. We shall consider a system isolated from its exterior by setting to zero outer mass fluxes, energy and entropy fluxes and assuming a free-slip condition[2]. We achieve this by setting

$$
\begin{aligned}
{}^{+}\mathbf{v}\cdot\mathbf{n} &= 0\ , && && (6.38a)\\
{}^{+}\mathbf{J}_{\alpha}^{\mathrm{M,diff}}\cdot\mathbf{n} &= 0\ , && \alpha\in K\ , && (6.38b)\\
({}^{+}\ \mathbf{n})_{\tau} &= \mathbf{0}\ , && && (6.38c)\\
{}^{+}\mathbf{J}_{e}\cdot\mathbf{n} &= 0\ , && && (6.38d)\\
{}^{+}\mathbf{J}_{\eta}\cdot\mathbf{n} &= 0\ . && && (6.38e)
\end{aligned}
$$

- **Non-active surface - Γ :** On the rest of the boundary we may prescribe any set of standard boundary conditions. Considering, for example also non-penetration conditions and free-slip, we can impose

$$
\begin{aligned}
\mathbf{v}\cdot\mathbf{n} &= 0\ , && && (6.39a)\\
\mathbf{J}_{\alpha}^{\mathrm{M,diff}}\cdot\mathbf{n} &= 0\ , && \alpha\in K\ , && (6.39b)\\
(\ \mathbf{n})_{\tau} &= \mathbf{0}\ , && && (6.39c)\\
\mathbf{J}_{\alpha}^{\mathrm{M,diff}}\cdot\mathbf{n} &= 0\ , && \alpha\in K\ , && (6.39d)\\
\mathbf{J}_{e}\cdot\mathbf{n} &= 0\ . && && (6.39e)
\end{aligned}
$$

- **Boundary of the active surface:** At the boundary of the active surface $\partial\Sigma$, see Fig 5.1 , we prescribe zero surface velocity and molar diffusive fluxes of all constituents and we impose insulating boundary conditions with respect to the energy and entropy fluxes:

$$
\begin{aligned}
{}^{\Sigma}\mathbf{v} &= \mathbf{0}\ , && && (6.40a)\\
\mathbf{J}_{\alpha}^{\mathrm{M,diff}} &= \mathbf{0}\ , && \alpha\in K_0\ , && (6.40b)\\
{}^{\Sigma}\mathbf{J}_{e}\cdot\mathbf{n}^{\Sigma} &= 0\ , && && (6.40c)\\
{}^{\Sigma}\mathbf{J}_{\eta}\cdot\mathbf{n}^{\Sigma} &= 0\ . && && (6.40d)
\end{aligned}
$$

[2] Alternatively, we could use no-slip conditions, i.e. take ${}^{+}\mathbf{v}=\mathbf{0}$ without specifying ${}^{+}\ \mathbf{n}$.

7. Constitutive modelling

7.1 Constitutive modelling - bulk

The constitutive relations in the bulk are delivered by specifying two scalar quantities – the specific molar Gibbs' free energy g^{M}, and the rate of entropy production Π_η – and constructing constitutive relations that ensure non-negativity of the entropy production. Here, with the exception of chemical and sorption kinetics, we look for constitutive relations within the framework of Classical Irreversible Thermodynamics (CIT) [23], which coincides for linear constitutive relations with the approach based on the principle of maximization of rate of entropy production [79].

7.1.1 Bulk Gibbs' free energy

We start from a fundamental thermodynamic relation (under the assumption of local equilibrium) defining the entropy density $\rho\eta$ as a function of internal energy density and mass densities of the constituents[1]

$$\rho\eta = \widehat{\rho\eta}(\rho e, \rho_\alpha) \ , \qquad \alpha\in K \ . \tag{7.1}$$

Then we define the specific entropy density $\hat\eta$ in terms of the specific internal energy e, the specific volume $\frac{1}{\rho}$, and the mass fractions c_α by

$$\hat\eta(e, \frac{1}{\rho}, c_\alpha) \stackrel{\text{def}}{=} \frac{1}{\rho}\widehat{\rho\eta}(\rho e, \rho c_\alpha) \ , \qquad \alpha\in K \ . \tag{7.2}$$

Assuming $\frac{\partial\hat\eta}{\partial e} > 0$, we can invert (7.2) as follows:

$$e = \hat e(\eta, \frac{1}{\rho}, c_\alpha) \ , \qquad \alpha\in K \ . \tag{7.3}$$

The partial derivatives of (7.3) define the fundamental quantities: the temperature ϑ, the thermodynamic pressure p and the chemical potentials μ_α:

$$\vartheta \stackrel{\text{def}}{=} \frac{\partial\hat e}{\partial\eta} \ , \qquad p \stackrel{\text{def}}{=} -\frac{\partial\hat e}{\partial\frac{1}{\rho}} \ , \qquad \mu_\alpha \stackrel{\text{def}}{=} \frac{\partial\hat e}{\partial c_\alpha} \ , \qquad \alpha\in K \ . \tag{7.4}$$

It is convenient to replace the entropy and density as primitive variables by temperature and pressure, which can be achieved by assuming invertibility of the first two relations in (7.4) and defining the specific Gibbs' free energy $g = \hat g(\vartheta, p, c_1, \dots, c_N)$ as the corresponding Legendre transform of $\hat e$ with respect to $\frac{1}{\rho}$ and η:

$$g \stackrel{\text{def}}{=} e - \vartheta\eta + \frac{p}{\rho} \qquad \text{and} \qquad \hat g(\vartheta, p, c_1, \dots, c_N) \sup_{\frac{1}{\rho},\eta} \left(\hat e\left(\eta, \frac{1}{\rho}, c_\alpha\right) - \vartheta\eta + \frac{p}{\rho}\right) \ . \tag{7.5}$$

Consequently, we obtain

$$\frac{\partial\hat g}{\partial\vartheta} = -\eta \ , \qquad \frac{\partial\hat g}{\partial p} = \frac{1}{\rho} \ , \qquad \frac{\partial\hat g}{\partial c_\alpha} = \mu_\alpha \ , \qquad \alpha\in K \ . \tag{7.6}$$

[1] Throughout the whole paper, the notation $f = \hat f(*_\alpha)$, $\alpha\in K$, abbreviates $f = \hat f(*_1, \dots, *_N)$.

Alternatively, in order to work with molar-based quantities, we define the molar Gibbs potential g^{M}, the molar Helmholtz free energy ψ^{M}, the molar internal energy e^{M} and the molar entropy η^{M} through the identities

$$c^{\mathrm{M}} g^{\mathrm{M}} \stackrel{\mathrm{def}}{=} \rho g \ , \qquad c^{\mathrm{M}} \psi^{\mathrm{M}} \stackrel{\mathrm{def}}{=} \rho \psi \ , \qquad c^{\mathrm{M}} e^{\mathrm{M}} \stackrel{\mathrm{def}}{=} \rho e \ , \qquad c^{\mathrm{M}} \eta^{\mathrm{M}} \stackrel{\mathrm{def}}{=} \rho \eta \ , \tag{7.7}$$

which is to be understood, for example for the Gibbs' free energy in the sense

$$\widehat{g^{\mathrm{M}}}(\vartheta, p, x_\alpha) \stackrel{\mathrm{def}}{=} \underbrace{\left(\sum_{\beta \in K} M_\beta x_\beta \right)}_{=\rho/c^{\mathrm{M}}} \hat{g}\left(\vartheta, p, \underbrace{\frac{M_\alpha x_\alpha}{\sum_{\beta \in K} M_\beta x_\beta}}_{c_\alpha} \right) , \qquad \alpha \in K \ . \tag{7.8}$$

This definition gives, with the help of (7.5) and the bulk Euler relation (7.13), the following identities

$$\frac{\partial \widehat{g^{\mathrm{M}}}}{\partial \vartheta} = -\eta^{\mathrm{M}} \ , \qquad \frac{\partial \widehat{g^{\mathrm{M}}}}{\partial p} = \frac{1}{c^{\mathrm{M}}} \ , \qquad \frac{\partial \widehat{g^{\mathrm{M}}}}{\partial x_\alpha} = \mu_\alpha^{\mathrm{M}} \ , \qquad \alpha \in K \ , \tag{7.9}$$

where the molar chemical potential is defined as

$$\mu_\alpha^{\mathrm{M}} \stackrel{\mathrm{def}}{=} M_\alpha \mu_\alpha \ , \qquad \alpha \in K \ . \tag{7.10}$$

In our application, we need not directly specify a particular functional form for the (molar) Gibbs' free energy, it suffices to choose the chemical potential. Here we could adopt the standard form for (possibly non-ideal) mixtures:

$$\mu_\alpha^{\mathrm{M}}(\vartheta, p, x_\beta) = \mu_\alpha^{\mathrm{M}0}(\vartheta, p) + R\vartheta \ln \zeta_\alpha(x_\beta) \ , \qquad \alpha, \beta \in K \ , \tag{7.11}$$

where ζ_α is the chemical activity and R is the universal gas constant. In the following, we however consider, for simplicity, an ideal mixture in the bulk where the activity equals the molar fraction, i.e. $\zeta_\alpha = x_\alpha$. This means that the molar chemical potential μ_α^{M} reads

$$\mu_\alpha^{\mathrm{M}} = \mu_\alpha^{\mathrm{M}0}(\vartheta, p) + R\vartheta \ln x_\alpha \ , \qquad \alpha \in K \ . \tag{7.12}$$

7.1.2 Entropy production

Taking the material time derivative (w.r.t. the mixture velocity) of $\rho g = c^{\mathrm{M}} \widehat{g^{\mathrm{M}}}$, using (7.9) and the following bulk Euler relation (derived in C.1, see C.162)

$$e - \vartheta \eta + \frac{p}{\rho} = \sum_{\alpha \in K} \mu_\alpha c_\alpha \qquad \Longleftrightarrow \qquad e^{\mathrm{M}} - \vartheta \eta^{\mathrm{M}} + \frac{p}{c^{\mathrm{M}}} = \sum_{\alpha \in K} \mu_\alpha^{\mathrm{M}} x_\alpha \ , \tag{7.13}$$

we obtain, after some manipulation, the following identity

$$\rho \vartheta \dot{\eta} = \rho \dot{e} - \frac{\dot{\rho}}{\rho} \left(p - \sum_{\alpha \in K} \mu_\alpha^{\mathrm{M}} c_\alpha^{\mathrm{M}} \right) - \sum_{\alpha \in K} \mu_\alpha^{\mathrm{M}} \dot{c_\alpha^{\mathrm{M}}} \ . \tag{7.14}$$

Employing the energy balance (6.30) and the mass balances (6.3) and (6.10), we obtain

$$\rho \vartheta \dot{\eta} = (\mathrm{P} + p) \operatorname{div} \mathbf{v} + \quad : \quad {}^{d} + \sum_{\alpha \in K} \mathbf{J}_\alpha^{\mathrm{M,diff}} \cdot \mathbf{b}_\alpha^{\mathrm{M}} - \operatorname{div} \mathbf{J}_e - \sum_{\alpha \in K} \mu_\alpha^{\mathrm{M}} r_\alpha^{\mathrm{M}} + \sum_{\alpha \in K} \mu_\alpha^{\mathrm{M}} \operatorname{div} \mathbf{J}_\alpha^{\mathrm{M,diff}} \ , \tag{7.15}$$

where $^{d} \stackrel{\text{def}}{=} \; - \frac{1}{3}\mathrm{tr}(\;)$. After division by ϑ and some manipulation, we arrive at

$$\rho\dot{\eta} = -\operatorname{div}\left(\frac{\mathbf{J}_e - \sum_{\alpha\in K}\mu_\alpha^{\mathrm{M}}\mathbf{J}_\alpha^{\mathrm{M,diff}}}{\vartheta}\right) + \frac{(\mathrm{P}+p)\operatorname{div}\mathbf{v}}{\vartheta} + \frac{:\;^{d}}{\vartheta} + \mathbf{J}_e\cdot\nabla\left(\frac{1}{\vartheta}\right)$$
$$- \sum_{\alpha\in K}\mathbf{J}_\alpha^{\mathrm{M,diff}}\cdot\left\{\nabla\left(\frac{\mu_\alpha^{\mathrm{M}}}{\vartheta}\right) - \frac{\mathbf{b}_\alpha^{\mathrm{M}}}{\vartheta}\right\} - \frac{1}{\vartheta}\sum_{\alpha\in K}\mu_\alpha^{\mathrm{M}} r_\alpha^{\mathrm{M}} \,. \tag{7.16}$$

Comparing (7.16) with the bulk entropy balance (6.34), we postulate the bulk entropy flux in the form

$$\mathbf{J}_\eta = \frac{\mathbf{J}_e - \sum_{\alpha\in K}\mu_\alpha^{\mathrm{M}}\mathbf{J}_\alpha^{\mathrm{M,diff}}}{\vartheta} \,. \tag{7.17}$$

This gives the bulk rate of entropy production as

$$\Pi_\eta = \underbrace{\frac{(\mathrm{P}+p)\operatorname{div}\mathbf{v}}{\vartheta} + \frac{:\;^{d}}{\vartheta}}_{\Pi_\eta^{\mathrm{mech}}} + \underbrace{\mathbf{J}_e\cdot\nabla\left(\frac{1}{\vartheta}\right) - \sum_{\alpha\in K}\mathbf{J}_\alpha^{\mathrm{M,diff}}\cdot\left\{\nabla\left(\frac{\mu_\alpha^{\mathrm{M}}}{\vartheta}\right) - \frac{\mathbf{b}_\alpha^{\mathrm{M}}}{\vartheta}\right\}}_{\Pi_\eta^{\mathrm{diff}}} \underbrace{-\frac{1}{\vartheta}\sum_{\alpha\in K}\mu_\alpha^{\mathrm{M}} r_\alpha^{\mathrm{M}}}_{\Pi_\eta^{\mathrm{chem}}} \,, \tag{7.18}$$

see [23]. It has the form of a generalized product of thermodynamic "affinities" and "fluxes" where the individual terms correspond to the entropy production due to mechanical dissipation Π_η^{mech} (volumetric and isochoric), energy and mass diffusion Π_η^{diff} and chemical reactions Π_η^{chem}, respectively.

7.1.3 Constitutive relations in the bulk

With the entropy production in the form of a generalized product of thermodynamic "affinities" and "fluxes", one can propose constitutive relations in such a form that the second law of thermodynamics – the non-negativity of the entropy production – is automatically satisfied. In the bulk, we consider a rheological model for a compressible viscous fluid and consider two types of linear constitutive relations for heat conduction and mass diffusion, one based on the classical CIT procedure, the other being of Maxwell-Stefan type.

Following the so-called Curie principle stating that a cross-coupling occurs only among terms of the same tensorial rank, it follows from (7.18) that a scalar cross-coupling is possible between mechanical compaction and chemical kinetics, and vectorial cross-coupling is possible between diffusive heat and mass transfer. Since for chemical reactions, the linear constitutive relations framework is too restrictive and probably valid only in very limited cases near the thermodynamic equilibrium, we shall follow the approach suggested by [11] and provide non-linear constitutive relations. Consequently, we do not consider the former cross-effects. The thermo-diffusion cross-coupling is considered only in the context of CIT, while for Maxwell-Stefan type relations for mass diffusion, cross-coupling with thermal conduction is also ignored for simplicity.

- **Volumetric and shear deformation - bulk rheology:**
  The first two terms in (7.18) denoted by Π_η^{mech} correspond to mechanical entropy production by compaction and isochoric deformations, respectively, and within CIT, the linear affinity-flux relations yield the classical model of a viscous compressible Newtonian fluid:

$$\mathrm{P} + p = \frac{3\lambda + 2\nu}{3}\operatorname{div}\mathbf{v} \,, \tag{7.19}$$
$$= 2\nu\;^{d} \,, \tag{7.20}$$

where λ and ν are viscosity parameters such that $\frac{3\lambda+2\nu}{3}\geq 0$ (bulk viscosity), $\nu\geq 0$ (shear viscosity) implying non-negativity of the contributions of these mechanical dissipation mechanisms to the entropy production. In view of (7.19) and (7.20), the Cauchy stress reads

$$= -p \ + \lambda \operatorname{div} \mathbf{v} \ + 2\nu \quad . \tag{7.21}$$

- **Thermo-diffusion - CIT:**
The thermo-diffusion contribution Π_η^{diff} to the entropy production in (7.18) within the CIT must be first recast into a product of independent thermodynamical fluxes and affinities. The dependence is due to the constraint (6.2). Notationally the easiest way is to switch from molar based to mass based quantities and eliminate for example the solvent flux $\mathbf{J}_N^{\text{diff}}$. This yields

$$\Pi_\eta^{\text{diff}} = \mathbf{J}_e \cdot \nabla\left(\frac{1}{\vartheta}\right) - \sum_{\alpha\in K\setminus\{N\}} \mathbf{J}_\alpha^{\text{diff}} \cdot \left\{\nabla\left(\frac{\mu_\alpha - \mu_N}{\vartheta}\right) - \frac{\mathbf{b}_\alpha - \mathbf{b}_N}{\vartheta}\right\}, \tag{7.22}$$

and, consequently, the CIT yields the following linear constitutive relations

$$\begin{pmatrix} -\mathbf{J}_1^{\text{diff}} \\ \vdots \\ -\mathbf{J}_{N-1}^{\text{diff}} \\ \mathbf{J}_e \end{pmatrix} = \underbrace{\begin{pmatrix} 11 & \cdots & 1,N-1 & 1,N \\ \vdots & & \vdots & \vdots \\ N-1,1 & \cdots & N-1,N-1 & N-1,N \\ N,1 & \cdots & N,N-1 & N,N \end{pmatrix}}_{\sim} \begin{pmatrix} \nabla\left(\frac{\mu_1-\mu_N}{\vartheta}\right) - \left(\frac{\mathbf{b}_1-\mathbf{b}_N}{\vartheta}\right) \\ \vdots \\ \nabla\left(\frac{\mu_{N-1}-\mu_N}{\vartheta}\right) - \left(\frac{\mathbf{b}_{N-1}-\mathbf{b}_N}{\vartheta}\right) \\ \nabla\left(\frac{1}{\vartheta}\right) \end{pmatrix} \tag{7.23}$$

where $\sim$ is a positive semi-definite matrix in order to comply with the second law of thermodynamics. The off-diagonal elements of $\sim$ are restricted (within CIT) by Onsager's reciprocity relations, e.g. [23], postulating symmetry of the matrix $\sim$. Alternatively, by adopting the same type of constitutive relations for molar based diffusion fluxes, employing the constraint (6.12), one arrives at

$$\begin{pmatrix} -\mathbf{J}_1^{\text{M,diff}} \\ \vdots \\ -\mathbf{J}_{N-1}^{\text{M,diff}} \\ \mathbf{J}_e \end{pmatrix} = \underbrace{\begin{pmatrix} \tilde{11} & \cdots & \tilde{1,N-1} & \tilde{1,N} \\ \vdots & & \vdots & \vdots \\ \tilde{N-1,1} & \cdots & \tilde{N-1,N-1} & \tilde{N-1,N} \\ N,1 & \cdots & N,N-1 & N,N \end{pmatrix}}_{\tilde{\sim}} \begin{pmatrix} \nabla\left(\frac{\mu_1^{\text{M}}-\mu_{N,1}^{\text{M}}}{\vartheta}\right) - \left(\frac{\mathbf{b}_1^{\text{M}}-\mathbf{b}_{N,1}^{\text{M}}}{\vartheta}\right) \\ \vdots \\ \nabla\left(\frac{\mu_{N-1}^{\text{M}}-\mu_{N,N-1}^{\text{M}}}{\vartheta}\right) - \left(\frac{\mathbf{b}_{N-1}^{\text{M}}-\mathbf{b}_{N,N-1}^{\text{M}}}{\vartheta}\right) \\ \nabla\left(\frac{1}{\vartheta}\right) \end{pmatrix} \tag{7.24}$$

where

$$\mu_{\alpha,\beta}^{\text{M}} \stackrel{\text{def}}{=} \frac{M_\alpha}{M_\beta}\mu_\beta^{\text{M}}, \qquad \mathbf{b}_{\alpha,\beta}^{\text{M}} \stackrel{\text{def}}{=} \frac{M_\alpha}{M_\beta}\mathbf{b}_\beta^{\text{M}} \qquad \alpha,\beta\in K\ , \tag{7.25}$$

and $\tilde{\ }$ is again a symmetric positive definite matrix.

- **Maxwell-Stefan diffusion:**
Alternatively, one may provide constitutive relations involving mass diffusion in the form of the so-called Maxwell-Stefan equations [66, 105], which express local force

balance between the frictional forces due to mutual motion of the constituents and the thermodynamic forces driving the diffusion. A derivation of Maxwell-Stefan equations within the Class-II mixture theory, where individual momenta balances are postulated, has been delivered in [11] by several ways. Here we briefly outline a possible derivation within a CIT setting, considering for simplicity, only the mass-diffusion contribution to the entropy production, i.e. ignoring a possible thermo-diffusional coupling. Taking into account only the mass-diffusion entropy production denoted by $\Pi_\eta^{\text{diff}-\text{m}}$, we have

$$\begin{aligned}\Pi_\eta^{\text{diff}-\text{m}} &\overset{\text{def}}{=} -\sum_{\alpha\in K}\mathbf{J}_\alpha^{\text{M,diff}}\cdot\left\{\nabla\left(\frac{\mu_\alpha^{\text{M}}}{\vartheta}\right)-\frac{\mathbf{b}_\alpha^{\text{M}}}{\vartheta}\right\}=-\sum_{\alpha\in K}\mathbf{J}_\alpha^{\text{diff}}\cdot\left\{\nabla\left(\frac{\mu_\alpha}{\vartheta}\right)-\frac{\mathbf{b}_\alpha}{\vartheta}\right\}\\ &=-\sum_{\alpha\in K}\mathbf{u}_\alpha^{\text{diff}}\cdot\left\{\rho_\alpha\nabla\left(\frac{\mu_\alpha}{\vartheta}\right)-\rho_\alpha\frac{\mathbf{b}_\alpha}{\vartheta}-\rho_\alpha\Lambda\right\}\ ,\end{aligned}\tag{7.26}$$

where in the last expression we have introduced the diffusive velocities

$$\mathbf{u}_\alpha^{\text{diff}}\overset{\text{def}}{=}\frac{\mathbf{J}_\alpha^{\text{diff}}}{\rho_\alpha}=\mathbf{v}_\alpha-\mathbf{v}\ ,\qquad \alpha\in K\ ,\tag{7.27}$$

and an auxiliary function Λ, which does not contribute to the entropy production due to the constraint (6.2). Choosing a value of Λ such that the sum of the cofactors vanishes, meaning that

$$\sum_{\alpha\in K}\left\{\rho_\alpha\nabla\left(\frac{\mu_\alpha}{\vartheta}\right)-\rho_\alpha\frac{\mathbf{b}_\alpha}{\vartheta}-\rho_\alpha\Lambda\right\}=0\ ,\tag{7.28}$$

which leads to

$$\Lambda=\frac{1}{\rho}\sum_{\alpha\in K}\left\{\rho_\alpha\nabla\left(\frac{\mu_\alpha}{\vartheta}\right)-\rho_\alpha\frac{\mathbf{b}_\alpha}{\vartheta}\right\}\ .\tag{7.29}$$

We can recast (7.26) to the form

$$\Pi_\eta^{\text{diff}-\text{m}}=-\sum_{\alpha\in K}\mathbf{u}_\alpha^{\text{diff}}\cdot\mathbf{d}_\alpha^{\text{diff}}\ ,\tag{7.30}$$

where the "diffusional thermodynamic forces" $\mathbf{d}_\alpha^{\text{diff}}$ take the form

$$\mathbf{d}_\alpha^{\text{diff}}\overset{\text{def}}{=}\rho_\alpha\left\{\nabla\left(\frac{\mu_\alpha}{\vartheta}\right)-\sum_{\beta\in K}c_\beta\nabla\left(\frac{\mu_\beta}{\vartheta}\right)-\frac{\mathbf{b}_\alpha-\mathbf{b}}{\vartheta}\right\}\ ,\qquad \alpha\in K\ ,\tag{7.31}$$

with $\mathbf{b}$ given by (6.22), and satisfy

$$\sum_{\alpha\in K}\mathbf{d}_\alpha^{\text{diff}}=\mathbf{0}\ .\tag{7.32}$$

This expression can be rewritten with the use of the bulk Gibbs-Duhem relation (C.163):

$$-\eta d\vartheta+\frac{1}{\rho}dp=\sum_{\alpha\in K}c_\alpha d\mu_\alpha\ ,\tag{7.33}$$

with differentials replaced by spatial gradients, and with the help of the bulk Euler relation (C.162) as follows[2]:

$$\mathbf{d}_\alpha^{\mathrm{diff}} = \rho_\alpha \nabla\left(\frac{\mu_\alpha}{\vartheta}\right) - \frac{c_\alpha}{\vartheta}\nabla p - \rho_\alpha h \nabla\left(\frac{1}{\vartheta}\right) - \rho_\alpha \frac{\mathbf{b}_\alpha - \mathbf{b}}{\vartheta} \ , \qquad \alpha \in K \ , \tag{7.34}$$

where h is the specific bulk enthalpy, defined as

$$h \stackrel{\mathrm{def}}{=} e + \frac{p}{\rho} \ . \tag{7.35}$$

The Maxwell-Stefan relations are now obtained from

$$\Pi_\eta^{\mathrm{diff-m}} = -\sum_{\alpha\in K} \mathbf{u}_\alpha^{\mathrm{diff}} \cdot \mathbf{d}_\alpha^{\mathrm{diff}} \stackrel{(7.32)}{=} -\sum_{\alpha\in K\setminus\{N\}} (\mathbf{u}_\alpha^{\mathrm{diff}} - \mathbf{u}_N^{\mathrm{diff}}) \cdot \mathbf{d}_\alpha^{\mathrm{diff}} \ , \tag{7.36}$$

as follows: employing the linear constitutive relations for $\mathbf{d}_\alpha^{\mathrm{diff}}$, $\alpha \in K \setminus \{N\}$ via a matrix $\tau_{\alpha\beta}$ of dimension $(N-1)\times(N-1)$:

$$\mathbf{d}_\alpha^{\mathrm{diff}} = -\sum_{\alpha\in K\setminus\{N\}} \tau_{\alpha\beta}(\mathbf{u}_\beta^{\mathrm{diff}} - \mathbf{u}_N^{\mathrm{diff}}) \ , \qquad \alpha \in K\setminus\{N\} \ , \tag{7.37}$$

and extending the matrix $\tau_{\alpha\beta}$ to $N \times N$ so that $\sum_{\beta\in K} \tau_{\alpha\beta} = 0$, $\alpha \in K$, yields the symmetrized expression

$$\mathbf{d}_\alpha^{\mathrm{diff}} = -\sum_{\alpha\in K} \tau_{\alpha\beta}(\mathbf{u}_\beta^{\mathrm{diff}} - \mathbf{u}_\alpha^{\mathrm{diff}}) \ , \qquad \alpha \in K \ . \tag{7.38}$$

Next, considering binary interactions, the phenomenological interaction coefficients $\tau_{\alpha\beta}$ can be modelled as [11]

$$\tau_{\alpha\beta} = -f_{\alpha\beta}\rho_\alpha\rho_\beta \ , \qquad \alpha,\beta \in K \ , \tag{7.39}$$

where $f_{\alpha\beta}$ are positive friction coefficients (for $\alpha \neq \beta$). Such a form ensures thermodynamic consistency $\Pi_\eta^{\mathrm{diff-m}} \geq 0$. Finally, assumption (7.32) reads under the relation (7.39) as follows

$$0 = \sum_{\alpha,\beta\in K} f_{\alpha\beta}\rho_\alpha\rho_\beta(\mathbf{u}_\alpha^{\mathrm{diff}} - \mathbf{u}_\beta^{\mathrm{diff}}) \Longrightarrow f_{\alpha\beta} = f_{\beta\alpha} \qquad \alpha,\beta \in K \ , \tag{7.40}$$

i.e. the matrix $f_{\alpha\beta}$ is symmetric. Rewriting back in terms of diffusive fluxes, we obtain the following form of the Maxwell-Stefan equations

$$-\sum_{\beta\in K} f_{\alpha\beta}(\rho_\beta \mathbf{J}_\alpha^{\mathrm{diff}} - \rho_\alpha \mathbf{J}_\beta^{\mathrm{diff}}) = \rho_\alpha \nabla\left(\frac{\mu_\alpha}{\vartheta}\right) - \frac{c_\alpha}{\vartheta}\nabla p - \rho_\alpha h \nabla\left(\frac{1}{\vartheta}\right) - \rho_\alpha \frac{\mathbf{b}_\alpha - \mathbf{b}}{\vartheta}, \qquad \alpha \in K, \tag{7.41}$$

together with the constraint (6.2). In the chemical engineering literature, molar based quantities are usually employed and the Maxwell-Stefan equations are written in the form

$$-\sum_{\beta\in K} \frac{x_\beta \mathbf{J}_\alpha^{\mathrm{M,diff}} - x_\alpha \mathbf{J}_\beta^{\mathrm{M,diff}}}{\mathrm{D}_{\alpha\beta}} = \frac{c_\alpha^{\mathrm{M}}}{R\vartheta}\nabla\mu_\alpha^{\mathrm{M}} - \frac{c_\alpha}{R\vartheta}\nabla p - \frac{\rho_\alpha h - c_\alpha^{\mathrm{M}}\mu_\alpha^{\mathrm{M}}}{R\vartheta}\nabla\ln\vartheta - \frac{\rho_\alpha}{R\vartheta}(\mathbf{b}_\alpha - \mathbf{b}) \ , \tag{7.42}$$

[2] From a derivation based on Class-II constitutive relations (i.e. resolving momentum balances of individual constituents), the relation (7.34) would be modified by replacing $\rho_\alpha h$ by ρh_α where h_α are partial specific enthalpies, see [11].

where $\alpha \in K$ and the Maxwell-Stefan diffusivity matrix D is defined by

$$\mathrm{D}_{\alpha\beta} \stackrel{\text{def}}{=} \frac{R}{c^{\mathrm{M}} M_\alpha M_\beta f_{\alpha\beta}} , \qquad \alpha, \beta \in K . \tag{7.43}$$

Provided that $f_{\alpha\beta} \geq \epsilon > 0$, $\alpha, \beta \in K, \alpha \neq \beta$, together with the constraint (6.2) the system (7.42) is invertible [see 12] and the inversion when employed in the balance equations ensures non-negativity of species concentrations, mathematically a very desirable property.

Chemical reactions:

We now introduce the notation and assumptions related to the chemical reactions in the bulk. The bulk chemical reactions are chemical reactions among the bulk species $\mathrm{A}_\alpha, \alpha \in K$. Symbolically we write these reactions as

$$\sum_{\alpha \in K} \delta_\alpha^{\zeta,f} \, \mathrm{A}_\alpha \quad \sum_{\alpha \in K} \delta_\alpha^{\zeta,b} \, \mathrm{A}_\alpha , \qquad \zeta = 1, \ldots, Z . \tag{7.44}$$

Here Z is the number of bulk chemical reactions, $\delta_\alpha^{\zeta,f}$, $\delta_\alpha^{\zeta,b}$ are the forward and backward stoichiometric coefficients of the α reactant in the ζ reaction. The stoichiometric coefficient of the combined (forward/backward) ζ reaction is denoted by

$$\delta_\alpha^\zeta \stackrel{\text{def}}{=} \delta_\alpha^{\zeta,b} - \delta_\alpha^{\zeta,f} , \qquad \alpha \in K, \quad \zeta = 1, \ldots, Z . \tag{7.45}$$

With the use of stoichiometry, the molar rate r_α^{M} of production of the α constituent in chemical reactions can be expressed as

$$r_\alpha^{\mathrm{M}} = \sum_{\zeta=1}^{Z} \delta_\alpha^\zeta (\mathcal{R}_\zeta^f - \mathcal{R}_\zeta^b) = \sum_{\zeta=1}^{Z} \delta_\alpha^\zeta \mathcal{R}_\zeta , \qquad \alpha \in K , \tag{7.46}$$

with $\mathcal{R}_\zeta^f$ and $\mathcal{R}_\zeta^b$ denoting the forward and backward reaction rates of the ζth chemical reaction and $\mathcal{R}_\zeta \stackrel{\text{def}}{=} \mathcal{R}_\zeta^f - \mathcal{R}_\zeta^b$. The atomic composition of the molecules A_α allows us to express the molar mass M_α as

$$M_\alpha = \sum_{b=1}^{\mathrm{R}} \mathrm{S}^{b\alpha} \mathcal{M}_b , \qquad \alpha \in K , \tag{7.47}$$

where R is the number of different types of atoms with atomic molar masses $\mathcal{M}_b$ entering the reactions and the matrix $\mathrm{S}^{b\alpha}$ captures the atomic composition of A_α.

Conservation of mass. *The following well-known orthogonality relation between the stoichiometric coefficients and the composition matrix, expressing the conservation of atoms in the individual chemical reactions, holds:*

$$\sum_{\alpha \in K} \mathrm{S}^{b\alpha} \delta_\alpha^\zeta = 0 , \qquad \zeta = 1, \ldots, Z, \quad b = 1, \ldots \mathrm{R} , \tag{7.48}$$

which immediately implies the conservation of mass in the chemical reactions (6.12) *since, by (7.46)–(7.48),*

$$\sum_{\alpha \in K} M_\alpha r_\alpha^M = \sum_{\zeta=1}^{Z} \mathcal{R}_\zeta \sum_{b=1}^{\mathrm{R}} \mathcal{M}_b \sum_{\alpha \in K} \mathcal{S}^{b\alpha} \delta_\alpha^\zeta = 0 . \tag{7.49}$$

The contribution to the bulk entropy production due to chemical reactions is given by (see (7.18))

$$\Pi_\eta^{\rm chem} = -\frac{1}{\vartheta}\sum_{\alpha\in K}\mu_\alpha^{\rm M} r_\alpha^{\rm M} \ . \tag{7.50}$$

Using the expression for the molar reaction rate (7.46), we can conclude that

$$\Pi_\eta^{\rm chem} = -\frac{1}{\vartheta}\sum_{\zeta=1}^{Z}(\mathcal{R}_\zeta^f - \mathcal{R}_\zeta^b)\mathcal{A}^\zeta \ , \tag{7.51}$$

where we introduced the affinity of the ζ bulk chemical reaction through

$$\mathcal{A}^\zeta \stackrel{\rm def}{=} \sum_{\alpha\in K}\mu_\alpha^{\rm M}\delta_\alpha^\zeta \ , \qquad \zeta = 1,\dots,Z \ . \tag{7.52}$$

Considering the following non-linear constitutive relation for $\mathcal{A}^\zeta$:

$$\mathcal{A}^\zeta = \beta^\zeta R\,\vartheta \ln\left(\frac{\mathcal{R}_\zeta^b}{\mathcal{R}_\zeta^f}\right) \ , \qquad \beta^\zeta \geq 0 \ , \qquad \zeta = 1,\dots,Z \ , \tag{7.53}$$

we observe that

$$\Pi_\eta^{\rm chem} = R\sum_{\zeta=1}^{Z}\beta^\zeta(\mathcal{R}_\zeta^f - \mathcal{R}_\zeta^b)(\ln\mathcal{R}_\zeta^f - \ln\mathcal{R}_\zeta^b) \ , \tag{7.54}$$

which implies that $\Pi_\eta^{\rm chem} \geq 0$ due to the monotone property of the logarithm. Particularly, for our ideal mixture model (7.12), we express the chemical affinity (7.52) as

$$\mathcal{A}^\zeta = \sum_{\alpha\in K}\mu_\alpha^{\rm M0}\delta_\alpha^\zeta + R\,\vartheta\ln\prod_{\alpha\in K}x_\alpha^{\delta_\alpha^\zeta} \ , \qquad \zeta = 1,\dots,Z \ . \tag{7.55}$$

Defining the equilibrium constant of the ζth reaction $\mathcal{K}_\zeta^{\rm chem}(\vartheta,p)$ through

$$-R\vartheta\ln\left(\mathcal{K}_\zeta^{\rm chem}(\vartheta,p)\right) \stackrel{\rm def}{=} \sum_{\alpha\in K}\mu_\alpha^{\rm M0}(\vartheta,p)\,\delta_\alpha^\zeta \ , \qquad \zeta = 1,\dots,Z \ , \tag{7.56}$$

and combining (7.53) and (7.55) together, yields

$$\prod_{\alpha\in K}x_\alpha^{\delta_\alpha^\zeta} = \mathcal{K}_\zeta^{\rm chem}(\vartheta,p)\left(\frac{\mathcal{R}_\zeta^b}{\mathcal{R}_\zeta^f}\right)^{\beta^\zeta} \ , \qquad \zeta = 1,\dots,Z \ . \tag{7.57}$$

One of the rates $\mathcal{R}_\zeta^f$, $\mathcal{R}_\zeta^b$ has to be modelled, while the other is given by relation (7.57). One possible choice which yields the standard reaction kinetics is as follows

$$\left(\mathcal{R}_\zeta^f\right)^{\beta^\zeta} = k_\zeta^f(\vartheta,p)\prod_{\alpha\in K}x_\alpha^{\delta_\alpha^{\zeta,f}} \ , \qquad \left(\mathcal{R}_\zeta^b\right)^{\beta^\zeta} = \ k_\zeta^b(\vartheta,p)\prod_{\alpha\in K}x_\alpha^{\delta_\alpha^{\zeta,b}} \ , \qquad \zeta = 1,\dots,Z \ , \tag{7.58}$$

and the coefficients $k_\zeta^f(\vartheta,p)$, $k_\zeta^b(\vartheta,p)$ must satisfy $\frac{k_\zeta^f(\vartheta,p)}{k_\zeta^b(\vartheta,p)} = \mathcal{K}_\zeta^{\rm chem}(\vartheta,p),\ \zeta = 1,\dots,Z.$

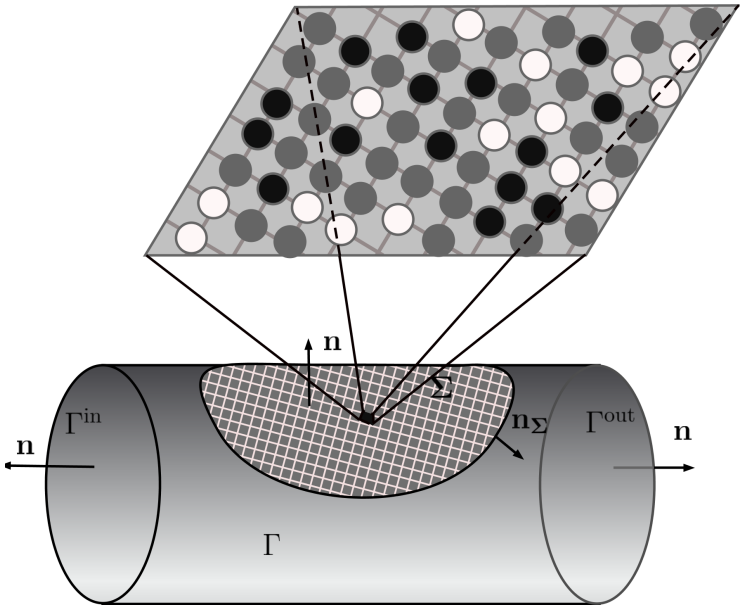

Figure 7.1: Sketch of a lattice model on the active surface Σ. The surface is represented by a regular grid with distinct adsorption sites, which can be either occupied by a molecule of adsorbate or empty (vacancy).

Observe that the bulk entropy production due to chemical reactions Π_η^{chem} vanishes only if $\mathcal{A}^\zeta = 0$, ζ=1, ..., Z (the so called principle of detailed balance). In that case, it follows from (7.55) and (7.56) that

$$\prod_{\alpha\in K} x_\alpha^{\delta_\alpha^\zeta} = \mathcal{K}_\zeta^{\mathrm{chem}}(\vartheta, p) \ , \qquad \zeta = 1, \dots, Z \ , \tag{7.59}$$

which is the standard equilibrium mass-action law.

Finally, let us note that a possible generalization that allows for cross-coupling between the individual reactions even in the framework of the above non-linear constitutive relations, is suggested in [11].

7.2 Constitutive modelling - active surface

The phenomenological (macroscopic) constitutive model for the surface thermodynamic potentials in our model is based on a microscopic idealization of the active surface treated as a monolayer homogeneous lattice with adsorption sites organized in a regular grid (see Fig. 7.1). The grid is occupied by N types of surface molecules (adsorbates) ${}^{\Sigma}\mathrm{A}_1, \dots, {}^{\Sigma}\mathrm{A}_N$ or by empty sites (vacancies) denoted ${}^{\Sigma}\mathrm{A}_0$. In the derivation of thermodynamic potentials in B.1, we focus on the derivation of a model, in which the molecules do not interact with each other and each molecule can occupy only one adsorption site, but we also show how the model can be generalized to include, for example, intermolecular interaction or multi-site adsorption. In the derivation, we consider the possibility that the grid itself may deform (stretch/compress) elastically. In what follows, we will further consider an incompressible limit of this model, where this elastic stretching or compression is negligible and the density of adsorption sites is constant.

7.2.1 Surface free energy

Considering a simple fixed monolayer single-site adsorption without mutual interaction among the adsorbed particles, one arrives at the following expressions for the molar surface Helmholtz free energy density (see B.1, (B.147))

$$ {}^{\Sigma}\psi^{\mathrm{M}} = -R\,{}^{\Sigma}\vartheta \sum_{\alpha\in K_0} {}^{\Sigma}x_\alpha(\ln {}^{\Sigma}q_\alpha({}^{\Sigma}\vartheta) - \ln {}^{\Sigma}x_\alpha) \ , \tag{7.60} $$

where ${}^{\Sigma}q_\alpha({}^{\Sigma}\vartheta)$ are the molecular partition functions depending on the surface temperature ${}^{\Sigma}\vartheta$, which correspond to the internal degrees of freedom of the adsorbed molecules. Adding a contribution resulting from possible stretching/compression of the lattice in a simple form ${}^{\Sigma}\psi_0^{\mathrm{M}}({}^{\Sigma}\vartheta, \frac{1}{{}^{\Sigma}c^{\mathrm{M}}})$, eliminating dependent ${}^{\Sigma}x_0{=}1{-}\sum_{\alpha\in K}{}^{\Sigma}x_\alpha$, we obtain ${}^{\Sigma}\psi^{\mathrm{M}} = \widehat{{}^{\Sigma}\psi^{\mathrm{M}}}({}^{\Sigma}\vartheta, \frac{1}{{}^{\Sigma}c^{\mathrm{M}}}, {}^{\Sigma}x_1, \ldots, {}^{\Sigma}x_N)$. Defining the corresponding surface molar Gibbs free energy ${}^{\Sigma}g^{\mathrm{M}} = \widehat{{}^{\Sigma}g^{\mathrm{M}}}({}^{\Sigma}\vartheta, {}^{\Sigma}\gamma, {}^{\Sigma}x_1, \ldots, {}^{\Sigma}x_N)$ via a Legendre transform of ${}^{\Sigma}\psi^{\mathrm{M}}$ with respect to $\frac{1}{{}^{\Sigma}c^{\mathrm{M}}}$:

$$ {}^{\Sigma}g^{\mathrm{M}} \stackrel{\mathrm{def}}{=} {}^{\Sigma}\psi^{\mathrm{M}} - \frac{{}^{\Sigma}\gamma}{{}^{\Sigma}c^{\mathrm{M}}} \quad \text{and} \quad \widehat{{}^{\Sigma}g^{\mathrm{M}}}({}^{\Sigma}\vartheta, {}^{\Sigma}\gamma, {}^{\Sigma}x_1, \ldots, {}^{\Sigma}x_N) \stackrel{\mathrm{def}}{=} \sup_{\frac{1}{{}^{\Sigma}c^{\mathrm{M}}}} \left(\widehat{{}^{\Sigma}\psi^{\mathrm{M}}}\left({}^{\Sigma}\vartheta, \frac{1}{{}^{\Sigma}c^{\mathrm{M}}}, {}^{\Sigma}x_\alpha\right) - \frac{{}^{\Sigma}\gamma}{{}^{\Sigma}c^{\mathrm{M}}} \right) \ , \tag{7.61} $$

one arrives at the following formula for the surface molar Gibbs free energy (see B.1, (B.151)):

$$ \begin{aligned} \widehat{{}^{\Sigma}g^{\mathrm{M}}}({}^{\Sigma}\vartheta, {}^{\Sigma}\gamma, {}^{\Sigma}x_1, \ldots, {}^{\Sigma}x_N) = {}^{\Sigma}g_0^{\mathrm{M}}({}^{\Sigma}\vartheta, {}^{\Sigma}\gamma) - R\,{}^{\Sigma}\vartheta \sum_{\alpha\in K} {}^{\Sigma}x_\alpha(\ln {}^{\Sigma}q_\alpha - \ln {}^{\Sigma}x_\alpha) \\ - R\,{}^{\Sigma}\vartheta \left(1{-}\sum_{\beta\in K} {}^{\Sigma}x_\beta\right)\left(\ln {}^{\Sigma}q_0 - \ln\left(1 - \sum_{\beta\in K} {}^{\Sigma}x_\beta\right)\right) \ , \end{aligned} \tag{7.62} $$

where ${}^{\Sigma}\gamma$ denotes the surface tension. From eq. (7.62), we recover the surface molar entropy density ${}^{\Sigma}\eta^{\mathrm{M}}$, the surface tension ${}^{\Sigma}\gamma$ and the surface chemical potentials (with respect to the vacancies) ${}^{\Sigma}\mu_\alpha^{\mathrm{M}}{-}{}^{\Sigma}\mu_0^{\mathrm{M}}$ as follows (see B.1, (B.152))

$$ \frac{\partial\, \widehat{{}^{\Sigma}g^{\mathrm{M}}}}{\partial\, {}^{\Sigma}\vartheta} = -{}^{\Sigma}\eta^{\mathrm{M}} \ , \qquad \frac{\partial \widehat{{}^{\Sigma}g^{\mathrm{M}}}}{\partial {}^{\Sigma}\gamma} = -\frac{1}{{}^{\Sigma}c^{\mathrm{M}}} \ , \qquad \frac{\partial\, \widehat{{}^{\Sigma}g^{\mathrm{M}}}}{\partial\, {}^{\Sigma}x_\alpha} = {}^{\Sigma}\mu_\alpha^{\mathrm{M}}{-}{}^{\Sigma}\mu_0^{\mathrm{M}} \ , \qquad \alpha{\in}K \ . \tag{7.63} $$

The last set of relations (7.63) in particular yields the following explicit relation for the molar chemical potentials (with respect to vacancies)

$$ {}^{\Sigma}\mu_\alpha^{\mathrm{M}}{-}{}^{\Sigma}\mu_0^{\mathrm{M}} = R\,{}^{\Sigma}\vartheta \left\{ \ln\left(\frac{q_0^\Sigma}{q_\alpha^\Sigma}\right) + \ln\left(\frac{{}^{\Sigma}x_\alpha}{1 - \sum_{\beta\in K} {}^{\Sigma}x_\beta}\right)\right\} \ , \qquad \alpha{\in}K_0 \ . \tag{7.64} $$

In the following, we shall employ the assumption of *incompressibility* of the lattice in the sense of the limit

$$ \frac{\partial}{\partial {}^{\Sigma}\gamma}\left(\frac{1}{{}^{\Sigma}c^{\mathrm{M}}}\right) = -\frac{\partial^2 \widehat{{}^{\Sigma}g^{\mathrm{M}}}}{\partial {}^{\Sigma}\gamma^2} \to 0 \quad \& \quad \frac{\partial}{\partial {}^{\Sigma}\vartheta}\left(\frac{1}{{}^{\Sigma}c^{\mathrm{M}}}\right) = -\frac{\partial^2 \widehat{{}^{\Sigma}g^{\mathrm{M}}}}{\partial {}^{\Sigma}\vartheta \partial {}^{\Sigma}\gamma} \to 0 \ , \tag{7.65} $$

which implies ${}^{\Sigma}c^{\mathrm{M}} \to$ const., since in view of (7.62) and (7.63), ${}^{\Sigma}c^{\mathrm{M}}$ depends only on $({}^{\Sigma}\vartheta, {}^{\Sigma}\gamma)$ as it holds $\frac{1}{{}^{\Sigma}c^{\mathrm{M}}} = -\frac{\partial {}^{\Sigma}g_0^{\mathrm{M}}({}^{\Sigma}\vartheta, {}^{\Sigma}\gamma)}{\partial {}^{\Sigma}\gamma}$. In this "relaxed" sense we also understand the condition (6.20).

Remarks

7.2.1 Model extension. *The presented model represents a rather simplified situation of monolayer single-site adsorption on a homogeneous lattice without interaction among the adsorbed molecules. If one would like to apply a more advanced model for the purpose of the macroscopic modelling, it is only necessary to identify the thermodynamic potentials (e.g. Gibbs, Helmholtz). The extended models are typically formulated in terms of the corresponding canonical partition function [see, e.g. 72, 81, 31, 84], the procedure outlined in B.1 provides the way how to identify the thermodynamic potentials. From this point of view, what we present here should be viewed as a framework that allows one to incorporate a much more sophisticated description of the catalytic surface properties.*

7.2.2 Surface entropy production

The specific surface densities of Gibbs, Helmholtz and internal energy and entropy are defined through the relations

$$\rho^{\Sigma\Sigma}g \stackrel{\text{def}}{=} {}^{\Sigma}c^{\mathrm{M}\Sigma}g^{\mathrm{M}}\,, \qquad \rho^{\Sigma\Sigma}\psi \stackrel{\text{def}}{=} {}^{\Sigma}c^{\mathrm{M}\Sigma}\psi^{\mathrm{M}}\,, \qquad \rho^{\Sigma\Sigma}e \stackrel{\text{def}}{=} {}^{\Sigma}c^{\mathrm{M}\Sigma}e^{\mathrm{M}}\,, \qquad \rho^{\Sigma\Sigma}\eta \stackrel{\text{def}}{=} {}^{\Sigma}c^{\mathrm{M}\Sigma}\eta^{\mathrm{M}}\,. \tag{7.66}$$

We start from the expression for the molar Gibbs potential

$${}^{\Sigma}g^{\mathrm{M}} = {}^{\Sigma}e^{\mathrm{M}} - {}^{\Sigma}\vartheta^{\Sigma}\eta^{\mathrm{M}} - \frac{{}^{\Sigma}\gamma}{{}^{\Sigma}c^{\mathrm{M}}}\,, \tag{7.67}$$

and apply a convective time derivative (with respect to the surface velocity ${}^{\Sigma}\mathbf{v}$) to ${}^{\Sigma}g^{\mathrm{M}} = \widehat{{}^{\Sigma}g^{\mathrm{M}}}({}^{\Sigma}\vartheta, {}^{\Sigma}\gamma, {}^{\Sigma}x_1, \ldots, {}^{\Sigma}x_N)$. After some manipulation with the use of relations (7.66), identities (7.63) and exploiting the surface Euler relation (derived in C.2, see (C.176))

$${}^{\Sigma}c^{\mathrm{M}\Sigma}\psi^{\mathrm{M}} - ({}^{\Sigma}\gamma + \mu_0^{\mathrm{M}\Sigma}c^{\mathrm{M}}) = \sum_{\alpha\in K}({}^{\Sigma}\mu_\alpha^{\mathrm{M}} - {}^{\Sigma}\mu_0^{\mathrm{M}})\,{}^{\Sigma}c_\alpha^{\mathrm{M}}\,, \tag{7.68}$$

we arrive at the following expression

$$\rho^{\Sigma\Sigma}\vartheta\dot{}^{\Sigma}\eta = {}^{\Sigma}\psi\rho\dot{}^{\Sigma} + \rho^{\Sigma\Sigma}e\dot{} - \sum_{\alpha\in K}({}^{\Sigma}\mu_\alpha^{\mathrm{M}} - {}^{\Sigma}\mu_0^{\mathrm{M}})\,{}^{\Sigma}c\dot{}_\alpha^{\mathrm{M}} \; - {}^{\Sigma}c\dot{}^{\mathrm{M}}\,{}^{\Sigma}\mu_0^{\mathrm{M}}\,.$$

Employing the surface mass and molar balances (6.6), (6.1.2), the symmetry of the surface stress tensor (6.27), the surface energy balance (6.33), and applying the lattice incompressibility in the sense (7.65), yields

$$\begin{aligned}\rho^{\Sigma\Sigma}\vartheta\dot{}^{\Sigma}\eta = {}&{}^{\Sigma}\psi\,(-\rho^{\Sigma}\,\mathrm{div}^{\Sigma}\,{}^{\Sigma}\mathbf{v} - [\![\rho\mathbf{v}]\!]\cdot\mathbf{n}) + {}^{\Sigma}\mathbb{T} : {}^{\Sigma}\mathbb{D} + \sum_{\alpha\in K}{}^{\Sigma}\mathbf{J}_\alpha^{\mathrm{M,diff}}\cdot{}^{\Sigma}\mathbf{b}_\alpha^{\mathrm{M}} - \mathrm{div}^{\Sigma}\,{}^{\Sigma}\mathbf{J}_e \\ &- \sum_{\alpha\in K}({}^{\Sigma}\mu_\alpha^{\mathrm{M}} - {}^{\Sigma}\mu_0^{\mathrm{M}})({}^{\Sigma}r_\alpha^{\mathrm{M}} + {}^{\Sigma}s_\alpha^{\mathrm{M}} - {}^{\Sigma}c_\alpha^{\mathrm{M}}\,\mathrm{div}^{\Sigma}\,{}^{\Sigma}\mathbf{v} - \mathrm{div}^{\Sigma}\,{}^{\Sigma}\mathbf{J}_\alpha^{\mathrm{M,diff}}) \\ &- \left[\!\!\left[\rho\left(e - {}^{\Sigma}e + \frac{1}{2}|\mathbf{v} - {}^{\Sigma}\mathbf{v}|^2\right)\mathbf{v}\right]\!\!\right]\cdot\mathbf{n} + [\![(\mathbf{v} - {}^{\Sigma}\mathbf{v})\cdot\mathbb{T}]\!]\,\mathbf{n} - [\![\mathbf{J}_e]\!]\cdot\mathbf{n}\;\,,\end{aligned} \tag{7.69}$$

where ${}^{\Sigma}\mathbb{D} \stackrel{\text{def}}{=} \frac{1}{2}\left(\nabla^{\Sigma\Sigma}\mathbf{v} + (\nabla^{\Sigma\Sigma}\mathbf{v})^{\mathrm{T}}\right)$ is the symmetric part of the surface velocity gradient. We split the surface stress tensor ${}^{\Sigma}\mathbb{T}$ into isotropic and traceless parts, see (6.25), which

yields

$$\begin{aligned}\rho^{\Sigma\,\Sigma}\vartheta^{\Sigma}\dot{\eta} = &\left(-\rho^{\Sigma\,\Sigma}\psi+{}^{\Sigma}\mathrm{P}+\sum_{\alpha\in K}({}^{\Sigma}\mu_\alpha^{\mathrm{M}}-{}^{\Sigma}\mu_0^{\mathrm{M}})^{\Sigma}c_\alpha^{\mathrm{M}}\right)\mathrm{div}^{\Sigma\,\Sigma}\mathbf{v}+{}^{\Sigma}\mathbb{S}:{}^{\Sigma}\mathbb{D}^d+\sum_{\alpha\in K}{}^{\Sigma}\mathbf{J}_\alpha^{\mathrm{M,diff}}\cdot{}^{\Sigma}\mathbf{b}_\alpha^{\mathrm{M}}-\mathrm{div}^{\Sigma\,\Sigma}\mathbf{J}_e\\ &-\sum_{\alpha\in K}({}^{\Sigma}\mu_\alpha^{\mathrm{M}}-{}^{\Sigma}\mu_0^{\mathrm{M}})({}^{\Sigma}r_\alpha^{\mathrm{M}}+{}^{\Sigma}s_\alpha^{\mathrm{M}})+\sum_{\alpha\in K}({}^{\Sigma}\mu_\alpha^{\mathrm{M}}-{}^{\Sigma}\mu_0^{\mathrm{M}})\,\mathrm{div}^{\Sigma\,\Sigma}\mathbf{J}_\alpha^{\mathrm{M,diff}}\\ &-\left[\!\!\left[\rho\left(e-{}^{\Sigma}e+\frac{1}{2}|\mathbf{v}-{}^{\Sigma}\mathbf{v}|^2+{}^{\Sigma}\psi\right)\mathbf{v}\right]\!\!\right]\cdot\mathbf{n}+[\![(\mathbf{v}-{}^{\Sigma}\mathbf{v})\cdot\mathbb{T}]\!]\,\mathbf{n}-[\![\mathbf{J}_e]\!]\cdot\mathbf{n}\,,\end{aligned}\tag{7.70}$$

where ${}^{\Sigma}\mathbb{D}^d \stackrel{\mathrm{def}}{=} {}^{\Sigma}\mathbb{D}-\frac{1}{2}\mathrm{tr}^{\Sigma}\mathbb{D}$ is the deviatoric (traceless) part of ${}^{\Sigma}\mathbb{D}$.

Dividing (7.70) by ${}^{\Sigma}\vartheta$, employing the surface Euler relation (7.68) on the first parenthesis on the r.h.s., and the definition of the surface pressure ${}^{\Sigma}p\stackrel{\mathrm{def}}{=}-{}^{\Sigma}\gamma-{}^{\Sigma}\mu_0^{\mathrm{M}}{}^{\Sigma}c^{\mathrm{M}}$ (see (C.175)), after rearranging the terms, we arrive at

$$\begin{aligned}\rho^{\Sigma}\dot{\Sigma}\eta = &-\mathrm{div}^{\Sigma}\left(\frac{{}^{\Sigma}\mathbf{J}_e-\sum_{\alpha\in K}({}^{\Sigma}\mu_\alpha^{\mathrm{M}}-{}^{\Sigma}\mu_0^{\mathrm{M}})^{\Sigma}\mathbf{J}_\alpha^{\mathrm{M,diff}}}{{}^{\Sigma}\vartheta}\right)+\frac{{}^{\Sigma}\mathrm{P}+{}^{\Sigma}p}{{}^{\Sigma}\vartheta}\,\mathrm{div}^{\Sigma\,\Sigma}\mathbf{v}+\frac{{}^{\Sigma}\mathbb{S}:{}^{\Sigma}\mathbb{D}^d}{{}^{\Sigma}\vartheta}+{}^{\Sigma}\mathbf{J}_e\cdot\nabla^{\Sigma}\left(\frac{1}{{}^{\Sigma}\vartheta}\right)\\ &-\sum_{\alpha\in K}\frac{({}^{\Sigma}\mu_\alpha^{\mathrm{M}}-{}^{\Sigma}\mu_0^{\mathrm{M}})}{{}^{\Sigma}\vartheta}({}^{\Sigma}r_\alpha^{\mathrm{M}}+{}^{\Sigma}s_\alpha^{\mathrm{M}})-\sum_{\alpha\in K}{}^{\Sigma}\mathbf{J}_\alpha^{\mathrm{M,diff}}\cdot\left\{\nabla^{\Sigma}\left(\frac{{}^{\Sigma}\mu_\alpha^{\mathrm{M}}-{}^{\Sigma}\mu_0^{\mathrm{M}}}{{}^{\Sigma}\vartheta}\right)-\frac{{}^{\Sigma}\mathbf{b}_\alpha^{\mathrm{M}}}{{}^{\Sigma}\vartheta}\right\}\\ &-\frac{1}{{}^{\Sigma}\vartheta}\left[\!\!\left[\rho\left(e-{}^{\Sigma}e+\frac{1}{2}|\mathbf{v}-{}^{\Sigma}\mathbf{v}|^2+{}^{\Sigma}\psi\right)\mathbf{v}\right]\!\!\right]\cdot\mathbf{n}+\frac{1}{{}^{\Sigma}\vartheta}[\![(\mathbf{v}-{}^{\Sigma}\mathbf{v})\cdot\mathbb{T}]\!]\,\mathbf{n}-\frac{1}{{}^{\Sigma}\vartheta}[\![\mathbf{J}_e]\!]\cdot\mathbf{n}\,.\end{aligned}\tag{7.71}$$

By comparing (7.71) with the surface entropy balance (6.35) and using (7.17), we obtain:

$$\begin{aligned}{}^{\Sigma}\Pi_\eta = &\,\mathrm{div}^{\Sigma}\left({}^{\Sigma}\mathbf{J}_\eta-\frac{{}^{\Sigma}\mathbf{J}_e-\sum_{\alpha\in K}({}^{\Sigma}\mu_\alpha^{\mathrm{M}}-{}^{\Sigma}\mu_0^{\mathrm{M}})^{\Sigma}\mathbf{J}_\alpha^{\mathrm{M,diff}}}{{}^{\Sigma}\vartheta}\right)+\frac{{}^{\Sigma}\mathrm{P}+{}^{\Sigma}p}{{}^{\Sigma}\vartheta}\,\mathrm{div}^{\Sigma\,\Sigma}\mathbf{v}+\frac{{}^{\Sigma}\mathbb{S}:{}^{\Sigma}\mathbb{D}^d}{{}^{\Sigma}\vartheta}+{}^{\Sigma}\mathbf{J}_e\cdot\nabla^{\Sigma}\left(\frac{1}{{}^{\Sigma}\vartheta}\right)\\ &-\sum_{\alpha\in K}\frac{{}^{\Sigma}\mu_\alpha^{\mathrm{M}}-{}^{\Sigma}\mu_0^{\mathrm{M}}}{{}^{\Sigma}\vartheta}{}^{\Sigma}r_\alpha^{\mathrm{M}}-\sum_{\alpha\in K}\frac{{}^{\Sigma}\mu_\alpha^{\mathrm{M}}-{}^{\Sigma}\mu_0^{\mathrm{M}}}{{}^{\Sigma}\vartheta}{}^{\Sigma}s_\alpha^{\mathrm{M}}-\sum_{\alpha\in K}{}^{\Sigma}\mathbf{J}_\alpha^{\mathrm{M,diff}}\cdot\left\{\nabla^{\Sigma}\left(\frac{{}^{\Sigma}\mu_\alpha^{\mathrm{M}}-{}^{\Sigma}\mu_0^{\mathrm{M}}}{{}^{\Sigma}\vartheta}\right)-\frac{{}^{\Sigma}\mathbf{b}_\alpha^{\mathrm{M}}}{{}^{\Sigma}\vartheta}\right\}\\ &-\frac{1}{{}^{\Sigma}\vartheta}\left[\!\!\left[\rho\left(e-{}^{\Sigma}\vartheta\eta+\frac{1}{2}|\mathbf{v}-{}^{\Sigma}\mathbf{v}|^2\right)\mathbf{v}\right]\!\!\right]\cdot\mathbf{n}+\frac{1}{{}^{\Sigma}\vartheta}[\![(\mathbf{v}-{}^{\Sigma}\mathbf{v})\cdot\mathbb{T}]\!]\cdot\mathbf{n}\\ &+\left[\!\!\left[\mathbf{J}_e\left(\frac{1}{\vartheta}-\frac{1}{{}^{\Sigma}\vartheta}\right)\right]\!\!\right]\cdot\mathbf{n}-\left[\!\!\left[\sum_{\alpha\in K}\frac{\mu_\alpha^{\mathrm{M}}}{\vartheta}\mathbf{J}_\alpha^{\mathrm{M,diff}}\right]\!\!\right]\cdot\mathbf{n}\,.\end{aligned}\tag{7.72}$$

Formula (7.72) suggests to identify the surface entropy flux as

$${}^{\Sigma}\mathbf{J}_\eta=\frac{{}^{\Sigma}\mathbf{J}_e-\sum_{\alpha\in K}({}^{\Sigma}\mu_\alpha^{\mathrm{M}}-{}^{\Sigma}\mu_0^{\mathrm{M}})^{\Sigma}\mathbf{J}_\alpha^{\mathrm{M,diff}}}{{}^{\Sigma}\vartheta}\,.\tag{7.73}$$

Furthermore, recalling that $\mathbf{J}_\alpha^{\mathrm{diff}}=\rho_\alpha(\mathbf{v}_\alpha-\mathbf{v})$, using (6.7), we obtain

$$\begin{aligned}\left[\!\!\left[\sum_{\alpha\in K}\frac{\mu_\alpha^{\mathrm{M}}}{\vartheta}\mathbf{J}_\alpha^{\mathrm{M,diff}}\right]\!\!\right]\cdot\mathbf{n}&=\left[\!\!\left[\sum_{\alpha\in K}\frac{\mu_\alpha}{\vartheta}\rho_\alpha(\mathbf{v}_\alpha-\mathbf{v})\right]\!\!\right]\cdot\mathbf{n}\\ &=-\sum_{\alpha\in K}\left(\frac{{}^{+}\mu_\alpha^{\mathrm{M}}+{}^{\Sigma}s_\alpha^{\mathrm{M}}}{{}^{+}\vartheta}+\frac{{}^{-}\mu_\alpha^{\mathrm{M}}-{}^{\Sigma}s_\alpha^{\mathrm{M}}}{{}^{-}\vartheta}\right)-\left[\!\!\left[\frac{1}{\vartheta}\sum_{\alpha\in K}\mu_\alpha^{\mathrm{M}}c_\alpha^{\mathrm{M}}\mathbf{v}\right]\!\!\right]\cdot\mathbf{n}\,.\end{aligned}\tag{7.74}$$

Employing the bulk Euler relation (7.13), together with the boundary conditions (see section 6.4) which exclude fluxes from the "outer" (+) side of Ω, and if we omit the $^{-}$ superscript, for brevity, we obtain the surface entropy production in the following form:

$${}^{\Sigma}\Pi_\eta={}^{\Sigma}\Pi_\eta^{\mathrm{i}}+{}^{\Sigma}\Pi_\eta^{\mathrm{t}}\,,\tag{7.75}$$

where ${}^{\Sigma}\Pi^{\mathrm{i}}_{\eta}$ represents the intrinsic surface entropy production due to processes inside the active surface Σ and ${}^{\Sigma}\Pi^{\mathrm{t}}_{\eta}$ corresponds to the transfer processes between the interface and the bulk, and these two terms take the form:

$$
\begin{aligned}
{}^{\Sigma}\Pi^{\mathrm{i}}_{\eta} \stackrel{\mathrm{def}}{=} & \underbrace{\left(\frac{{}^{\Sigma}\mathrm{P}+{}^{\Sigma}p}{{}_{\Sigma}\vartheta}\right)\mathrm{div}^{\Sigma}\,{}^{\Sigma}\mathbf{v} + \frac{{}^{\Sigma}\quad:{}^{\Sigma}\quad d}{{}_{\Sigma}\vartheta}}_{{}^{\Sigma}\Pi^{\mathrm{i,mech}}_{\eta}} \\
& \underbrace{-\sum_{\alpha\in K}{}^{\Sigma}\mathbf{J}^{\mathrm{M,diff}}_{\alpha}\cdot\left\{\nabla^{\Sigma}\left(\frac{{}^{\Sigma}\mu^{\mathrm{M}}_{\alpha}-{}^{\Sigma}\mu^{\mathrm{M}}_{0}}{{}_{\Sigma}\vartheta}\right)-\left(\frac{{}^{\Sigma}\mathbf{b}^{\mathrm{M}}_{\alpha}}{{}_{\Sigma}\vartheta}\right)\right\}+{}^{\Sigma}\mathbf{J}_{e}\cdot\nabla^{\Sigma}\left(\frac{1}{{}_{\Sigma}\vartheta}\right)}_{{}^{\Sigma}\Pi^{\mathrm{i,diff}}_{\eta}} \\
& \underbrace{-\sum_{\alpha\in K}\frac{{}^{\Sigma}\mu^{\mathrm{M}}_{\alpha}-{}^{\Sigma}\mu^{\mathrm{M}}_{0}}{{}_{\Sigma}\vartheta}\,{}^{\Sigma}r^{\mathrm{M}}_{\alpha}}_{{}^{\Sigma}\Pi^{\mathrm{i,chem}}_{\eta}} = {}^{\Sigma}\Pi^{\mathrm{i,mech}}_{\eta}+{}^{\Sigma}\Pi^{\mathrm{i,diff}}_{\eta}+{}^{\Sigma}\Pi^{\mathrm{i,chem}}_{\eta}\ , \qquad (7.76)
\end{aligned}
$$

$$
\begin{aligned}
{}^{\Sigma}\Pi^{\mathrm{t}}_{\eta} \stackrel{\mathrm{def}}{=} & -\sum_{\alpha\in K}\left(\frac{{}^{\Sigma}\mu^{\mathrm{M}}_{\alpha}-{}^{\Sigma}\mu^{\mathrm{M}}_{0}}{{}_{\Sigma}\vartheta}-\frac{\mu^{\mathrm{M}}_{\alpha}}{\vartheta}\right){}^{\Sigma}s^{\mathrm{M}}_{\alpha}-\frac{1}{{}_{\Sigma}\vartheta}(\mathbf{v}-{}^{\Sigma}\mathbf{v})_{\tau}\cdot(\ \ \mathbf{n})_{\tau}-\frac{1}{{}_{\Sigma}\vartheta}\left(\mathbf{n}\cdot\ \ {}^{\mathrm{e}}\mathbf{n}-\frac{1}{2}\rho|\mathbf{v}-{}^{\Sigma}\mathbf{v}|^{2}\right)\mathbf{v}\cdot\mathbf{n} \\
& -\left(\mathbf{J}_{e}\cdot\mathbf{n}+\rho\left(e+\frac{p}{\rho}\right)\mathbf{v}\cdot\mathbf{n}\right)\left(\frac{1}{\vartheta}-\frac{1}{{}_{\Sigma}\vartheta}\right)\ . \qquad (7.77)
\end{aligned}
$$

where we introduced the bulk "extra stress" tensor

$$
{}^{\mathrm{e}} \stackrel{\mathrm{def}}{=} (\mathrm{P}+p)\ +\quad . \qquad (7.78)
$$

Our strategy (motivated by the CIT framework) is to regroup the terms in both groups in the form of a generalized product of thermodynamic "fluxes" and "affinities". While the expression (7.76) is an exact counterpart of (7.18), the terms in the transfer part (7.77) are more challenging and allow multiple possibilities for the construction of the corresponding constitutive relations. We discuss two possibilities in Section 7.2.3.

7.2.3 Constitutive relations on the active surface

Concerning the constitutive relations we treat the intrinsic and transfer entropy production terms (7.76) and (7.77) separately, meaning that we do not consider any cross-coupling effects between them.

Intrinsic surface processes

The processes of surface entropy production due to mechanical dissipation ${}^{\Sigma}\Pi^{\mathrm{i,mech}}_{\eta}$ (surface compression plus surface shear deformation), entropy production due to surface chemical reactions ${}^{\Sigma}\Pi^{\mathrm{i,chem}}_{\eta}$ and, finally, entropy production due to diffusion ${}^{\Sigma}\Pi^{\mathrm{i,diff}}_{\eta}$ (of heat and of mass), are treated analogously to the dissipative processes considered in the bulk. Again, for simplicity, we do not take into account the mechano-chemical cross coupling, allowing only the "vectorial" coupling by thermo-diffusion.

- **Surface compaction and shear deformation - surface rheology:**
  Concerning the mechanical contribution to the surface entropy production, the CIT

constitutive relations suggest the following surface rheological model

$$ {}^{\Sigma}\mathrm{P}+{}^{\Sigma}p=({}^{\Sigma}\lambda+{}^{\Sigma}\nu)\,\mathrm{div}^{\Sigma}\,{}^{\Sigma}\mathbf{v}\ , \tag{7.79} $$

$$ {}^{\Sigma}\quad=2\,{}^{\Sigma}\nu\,{}^{\Sigma}\quad{}^{d}\ , \tag{7.80} $$

where ${}^{\Sigma}\nu$ and ${}^{\Sigma}\lambda$ are viscosity parameters, such that ${}^{\Sigma}\nu\geq 0$ and ${}^{\Sigma}\lambda+{}^{\Sigma}\nu\geq 0$, which implies that ${}^{\Sigma}\Pi_{\eta}^{\mathrm{i,mech}}\geq 0$. The surface Cauchy stress then reads

$$ {}^{\Sigma}\quad=-{}^{\Sigma}p\,{}^{\Sigma}\quad+{}^{\Sigma}\lambda\,\mathrm{div}^{\Sigma}\,{}^{\Sigma}\mathbf{v}\,{}^{\Sigma}\quad+2{}^{\Sigma}\nu\,{}^{\Sigma}\quad\ . \tag{7.81} $$

- *Surface chemical reactions*
  Chemical reactions among the surface species ${}^{\Sigma}\mathrm{A}_{\alpha}$, $\alpha\in K_0$, can be symbolically written as follows:

$$ \sum_{\alpha\in K_0}{}^{\Sigma}\delta_{\alpha}^{\zeta,f}\ {}^{\Sigma}\mathrm{A}_{\alpha}\quad\sum_{\alpha\in K_0}{}^{\Sigma}\delta_{\alpha}^{\zeta,b}\ {}^{\Sigma}\mathrm{A}_{\alpha}\ ,\qquad \zeta=1,\ldots,{}^{\Sigma}Z\ . \tag{7.82} $$

  Here ${}^{\Sigma}Z$ is the number of surface chemical reactions, ${}^{\Sigma}\delta_{\alpha}^{\zeta,f}$, ${}^{\Sigma}\delta_{\alpha}^{\zeta,b}$ are the forward and backward surface stoichiometric coefficients of the αth reactant in the ζth reaction, respectively. Since in general the free sites can be evacuated or, conversely, occupied during a surface chemical reaction, we formally add the vacancies ${}^{\Sigma}\mathrm{A}_0$ into the reaction mechanisms with the corresponding stoichiometric coefficients ${}^{\Sigma}\delta_{0}^{\zeta,f}$, ${}^{\Sigma}\delta_{0}^{\zeta,b}$. Denoting the stoichiometric coefficient of the combined (forward/backward ζth reaction) by

$$ {}^{\Sigma}\delta_{\alpha}^{\zeta}\stackrel{\mathrm{def}}{=}{}^{\Sigma}\delta_{\alpha}^{\zeta,b}-{}^{\Sigma}\delta_{\alpha}^{\zeta,f}\ ,\qquad \alpha\in K_0\ ,\quad \zeta=1,\ldots{}^{\Sigma}Z\ , \tag{7.83} $$

  we impose for the vacancies the condition

$$ {}^{\Sigma}\delta_{0}^{\zeta}\stackrel{\mathrm{def}}{=}-\sum_{\alpha\in K}{}^{\Sigma}\delta_{\alpha}^{\zeta}\ ,\qquad \zeta=1,\ldots,{}^{\Sigma}Z\ , \tag{7.84} $$

  stating that the total number of sites (occupied and vacant) does not change in the chemical reactions[3]. With the use of stoichiometry, the molar rate ${}^{\Sigma}r_{\alpha}^{\mathrm{M}}$ of production of the α constituent in surface chemical reactions can be expressed as

$$ {}^{\Sigma}r_{\alpha}^{\mathrm{M}}=\sum_{a=1}^{{}^{\Sigma}Z}{}^{\Sigma}\delta_{\alpha}^{\zeta}({}^{\Sigma}\mathcal{R}_{\zeta}^{f}-{}^{\Sigma}\mathcal{R}_{\zeta}^{b})=\sum_{a=1}^{{}^{\Sigma}Z}{}^{\Sigma}\delta_{\alpha}^{\zeta}\,{}^{\Sigma}\mathcal{R}_{\zeta}\ ,\qquad \alpha\in K_0\ , \tag{7.85} $$

  where ${}^{\Sigma}\mathcal{R}_{\zeta}^{f}$ and ${}^{\Sigma}\mathcal{R}_{\zeta}^{b}$ denote the forward and backward reaction rate of the ζth surface chemical reaction and ${}^{\Sigma}\mathcal{R}_{\zeta}\stackrel{\mathrm{def}}{=}{}^{\Sigma}\mathcal{R}_{\zeta}^{f}-{}^{\Sigma}\mathcal{R}_{\zeta}^{b}$.

  The surface chemical reaction contribution to the surface entropy production (7.76) is

$$ {}^{\Sigma}\Pi_{\eta}^{\mathrm{i,chem}}=-\sum_{\alpha\in K}\frac{{}^{\Sigma}\mu_{\alpha}^{\mathrm{M}}-{}^{\Sigma}\mu_{0}^{\mathrm{M}}}{{}_{\Sigma}\vartheta}\,{}^{\Sigma}r_{\alpha}^{\mathrm{M}}\ . \tag{7.86} $$

  Using the expression for the molar reaction rate (7.85), we can rewrite it as

$$ {}^{\Sigma}\Pi_{\eta}^{\mathrm{i,chem}}=-\frac{1}{{}_{\Sigma}\vartheta}\sum_{a=1}^{{}^{\Sigma}Z}({}^{\Sigma}\mathcal{R}_{\zeta}^{f}-{}^{\Sigma}\mathcal{R}_{\zeta}^{b})\,{}^{\Sigma}\mathcal{A}^{\zeta} \tag{7.87} $$

[3] In fact (7.84) holds in this particular form if each surface molecule occupies exactly one site and can be easily modified in the multi-site adsorption case by assuming ${}^{\Sigma}\delta_{0}^{\zeta}\stackrel{\mathrm{def}}{=}-\sum_{\alpha\in K}r_{\alpha}\,{}^{\Sigma}\delta_{\alpha}^{\zeta}$, $\zeta=1,\ldots,{}^{\Sigma}Z$, where r_{α} is the number of adsorption sites occupied by a molecule of type α.

where we define the affinity of the ζth surface chemical reaction as

$$ {}^{\Sigma}\mathcal{A}^{\zeta} \stackrel{\text{def}}{=} \sum_{\alpha\in K} ({}^{\Sigma}\mu_{\alpha}^{\mathrm{M}} - {}^{\Sigma}\mu_{0}^{\mathrm{M}})\,{}^{\Sigma}\delta_{\alpha}^{\zeta} \ . \tag{7.88} $$

Considering the following nonlinear constitutive relation for ${}^{\Sigma}\mathcal{A}^{\zeta}$:

$$ {}^{\Sigma}\mathcal{A}^{\zeta} = {}^{\Sigma}\beta^{\zeta} R\, {}^{\Sigma}\vartheta \ln\left(\frac{{}^{\Sigma}\mathcal{R}_{\zeta}^{b}}{{}^{\Sigma}\mathcal{R}_{\zeta}^{f}}\right) \ , \qquad {}^{\Sigma}\beta^{\zeta} \geq 0 \ , \qquad \zeta = 1, \dots, {}^{\Sigma}Z \ . \tag{7.89} $$

we obtain

$$ {}^{\Sigma}\Pi_{\eta}^{\mathrm{i,chem}} = R \sum_{\zeta=1}^{Z} {}^{\Sigma}\beta^{\zeta} ({}^{\Sigma}\mathcal{R}_{\zeta}^{f} - {}^{\Sigma}\mathcal{R}_{\zeta}^{b})(\ln {}^{\Sigma}\mathcal{R}_{\zeta}^{f} - \ln {}^{\Sigma}\mathcal{R}_{\zeta}^{b}) \ , \tag{7.90} $$

which implies that ${}^{\Sigma}\Pi_{\eta}^{\mathrm{i,chem}} \geq 0$ due to the monotone property of logarithm. Particularly, for our model, we can further use the expression for the chemical potential (7.64) and express the chemical affinity (7.88) as

$$ {}^{\Sigma}\mathcal{A}^{\zeta} = R\, {}^{\Sigma}\vartheta \left\{ \ln \prod_{\alpha\in K} \left(\frac{q_0^{\Sigma}}{q_{\alpha}^{\Sigma}}\right)^{{}^{\Sigma}\delta_{\alpha}^{\zeta}} + \ln \prod_{\alpha\in K} \left(\frac{{}^{\Sigma}x_{\alpha}}{1 - \sum_{\beta\in K} {}^{\Sigma}x_{\beta}}\right)^{{}^{\Sigma}\delta_{\alpha}^{\zeta}} \right\} \ , \qquad \zeta = 1, \dots, {}^{\Sigma}Z \ . \tag{7.91} $$

Introducing the surface equilibrium constant of the ζth reaction ${}^{\Sigma}\mathcal{K}_{\zeta}^{\mathrm{chem}}$ through

$$ {}^{\Sigma}\mathcal{K}_{\zeta}^{\mathrm{chem}}({}^{\Sigma}\vartheta) \stackrel{\text{def}}{=} \prod_{\alpha\in K} \left(\frac{{}^{\Sigma}q_{\alpha}}{{}^{\Sigma}q_{0}}\right)^{{}^{\Sigma}\delta_{\alpha}^{\zeta}} \ , \qquad \zeta = 1, \dots, {}^{\Sigma}Z \ , \tag{7.92} $$

and by comparing (7.89) and (7.91), we obtain

$$ \prod_{\alpha\in K} \left(\frac{{}^{\Sigma}x_{\alpha}}{1 - \sum_{\beta=1}^{K} {}^{\Sigma}x_{\beta}}\right)^{{}^{\Sigma}\delta_{\alpha}^{\zeta}} = {}^{\Sigma}\mathcal{K}_{\zeta}^{\mathrm{chem}}({}^{\Sigma}\vartheta) \left(\frac{{}^{\Sigma}\mathcal{R}_{\zeta}^{b}}{{}^{\Sigma}\mathcal{R}_{\zeta}^{f}}\right)^{{}^{\Sigma}\beta^{\zeta}} \ , \qquad \zeta = 1, \dots, {}^{\Sigma}Z \ . \tag{7.93} $$

One of the rates ${}^{\Sigma}\mathcal{R}_{\zeta}^{f}$, ${}^{\Sigma}\mathcal{R}_{\zeta}^{b}$ has still to be modelled, while the other is then given by relation (7.93). Following the method presented in Section 7.1.2, one possible choice of the reaction kinetics would be

$$ \left({}^{\Sigma}\mathcal{R}_{\zeta}^{f}\right)^{{}^{\Sigma}\beta^{\zeta}} = {}^{\Sigma}k_{\zeta}^{f}({}^{\Sigma}\vartheta) \prod_{\alpha\in K} \left(\frac{{}^{\Sigma}x_{\alpha}}{1 - \sum_{\beta=1}^{K} {}^{\Sigma}x_{\beta}}\right)^{{}^{\Sigma}\delta_{\alpha}^{\zeta,f}} \ , \qquad \zeta = 1, \dots, {}^{\Sigma}Z \ , \tag{7.94a} $$

$$ \left(\mathcal{R}_{\zeta}^{b}\right)^{\beta_a} = {}^{\Sigma}k_{\zeta}^{b}({}^{\Sigma}\vartheta) \prod_{\alpha\in K} \left(\frac{{}^{\Sigma}x_{\alpha}}{1 - \sum_{\beta=1}^{K} {}^{\Sigma}x_{\beta}}\right)^{{}^{\Sigma}\delta_{\alpha}^{\zeta,b}} \ , \qquad \zeta = 1, \dots, {}^{\Sigma}Z \ , \tag{7.94b} $$

where ${}^{\Sigma}\delta_{\alpha}^{\zeta,f}$, ${}^{\Sigma}\delta_{\alpha}^{\zeta,b}$ are the forward and backward stoichiometric coefficients of the ζth reaction, see (7.83), and the coefficients ${}^{\Sigma}k_{\zeta}^{f}({}^{\Sigma}\vartheta)$, ${}^{\Sigma}k_{\zeta}^{b}({}^{\Sigma}\vartheta)$ must satisfy $\frac{{}^{\Sigma}k_{\zeta}^{f}({}^{\Sigma}\vartheta)}{{}^{\Sigma}k_{\zeta}^{b}({}^{\Sigma}\vartheta)} = {}^{\Sigma}\mathcal{K}_{\zeta}^{\mathrm{chem}}({}^{\Sigma}\vartheta)$, $\zeta = 1, \dots, {}^{\Sigma}Z$.

Observe that, as a consequence of the fact that the logarithm is strictly monotone, the surface entropy production due to the chemical reactions ${}^{\Sigma}\Pi_{\eta}^{\mathrm{i,chem}}$ vanishes only

if ${}^{\Sigma}\mathcal{A}^{\zeta}=0$, $\zeta=1,\dots,{}^{\Sigma}Z$, which is the so-called principle of detailed balance. In that case we have

$$\prod_{\alpha\in K}\left(\frac{{}^{\Sigma}x_{\alpha}}{1-\sum_{\beta=1}^{K}{}^{\Sigma}x_{\beta}}\right)^{{}^{\Sigma}\delta_{\alpha}^{\zeta}}={}^{\Sigma}\mathcal{K}_{\zeta}^{\mathrm{chem}}({}^{\Sigma}\vartheta)\ ,\qquad \zeta=1,\dots,{}^{\Sigma}Z\ , \tag{7.95}$$

representing the surface equilibrium mass-action law.

- **Thermo-diffusion – CIT:**
Analogously as in the bulk, the constitutive relations for thermo-diffusion (within CIT) take the following form

$$\begin{pmatrix} -{}^{\Sigma}\mathbf{J}_{1}^{\mathrm{M,diff}} \\ \vdots \\ -{}^{\Sigma}\mathbf{J}_{N-1}^{\mathrm{M,diff}} \\ {}^{\Sigma}\mathbf{J}_{e} \end{pmatrix}= \tag{7.96}$$

$$\underbrace{\begin{pmatrix} {}^{\Sigma}_{1,1} & \cdots & {}^{\Sigma}_{1,N-1} & {}^{\Sigma}_{1,N} \\ \vdots & & \vdots & \vdots \\ {}^{\Sigma}_{N-1,1} & \cdots & {}^{\Sigma}_{N-1,N-1} & {}^{\Sigma}_{N-1,N} \\ {}^{\Sigma}_{N,1} & \cdots & {}^{\Sigma}_{N,N-1} & {}^{\Sigma}_{N,N} \end{pmatrix}}_{\Sigma}\begin{pmatrix} \nabla^{\Sigma}\left(\frac{{}^{\Sigma}\bar{\mu}_{1}^{\mathrm{M}}-{}^{\Sigma}\bar{\mu}_{N,1}^{\mathrm{M}}}{{}^{\Sigma}\vartheta}\right)-\left(\frac{{}^{\Sigma}\mathbf{b}_{1}^{\mathrm{M}}-{}^{\Sigma}\mathbf{b}_{N,1}^{\mathrm{M}}}{{}^{\Sigma}\vartheta}\right) \\ \vdots \\ \nabla^{\Sigma}\left(\frac{{}^{\Sigma}\bar{\mu}_{N-1}^{\mathrm{M}}-{}^{\Sigma}\bar{\mu}_{N,N-1}^{\mathrm{M}}}{{}^{\Sigma}\vartheta}\right)-\left(\frac{{}^{\Sigma}\mathbf{b}_{N-1}^{\mathrm{M}}-{}^{\Sigma}\mathbf{b}_{N,N-1}^{\mathrm{M}}}{{}^{\Sigma}\vartheta}\right) \\ \nabla^{\Sigma}\left(\frac{1}{{}^{\Sigma}\vartheta}\right) \end{pmatrix}, \tag{7.97}$$

where

$${}^{\Sigma}\bar{\mu}_{\alpha}^{\mathrm{M}}\overset{\mathrm{def}}{=}{}^{\Sigma}\mu_{\alpha}^{\mathrm{M}}-{}^{\Sigma}\mu_{0}^{\mathrm{M}}\ ,\qquad {}^{\Sigma}\bar{\mu}_{\alpha,\beta}^{\mathrm{M}}\overset{\mathrm{def}}{=}\frac{M_{\alpha}}{M_{\beta}}{}^{\Sigma}\bar{\mu}_{\beta}^{\mathrm{M}}\ ,\qquad {}^{\Sigma}\mathbf{b}_{\alpha,\beta}^{\mathrm{M}}\overset{\mathrm{def}}{=}\frac{M_{\alpha}}{M_{\beta}}{}^{\Sigma}\mathbf{b}_{\beta}^{\mathrm{M}}\ ,\qquad \alpha,\beta\in K\ . \tag{7.98}$$

and where ${}^{\Sigma}$ is a symmetric positive semi-definite matrix in order to guarantee ${}^{\Sigma}\Pi_{\eta}^{\mathrm{i,diff}}\geq 0$. The diagonal of the matrix corresponds to the surface Fick's laws for mass diffusion (the first $N-1$ entries) and surface Fourier's law for heat conduction (last entry), respectively. The off-diagonal terms represent the cross-coupling effects which are restricted (within CIT) by Onsager reciprocity relations, [e.g. 23], postulating symmetry of the matrix ${}^{\Sigma}$.

- **Thermo-diffusion – Maxwell-Stefan equations:**
Alternatively, the constitutive relations for surface mass diffusion can take the form of Maxwell-Stefan equations. Starting from ${}^{\Sigma}\Pi_{\eta}^{\mathrm{i,diff-m}}\overset{\mathrm{def}}{=}-\sum_{\alpha\in K}{}^{\Sigma}\mathbf{J}_{\alpha}^{\mathrm{M,diff}}\cdot\left\{\nabla^{\Sigma}\left(\frac{{}^{\Sigma}\mu_{\alpha}^{\mathrm{M}}-{}^{\Sigma}\mu_{0}^{\mathrm{M}}}{{}^{\Sigma}\vartheta}\right)-\left(\frac{{}^{\Sigma}\mathbf{b}_{\alpha}^{\mathrm{M}}}{{}^{\Sigma}\vartheta}\right)\right\}$, one proceeds analogously as in the bulk, see the computation between (7.26) and (7.43), using the surface Euler relation (7.68) and the surface Gibbs-Duhem relation (C.177) in the incompressible limit (i.e. for ${}^{\Sigma}c^{\mathrm{M}}$=const.), one obtains the following form of the surface Maxwell-Stefan system:

$$\begin{aligned}-\sum_{\beta\in K}\frac{{}^{\Sigma}x_{\beta}\,{}^{\Sigma}\mathbf{J}_{\alpha}^{\mathrm{M,diff}}-{}^{\Sigma}x_{\alpha}\,{}^{\Sigma}\mathbf{J}_{\beta}^{\mathrm{M,diff}}}{{}^{\Sigma}\mathrm{D}_{\alpha\beta}}&=\frac{{}^{\Sigma}c_{\alpha}^{\mathrm{M}}}{R\,{}^{\Sigma}\vartheta}\nabla^{\Sigma}{}^{\Sigma}\bar{\mu}_{\alpha}^{\mathrm{M}}-\frac{{}^{\Sigma}c_{\alpha}}{R\,{}^{\Sigma}\vartheta}\nabla^{\Sigma}{}^{\Sigma}p-\frac{\rho_{\alpha}^{\Sigma}{}^{\Sigma}h-{}^{\Sigma}c_{\alpha}^{\mathrm{M}}\,{}^{\Sigma}\bar{\mu}_{\alpha}^{\mathrm{M}}}{R\,{}^{\Sigma}\vartheta}\nabla^{\Sigma}\ln{}^{\Sigma}\vartheta\\&\quad-\frac{\rho_{\alpha}^{\Sigma}}{R\,{}^{\Sigma}\vartheta}({}^{\Sigma}\mathbf{b}_{\alpha}-{}^{\Sigma}\mathbf{b})\ ,\ \alpha\in K\ ,\end{aligned} \tag{7.99}$$

where ${}^{\Sigma}h$ is the specific surface enthalpy defined as[4]

$$ {}^{\Sigma}h \stackrel{\text{def}}{=} {}^{\Sigma}e + \frac{{}^{\Sigma}p}{\rho^{\Sigma}} \ . \tag{7.100} $$

The surface Maxwell-Stefan diffusivity matrix possesses the following structure:

$$ {}^{\Sigma}\mathrm{D}_{\alpha\beta} = \frac{R}{{}^{\Sigma}c^{\mathrm{M}}\, M_\alpha M_\beta {}^{\Sigma}f_{\alpha\beta}} \ , \qquad \alpha,\beta\in K \ , \tag{7.101} $$

with ${}^{\Sigma}f_{\alpha\beta}$ being a symmetric surface friction coefficient matrix with positive entries ${}^{\Sigma}f_{\alpha,\beta}\geq{}^{\Sigma}\epsilon>0$, $\alpha,\beta\in K$.

Transfer processes

We wish to exploit the entropy production arising due to the transfer of mass, momenta and energy between the bulk and surface phases. We recall that we have identified the corresponding contribution in (7.77) as

$$ \begin{aligned} {}^{\Sigma}\Pi^{\mathrm{t}}_{\eta} = &- \sum_{\alpha\in K}\left(\frac{{}^{\Sigma}\mu^{\mathrm{M}}_{\alpha}-{}^{\Sigma}\mu^{\mathrm{M}}_{0}}{{}^{\Sigma}\vartheta}-\frac{\mu^{\mathrm{M}}_{\alpha}}{\vartheta}\right){}^{\Sigma}s^{\mathrm{M}}_{\alpha} - \frac{1}{{}_{\Sigma}\vartheta}(\mathbf{v}-{}^{\Sigma}\mathbf{v})_{\tau}\cdot(\ \mathbf{n})_{\tau} - \frac{1}{{}_{\Sigma}\vartheta}\left(\mathbf{n}\cdot\ {}^{\mathrm{e}}\mathbf{n}-\frac{1}{2}\rho|\mathbf{v}-{}^{\Sigma}\mathbf{v}|^2\right)\mathbf{v}\cdot\mathbf{n} \\ &- \left(\mathbf{J}_e\cdot\mathbf{n}+\rho\left(e+\frac{p}{\rho}\right)\mathbf{v}\cdot\mathbf{n}\right)\left(\frac{1}{\vartheta}-\frac{1}{{}_{\Sigma}\vartheta}\right) \ . \end{aligned} \tag{7.102} $$

Concerning the linear constitutive relations that can be obtained from this expression, several different suggestions can be found in the literature. Surprisingly, some of those seem to violate the principle of material frame indifference [independence of the form of the constitutive relations on the observer, see 110]. For example in [86] (eq. 63) a non-objective (for $\vartheta\neq{}^{\Sigma}\vartheta$) term $\mathbf{v}/\vartheta-{}^{\Sigma}\mathbf{v}/{}^{\Sigma}\vartheta$ is considered as an affinity for the constitutive relation of the type (7.116) for surface friction, or the non-objective "velocity-modifed chemical potentials" $\tilde{\mu}_\alpha \stackrel{\text{def}}{=} \mu_\alpha-|\mathbf{v}|^2/2$ [appearing also in 7, see eq. (4.6.7)] are introduced.

Here, we propose the following two possible forms of constitutive relations (Model A and Model B) that are both consistent with the principle of material frame indifference. The Model B in addition provides compatibility with the jump conditions across interfaces.

Transfer model A

In the first approach, we follow [10], where the author argues that the "affinity" $\mathbf{v}\cdot\mathbf{n}$ cannot be considered independently of the sorption rates ${}^{\Sigma}s^{\mathrm{M}}_{\alpha}$. Indeed the relation (6.16) that expresses mass conservation for sorption, together with the considered boundary conditions imply

$$ \sum_{\alpha\in K} M_\alpha {}^{\Sigma}s^{\mathrm{M}}_{\alpha} = \rho\mathbf{v}\cdot\mathbf{n} \ . \tag{7.103} $$

[4]Here, the same remark applies as in the bulk case, i.e. if the Maxwell-Stefan relations were derived within so-called Class II mixture theory (where individual velocities of mixture constituents are taken as independent variables), the terms $\rho^{\Sigma}_{\alpha}h$ would be replaced by $\rho^{\Sigma}{}^{\Sigma}h_\alpha$ where ${}^{\Sigma}h_\alpha$ are partial surface enthalphies.

Therefore, providing independently constitutive relations for the first and the third term on the right-hand side of (7.102), as it is presented in [7] or [86], contradicts (7.103). On the other hand, [10] suggests to insert (7.103) into (7.102) to obtain

$$
{}^{\Sigma}\Pi_{\eta}^{\mathrm{t(A)}} \overset{\mathrm{def}}{=} \underbrace{-\sum_{\alpha\in K}\left(\frac{{}^{\Sigma}\mu_{\alpha}^{\mathrm{M}}-{}^{\Sigma}\mu_{0}^{\mathrm{M}}}{{}^{\Sigma}\vartheta}-\frac{\mu_{\alpha}^{\mathrm{M}}}{\vartheta}+\frac{M_{\alpha}}{{}^{\Sigma}\vartheta}\left\{\frac{\mathbf{n}\cdot\ {}^{\mathrm{e}}\mathbf{n}}{\rho}-\frac{1}{2}|\mathbf{v}-{}^{\Sigma}\mathbf{v}|^{2}\right\}\right){}^{\Sigma}s_{\alpha}^{\mathrm{M}}}_{{}^{\Sigma}\Pi_{\eta}^{\mathrm{sor(A)}}} \underbrace{-\frac{1}{{}^{\Sigma}\vartheta}(\mathbf{v}-{}^{\Sigma}\mathbf{v})_{\tau}\cdot(\ \mathbf{n})_{\tau}}_{{}^{\Sigma}\Pi_{\eta}^{\mathrm{fric(A)}}}
$$

$$
\underbrace{-\left(\mathbf{J}_{e}\cdot\mathbf{n}+\rho\left(e+\frac{p}{\rho}\right)\mathbf{v}\cdot\mathbf{n}\right)\left(\frac{1}{\vartheta}-\frac{1}{{}^{\Sigma}\vartheta}\right)}_{{}^{\Sigma}\Pi_{\eta}^{\mathrm{et(A)}}} = {}^{\Sigma}\Pi_{\eta}^{\mathrm{sor(A)}}+{}^{\Sigma}\Pi_{\eta}^{\mathrm{fric(A)}}+{}^{\Sigma}\Pi_{\eta}^{\mathrm{et(A)}}\ . \tag{7.104}
$$

We can interpret the respective entropy production contributions as due to (i) sorption (ii) surface friction and (iii) energy transfer across the interface. Following this approach we can formulate the constitutive relations. For simplicity and due to the nonlinear character of the constitutive relations for sorption, we do not consider any cross-coupling effects among these dissipative mechanisms. Let us discuss the individual mechanisms in detail.

- *Sorption*
  Sorption can be formally viewed as a special type of chemical transformation involving a bulk substance, its surface counterpart and vacancies. This can be written as

$$
\mathrm{A}_{\alpha}+{}^{\Sigma}\mathrm{A}_{0} \qquad {}^{\Sigma}\mathrm{A}_{\alpha}\ , \qquad \alpha\in K\ . \tag{7.105}
$$

  The forward direction represents the adsorption process resulting in transformation of the bulk constituent A_α into the corresponding surface constituent ${}^{\Sigma}\mathrm{A}_{\alpha}$, filling the vacancies[5]. The reverse process, i.e. evacuation of the site occupied by ${}^{\Sigma}\mathrm{A}_{\alpha}$ and its transfer to the bulk (forming A_α) creating a vacancy ${}^{\Sigma}\mathrm{A}_{0}$ in the process, is called desorption. The molar rate of transfer of the αth constituent between the bulk and the surface ${}^{\Sigma}s_{\alpha}^{\mathrm{M}}$ is equal to the difference between the adsorption and the desorption rates:

$$
{}^{\Sigma}s_{\alpha}^{\mathrm{M}} = {}^{\Sigma}s_{\alpha}^{\mathrm{M}ad}-{}^{\Sigma}s_{\alpha}^{\mathrm{M}de} \qquad \alpha\in K. \tag{7.106}
$$

  The sorption contribution to the surface entropy production (7.104) reads

$$
{}^{\Sigma}\Pi_{\eta}^{\mathrm{sor(A)}} = -\sum_{\alpha\in K}\left(\frac{{}^{\Sigma}\mu_{\alpha}^{\mathrm{M}}-{}^{\Sigma}\mu_{0}^{\mathrm{M}}}{{}^{\Sigma}\vartheta}-\frac{\mu_{\alpha}^{\mathrm{M}}}{\vartheta}+\frac{M_{\alpha}\Upsilon^{(\mathrm{A})}}{{}^{\Sigma}\vartheta\,\rho}\right){}^{\Sigma}s_{\alpha}^{\mathrm{M}}\ , \tag{7.107}
$$

  where we abbreviated

$$
\Upsilon^{(\mathrm{A})} \overset{\mathrm{def}}{=} \mathbf{n}\cdot\ {}^{\mathrm{e}}\mathbf{n}-\frac{1}{2}\rho|\mathbf{v}-{}^{\Sigma}\mathbf{v}|^{2}\ . \tag{7.108}
$$

  With the choice of chemical potentials in the bulk (7.12) and on the surface (7.64), we obtain

$$
{}^{\Sigma}\Pi_{\eta}^{\mathrm{sor(A)}} = -R\sum_{\alpha\in K}\left[\left(\ln\left(\frac{{}^{\Sigma}q_{0}({}^{\Sigma}\vartheta)}{{}^{\Sigma}q_{\alpha}({}^{\Sigma}\vartheta)}\right)-\frac{\mu_{\alpha}^{\mathrm{M}0}(\vartheta,p)}{R\vartheta}+\frac{M_{\alpha}\Upsilon^{(\mathrm{A})}}{R\,\rho\,{}^{\Sigma}\vartheta}\right)+\ln\left(\frac{{}^{\Sigma}x_{\alpha}}{x_{\alpha}(1-\sum_{\beta\in K}{}^{\Sigma}x_{\beta})}\right)\right]{}^{\Sigma}s_{\alpha}^{\mathrm{M}}. \tag{7.109}
$$

[5] The stoichiometry in (7.105) describes *single-site adsorption*, i.e. the case when each molecule occupies exactly one adsorption site. For multi-site adsorption, (7.105) should be replaced by $\mathrm{A}_{\alpha}+r_{\alpha}\,{}^{\Sigma}\mathrm{A}_{0}$ ${}^{\Sigma}\mathrm{A}_{\alpha}$, $\alpha\in K$, where r_α is the number of sites occupied by the αth constituent.

Introducing the equilibrium sorption constants $\mathcal{K}_\alpha^{\mathrm{sor}}({}^\Sigma\vartheta,\vartheta,p)$ through

$$\mathcal{K}_\alpha^{\mathrm{sor}}({}^\Sigma\vartheta,\vartheta,p) \stackrel{\mathrm{def}}{=} \left(\frac{{}^\Sigma q_\alpha({}^\Sigma\vartheta)}{{}^\Sigma q_0({}^\Sigma\vartheta)}\right)\exp\left(\frac{\mu_\alpha^{\mathrm{M}0}(\vartheta,p)}{R\vartheta}\right)\ , \qquad \alpha\in K\ , \tag{7.110}$$

we get, using also (7.106)

$${}^\Sigma\Pi_\eta^{\mathrm{sor(A)}} = R\sum_{\alpha\in K}\ln\left(\mathcal{K}_\alpha^{\mathrm{sor}}\exp\left(-\frac{M_\alpha\Upsilon^{(\mathrm{A})}}{R\,\rho\,{}^\Sigma\vartheta}\right)\frac{x_\alpha(1-\sum_{\beta\in K}{}^\Sigma x_\beta)}{{}^\Sigma x_\alpha}\right)({}^\Sigma s_\alpha^{\mathrm{M}ad}-{}^\Sigma s_\alpha^{\mathrm{M}de})\ . \tag{7.111}$$

Proposing the following non-linear constitutive relations:

$$\frac{{}^\Sigma s_\alpha^{\mathrm{M}ad}}{{}^\Sigma s_\alpha^{\mathrm{M}de}} = \mathcal{K}_\alpha^{\mathrm{sor}}\exp\left(-\frac{M_\alpha\Upsilon^{(\mathrm{A})}}{R\,\rho\,{}^\Sigma\vartheta}\right)\frac{x_\alpha(1-\sum_{\beta\in K}{}^\Sigma x_\beta)}{{}^\Sigma x_\alpha}\ , \qquad \alpha\in K\ , \tag{7.112}$$

and referring to the monotone property of the logarithm, we observe that ${}^\Sigma\Pi_\eta^{\mathrm{sor(A)}}\geq 0$. One of the rates ${}^\Sigma s_\alpha^{\mathrm{M}ad}$, ${}^\Sigma s_\alpha^{\mathrm{M}de}$ still has to be modelled, while the other follows from (7.112). Since in equilibrium ${\Upsilon^{(\mathrm{A})}}_{\mathrm{eq}}=0$, and ${}^\Sigma s_\alpha^{\mathrm{M}ad}={}^\Sigma s_\alpha^{\mathrm{M}de}$, the equilibrium condition for sorption reads

$$1 = \mathcal{K}_\alpha^{\mathrm{sor}}\frac{x_\alpha(1-\sum_{\beta\in K}{}^\Sigma x_\beta)}{{}^\Sigma x_\alpha}\ . \tag{7.113}$$

This is the well-known Langmuir adsorption isotherm [see, e.g. 1]. Motivated by the kinetic derivation of the Langmuir adsorption isotherm [see 56], the following constitutive relations seem plausible:

$${}^\Sigma s_\alpha^{\mathrm{M}ad} = {}^\Sigma k_\alpha^{\mathrm{ad-sor}}\ x_\alpha(1-\sum_{\beta\in K}{}^\Sigma x_\beta)\ , \qquad \alpha\in K\ , \tag{7.114a}$$

$${}^\Sigma s_\alpha^{\mathrm{M}de} = {}^\Sigma k_\alpha^{\mathrm{de-sor}}\ {}^\Sigma x_\alpha\ , \qquad \alpha\in K\ , \tag{7.114b}$$

where by comparison with (7.112) the adsorption/desorption rate coefficients ${}^\Sigma k_\alpha^{\mathrm{ad-sor}}$, ${}^\Sigma k_\alpha^{\mathrm{de-sor}}$ must satisfy

$$\frac{{}^\Sigma k_\alpha^{\mathrm{ad-sor}}}{{}^\Sigma k_\alpha^{\mathrm{de-sor}}} = \mathcal{K}_\alpha^{\mathrm{sor}}\exp\left(-\frac{M_\alpha\Upsilon^{(\mathrm{A})}}{R\,\rho\,{}^\Sigma\vartheta}\right)\ , \qquad \alpha\in K\ . \tag{7.115}$$

Henry isotherm. *In [10] sorption constitutive relations are provided for a fluid-fluid interface in a similar spirit. For an ideal mixture model due to the absence of the constraint* (6.20) *of fixed adsorption sites, this leads to the so-called Henry isotherm and associated sorption kinetics.*

Non-absorbing species. *While we assume implicitly that all bulk constituents can adsorb, i.e. that they have their surface counterparts, we will argue that this is not a restrictive assumption. Assuming that a particular bulk specie A_α has very big (positive) bonding energy, we obtain $q_\alpha\to 0+$ (take $\epsilon_j\to+\infty$, $\forall j$ in the definition of ${}^\Sigma q_\alpha$ in the discussion under* (B.135)*). In view of* (7.110)*, this implies $\mathcal{K}_\alpha^{\mathrm{sor}}\to 0+$ for such species, and consequently, as a result of* (7.113)*, we arrive at ${}^\Sigma x_\alpha\to 0+$, meaning that these species cannot accumulate on the active surface Σ and are thus effectively non-adsorbing.*

- **Surface friction:**
  We propose the following simple linear relation, the so-called Navier-slip condition, between the tangential slip velocity and the tangential component of the surface traction force:

$$(\ \mathbf{n})_\tau = -\,k(\mathbf{v}-{}^\Sigma\mathbf{v})_\tau\ , \tag{7.116}$$

  where $k \geq 0$ in order to ensure ${}^\Sigma\Pi_\eta^{\mathrm{fric(A)}}\geq 0$.

- **Energy transfer across the interface:**
  For the combined conductive and convective latent heat flux across the interface, we consider the following linear constitutive relation

$$\mathbf{J}_e\cdot\mathbf{n}+\rho(\mathbf{v}\cdot\mathbf{n})\left(e+\frac{p}{\rho}\right) = -\,\kappa\left(\frac{1}{\vartheta}-\frac{1}{{}^\Sigma\vartheta}\right)\ , \tag{7.117}$$

  where $\kappa\geq 0$ implies ${}^\Sigma\Pi_\eta^{\mathrm{et(A)}}\geq 0$. The left-hand side represents the diffusive energy flux plus the convective enthalpy flux into the interface and such form can be found e.g. in [32].

Transfer model B:

An alternative constitutive model for the transfer processes follows from the requirement of compatibility with the jump conditions in the following sense. Taking into account the outer domain (which we now effectively ignore due to the choice of the boundary conditions) and considering a limit situation in which all the interfacial processes vanish, in particular neglecting transfer of surface mass, surface momenta and surface energy along the interface, we should recover the traditional jump conditions from the theory of continuum mechanics with an internal surface of discontinuity [e.g. 45]. In order to achieve this, we first rewrite (7.77) equivalently as follows

$$\begin{aligned}
{}^\Sigma\Pi_\eta^{\mathrm{t}} = &-\sum_{\alpha\in K}\left(\frac{{}^\Sigma\mu_\alpha^{\mathrm{M}}-{}^\Sigma\mu_0^{\mathrm{M}}}{{}^\Sigma\vartheta}-\frac{\mu_\alpha^{\mathrm{M}}}{\vartheta}\right){}^\Sigma s_\alpha^{\mathrm{M}} \ -\frac{1}{\vartheta}(\mathbf{v}-{}^\Sigma\mathbf{v})_\tau\cdot((\ \mathbf{n})_\tau-\rho\mathbf{v}\cdot\mathbf{n}\,(\mathbf{v}-{}^\Sigma\mathbf{v})_\tau)\\
&-\frac{1}{\vartheta}\left(\mathbf{n}\cdot\ {}^{\mathrm{e}}\mathbf{n}-\rho(\mathbf{v}\cdot\mathbf{n})^2+\rho\frac{|\mathbf{v}-{}^\Sigma\mathbf{v}|^2}{2}\right)\mathbf{v}\cdot\mathbf{n}\\
&-\left(\mathbf{J}_e\cdot\mathbf{n}+\rho\left(e+\frac{p}{\rho}+\frac{|\mathbf{v}-{}^\Sigma\mathbf{v}|^2}{2}\right)\mathbf{v}\cdot\mathbf{n}-(\ {}^{\mathrm{e}}\mathbf{n})\cdot(\mathbf{v}-{}^\Sigma\mathbf{v})\right)\left(\frac{1}{\vartheta}-\frac{1}{{}^\Sigma\vartheta}\right)\ .
\end{aligned} \tag{7.118}$$

As in the previous Model A, we cannot keep the third term on the right-hand side with "affinity" $\mathbf{v}\cdot\mathbf{n}$ as independent, due to the constraint (7.103). Proceeding as before by absorbing this term into the first term on the right-hand side of (7.118), we obtain

$$\begin{aligned}
{}^\Sigma\Pi_\eta^{\mathrm{t(B)}} \stackrel{\mathrm{def}}{=} &\underbrace{-\sum_{\alpha\in K}\left(\frac{{}^\Sigma\mu_\alpha^{\mathrm{M}}-{}^\Sigma\mu_0^{\mathrm{M}}}{{}^\Sigma\vartheta}-\frac{\mu_\alpha^{\mathrm{M}}}{\vartheta}+\frac{M_\alpha}{\vartheta\rho}\Upsilon^{(\mathrm{B})}\right){}^\Sigma s_\alpha^{\mathrm{M}}}_{{}^\Sigma\Pi_\eta^{\mathrm{sor(B)}}}\ \underbrace{-\frac{1}{\vartheta}(\mathbf{v}-{}^\Sigma\mathbf{v})_\tau\cdot((\ \mathbf{n})_\tau-\rho\mathbf{v}\cdot\mathbf{n}\,(\mathbf{v}-{}^\Sigma\mathbf{v})_\tau)}_{{}^\Sigma\Pi_\eta^{\mathrm{fric(B)}}}\\
&\underbrace{-\left(\mathbf{J}_e\cdot\mathbf{n}+\rho\left(e+\frac{p}{\rho}+\frac{|\mathbf{v}-{}^\Sigma\mathbf{v}|^2}{2}\right)\mathbf{v}\cdot\mathbf{n}-\ {}^{\mathrm{e}}\mathbf{n}\cdot(\mathbf{v}-{}^\Sigma\mathbf{v})\right)\left(\frac{1}{\vartheta}-\frac{1}{{}^\Sigma\vartheta}\right)}_{{}^\Sigma\Pi_\eta^{\mathrm{et(B)}}}\\
&={}^\Sigma\Pi_\eta^{\mathrm{sor(B)}}+{}^\Sigma\Pi_\eta^{\mathrm{fric(B)}}+{}^\Sigma\Pi_\eta^{\mathrm{et(B)}}\ ,
\end{aligned} \tag{7.119}$$

where we abbreviated

$$\Upsilon^{(\mathrm{B})} \stackrel{\text{def}}{=} \mathbf{n}\cdot\ {}^{\mathrm{e}}\mathbf{n} - \rho(\mathbf{v}\cdot\mathbf{n})^2 + \frac{1}{2}\rho|\mathbf{v}-{}^{\Sigma}\mathbf{v}|^2 \ . \tag{7.120}$$

Concerning the constitutive relations for the three dissipative mechanisms: sorption, surface friction and energy transfer, as in the formulation of Model B, we provide non-linear logarithmic constitutive relations for the sorption rates and linear constitutive relations for the latter two. We obtain the following relations

- *Sorption*
  The sorption kinetics for Model B differs (provided we use the same type of logarithmic constitutive relation) only in the form of the factor Υ.

$$\frac{{}^{\Sigma}s_{\alpha}^{\mathrm{M}ad}}{{}^{\Sigma}s_{\alpha}^{\mathrm{M}de}} = K_{\alpha}^{\mathrm{sor}} \exp\left(-\frac{M_{\alpha}\Upsilon^{(\mathrm{B})}}{R\,\rho\,{}^{\Sigma}\vartheta}\right) \frac{x_{\alpha}(1-\sum_{\beta\in K}{}^{\Sigma}x_{\beta})}{{}^{\Sigma}x_{\alpha}} \ . \tag{7.121}$$

  Again, one of the rates ${}^{\Sigma}s_{\alpha}^{\mathrm{M}ad}$, ${}^{\Sigma}s_{\alpha}^{\mathrm{M}de}$ still has to be modelled, while the other follows from (7.121). Again, in equilibrium ${\Upsilon^{(\mathrm{B})}}_{\mathrm{eq}}=0$, so the zero entropy production condition for sorption equilibrium implies the Langmuir adsorption isotherm (7.113). A kinetics constitutive relation of the form (7.114) is again possible, replacing only $\Upsilon^{(\mathrm{A})}$ by $\Upsilon^{(\mathrm{B})}$ in (7.115).

- **Surface friction:** Using a linear constitutive relation, the following alternative form of the Navier-slip condition is obtained

$$(\ \mathbf{n})_{\tau} - \rho\mathbf{v}\cdot\mathbf{n}\,(\mathbf{v}-{}^{\Sigma}\mathbf{v})_{\tau} = -k(\mathbf{v}-{}^{\Sigma}\mathbf{v})_{\tau} \ , \tag{7.122}$$

  where $k \geq 0$ in order to ensure that ${}^{\Sigma}\Pi_{\eta}^{\mathrm{fric(B)}}\geq 0$. This model of surface friction differs from Model A by the presence of a momentum exchange term due to mass transfer $-\rho\mathbf{v}\cdot\mathbf{n}\,(\mathbf{v}-{}^{\Sigma}\mathbf{v})_{\tau}$, which can be found for example in [7] or [86], but here it is expressed in a frame-indifferent form [6], while in [86] the generally non-objective term $\frac{\mathbf{v}_{\tau}}{\vartheta}-\frac{{}^{\Sigma}\mathbf{v}_{\tau}}{{}^{\Sigma}\vartheta}$ is present.

- **Energy transfer across the interface:**
  For the combined conductive and convective latent heat flux across the interface Model B, we consider a linear constitutive relation of the form

$$\mathbf{J}_e\cdot\mathbf{n} + \rho\left(e+\frac{p}{\rho}+\frac{|\mathbf{v}-{}^{\Sigma}\mathbf{v}|^2}{2}\right)\mathbf{v}\cdot\mathbf{n} - (\ {}^{\mathrm{e}}\mathbf{n})\cdot(\mathbf{v}-{}^{\Sigma}\mathbf{v}) = -\kappa\left(\frac{1}{\vartheta}-\frac{1}{{}^{\Sigma}\vartheta}\right) \ , \tag{7.123}$$

  where $\kappa\geq 0$ in order to ensure that ${}^{\Sigma}\Pi_{\eta}^{\mathrm{et(B)}}\geq 0$. This model differs from Model A by the presence of a "kinetic" term $\frac{\rho|\mathbf{v}-{}^{\Sigma}\mathbf{v}|^2}{2}$ in the convective contribution and by the extra stress power $(\ {}^{\mathrm{e}}\mathbf{n})\cdot(\mathbf{v}-{}^{\Sigma}\mathbf{v})$. Let us note that kinetic terms of the first type are present both for instance in [7] or [86], but unlike here, in a non-objective form. The motivation for the presence of the second terms is clarified below.

[6] The term $\mathbf{v}\cdot\mathbf{n}$ is not frame indifferent but it stands throughout the manuscript for a frame indifferent term $(\mathbf{v}-{}^{\Sigma}\mathbf{v})\cdot\mathbf{n}$, where we consistently omit the term ${}^{\Sigma}\mathbf{v}\cdot\mathbf{n}$ working in a frame where the boundary is fixed.

Let us now consider the situation described at the beginning of the part devoted to the derivation of Model B. This means that we do not ignore the outer domain and, simultaneously, that we reduce the interface to just a discontinuity between the two bulk subdomains. In particular we do not allow accumulation of mass, energy, stress or entropy in the interface, and also the surface fluxes and surface chemical reaction rates are identically zero, i.e. we set $\rho_\alpha^\Sigma{=}0$, ${}^\Sigma e{=}0$, ${}^\Sigma\eta{=}\,0$, ${}^\Sigma\mu_\alpha^{\mathrm{M}}{=}0$, and $\mathbf{J}_e^\Sigma{=}0$, ${}^\Sigma\mathbb{T}{=}\mathbf{0}$, ${}^\Sigma\mathbf{J}_\alpha^{\mathrm{diff}}{=}\mathbf{0}$, ${}^\Sigma r_\alpha{=}0$, for all $\alpha{\in}K_0$. The surface mass, momentum and energy balances (6.4), (6.24) (6.33) then reduce to the following jump conditions

$$\llbracket\rho_\alpha\mathbf{v}_\alpha\rrbracket\cdot\mathbf{n}=0\ ,\ \ \alpha{\in}K \quad\Longrightarrow\quad \llbracket\rho\mathbf{v}\rrbracket\cdot\mathbf{n}=0\ , \tag{7.124a}$$

$$\llbracket\rho\mathbf{v}\otimes\mathbf{v}-\mathbb{T}\rrbracket\,\mathbf{n}=\mathbf{0}\ , \tag{7.124b}$$

$$\llbracket\mathbf{J}_e\rrbracket\cdot\mathbf{n}+\left\llbracket\rho\left(e+\frac{1}{2}|\mathbf{v}{-}{}^\Sigma\mathbf{v}|^2\right)\mathbf{v}\right\rrbracket\cdot\mathbf{n}-\llbracket(\mathbf{v}{-}{}^\Sigma\mathbf{v})\cdot\mathbb{T}\rrbracket\,\mathbf{n}=0 \tag{7.124c}$$

$$\overset{(7.124a),(7.124b)}{\Longrightarrow}\ \llbracket\mathbf{J}_e\rrbracket\cdot\mathbf{n}+\left\llbracket\rho\left(e{+}\frac{1}{2}|\mathbf{v}|^2\right)\mathbf{v}\right\rrbracket\cdot\mathbf{n}-\llbracket\mathbf{v}\cdot\mathbb{T}\rrbracket\,\mathbf{n}=0\ . \tag{7.124d}$$

The surface entropy production due to transfer processes across the interface (7.119) if the outer (+) part of the domain is taken into account reads as follows (recall that we consider $\mathbf{n}={}^-\mathbf{n}=-{}^+\mathbf{n}$):

$$\begin{aligned}
{}^\Sigma\Pi_\eta^{\mathrm{t}}=&\sum_{\alpha\in K}\left(\frac{{}^+\mu_\alpha^{\mathrm{M}}}{{}^+\vartheta}-\frac{M_\alpha}{{}^+\vartheta\,{}^+\rho}{}^+\Upsilon^{(\mathrm{B})}\right){}^{+\Sigma}s_\alpha^{\mathrm{M}}+\sum_{\alpha\in K}\left(\frac{{}^-\mu_\alpha^{\mathrm{M}}}{{}^-\vartheta}-\frac{M_\alpha}{{}^-\vartheta\,{}^-\rho}{}^-\Upsilon^{(\mathrm{B})}\right){}^{-\Sigma}s_\alpha^{\mathrm{M}}\\
&-\frac{1}{{}^+\vartheta}({}^+\mathbf{v}{-}{}^\Sigma\mathbf{v})_\tau\cdot\left(({}^+\mathbb{T}^{\mathrm{e}}{}^+\mathbf{n})_\tau-{}^+\rho\,{}^+\mathbf{v}\cdot{}^+\mathbf{n}\,({}^+\mathbf{v}{-}{}^\Sigma\mathbf{v})_\tau\right)\\
&-\frac{1}{{}^-\vartheta}({}^-\mathbf{v}{-}{}^\Sigma\mathbf{v})_\tau\cdot\left(({}^-\mathbb{T}^{\mathrm{e}}{}^-\mathbf{n})_\tau-{}^-\rho\,{}^-\mathbf{v}\cdot{}^-\mathbf{n}\,({}^-\mathbf{v}{-}{}^\Sigma\mathbf{v})_\tau\right)\\
&-\left({}^+\mathbf{J}_e\cdot{}^+\mathbf{n}+{}^+\rho\left({}^+e+\frac{{}^+p}{{}^+\rho}+\frac{|{}^+\mathbf{v}{-}{}^\Sigma\mathbf{v}|^2}{2}\right){}^+\mathbf{v}\cdot{}^+\mathbf{n}-{}^+\mathbb{T}^{\mathrm{e}}{}^+\mathbf{n}\cdot({}^+\mathbf{v}{-}{}^\Sigma\mathbf{v})\right)\left(\frac{1}{{}^+\vartheta}{-}\frac{1}{{}^\Sigma\vartheta}\right)\\
&-\left({}^-\mathbf{J}_e\cdot{}^-\mathbf{n}+{}^-\rho\left({}^-e+\frac{{}^-p}{{}^-\rho}+\frac{|{}^-\mathbf{v}{-}{}^\Sigma\mathbf{v}|^2}{2}\right){}^-\mathbf{v}\cdot{}^-\mathbf{n}-{}^-\mathbb{T}^{\mathrm{e}}{}^-\mathbf{n}\cdot({}^-\mathbf{v}{-}{}^\Sigma\mathbf{v})\right)\left(\frac{1}{{}^-\vartheta}{-}\frac{1}{{}^\Sigma\vartheta}\right)\ ,
\end{aligned}\tag{7.125}$$

i.e. compared with (7.119), each term is present twice with a contribution from the positive and negative side of the interface. In view of the definition (6.7) and condition (7.124a) ${}^{-\Sigma}s_\alpha{=}{-}{}^{+\Sigma}s_\alpha$, $\alpha{\in}K$ and we can thus add the two sums in the first row of (7.125) which yields

$$\begin{aligned}
{}^\Sigma\Pi_\eta^{\mathrm{t}}=&-\sum_{\alpha\in K}\left(\frac{{}^+\mu_\alpha^{\mathrm{M}}-\frac{M_\alpha{}^+\Upsilon^{(\mathrm{B})}}{{}^+\rho}}{{}^+\vartheta}-\frac{{}^-\mu_\alpha^{\mathrm{M}}-\frac{M_\alpha{}^-\Upsilon^{(\mathrm{B})}}{{}^-\rho}}{{}^-\vartheta}\right){}^{-\Sigma}s_\alpha^{\mathrm{M}}\\
&-\frac{1}{{}^+\vartheta}({}^+\mathbf{v}{-}{}^\Sigma\mathbf{v})_\tau\cdot\left(({}^+\mathbb{T}^{\mathrm{e}}{}^+\mathbf{n})_\tau-{}^+\rho\,{}^+\mathbf{v}\cdot{}^+\mathbf{n}\,({}^+\mathbf{v}{-}{}^\Sigma\mathbf{v})_\tau\right)\\
&-\frac{1}{{}^-\vartheta}({}^-\mathbf{v}{-}{}^\Sigma\mathbf{v})_\tau\cdot\left(({}^-\mathbb{T}^{\mathrm{e}}{}^-\mathbf{n})_\tau-{}^-\rho\,{}^-\mathbf{v}\cdot{}^-\mathbf{n}\,({}^-\mathbf{v}{-}{}^\Sigma\mathbf{v})_\tau\right)\\
&-\left({}^+\mathbf{J}_e\cdot{}^+\mathbf{n}+{}^+\rho\left({}^+e+\frac{{}^+p}{{}^+\rho}+\frac{|{}^+\mathbf{v}{-}{}^\Sigma\mathbf{v}|^2}{2}\right){}^+\mathbf{v}\cdot{}^+\mathbf{n}-{}^+\mathbb{T}^{\mathrm{e}}{}^+\mathbf{n}\cdot({}^+\mathbf{v}{-}{}^\Sigma\mathbf{v})\right)\left(\frac{1}{{}^+\vartheta}{-}\frac{1}{{}^\Sigma\vartheta}\right)\\
&-\left({}^-\mathbf{J}_e\cdot{}^-\mathbf{n}+{}^-\rho\left({}^-e+\frac{{}^-p}{{}^-\rho}+\frac{|{}^-\mathbf{v}{-}{}^\Sigma\mathbf{v}|^2}{2}\right){}^-\mathbf{v}\cdot{}^-\mathbf{n}-{}^-\mathbb{T}^{\mathrm{e}}{}^-\mathbf{n}\cdot({}^-\mathbf{v}{-}{}^\Sigma\mathbf{v})\right)\left(\frac{1}{{}^-\vartheta}{-}\frac{1}{{}^\Sigma\vartheta}\right)\ .
\end{aligned}\tag{7.126}$$

The first term represents entropy production due to transfer of mass of individual species across the interface, the second and third are entropy productions due to frictional dissipation and the last two are entropy productions due to energy transfer across the interface. For the first mechanism we could adopt for example linear constitutive relation

$$ {}^{-\Sigma}s_\alpha^{\mathrm{M}} = -{}^{+\Sigma}s_\alpha^{\mathrm{M}} = -\mathrm{L}\left(\frac{{}^{+}\mu_\alpha^{\mathrm{M}} - \frac{M_\alpha {}^{+}\Upsilon^{(\mathrm{B})}}{{}^{+}\rho}}{{}^{+}\vartheta} - \frac{{}^{-}\mu_\alpha^{\mathrm{M}} - \frac{M_\alpha {}^{-}\Upsilon^{(\mathrm{B})}}{{}^{-}\rho}}{{}^{-}\vartheta} \right) , \qquad \mathrm{L}{\geq}0 , \tag{7.127} $$

or, possibly include also cross-couplings via some positive definite symmetric matrix, or provide a non-linear constitutive relation via any monotone function of the affinity $\frac{{}^{+}\mu_\alpha^{\mathrm{M}} - \frac{M_\alpha {}^{+}\Upsilon^{(\mathrm{B})}}{{}^{+}\rho}}{{}^{+}\vartheta} - \frac{{}^{-}\mu_\alpha^{\mathrm{M}} - \frac{M_\alpha {}^{-}\Upsilon^{(\mathrm{B})}}{{}^{-}\rho}}{{}^{-}\vartheta}$, all these choices lead to compatibility with the second law of thermodynamics. Note that (7.127) together with (6.7) implies the mass jump condition (7.124a).

Let us postulate for the latter two mechanisms (friction and energy transfer) the following linear constitutive relations (compare with (7.122) and (7.123)):

$$ ({}^{+}\mathbb{S}\,{}^{+}\mathbf{n})_\tau - {}^{+}\rho\,{}^{+}\mathbf{v}\cdot{}^{+}\mathbf{n}\,({}^{+}\mathbf{v}-{}^{\Sigma}\mathbf{v})_\tau = -{}^{+}k({}^{+}\mathbf{v}-{}^{\Sigma}\mathbf{v})_\tau , \qquad {}^{+}k{\geq}0 , \tag{7.128a} $$

$$ ({}^{-}\mathbb{S}\,{}^{-}\mathbf{n})_\tau - {}^{-}\rho\,{}^{-}\mathbf{v}\cdot{}^{-}\mathbf{n}\,({}^{-}\mathbf{v}-{}^{\Sigma}\mathbf{v})_\tau = -{}^{-}k({}^{-}\mathbf{v}-{}^{\Sigma}\mathbf{v})_\tau , \qquad {}^{-}k{\geq}0 , \tag{7.128b} $$

and

$$ {}^{+}\mathbf{J}_e\cdot{}^{+}\mathbf{n} + {}^{+}\rho\left({}^{+}e + \frac{{}^{+}p}{{}^{+}\rho} + \frac{|{}^{+}\mathbf{v}-{}^{\Sigma}\mathbf{v}|^2}{2}\right){}^{+}\mathbf{v}\cdot{}^{+}\mathbf{n} - {}^{+}\mathbb{T}^{\mathrm{e}}{}^{+}\mathbf{n}\cdot({}^{+}\mathbf{v}-{}^{\Sigma}\mathbf{v}) = -{}^{+}\kappa\left(\frac{1}{{}^{+}\vartheta}-\frac{1}{{}^{\Sigma}\vartheta}\right) , \ {}^{+}\kappa{\geq}0, \tag{7.129a} $$

$$ {}^{-}\mathbf{J}_e\cdot{}^{-}\mathbf{n} + {}^{-}\rho\left({}^{-}e + \frac{{}^{-}p}{{}^{-}\rho} + \frac{|{}^{-}\mathbf{v}-{}^{\Sigma}\mathbf{v}|^2}{2}\right){}^{-}\mathbf{v}\cdot{}^{-}\mathbf{n} - {}^{-}\mathbb{T}^{\mathrm{e}}{}^{-}\mathbf{n}\cdot({}^{-}\mathbf{v}-{}^{\Sigma}\mathbf{v}) = -{}^{-}\kappa\left(\frac{1}{{}^{-}\vartheta}-\frac{1}{{}^{\Sigma}\vartheta}\right) , \ {}^{-}\kappa{\geq}0. \tag{7.129b} $$

Let us inspect the first set of equations first. Summing the two equations in (7.128), we then obtain, with the use of (7.124a),

$$ (\llbracket\mathbb{S} - \rho(\mathbf{v}\otimes\mathbf{v})\rrbracket\,\mathbf{n})_\tau + {}^{\Sigma}\mathbf{v}_\tau \underbrace{\llbracket\rho\mathbf{v}\rrbracket\cdot\mathbf{n}}_{=0} = +{}^{+}k({}^{+}\mathbf{v}-{}^{\Sigma}\mathbf{v})_\tau + {}^{-}k({}^{-}\mathbf{v}-{}^{\Sigma}\mathbf{v})_\tau . \tag{7.130} $$

Consequently, the constitutive relations for friction are compatible with the jump condition (7.124b) as long as the right-hand side vanishes, which can be achieved for example by (i) equating the two slip coefficients ${}^{+}k$ and ${}^{-}k$ (which is reasonable since the interface in this situation does not have any internal structure that would allow one to distinguish between them) and (ii) defining the so-far unspecified (due to the absence of mass transport within the interface) surface velocity ${}^{\Sigma}\mathbf{v}_\tau$ simply as an average: ${}^{\Sigma}\mathbf{v}_\tau = \frac{1}{2}({}^{+}\mathbf{v}_\tau + {}^{-}\mathbf{v}_\tau)$.

By summing the second pair of equations (7.129), we obtain

$$ \llbracket\mathbf{J}_e\rrbracket\cdot\mathbf{n} + \left\llbracket\rho\left(e + \frac{|\mathbf{v}-{}^{\Sigma}\mathbf{v}|^2}{2}\right)\mathbf{v}\right\rrbracket\cdot\mathbf{n} - \llbracket(\mathbf{v}-{}^{\Sigma}\mathbf{v})\cdot\mathbb{T}\rrbracket\,\mathbf{n} = {}^{+}\kappa\left(\frac{1}{{}^{+}\vartheta}-\frac{1}{{}^{\Sigma}\vartheta}\right) + {}^{-}\kappa\left(\frac{1}{{}^{-}\vartheta}-\frac{1}{{}^{\Sigma}\vartheta}\right) , \tag{7.131} $$

i.e. the energy transfer constitutive relation is compatible with the energy jump condition (7.124c) as long as the right hand-side vanishes. This can be achieved, for example by (i)

equating ${}^{+}\kappa={}^{-}\kappa$ (by the same logic as for the friction coefficients k above), and (ii) defining the intefacial coldness $\frac{1}{{}^{\Sigma}\vartheta}$ (yet unspecified due to the absence of the notion of interfacial energy and thus temperature in this situation) as an average of the two bulk values, i.e. setting $\frac{1}{{}^{\Sigma}\vartheta} = \frac{1}{2}\left(\frac{1}{{}^{+}\vartheta}+\frac{1}{{}^{-}\vartheta}\right)$.

To summarize, the constitutive relations proposed for transfer processes across the interface are compatible with the jump conditions in the case when the interface reduces to a discontinuity (meaning that it does not have any internal structure), provided that (i) we do not distinguish between the energy transfer coefficients κ and also the slip coefficients k from the positive and negative sides of the interface, and (ii) we define the interfacial velocity ${}^{\Sigma}\mathbf{v}$ and coldness $(\frac{1}{{}^{\Sigma}\vartheta})$, (both undetermined due to absence of the notion of mass transfer along the interface and of the surface energy) as averages of the bulk values.

Remarks

7.2.2 Young-Laplace condition. *In derivations of both Models A and B, we used the observation that the affinity* $\mathbf{v}\cdot\mathbf{n}$ *cannot be taken as being independent of the sorption rates in (7.102) and, by using* (7.103)*, we absorbed them in the "sorption" part of the entropy production. Ignoring this issue, [32] propose constitutive relations with affinity* $\mathbf{v}\cdot\mathbf{n}$ *and show, as a consequence, the well-known Young-Laplace condition. We wish to emphasize that the Young-Laplace condition can be obtained also within the presented framework. Indeed, let us inspect the normal component of (6.24) in equilibrium when the terms* $\mathbb{T}^{\mathrm{e}}$*,* $\rho\mathbf{v}\cdot\mathbf{n}$*,* ${}^{\Sigma}\mathbf{v}$ *vanish and* ${}^{\Sigma}\mathbb{T}$ *reduces to the surface pressure* ${}^{\Sigma}\mathbb{T}^{\mathrm{equil}} = -{}^{\Sigma}p^{\Sigma}\mathbb{I}$*. Assuming the presence of a fluid on the positive (outer) side of the interface with associated equilibrium stress* ${}^{+}\mathbb{T}^{\mathrm{equil}} = -{}^{+}p\mathbb{I}$*, we obtain*

$$[\![p]\!] = \mathrm{div}^{\Sigma}\left(-{}^{\Sigma}p^{\Sigma}\mathbb{I}\right)\cdot\mathbf{n} + \rho^{\Sigma\Sigma}\mathbf{b}\cdot\mathbf{n}\ .$$

Assuming further that the surface force ${}^{\Sigma}\mathbf{b}$ *is tangential and using the identity*

$$\mathrm{div}^{\Sigma}\left(-{}^{\Sigma}p^{\Sigma}\mathbb{I}\right) = -{}^{\Sigma}p^{\Sigma}\mathbb{B}:{}^{\Sigma}\mathbb{I} = -2{}^{\Sigma}p^{\Sigma}\mathrm{H},$$

where ${}^{\Sigma}\mathbb{B}$ *is the surface curvature tensor and* ${}^{\Sigma}\mathrm{H}$ *is the mean curvature [97], we finally obtain the following relation for the equilibrium bulk pressure jump*

$$[\![p]\!] = -2{}^{\Sigma}\mathrm{H}\,{}^{\Sigma}p\ .$$

This differs from the standard Young-Laplace condition by the presence of surface pressure rather than surface tension on the right-hand side. For a fluid-fluid interface, however, ${}^{\Sigma}\gamma = -{}^{\Sigma}p$*, which follows from (C.174) and (C.175) and from the fact that* ${}^{\Sigma}\mu_0^M{=}0$ *since there is no sensible notion of vacancies in this case. We therefore recover the classical form of the Young-Laplace condition.*

7.2.3 Alternative closure. *In [26], a dependence of the type (7.103) is also considered and applied in several ways. One is similar to our approach (elimination of* $\mathbf{v}\cdot\mathbf{n}$ *terms), or alternatively by eliminating one of the sorption rates and providing "compaction" constitutive relation with affinity* $\mathbf{v}\cdot\mathbf{n}$ *[as in 8, 32, 86]. Since the resulting constitutive formulae then depend on the choice of the eliminated sorption rate, we do not see any objective preference for such a choice.*

7.3 Summary of the model

In this last section, we summarize the model derived in this study, i.e. we recall all the balance equations, constraints and constitutive relations. The purpose of this section is to serve as a starting point for the mathematical analysis of the model of heterogeneous catalysis or, as a starting point for its numerical implementation.

7.3.1 Summary of the model - bulk

- **Balance equations - bulk**

  - Mass balance:

$$\frac{\partial \rho}{\partial t} + \operatorname{div} \rho \mathbf{v} = 0 \ ,$$
$$\dot{c_\alpha^{\mathrm{M}}} + c_\alpha^{\mathrm{M}} \operatorname{div} \mathbf{v} + \operatorname{div} \mathbf{J}_\alpha^{\mathrm{M,diff}} = r_\alpha^{\mathrm{M}} \ , \qquad \alpha \in K \setminus \{N\} \ .$$

  - Linear and angular momentum balance:

$$\frac{\partial(\rho \mathbf{v})}{\partial t} + \operatorname{div}(\rho \mathbf{v} \otimes \mathbf{v}) = \operatorname{div} \quad + \rho \mathbf{b} \ , \qquad = \ ^{\mathrm{T}} \ .$$

  - Energy balance (total energy):

$$\frac{\partial}{\partial t}\left(\rho(e + \frac{1}{2}|\mathbf{v}|^2)\right) + \operatorname{div}\left(\rho(e + \frac{1}{2}|\mathbf{v}|^2)\mathbf{v}\right) = -\operatorname{div} \mathbf{J}_e + \operatorname{div}(\ \ \mathbf{v}) + \rho \mathbf{b} \cdot \mathbf{v} + \sum_{\alpha \in K} \mathbf{J}_\alpha^{\mathrm{M,diff}} \cdot \mathbf{b}_\alpha^{\mathrm{M}} + q \ .$$

  - Energy balance (reduced form for the internal energy):

$$\rho \dot{e} = \quad : \quad -\operatorname{div} \mathbf{J}_e + \sum_{\alpha \in K} \mathbf{J}_\alpha^{\mathrm{M,diff}} \cdot \mathbf{b}_\alpha^{\mathrm{M}} + q \ ,$$

- **Constraints - bulk**

$$\sum_{\alpha \in K} M_\alpha c_\alpha^{\mathrm{M}} = \rho, \quad \sum_{\alpha \in K} M_\alpha \mathbf{J}_\alpha^{\mathrm{M,diff}} = \mathbf{0}, \quad \sum_{\alpha \in K} M_\alpha r_\alpha^{\mathrm{M}} = 0 \ .$$

- **Constitutive relations - bulk**

  - Rheology

$$= -p \ + \lambda \operatorname{div} \mathbf{v} \quad + 2\nu \quad , \qquad \nu \geq 0, \text{ and } 3\lambda + 2\nu \geq 0 \ .$$

- Thermo-diffusion (coupled) CIT

$$\begin{pmatrix} -\mathbf{J}_1^{\mathrm{M,diff}} \\ \vdots \\ -\mathbf{J}_{N-1}^{\mathrm{M,diff}} \\ \mathbf{J}_e \end{pmatrix} = \underbrace{\begin{pmatrix} \tilde{} & \cdots & \tilde{} & \tilde{} \\ 11 & & 1,N-1 & 1,N \\ \vdots & & \vdots & \vdots \\ \tilde{} & & \tilde{} & \tilde{} \\ N-1,1 & \cdots & N-1,N-1 & N-1,N \\ N,1 & \cdots & N,N-1 & N,N \end{pmatrix}}_{\tilde{}} \begin{pmatrix} \nabla\left(\frac{\mu_1^{\mathrm{M}}-\mu_{N,1}^{\mathrm{M}}}{\vartheta}\right) - \left(\frac{\mathbf{b}_1^{\mathrm{M}}-\mathbf{b}_{N,1}^{\mathrm{M}}}{\vartheta}\right) \\ \vdots \\ \nabla\left(\frac{\mu_{N-1}^{\mathrm{M}}-\mu_{N,N-1}^{\mathrm{M}}}{\vartheta}\right) - \left(\frac{\mathbf{b}_{N-1}^{\mathrm{M}}-\mathbf{b}_{N,N-1}^{\mathrm{M}}}{\vartheta}\right) \\ \nabla\left(\frac{1}{\vartheta}\right) \end{pmatrix},$$

where

$$\mu_{\alpha,\beta}^{\mathrm{M}} = \frac{M_\alpha}{M_\beta}\mu_\beta^{\mathrm{M}}\ , \qquad \mathbf{b}_{\alpha,\beta}^{\mathrm{M}} = \frac{M_\alpha}{M_\beta}\mathbf{b}_\beta^{\mathrm{M}}\ , \qquad \alpha,\beta\in K\ ,$$

and $\tilde{}$ is a symmetric positive definite matrix.

- Alternative diffusion constitutive relations - Maxwell-Stefan diffusion + Fourier heat conduction:

$$-\sum_{\beta\in K}\frac{x_\beta\mathbf{J}_\alpha^{\mathrm{M,diff}} - x_\alpha\mathbf{J}_\beta^{\mathrm{M,diff}}}{D_{\alpha\beta}} = \frac{c_\alpha^{\mathrm{M}}}{R\vartheta}\nabla\mu_\alpha^{\mathrm{M}} - \frac{c_\alpha}{R\vartheta}\nabla p - \frac{\rho_\alpha h - c_\alpha^{\mathrm{M}}\mu_\alpha^{\mathrm{M}}}{R\vartheta}\nabla\ln\vartheta - \frac{\rho_\alpha}{R\vartheta}(\mathbf{b}_\alpha - \mathbf{b})\ ,$$

$$\mathbf{J}_e = \kappa\nabla\left(\frac{1}{\vartheta}\right)\ , \qquad \kappa\geq 0\ , \qquad \alpha\in K\ ,$$

where the Maxwell-Stefan diffusivity matrix D has the following structure

$$\mathrm{D}_{\alpha\beta} \stackrel{\mathrm{def}}{=} \frac{R}{c^{\mathrm{M}}M_\alpha M_\beta f_{\alpha\beta}}\ , \qquad \alpha,\beta\in K\ .$$

where $f_{\alpha\beta} = f_{\beta\alpha} \geq \delta > 0, \quad \alpha,\beta\in K, \alpha\neq\beta.$

- Chemical reactions:

$$r_\alpha^{\mathrm{M}} = \sum_{\zeta=1}^{Z}\nu_\alpha^\zeta(\mathcal{R}_\zeta^f - \mathcal{R}_\zeta^b) = \sum_{\zeta=1}^{Z}\nu_\alpha^\zeta\mathcal{R}_\zeta\ , \qquad \alpha\in K\ ,$$

where the forward and backward reaction rates $\mathcal{R}_\zeta^f$, $\mathcal{R}_\zeta^b$ satisfy

$$\prod_{\alpha\in K} x_\alpha^{\nu_\alpha^\zeta} = \mathcal{K}_\zeta^{\mathrm{chem}}(\vartheta,p)\left(\frac{\mathcal{R}_\zeta^f}{\mathcal{R}_\zeta^b}\right)^\beta\ , \qquad \zeta = 1,\ldots,Z\ ,$$

which can be ensured for example by the following ansatz of reaction kinetics

$$\left(\mathcal{R}_\zeta^f\right)^\beta = k_\zeta^f(\vartheta,p)\prod_{\alpha\in K} x_\alpha^{\delta_\alpha^{\zeta,f}}\ , \qquad \left(\mathcal{R}_\zeta^b\right)^\beta = k_\zeta^b(\vartheta,p)\prod_{\alpha\in K} x_\alpha^{\delta_\alpha^{\zeta,b}}\ , \qquad \zeta = 1,\ldots,Z\ ,$$

where $\delta_\alpha^{\zeta,f}$, $\delta_\alpha^{\zeta,b}$ are the forward and backward stoichiometric coefficients of the ζth reaction, and coefficients $k_\zeta^f(\vartheta,p)$, $k_\zeta^b(\vartheta,p)$ must satisfy $\frac{k_\zeta^f(\vartheta,p)}{k_\zeta^b(\vartheta,p)} = \mathcal{K}_\zeta^{\mathrm{chem}}(\vartheta,p)$, $\zeta = 1,\ldots,Z$.

7.3.2 Summary of the model - active surface

- **Balance equations - active surface**
  - Mass balance:

$$\frac{\partial\,\rho^{\Sigma}}{\partial t}+\operatorname{div}^{\Sigma}\left(\rho^{\Sigma}\,{}^{\Sigma}\mathbf{v}\right)=-\left[\!\left[\rho\mathbf{v}\right]\!\right]\cdot\mathbf{n}\;,$$

$$\frac{\partial^{\Sigma}c_{\alpha}^{\mathrm{M}}}{\partial t}+\operatorname{div}^{\Sigma}\left({}^{\Sigma}c_{\alpha}^{\mathrm{M}}\,{}^{\Sigma}\mathbf{v}\right)+\operatorname{div}^{\Sigma}\,{}^{\Sigma}\mathbf{J}_{\alpha}^{\mathrm{M,diff}}={}^{\Sigma}r_{\alpha}^{\mathrm{M}}\;+{}^{\Sigma}s_{\alpha}^{\mathrm{M}}\;,\qquad\alpha\in K\setminus\{N\}\;.$$

  - Linear + angular momentum balance:

$$\frac{\partial(\rho^{\Sigma\Sigma}\mathbf{v})}{\partial t}+\operatorname{div}^{\Sigma}\left(\rho^{\Sigma\Sigma}\mathbf{v}\otimes{}^{\Sigma}\mathbf{v}\right)+\left[\!\left[\rho\mathbf{v}\otimes\mathbf{v}-\mathbb{T}\right]\!\right]\mathbf{n}=\operatorname{div}^{\Sigma}\,{}^{\Sigma}\mathbb{T}+\rho^{\Sigma\Sigma}\mathbf{b}\;,\qquad{}^{\Sigma}\mathbb{T}={}^{\Sigma}\mathbb{T}^{\mathrm{T}}\;.$$

  - Energy balance (total energy):

$$\frac{\partial\left(\rho^{\Sigma}({}^{\Sigma}e+\frac{1}{2}|{}^{\Sigma}\mathbf{v}|^{2})\right)}{\partial t}+\operatorname{div}^{\Sigma}\left(\rho^{\Sigma}({}^{\Sigma}e+\frac{1}{2}|{}^{\Sigma}\mathbf{v}|^{2})\,{}^{\Sigma}\mathbf{v}\right)-\operatorname{div}^{\Sigma}\left({}^{\Sigma}\mathbb{T}\,{}^{\Sigma}\mathbf{v}\right)-\rho^{\Sigma\Sigma}\mathbf{v}\cdot{}^{\Sigma}\mathbf{b}$$
$$-\sum_{\alpha\in K}{}^{\Sigma}\mathbf{J}_{\alpha}^{\mathrm{diff}}\cdot{}^{\Sigma}\mathbf{b}_{\alpha}+\operatorname{div}^{\Sigma}\,{}^{\Sigma}\mathbf{J}_{e}-{}^{\Sigma}\mathrm{s}_{e}+\left[\!\!\left[\rho(e+\frac{1}{2}|\mathbf{v}|^{2})\mathbf{v}-\mathbf{v}\cdot\mathbb{T}+\mathbf{J}_{e}\right]\!\!\right]\cdot\mathbf{n}=0\;.$$

  - Energy balance (reduced form for internal energy):

$$\rho^{\Sigma}\overset{\circ}{{}^{\Sigma}e}={}^{\Sigma}\mathbb{T}:\nabla^{\Sigma\Sigma}\mathbf{v}+\sum_{\alpha\in K}{}^{\Sigma}\mathbf{J}_{\alpha}^{\mathrm{diff}}\cdot{}^{\Sigma}\mathbf{b}_{\alpha}-\operatorname{div}^{\Sigma}\,{}^{\Sigma}\mathbf{J}_{e}$$
$$-\left[\!\!\left[\rho\left(e-{}^{\Sigma}e+\frac{1}{2}|\mathbf{v}-{}^{\Sigma}\mathbf{v}|^{2}\right)\mathbf{v}\right]\!\!\right]\cdot\mathbf{n}+\left[\!\left[(\mathbf{v}-{}^{\Sigma}\mathbf{v})\cdot\mathbb{T}\right]\!\right]\mathbf{n}-\left[\!\left[\mathbf{J}_{e}\right]\!\right]\cdot\mathbf{n}\;.\qquad(7.132)$$

- **Constraints - active surface**

$$\sum_{\alpha\in K}M_{\alpha}\,{}^{\Sigma}c_{\alpha}^{\mathrm{M}}=\rho^{\Sigma},\;\sum_{\alpha\in K}M_{\alpha}\,{}^{\Sigma}\mathbf{J}_{\alpha}^{\mathrm{M,diff}}=\mathbf{0},\;\sum_{\alpha\in K}M_{\alpha}\,{}^{\Sigma}r_{\alpha}^{\mathrm{M}}=0,\;\sum_{\alpha\in K}M_{\alpha}\,{}^{\Sigma}s_{\alpha}^{\mathrm{M}}=-\left[\!\left[\rho\mathbf{v}\right]\!\right]\cdot\mathbf{n},$$
$${}^{\Sigma}c^{\mathrm{M}}=\mathrm{const}\,.$$

- **Constitutive relations - active surface**
  - Rheology:

$${}^{\Sigma}\mathbb{T}=-{}^{\Sigma}p\,{}^{\Sigma}\mathbb{I}+{}^{\Sigma}\lambda\operatorname{div}^{\Sigma}\,{}^{\Sigma}\mathbf{v}\,{}^{\Sigma}\mathbb{I}+2{}^{\Sigma}\nu\,{}^{\Sigma}\mathbb{D}\;.$$

  - Thermo-diffusion (coupled – CIT):

$$\begin{pmatrix}-{}^{\Sigma}\mathbf{J}_{1}^{\mathrm{M,diff}}\\ \vdots\\ -{}^{\Sigma}\mathbf{J}_{K-1}^{\mathrm{M,diff}}\\ {}^{\Sigma}\mathbf{J}_{e}\end{pmatrix}=$$

$$\underbrace{\begin{pmatrix}{}^{\Sigma}\mathbb{L}_{1,1}&\cdots&{}^{\Sigma}\mathbb{L}_{1,N-1}&{}^{\Sigma}\mathbb{L}_{1,N}\\ \vdots&&\vdots&\vdots\\ {}^{\Sigma}\mathbb{L}_{N-1,1}&\cdots&{}^{\Sigma}\mathbb{L}_{N-1,N-1}&{}^{\Sigma}\mathbb{L}_{N-1,N}\\ {}^{\Sigma}\mathbb{L}_{N,1}&\cdots&{}^{\Sigma}\mathbb{L}_{N,N-1}&{}^{\Sigma}\mathbb{L}_{N,N}\end{pmatrix}}_{{}^{\Sigma}\mathbb{L}}\begin{pmatrix}\nabla^{\Sigma}\left(\frac{{}^{\Sigma}\bar{\mu}_{1}^{\mathrm{M}}-{}^{\Sigma}\bar{\mu}_{K,1}^{\mathrm{M}}}{{}^{\Sigma}\vartheta}\right)-\left(\frac{{}^{\Sigma}\mathbf{b}_{1}^{\mathrm{M}}-{}^{\Sigma}\mathbf{b}_{K,1}^{\mathrm{M}}}{{}^{\Sigma}\vartheta}\right)\\ \vdots\\ \nabla^{\Sigma}\left(\frac{{}^{\Sigma}\bar{\mu}_{K-1}^{\mathrm{M}}-{}^{\Sigma}\bar{\mu}_{K,K-1}^{\mathrm{M}}}{{}^{\Sigma}\vartheta}\right)-\left(\frac{{}^{\Sigma}\mathbf{b}_{K-1}^{\mathrm{M}}-{}^{\Sigma}\mathbf{b}_{K,K-1}^{\mathrm{M}}}{{}^{\Sigma}\vartheta}\right)\\ \nabla^{\Sigma}\left(\frac{1}{{}^{\Sigma}\vartheta}\right)\end{pmatrix}$$

where ${}^{\Sigma}$ is a symmetric positive semi-definite matrix and

$$ {}^{\Sigma}\bar{\mu}^{\mathrm{M}}_{\alpha} = {}^{\Sigma}\mu^{\mathrm{M}}_{\alpha} - {}^{\Sigma}\mu^{\mathrm{M}}_{0} \ , \qquad {}^{\Sigma}\bar{\mu}^{\mathrm{M}}_{\alpha,\beta} = \frac{M_\alpha}{M_\beta}\,{}^{\Sigma}\bar{\mu}^{\mathrm{M}}_{\beta} \ , \qquad {}^{\Sigma}\mathbf{b}^{\mathrm{M}}_{\alpha,\beta} = \frac{M_\alpha}{M_\beta}\,{}^{\Sigma}\mathbf{b}^{\mathrm{M}}_{\beta} \ , \qquad \alpha,\beta \in K \ . $$

- Alternative diffusion constitutive relations – Maxwell-Stefan diffusion + Fourier heat conduction:

$$ \begin{aligned} -\sum_{\beta\in K} \frac{{}^{\Sigma}x_\beta\,{}^{\Sigma}\mathbf{J}^{\mathrm{M,diff}}_{\alpha} - {}^{\Sigma}x_\alpha\,{}^{\Sigma}\mathbf{J}^{\mathrm{M,diff}}_{\beta}}{{}^{\Sigma}\mathrm{D}_{\alpha\beta}} &= \frac{{}^{\Sigma}c^{\mathrm{M}}_{\alpha}}{R\,{}^{\Sigma}\vartheta}\nabla^{\Sigma}{}^{\Sigma}\bar{\mu}^{\mathrm{M}}_{\alpha} - \frac{\rho^{\Sigma}_{\alpha}}{R\,\rho^{\Sigma}\,{}^{\Sigma}\vartheta}\nabla^{\Sigma}{}^{\Sigma}p \\ &\quad - \frac{\rho^{\Sigma}{}^{\Sigma}h - {}^{\Sigma}c^{\mathrm{M}}_{\alpha}\,{}^{\Sigma}\bar{\mu}^{\mathrm{M}}_{\alpha}}{R\,{}^{\Sigma}\vartheta}\nabla^{\Sigma}\ln{}^{\Sigma}\vartheta - \frac{\rho^{\Sigma}_{\alpha}}{R\,{}^{\Sigma}\vartheta}({}^{\Sigma}\mathbf{b}_{\alpha} - {}^{\Sigma}\mathbf{b}) \ , \quad \alpha\in K \ , \\ {}^{\Sigma}\mathbf{J}_{e} &= {}^{\Sigma}\kappa\nabla^{\Sigma}\left(\frac{1}{{}^{\Sigma}\vartheta}\right), \qquad {}^{\Sigma}\kappa \geq 0 \ , \end{aligned} $$

and the Maxwell-Stefan diffusivity matrix possesses the following structure:

$$ {}^{\Sigma}\mathrm{D}_{\alpha\beta} = \frac{R}{{}^{\Sigma}c^{\mathrm{M}}\,M_\alpha M_\beta\,{}^{\Sigma}f_{\alpha\beta}} \ , \qquad \alpha,\beta\in K \ , $$

with ${}^{\Sigma}f_{\alpha\beta}$ being a symmetric surface friction coefficient matrix with positive entries ${}^{\Sigma}f_{\alpha,\beta} \geq {}^{\Sigma}\delta > 0$, $\alpha,\beta\in K$.

- Chemical reactions:

$$ {}^{\Sigma}r^{\mathrm{M}}_{\alpha} = \sum_{a=1}^{{}^{\Sigma}Z} {}^{\Sigma}\delta^{\zeta}_{\alpha}({}^{\Sigma}\mathcal{R}^{f}_{\zeta} - {}^{\Sigma}\mathcal{R}^{b}_{\zeta}) = \sum_{a=1}^{{}^{\Sigma}Z} {}^{\Sigma}\delta^{\zeta}_{\alpha}\,{}^{\Sigma}\mathcal{R}_{\zeta} \ , \qquad \alpha\in K \ , $$

with ${}^{\Sigma}\mathcal{R}^{f}_{\zeta}$ and ${}^{\Sigma}\mathcal{R}^{b}_{\zeta}$ denoting the forward and backward reaction rate of the ζth surface chemical reaction and ${}^{\Sigma}\mathcal{R}_{\zeta} \overset{\text{def}}{=} {}^{\Sigma}\mathcal{R}^{f}_{\zeta} - {}^{\Sigma}\mathcal{R}^{b}_{\zeta}$. The forward and backward reaction rates satisfy

$$ \prod_{\alpha\in K}\left(\frac{{}^{\Sigma}x_\alpha}{1-\sum_{\beta=1}^{K}{}^{\Sigma}x_\beta}\right)^{{}^{\Sigma}\delta^{\zeta}_{\alpha}} = {}^{\Sigma}\mathcal{K}^{\mathrm{chem}}_{\zeta}\left(\frac{{}^{\Sigma}\mathcal{R}^{f}_{\zeta}}{{}^{\Sigma}\mathcal{R}^{b}_{\zeta}}\right)^{{}^{\Sigma}\beta\zeta} \ , \qquad \zeta = 1,\ldots,{}^{\Sigma}Z \ . $$

One particular ansatz for reaction kinetics reads

$$ \left({}^{\Sigma}\mathcal{R}^{f}_{\zeta}\right)^{{}^{\Sigma}\beta\zeta} = {}^{\Sigma}k^{f}_{\zeta}\prod_{\alpha\in K}\left(\frac{{}^{\Sigma}x_\alpha}{1-\sum_{\beta=1}^{K}{}^{\Sigma}x_\beta}\right)^{{}^{\Sigma}\delta^{\zeta,f}_{\alpha}} , \left(\mathcal{R}^{b}_{\zeta}\right)^{\beta_a} = {}^{\Sigma}k^{b}_{\zeta}\prod_{\alpha\in K}\left(\frac{{}^{\Sigma}x_\alpha}{1-\sum_{\beta=1}^{K}{}^{\Sigma}x_\beta}\right)^{{}^{\Sigma}\delta^{\zeta,b}_{\alpha}} , $$

where $\zeta = 1,\ldots,{}^{\Sigma}Z$, and ${}^{\Sigma}\delta^{\zeta,f}_{\alpha}$, ${}^{\Sigma}\delta^{\zeta,b}_{\alpha}$ are the forward and backward stoichiometric coefficients of the ζth reaction and coefficients ${}^{\Sigma}k^{f}_{\zeta}$, ${}^{\Sigma}k^{b}_{\zeta}$ must satisfy $\frac{{}^{\Sigma}k^{f}_{\zeta}}{{}^{\Sigma}k^{b}_{\zeta}} = {}^{\Sigma}\mathcal{K}^{\mathrm{chem}}_{\zeta}$, $\zeta = 1,\ldots,{}^{\Sigma}Z$.

- Sorption:
The adsorption and desorption rates satisfy

$$ \frac{{}^{\Sigma}s^{\mathrm{M}\,ad}_{\alpha}}{{}^{\Sigma}s^{\mathrm{M}\,de}_{\alpha}} = \mathcal{K}^{\mathrm{sor}}_{\alpha}\exp\left(-\frac{M_\alpha\Upsilon^{(\mathrm{A,B})}}{R\,\rho\,{}^{\Sigma}\vartheta}\right)\frac{x_\alpha(1-\sum_{\beta\in K}{}^{\Sigma}x_\beta)}{{}^{\Sigma}x_\alpha} \ , $$

where

$$\text{Model A:} \qquad \Upsilon^{(\mathrm{A})} = \mathbf{n}\cdot\ {}^{\mathrm{e}}\mathbf{n} - \frac{1}{2}\rho|\mathbf{v}-{}^{\Sigma}\mathbf{v}|^2 \ ,$$

$$\text{Model B:} \qquad \Upsilon^{(\mathrm{B})} = \mathbf{n}\cdot\ {}^{\mathrm{e}}\mathbf{n} - \rho(\mathbf{v}\cdot\mathbf{n})^2 + \frac{1}{2}\rho|\mathbf{v}-{}^{\Sigma}\mathbf{v}|^2 \ .$$

One possible choice of the adsorption/desorption kinetics is as follows

$${}^{\Sigma}s_{\alpha}^{\mathrm{M}ad} = {}^{\Sigma}k_{\alpha}^{\mathrm{ad-sor}}\ x_{\alpha}(1-\sum_{\beta\in K}{}^{\Sigma}x_{\beta}) \ , \qquad \alpha\in K \ ,$$

$${}^{\Sigma}s_{\alpha}^{\mathrm{M}de} = {}^{\Sigma}k_{\alpha}^{\mathrm{de-sor}}\ {}^{\Sigma}x_{\alpha} \ , \qquad \alpha\in K \ ,$$

where the adsorption/desorption rate coefficients ${}^{\Sigma}k_{\alpha}^{\mathrm{ad-sor}}$, ${}^{\Sigma}k_{\alpha}^{\mathrm{de-sor}}$ satisfy

$$\frac{{}^{\Sigma}k_{\alpha}^{\mathrm{ad-sor}}}{{}^{\Sigma}k_{\alpha}^{\mathrm{de-sor}}} = \mathcal{K}_{\alpha}^{\mathrm{sor}}\exp\left(-\frac{M_{\alpha}\Upsilon^{(\mathrm{A,B})}}{R\,\rho\,{}^{\Sigma}\vartheta}\right) \ , \qquad \alpha\in K \ .$$

- Surface friction:

$$\text{Model A:} \qquad (\ \mathbf{n})_{\tau} = -k(\mathbf{v}-{}^{\Sigma}\mathbf{v})_{\tau} \ ,$$

$$\text{Model B :} \qquad (\ \mathbf{n})_{\tau} - \rho\mathbf{v}\cdot\mathbf{n}\,(\mathbf{v}-{}^{\Sigma}\mathbf{v})_{\tau} = -k(\mathbf{v}-{}^{\Sigma}\mathbf{v})_{\tau} \ ,$$

where $k\geq 0$.

- Energy transfer across the interface:

$$\text{Model A:} \qquad \mathbf{J}_e\cdot\mathbf{n} + \rho(\mathbf{v}\cdot\mathbf{n})\left(e+\frac{p}{\rho}\right) = -\kappa\left(\frac{1}{\vartheta}-\frac{1}{{}^{\Sigma}\vartheta}\right) \ ,$$

$$\text{Model B:} \qquad \mathbf{J}_e\cdot\mathbf{n} + \rho\left(e+\frac{p}{\rho}+\frac{|\mathbf{v}-{}^{\Sigma}\mathbf{v}|^2}{2}\right)\mathbf{v}\cdot\mathbf{n} - (\ {}^{\mathrm{e}}\mathbf{n})\cdot(\mathbf{v}-{}^{\Sigma}\mathbf{v}) = -\kappa\left(\frac{1}{\vartheta}-\frac{1}{{}^{\Sigma}\vartheta}\right) \ ,$$

where $\kappa\geq 0$.

Appendices

Appendix B

B.1 Statistical lattice model - surface free energy

In order to develop a (two-dimensional) continuum description of the active surface, let us consider a (finite) surface element $\mathrm{d}\Sigma$ with corresponding surface measure $|\mathrm{d}\Sigma|$, which is assumed to contain ${}^{\mathrm{d}\Sigma}\mathrm{N}_s$ adsorption sites, assuming ${}^{\mathrm{d}\Sigma}\mathrm{N}_S \gg 1$ in order to allow for sensible spatial averaging and passing to the thermodynamic limit. Thermodynamic properties of the lattice can be derived by means of lattice statistical mechanics and, despite the fact that it can be found in classical references [see e.g. 43, 64], we outline the method of derivation for the sake of completeness.

A reasonable starting point is the canonical partition function for the ensemble of $N+1$ surface molecules (including vacancies) in the following form

$$ {}^{\mathrm{d}\Sigma}\mathrm{Q} = G({}^{\mathrm{d}\Sigma}\mathrm{N}_S, {}^{\mathrm{d}\Sigma}\mathrm{N}_0, \ldots, {}^{\mathrm{d}\Sigma}\mathrm{N}_N) \prod_{\alpha \in K_0} {}^{\Sigma}q_\alpha({}^{\mathrm{d}\Sigma}\vartheta)^{{}^{\mathrm{d}\Sigma}\mathrm{N}_\alpha} \exp\left(-\frac{\bar{E}_c}{k_B {}^{\mathrm{d}\Sigma}\vartheta}\right) , \tag{B.134} $$

In this expression, G is a factor expressing the number of spatial configurations of the given numbers ${}^{\mathrm{d}\Sigma}\mathrm{N}_0, \ldots {}^{\mathrm{d}\Sigma}\mathrm{N}_N$ of surface species. In the simplest case of single-site adsorption, i.e. when each surface species can occupy only one adsoprtion site G, takes the simple combinatoric form

$$ G({}^{\mathrm{d}\Sigma}\mathrm{N}_s, {}^{\mathrm{d}\Sigma}\mathrm{N}_0, \ldots, {}^{\mathrm{d}\Sigma}\mathrm{N}_N) = \frac{{}^{\mathrm{d}\Sigma}\mathrm{N}_S!}{{}^{\mathrm{d}\Sigma}\mathrm{N}_0! \ldots {}^{\mathrm{d}\Sigma}\mathrm{N}_N!} . \tag{B.135} $$

Next, ${}^{\Sigma}q_\alpha \stackrel{\mathrm{def}}{=} \sum_j \omega_j \exp\left(-\frac{\epsilon_j}{k^{\mathrm{d}\Sigma}\vartheta}\right)$, are the molecular partition functions representing the internal degrees of freedom of the molecules. The sum goes over all molecular configurations with energies ϵ_j and degeneracies ω_j. In what follows, we will not employ this definition of ${}^{\Sigma}q_\alpha$ and simply consider it as a given function of the local patch temperature ${}^{\mathrm{d}\Sigma}\vartheta$. Finally, $\bar{E}_c$ is the average configuration energy representing the closest-neighbour interaction of the adsorbed species (in the Bragg-Williams approximation) and k_B is the Boltzmann constant. Neglecting the interaction among the adsorbed species in the first step, we set $\bar{E}_c = 0$ in (B.134).

From the canonical partition function (B.134), we obtain the Helmholtz free energy of the patch $\mathrm{d}\Sigma$ as follows [e.g. 64]

$$ {}^{\mathrm{d}\Sigma}F = -k_B {}^{\mathrm{d}\Sigma}\vartheta \ln {}^{\mathrm{d}\Sigma}\mathrm{Q} , \tag{B.136} $$

which under the assumptions $\bar{E}_c{=}0$ and ansatz (B.135) can be expressed using the Stirling approximation $\ln N! {\sim} N \ln N {-} N$ as follows

$$ {}^{\mathrm{d}\Sigma}F = k_B {}^{\mathrm{d}\Sigma}\vartheta \sum_{\alpha \in K_0} {}^{\mathrm{d}\Sigma}\mathrm{N}_\alpha \ln\left({}^{\Sigma}q_\alpha^{-1} \frac{{}^{\mathrm{d}\Sigma}\mathrm{N}_\alpha}{{}^{\mathrm{d}\Sigma}\mathrm{N}_s}\right) = k^{\mathrm{d}\Sigma}\vartheta \sum_{\alpha \in K_0} {}^{\mathrm{d}\Sigma}\mathrm{N}_\alpha \ln\left({}^{\Sigma}q_\alpha^{-1\,\mathrm{d}\Sigma}x_\alpha\right) , \tag{B.137} $$

where we introduced the patch surface coverage

$$ {}^{\mathrm{d}\Sigma}x_\alpha \stackrel{\mathrm{def}}{=} \frac{{}^{\mathrm{d}\Sigma}\mathrm{N}_\alpha}{{}^{\mathrm{d}\Sigma}\mathrm{N}_S} , \qquad \alpha {\in} K_0 . \tag{B.138} $$

The molar Helmholtz free-energy density defined as ${}^{\mathrm{d}\Sigma}\psi^{\mathrm{M}} \overset{\text{def}}{=} {}^{\mathrm{d}\Sigma}F\frac{N_A}{{}^{\mathrm{d}\Sigma}\mathrm{N}_S}$, where N_A is the Avogardo number, consequently reads

$$ {}^{\mathrm{d}\Sigma}\psi^{\mathrm{M}} = -R\,{}^{\mathrm{d}\Sigma}\vartheta \sum_{\alpha\in K_0} {}^{\mathrm{d}\Sigma}x_\alpha(\ln {}^{\Sigma}q_\alpha - \ln {}^{\mathrm{d}\Sigma}x_\alpha) \ , \tag{B.139} $$

where the universal gas constant R was introduced as $R = k_B\,N_A$. Immediately from the canonical partition function, we can also evaluate the molar chemical potentials as follows [64]

$$ {}^{\mathrm{d}\Sigma}\mu_\alpha^{\mathrm{M}} \overset{\text{def}}{=} -R\,{}^{\mathrm{d}\Sigma}\vartheta \left.\frac{\partial \ln {}^{\mathrm{d}\Sigma}\mathrm{Q}}{\partial {}^{\mathrm{d}\Sigma}\mathrm{N}_\alpha}\right|_{|\mathrm{d}\Sigma|,{}^{\mathrm{d}\Sigma}\vartheta,{}^{\mathrm{d}\Sigma}\mathrm{N}_{\beta\neq\alpha}} = R\,{}^{\mathrm{d}\Sigma}\vartheta \ln\left({}^{\Sigma}q_\alpha^{-1\,\mathrm{d}\Sigma}x_\alpha\right) \ , \qquad \alpha\in K_0 \ . \tag{B.140} $$

So far we ignored possible stretching or compression of the lattice. We essentially only considered combinatoric contributions to the partition function plus internal degrees of freedom at each site. In order to include such an effect, we extend the patch surface free energy by a term ${}^{\mathrm{d}\Sigma}\psi_0^{\mathrm{M}}$ and impose

$$ {}^{\mathrm{d}\Sigma}\psi^{\mathrm{M}} = {}^{\mathrm{d}\Sigma}\psi^{\mathrm{M}}{}_0\left({}^{\mathrm{d}\Sigma}\vartheta, \frac{1}{{}^{\mathrm{d}\Sigma}c^{\mathrm{M}}}\right) - R\,{}^{\mathrm{d}\Sigma}\vartheta \sum_{\alpha\in K_0} {}^{\mathrm{d}\Sigma}x_\alpha(\ln {}^{\Sigma}q_\alpha - \ln {}^{\mathrm{d}\Sigma}x_\alpha) \tag{B.141} $$

where

$$ {}^{\mathrm{d}\Sigma}c^{\mathrm{M}} \overset{\text{def}}{=} \frac{1}{N_A}\frac{{}^{\mathrm{d}\Sigma}\mathrm{N}_S}{|d\Sigma|} \tag{B.142} $$

is the surface molar concentration of the adsorption sites, which captures the stretching/compression effects of the lattice. Since only $\sum_{\beta\in K_0} {}^{\mathrm{d}\Sigma}x_\beta = 1$, we can eliminate ${}^{\mathrm{d}\Sigma}x_0$ and consider ${}^{\mathrm{d}\Sigma}\psi^{\mathrm{M}} = {}^{\mathrm{d}\Sigma}\psi^{\mathrm{M}}({}^{\mathrm{d}\Sigma}\vartheta, \frac{1}{{}^{\mathrm{d}\Sigma}c^{\mathrm{M}}}, {}^{\mathrm{d}\Sigma}x_1, \ldots, {}^{\mathrm{d}\Sigma}x_N)$ defined by

$$ \begin{aligned} {}^{\mathrm{d}\Sigma}\psi^{\mathrm{M}}({}^{\mathrm{d}\Sigma}\vartheta, \frac{1}{{}^{\mathrm{d}\Sigma}c^{\mathrm{M}}}, {}^{\mathrm{d}\Sigma}x_1, \ldots, {}^{\mathrm{d}\Sigma}x_N) \overset{\text{def}}{=} {}^{\mathrm{d}\Sigma}\psi^{\mathrm{M}}{}_0({}^{\mathrm{d}\Sigma}\vartheta, \frac{1}{{}^{\mathrm{d}\Sigma}c^{\mathrm{M}}}) - R\,{}^{\mathrm{d}\Sigma}\vartheta \sum_{\alpha\in K} {}^{\mathrm{d}\Sigma}x_\alpha(\ln {}^{\Sigma}q_\alpha - \ln {}^{\mathrm{d}\Sigma}x_\alpha) \\ - R\,{}^{\mathrm{d}\Sigma}\vartheta \left(1 - \sum_{\beta\in K} {}^{\mathrm{d}\Sigma}x_\beta\right)\left(\ln {}^{\Sigma}q_0 - \ln\left(1 - \sum_{\beta\in K} {}^{\mathrm{d}\Sigma}x_\beta\right)\right) \ , \end{aligned} \tag{B.143} $$

By direct calculation, with the use of (B.140), we arrive at the expected relation

$$ \frac{\partial\, {}^{\mathrm{d}\Sigma}\psi^{\mathrm{M}}}{\partial\, {}^{\mathrm{d}\Sigma}x_\alpha} = {}^{\mathrm{d}\Sigma}\mu_\alpha^{\mathrm{M}} - {}^{\mathrm{d}\Sigma}\mu_0^{\mathrm{M}} = R\,{}^{\mathrm{d}\Sigma}\vartheta\left\{\ln\left(\frac{q_0^\Sigma}{q_\alpha^\Sigma}\right) + \ln\left(\frac{{}^{\mathrm{d}\Sigma}x_\alpha}{1 - \sum_{\beta\in K} {}^{\mathrm{d}\Sigma}x_\beta}\right)\right\} \ , \qquad \alpha\in K \ . \tag{B.144} $$

The molar surface entropy density ${}^{\mathrm{d}\Sigma}\eta^{\mathrm{M}}$ can be obtained from ${}^{\mathrm{d}\Sigma}\psi^{\mathrm{M}}$ using the identity (see e.g. [64]):

$$ \frac{\partial\, {}^{\mathrm{d}\Sigma}\psi^{\mathrm{M}}}{\partial\, {}^{\mathrm{d}\Sigma}\vartheta} = -{}^{\mathrm{d}\Sigma}\eta^{\mathrm{M}} \ , \tag{B.145} $$

and finally, we define the surface tension on the patch by

$$ {}^{\mathrm{d}\Sigma}\gamma \overset{\text{def}}{=} \frac{\partial\, {}^{\mathrm{d}\Sigma}\psi^{\mathrm{M}}}{\partial\left(\frac{1}{{}^{\mathrm{d}\Sigma}c^{\mathrm{M}}}\right)} \ . \tag{B.146} $$

We have obtained a complete thermodynamic description of the patch $d\Sigma$. Motivated by the preceding expressions, we assume that in the considered multi-component continuum framework the surface molar Helmholtz free energy density takes the form identical to (B.141), or (B.143). This means that we set:

$$ {}^{\Sigma}\psi^{\mathrm{M}} \stackrel{\mathrm{def}}{=} {}^{\Sigma}\psi_0^{\mathrm{M}} - R\,{}^{\Sigma}\vartheta \sum_{\alpha\in K_0} {}^{\Sigma}x_\alpha(\ln {}^{\Sigma}q_\alpha - \ln {}^{\Sigma}x_\alpha) \tag{B.147} $$

or, again, expressed in terms of the independent variables ${}^{\Sigma}\vartheta, \frac{1}{{}^{\Sigma}c^{\mathrm{M}}}, {}^{\Sigma}x_1, \ldots, {}^{\Sigma}x_N$, we define ${}^{\Sigma}\widehat{\psi^{\mathrm{M}}}$ by

$$ \begin{aligned} {}^{\Sigma}\widehat{\psi^{\mathrm{M}}}({}^{\Sigma}\vartheta, \frac{1}{{}^{\Sigma}c^{\mathrm{M}}}, {}^{\Sigma}x_1, \ldots, {}^{\Sigma}x_N) &= {}^{\Sigma}\widehat{\psi_0^{\mathrm{M}}}({}^{\Sigma}\vartheta, \frac{1}{{}^{\Sigma}c^{\mathrm{M}}}) - R\,{}^{\Sigma}\vartheta \sum_{\alpha\in K} {}^{\Sigma}x_\alpha(\ln {}^{\Sigma}q_\alpha - \ln {}^{\Sigma}x_\alpha) \\ &\quad - R\,{}^{\Sigma}\vartheta \left(1 - \sum_{\beta\in K} {}^{\Sigma}x_\beta\right)\left(\ln {}^{\Sigma}q_0 - \ln\left(1 - \sum_{\beta\in K} {}^{\Sigma}x_\beta\right)\right) \ . \end{aligned} \tag{B.148} $$

From the above, we can again recover the surface molar entropy density ${}^{\Sigma}\eta^{\mathrm{M}}$, the surface tension ${}^{\Sigma}\gamma$ and the surface chemical potentials (with respect to vacancies) ${}^{\Sigma}\mu_\alpha^{\mathrm{M}} - {}^{\Sigma}\mu_0^{\mathrm{M}}$:

$$ \frac{\partial\, {}^{\Sigma}\widehat{\psi^{\mathrm{M}}}}{\partial\, {}^{\Sigma}\vartheta} = -{}^{\Sigma}\eta^{\mathrm{M}} \ , \tag{B.149a} $$

$$ \frac{\partial {}^{\Sigma}\widehat{\psi^{\mathrm{M}}}}{\partial(\frac{1}{{}^{\Sigma}c^{\mathrm{M}}})} = {}^{\Sigma}\gamma \ , \tag{B.149b} $$

$$ \frac{\partial\, {}^{\Sigma}\widehat{\psi^{\mathrm{M}}}}{\partial\, {}^{\Sigma}x_\alpha} = {}^{\Sigma}\mu_\alpha^{\mathrm{M}} - {}^{\Sigma}\mu_0^{\mathrm{M}} = R\,{}^{\Sigma}\vartheta \left\{ \ln\left(\frac{q_0^\Sigma}{q_\alpha^\Sigma}\right) + \ln\left(\frac{{}^{\Sigma}x_\alpha}{1 - \sum_{\beta\in K} {}^{\Sigma}x_\beta}\right)\right\}, \qquad \alpha\in K \ . \tag{B.149c} $$

In order to treat the surface "incompressibility" constraint, it is convenient to work with the surface Gibbs potential defined through the Legendre transform of ${}^{\Sigma}\widehat{\psi^{\mathrm{M}}}$ with respect to $\frac{1}{{}^{\Sigma}c^{\mathrm{M}}}$. Defining

$$ {}^{\Sigma}g^{\mathrm{M}} \stackrel{\mathrm{def}}{=} {}^{\Sigma}\psi^{\mathrm{M}} - \frac{{}^{\Sigma}\gamma}{{}^{\Sigma}c^{\mathrm{M}}} \ , \quad \text{and} \quad {}^{\Sigma}\widehat{g^{\mathrm{M}}}({}^{\Sigma}\vartheta, {}^{\Sigma}\gamma, {}^{\Sigma}x_1, \ldots, {}^{\Sigma}x_N) \stackrel{\mathrm{def}}{=} \sup_{\frac{1}{{}^{\Sigma}c^{\mathrm{M}}}} \left({}^{\Sigma}\widehat{\psi^{\mathrm{M}}}\left({}^{\Sigma}\vartheta, \frac{1}{{}^{\Sigma}c^{\mathrm{M}}}, {}^{\Sigma}x_\alpha\right) - \frac{{}^{\Sigma}\gamma}{{}^{\Sigma}c^{\mathrm{M}}}\right) \ , \tag{B.150} $$

and using the surface Helmholtz free energy (B.148), the corresponding surface Gibbs' free energy reads

$$ \begin{aligned} {}^{\Sigma}\widehat{g^{\mathrm{M}}}({}^{\Sigma}\vartheta, {}^{\Sigma}\gamma, {}^{\Sigma}x_1, \ldots, {}^{\Sigma}x_N) &= {}^{\Sigma}\widehat{g_0^{\mathrm{M}}}({}^{\Sigma}\vartheta, {}^{\Sigma}\gamma) - R\,{}^{\Sigma}\vartheta \sum_{\alpha\in K} {}^{\Sigma}x_\alpha(\ln {}^{\Sigma}q_\alpha - \ln {}^{\Sigma}x_\alpha) \\ &\quad - R\,{}^{\Sigma}\vartheta \left(1 - \sum_{\beta\in K} {}^{\Sigma}x_\beta\right)\left(\ln {}^{\Sigma}q_0 - \ln\left(1 - \sum_{\beta\in K} {}^{\Sigma}x_\beta\right)\right) \ , \end{aligned} \tag{B.151} $$

and we obtain in the standard manner the identities

$$ \frac{\partial\, {}^{\Sigma}\widehat{g^{\mathrm{M}}}}{\partial\, {}^{\Sigma}\vartheta} = -{}^{\Sigma}\eta^{\mathrm{M}} \ , \qquad \frac{\partial {}^{\Sigma}\widehat{g^{\mathrm{M}}}}{\partial {}^{\Sigma}\gamma} = -\frac{1}{{}^{\Sigma}c^{\mathrm{M}}} \ , \qquad \frac{\partial\, {}^{\Sigma}\widehat{g^{\mathrm{M}}}}{\partial\, {}^{\Sigma}x_\alpha} = {}^{\Sigma}\mu_\alpha^{\mathrm{M}} - {}^{\Sigma}\mu_0^{\mathrm{M}} \ , \qquad \alpha\in K \ . \tag{B.152} $$

Remark. The simple lattice model discussed in this section can be generalized in many ways, see, for instance [85] and references therein. In order to take into account for the nearest neighbour interaction of the adsorbed molecules, one may take in (B.134) $\bar{E}_c = \sum_{\alpha\in K}\sum_{\beta\in K}\bar{N}_{\alpha\beta}\epsilon_{\alpha\beta}$, where $\bar{N}_{\alpha\beta}$ is the average number of neighbouring molecules of α and β type, and $\epsilon_{\alpha\beta}$ is the corresponding interaction energy. For single site adsorption the average number of neighbours can be estimated using the assumption of completely random distribution as $Z\frac{{}^{\mathrm{d}\Sigma}\mathrm{N}_\alpha\,{}^{\mathrm{d}\Sigma}\mathrm{N}_\beta}{{}^{\mathrm{d}\Sigma}\mathrm{N}_S}$ where Z is a configuration number of the lattice (number of nearest neighbours for each adsorption site). Alternatively, in order to capture multi-site adsorption, one typically needs to modify the configuration factor G in the canonical partition function (B.134). A classical example of such a generalization is the model of [72], which can be for a single-component adsorption expressed through the canonical partition function

$$G = \frac{{}^{\mathrm{d}\Sigma}\mathrm{N}_S!}{{}^{\mathrm{d}\Sigma}\mathrm{N}_1!({}^{\mathrm{d}\Sigma}\mathrm{N}_S - r\ {}^{\mathrm{d}\Sigma}\mathrm{N}_1)!}\frac{\zeta^{{}^{\mathrm{d}\Sigma}\mathrm{N}_1}}{{}_{\mathrm{d}\Sigma}\mathrm{N}_S{}^{(r-1)^{\mathrm{d}\Sigma}\mathrm{N}_1}}\ ,$$

where r is the number of sites occupied by each molecule and ζ is a parameter related to properties of the molecule. With such a modified canonical partition function, one then proceeds in an analogous manner as in the presented derivation, that is, by employing (B.136), one finds the Helmholtz free energy of the surface patch, computes the chemical potentials and all of the necessary macroscopic thermodynamic quantities.

Appendix C

C.1 Euler relation in bulk

We perform the derivation in molar-based quantities, but the procedure can be easily recast into a mass-based derivation. Let us start from the constitutive assumption on the density of the Helmholtz free energy $c^{\mathrm{M}}\psi^{\mathrm{M}}$ in the form

$$c^{\mathrm{M}}\psi^{\mathrm{M}} \stackrel{\mathrm{def}}{=} c^{\mathrm{M}}\psi^{\mathrm{M}}(\vartheta, c^{\mathrm{M}}_{\alpha}) \ , \qquad \alpha\in K. \tag{C.153}$$

From here, the molar Helmholtz free energy $\widehat{\psi^{\mathrm{M}}}$ can be defined as a function of ϑ, $\frac{1}{c^{\mathrm{M}}}$, x_α, using

$$\widehat{\psi^{\mathrm{M}}}\left(\vartheta, \frac{1}{c^{\mathrm{M}}}, x_\alpha\right) \stackrel{\mathrm{def}}{=} \frac{c^{\mathrm{M}}\psi^{\mathrm{M}}(\vartheta, c^{\mathrm{M}}x_\alpha)}{c^{\mathrm{M}}} \ , \qquad \alpha\in K. \tag{C.154}$$

As a consequence, we have that

$$\left.\frac{\partial c^{\mathrm{M}}\psi^{\mathrm{M}}}{\partial c^{\mathrm{M}}_{\alpha}}\right|_{\vartheta, c^{\mathrm{M}}_{\beta\neq\alpha}} = \left.\frac{\partial\widehat{\psi^{\mathrm{M}}}}{\partial x_\alpha}\right|_{\vartheta, \frac{1}{c^{\mathrm{M}}}, x_{\beta\neq\alpha}} \qquad \alpha\in K \ , \tag{C.155}$$

$$\left.\frac{\partial c^{\mathrm{M}}\psi^{\mathrm{M}}}{\partial\vartheta}\right|_{c^{\mathrm{M}}_{\beta}} = c^{\mathrm{M}} \left.\frac{\partial\widehat{\psi^{\mathrm{M}}}}{\partial\vartheta}\right|_{\frac{1}{c^{\mathrm{M}}}, x_\beta} . \tag{C.156}$$

Taking the material time derivative of $c^{\mathrm{M}}\psi^{\mathrm{M}}$ and of $c^{\mathrm{M}}\widehat{\psi^{\mathrm{M}}}$, we obtain

$$\dot{c^{\mathrm{M}}\psi^{\mathrm{M}}} = \frac{\partial(c^{\mathrm{M}}\psi^{\mathrm{M}})}{\partial\vartheta}\dot{\vartheta} + \sum_{\alpha\in K}\frac{\partial(c^{\mathrm{M}}\psi^{\mathrm{M}})}{\partial c^{\mathrm{M}}_{\alpha}}\dot{c^{\mathrm{M}}_{\alpha}} \ , \tag{C.157}$$

$$\dot{\overline{c^{\mathrm{M}}\widehat{\psi^{\mathrm{M}}}}} = \dot{c^{\mathrm{M}}}\widehat{\psi^{\mathrm{M}}} + c^{\mathrm{M}}\left(\frac{\partial\widehat{\psi^{\mathrm{M}}}}{\partial\vartheta}\dot{\vartheta} + \frac{\partial\widehat{\psi^{\mathrm{M}}}}{\partial\frac{1}{c^{\mathrm{M}}}}\dot{\overline{\left(\frac{1}{c^{\mathrm{M}}}\right)}} + \sum_{\alpha\in K}\frac{\partial\widehat{\psi^{\mathrm{M}}}}{\partial x_\alpha}\dot{x_\alpha}\right) . \tag{C.158}$$

Expressing in (C.158) $x_\alpha = \frac{c^{\mathrm{M}}_{\alpha}}{c^{\mathrm{M}}}$ and comparing with (C.157), we obtain with the use of (C.155) and (C.156):

$$\dot{c^{\mathrm{M}}}\left(\widehat{\psi^{\mathrm{M}}} - \frac{1}{c^{\mathrm{M}}}\frac{\partial\widehat{\psi^{\mathrm{M}}}}{\partial\frac{1}{c^{\mathrm{M}}}} - \sum_{\alpha\in K}\frac{\partial\widehat{\psi^{\mathrm{M}}}}{\partial x_\alpha}x_\alpha\right) = 0 \ . \tag{C.159}$$

Requiring that (C.159) holds for arbitrary $\dot{c^{\mathrm{M}}}$, we conclude that the expression in the parenthesis must be identically equal to zero. Defining the thermodynamic pressure and the chemical potentials in the standard manner, i.e. by writing

$$p \stackrel{\mathrm{def}}{=} -\frac{\partial\widehat{\psi^{\mathrm{M}}}}{\partial\frac{1}{c^{\mathrm{M}}}} \ , \qquad \mu^{\mathrm{M}}_{\alpha} \stackrel{\mathrm{def}}{=} \frac{\partial\widehat{\psi^{\mathrm{M}}}}{\partial x_\alpha} \ , \qquad \alpha\in K \ , \tag{C.160}$$

this assertion can be rewritten as follows:

$$\psi^{\mathrm{M}} + \frac{p}{c^{\mathrm{M}}} = \sum_{\alpha\in K}\mu^{\mathrm{M}}_{\alpha}x_\alpha \ , \tag{C.161}$$

which is the Euler relation known from classical equilibrium thermodynamics. Multiplying by c^{M} and using $c^{\mathrm{M}}\psi^{\mathrm{M}} = \rho\psi$, we can rewrite it in a more familiar form:

$$c^{\mathrm{M}}\psi^{\mathrm{M}} + p = \sum_{\alpha\in K} \mu_\alpha^{\mathrm{M}} c_\alpha^{\mathrm{M}} \qquad \Longleftrightarrow \qquad \psi + \frac{p}{\rho} = \sum_{\alpha\in K} \mu_\alpha c_\alpha \ . \tag{C.162}$$

Taking a differential of (C.162) and employing relations (C.160) and the thermodynamic relation $\eta^{\mathrm{M}} = -\frac{\partial\psi^{\mathrm{M}}}{\partial\vartheta}$, one also obtains immediately the Gibbs-Duhem relation

$$-\eta^{\mathrm{M}} c^{\mathrm{M}} d\vartheta + dp = \sum_{\alpha\in K} c_\alpha^{\mathrm{M}} d\mu_\alpha^{\mathrm{M}} \qquad \Longleftrightarrow \qquad -\eta d\vartheta + \frac{1}{\rho} dp = \sum_{\alpha\in K} c_\alpha d\mu_\alpha \ . \tag{C.163}$$

C.2 Euler relation on surface

We proceed analogously as in C.1, namely, we start by postulating the constitutive form of ${}^{\Sigma}c^{\mathrm{M}}\,{}^{\Sigma}\psi^{\mathrm{M}} = \rho^{\Sigma\Sigma}\psi$:

$${}^{\Sigma}c^{\mathrm{M}}{}^{\Sigma}\psi^{\mathrm{M}} \stackrel{\mathrm{def}}{=} {}^{\Sigma}c^{\mathrm{M}}{}^{\Sigma}\psi^{\mathrm{M}}\big({}^{\Sigma}\vartheta, {}^{\Sigma}c_\alpha^{\mathrm{M}}\big) \qquad \alpha\in K_0. \tag{C.164}$$

and the molar Helmholtz free energy as

$$\widehat{{}^{\Sigma}\psi^{\mathrm{M}}}\big(\vartheta, {}^{\Sigma}c^{\mathrm{M}}, {}^{\Sigma}x_\alpha\big) \stackrel{\mathrm{def}}{=} \frac{{}^{\Sigma}c^{\mathrm{M}}{}^{\Sigma}\psi^{\mathrm{M}}\big({}^{\Sigma}\vartheta, {}^{\Sigma}c^{\mathrm{M}}{}^{\Sigma}x_\alpha\big)}{{}^{\Sigma}c^{\mathrm{M}}} \ , \qquad \alpha\in K_0. \tag{C.165}$$

Using the identity

$${}^{\Sigma}\dot{c}^{\mathrm{M}}{}^{\Sigma}\psi^{\mathrm{M}} = \dot{\overline{{}^{\Sigma}c^{\mathrm{M}}\widehat{{}^{\Sigma}\psi^{\mathrm{M}}}}} \ , \tag{C.166}$$

by analogous computation as for the bulk quantities, we arrive at

$${}^{\Sigma}c^{\mathrm{M}}{}^{\Sigma}\psi^{\mathrm{M}} + \big({}^{\Sigma}c^{\mathrm{M}}\big)^2 \frac{\partial\widehat{{}^{\Sigma}\psi^{\mathrm{M}}}}{\partial{}^{\Sigma}c^{\mathrm{M}}} - \sum_{\alpha\in K_0} \left.\frac{\partial\widehat{{}^{\Sigma}\psi^{\mathrm{M}}}}{\partial{}^{\Sigma}x_\alpha}\right|_{\vartheta, {}^{\Sigma}c^{\mathrm{M}}, {}^{\Sigma}x_{\beta\neq\alpha}} {}^{\Sigma}c_\alpha^{\mathrm{M}} = 0 \ . \tag{C.167}$$

Defining the surface molar chemical potential

$${}^{\Sigma}\mu_\alpha^{\mathrm{M}} \stackrel{\mathrm{def}}{=} \left.\frac{\partial\widehat{{}^{\Sigma}\psi^{\mathrm{M}}}}{\partial{}^{\Sigma}x_\alpha}\right|_{\vartheta, {}^{\Sigma}c^{\mathrm{M}}, {}^{\Sigma}x_{\beta\neq\alpha}} = \left.\frac{\partial{}^{\Sigma}c^{\mathrm{M}}{}^{\Sigma}\psi^{\mathrm{M}}}{\partial{}^{\Sigma}c_\alpha^{\mathrm{M}}}\right|_{\vartheta, {}^{\Sigma}c_{\beta\neq\alpha}^{\mathrm{M}}} = \left.\frac{\partial\rho^{\Sigma\Sigma}\psi}{\partial{}^{\Sigma}c_\alpha^{\mathrm{M}}}\right|_{\vartheta, {}^{\Sigma}c_{\beta\neq\alpha}^{\mathrm{M}}} \ , \qquad \alpha\in K_0 \ , \tag{C.168}$$

we obtain

$$\rho^{\Sigma\Sigma}\psi + \big({}^{\Sigma}c^{\mathrm{M}}\big)^2 \frac{\partial\widehat{{}^{\Sigma}\psi^{\mathrm{M}}}}{\partial{}^{\Sigma}c^{\mathrm{M}}} = \sum_{\alpha\in K_0} {}^{\Sigma}\mu_\alpha^{\mathrm{M}}\,{}^{\Sigma}c_\alpha^{\mathrm{M}} \ . \tag{C.169}$$

Defining the surface tension as

$${}^{\Sigma}\gamma \stackrel{\mathrm{def}}{=} \frac{\partial\widehat{{}^{\Sigma}\psi^{\mathrm{M}}}}{\partial\frac{1}{{}^{\Sigma}c^{\mathrm{M}}}} \ , \tag{C.170}$$

we obtain the surface Euler relation in the form

$${}^{\Sigma}c^{\mathrm{M}}{}^{\Sigma}\psi^{\mathrm{M}} - {}^{\Sigma}\gamma = \sum_{\alpha\in K_0} {}^{\Sigma}\mu_\alpha^{\mathrm{M}}\,{}^{\Sigma}c_\alpha^{\mathrm{M}} \iff \rho^{\Sigma\Sigma}\psi - {}^{\Sigma}\gamma = \sum_{\alpha\in K_0} {}^{\Sigma}\mu_\alpha^{\mathrm{M}}\,{}^{\Sigma}c_\alpha^{\mathrm{M}} \ . \tag{C.171}$$

Alternatively, using

$$\sum_{\alpha\in K_0} {}^{\Sigma}\mu_\alpha^{\mathrm{M}}\,{}^{\Sigma}c_\alpha^{\mathrm{M}} = \sum_{\alpha\in K} \big({}^{\Sigma}\mu_\alpha^{\mathrm{M}} - {}^{\Sigma}\mu_0^{\mathrm{M}}\big){}^{\Sigma}c_\alpha^{\mathrm{M}} + {}^{\Sigma}c^{\mathrm{M}}{}^{\Sigma}\mu_0^{\mathrm{M}} \ , \tag{C.172}$$

we can rewrite the surface Euler relation in the form

$$ {}^{\Sigma}c^{\mathrm{M}\,{}^{\Sigma}}\psi^{\mathrm{M}} - ({}^{\Sigma}\gamma + \mu_0^{\mathrm{M}\,{}^{\Sigma}}c^{\mathrm{M}}) = \sum_{\alpha\in K} ({}^{\Sigma}\mu_\alpha^{\mathrm{M}} - {}^{\Sigma}\mu_0^{\mathrm{M}})\, {}^{\Sigma}c_\alpha^{\mathrm{M}} \ . \tag{C.173} $$

Note that for a vacant surface, for which $\rho^{\Sigma} = 0$ and ${}^{\Sigma}c_\alpha^{\mathrm{M}} = 0$, $\alpha\in K$, and ${}^{\Sigma}c_0^{\mathrm{M}} = {}^{\Sigma}c^{\mathrm{M}}$, the Euler relation (C.171) yields

$$ {}^{\Sigma}\gamma^* \stackrel{\mathrm{def}}{=} {}^{\Sigma}\gamma|_{c_0^{\mathrm{M}}={}^{\Sigma}c^{\mathrm{M}},c_{\alpha\neq 0}^{\mathrm{M}}=0} = - {}^{\Sigma}\mu_0^{\mathrm{M}\,{}^{\Sigma}}c^{\mathrm{M}}|_{c_0^{\mathrm{M}}={}^{\Sigma}c^{\mathrm{M}},c_{\alpha\neq 0}^{\mathrm{M}}=0} \ . \tag{C.174} $$

Assuming ${}^{\Sigma}\mu_0^{\mathrm{M}}$=const and defining the surface pressure ${}^{\Sigma}p$ as the difference between the surface tension of the surface without any adsorbants and the actual surface tension, see [64], i.e. as

$$ {}^{\Sigma}p \stackrel{\mathrm{def}}{=} {}^{\Sigma}\gamma^* - {}^{\Sigma}\gamma \ , \tag{C.175} $$

the surface Euler relation becomes

$$ {}^{\Sigma}c^{\mathrm{M}\,{}^{\Sigma}}\psi^{\mathrm{M}} + {}^{\Sigma}p = \sum_{\alpha\in K} ({}^{\Sigma}\mu_\alpha^{\mathrm{M}} - {}^{\Sigma}\mu_0^{\mathrm{M}})\, {}^{\Sigma}c_\alpha^{\mathrm{M}} \ . \tag{C.176} $$

By the same argument as in the bulk, i.e. taking differential of (C.171), and employing the thermodynamic relations, one arrives at the surface Gibbs-Duhem relation

$$ -{}^{\Sigma}\eta^{\mathrm{M}\,{}^{\Sigma}}c^{\mathrm{M}} d^{\Sigma}\vartheta - d^{\Sigma}\gamma = \sum_{\alpha\in K_0} {}^{\Sigma}c_\alpha^{\mathrm{M}} d^{\Sigma}\mu_\alpha^{\mathrm{M}} \Longleftrightarrow -{}^{\Sigma}\eta^{\mathrm{M}\,{}^{\Sigma}}c^{\mathrm{M}} d^{\Sigma}\vartheta + d^{\Sigma}p = \sum_{\alpha\in K} {}^{\Sigma}c_\alpha^{\mathrm{M}} d({}^{\Sigma}\mu_\alpha^{\mathrm{M}} - {}^{\Sigma}\mu_0^{\mathrm{M}}) - {}^{\Sigma}\mu_0^{\mathrm{M}} d^{\Sigma}c^{\mathrm{M}}. \tag{C.177} $$

Bibliography

[1] A.W. Adamson. *Physical chemistry of surfaces*. A Wiley-Interscience publication. Wiley, 1990.

[2] P.R. Amestoy, I.S. Duff, and J.-Y. L'Excellent. Multifrontal parallel distributed symmetric and unsymmetric solvers. *Computer Methods in Applied Mechanics and Engineering*, 184(2):501 – 520, 2000.

[3] SP Antal, RT Lahey, and JE Flaherty. Analysis of phase distribution in fully developed laminar bubbly two-phase flow. *International Journal of Multiphase Flow*, 17(5):635–652, 1991.

[4] P Atkins. Atkins physical chemistry, 2006.

[5] AB Basset. A treatise on hydrodynamics vol i. deighton, bell and co, london george bell and sons, 1888.

[6] G Batchelor. An introduction to fluid mechanics (cambridge. *Press, Cambridge UK*, 1967.

[7] D Bedeaux. Nonequilibrium thermodynamics and statistical physics of surfaces. *Adv. Chem. Phys*, 64(47):C109, 1986.

[8] D. Bedeaux, A.M. Albano, and P. Mazur. Boundary conditions and non-equilibrium thermodynamics. *Physica A: Statistical Mechanics and its Applications*, 82(3):438 – 462, 1976.

[9] P Bogacki and Lawrence F Shampine. An efficient runge-kutta (4, 5) pair. *Computers & Mathematics with Applications*, 32(6):15–28, 1996.

[10] D. Bothe. On the multiphysics of mass transfer across fluid interfaces. *arXiv: 1501.05610*, 2015.

[11] D. Bothe and W. Dreyer. Continuum thermodynamics of chemically reacting fluid mixtures. *Acta Mechanica*, 226(6):1757–1805, 2015.

[12] Dieter Bothe. *On the Maxwell-Stefan Approach to Multicomponent Diffusion*, pages 81–93. Springer Basel, Basel, 2011.

[13] Joseph Boussinesq. Sur la résistance qu'oppose un liquide indéfini en repos. *CR Acad. Sci. Paris*, 100:935–937, 1885.

[14] C.E. Brennen. *Fundamentals of Multiphase Flow*. Cambridge University Press, 2005.

[15] Phillip P Brown and Desmond F Lawler. Sphere drag and settling velocity revisited. *Journal of environmental engineering*, 129(3):222–231, 2003.

[16] John J Carroll, John D Slupsky, and Alan E Mather. The solubility of carbon dioxide in water at low pressure. *Journal of Physical and Chemical Reference Data*, 20(6):1201–1209, 1991.

[17] MW Chase. Nist-janaf thermochemical tables (journal of physical and chemical reference data monograph no. 9). *American Institute of Physics*, 1998.

[18] R Clift, JR Grace, and ME Weber. Bubbles, drops and particles. 1978.

[19] Roland Clift, John R Grace, and Martin E Weber. *Bubbles, drops, and particles*. Courier Corporation, 2005.

[20] Livija Cveticanin. *Dynamics of machines with variable mass*. CRC Press, 1998.

[21] John Dalton. On the constitution of mixed gases, on the force of steam of vapour from water and other liquids in different temperatures, both in a torricellia vacuum and in air; on evaporation; and on the expansion of gases by heat. *Memoirs, Literary and Philosophical Society of Manchester*, 5(2):536–602, 1802.

[22] Carter Dan and Wing Jonathan. Fuel cell industry review 2013. *Fuel Cell Today: Hertfordshire, UK*, 2013.

[23] S.R. de Groot and P. Mazur. *Non-equilibrium Thermodynamics*. Dover Books on Physics. Dover Publications, 1984.

[24] Arthur R Deemer and John C Slattery. Balance equations and structural models for phase interfaces. *International Journal of Multiphase Flow*, 4(2):171–192, 1978.

[25] D. Do Duong. *Adsorption analysis: equilibria and kinetics*, volume 2 of *Series on chemical engineering*. Imperial College Press, London, 1998.

[26] W. Dreyer. On jump conditions at phase boundaries for ordered and disordered phases. *WIAS Preprint*, 869, 2003.

[27] D. A. Edwards, H. Brenner, and D. T. Wasan. *Interfacial Transport Processes and Rheology*. Butterworth-Heinemann, Boston, 1991.

[28] DA Edwards, H Brenner, and DT Wasan. Interfacial transport processes and rheology, 1991. *Bufferworth-Heinemann, Boston*, 1991.

[29] SE Elghobashi and TW Abou-Arab. A two-equation turbulence model for two-phase flows. *The Physics of Fluids*, 26(4):931–938, 1983.

[30] LS Fan and C Zhu. Principles of gas-solid flows. 1999.

[31] Vasiliy Fefelov, Vitaly Gorbunov, Alexander Myshlyavtsev, and Marta Myshlyavtseva. Statistical thermodynamics of lattice gas models of multisite adsorption. In Ricardo Morales-Rodriguez, editor, *Thermodynamics - Fundamentals and Its Application in Science*, chapter 15. InTech, Rijeka, 2012.

[32] R. Gatignol and R. Prud'Homme. *Mechanic and Thermodynamic Modeling of Fluid Interfaces*. World Scientific Publishing, Singapore, 2001.

[33] J.W. Gibbs. *The collected works of J. Willard Gibbs, vol. 1*. Yale University Press, New Haven, 1928.

[34] J.W. Gibbs, H.A. Bumstead, R.G. Van Name, and W.R. Longley. *The collected works of J. Willard Gibbs*. Number sv. 2 in The Collected Works of J. Willard Gibbs. Longmans, Green and Co., 1902.

[35] Martin Grasemann and Gábor Laurenczy. Formic acid as a hydrogen source-recent developments and future trends. *Energy & Environmental Science*, 5(8):8171–8181, 2012.

[36] Dwight E Gray. American institute of physics (aip). handbook. *AIP Advances*, 1, 1963.

[37] Don W Green. Perry's chemical engineering handbook. *McGrawHill Professional*, 2007.

[38] A Haider and O Levenspiel. Drag coefficient and terminal velocity of spherical and nonspherical particles. *Powder technology*, 58(1):63–70, 1989.

[39] David Halliday and Robert Resnick. *Fundamentals of physics*. John Wiley & Sons, 1981.

[40] W.M. Haynes. *CRC Handbook of Chemistry and Physics*. 94th Edition. CRC Press, 2014.

[41] William Henry. Experiments on the quantity of gases absorbed by water, at different temperatures, and under different pressures. *Philosophical Transactions of the Royal Society of London*, 93:29–276, 1803.

[42] Jukka Hietala, Antti Vuori, Pekka Johnsson, Ilkka Pollari, Werner Reutemann, and Heinz Kieczka. *Formic Acid*. Wiley-VCH Verlag GmbH & Co. KGaA, 2000.

[43] L.T. Hill. *An introduction to statistical thermodynamics*. Addison-Wesley Publishing Company, London, 1960.

[44] Thomas JR Hughes, Leopoldo P Franca, and Marc Balestra. A new finite element formulation for computational fluid dynamics: V. circumventing the babuška-brezzi condition: a stable petrov-galerkin formulation of the stokes problem accommodating equal-order interpolations. *Computer Methods in Applied Mechanics and Engineering*, 59(1):85–99, 1986.

[45] K. Hutter and K. Jöhnk. *Continuum methods of physical modeling*. Springer-Verlag, Berlin, 2004. Continuum mechanics, dimensional analysis, turbulence.

[46] E Iglesia and M Boudart. Decomposition of formic acid on copper, nickel, and copper-nickel alloys: Iii. catalytic decomposition on nickel and copper-nickel alloys. *Journal of Catalysis*, 81(1):224–238, 1983.

[47] E. Isaacson and H.B. Keller. *Analysis of Numerical Methods*. Dover Books on Mathematics. Dover Publications, 1994.

[48] Hugo A Jakobsen. Chemical reactor modeling. *Multiphase Reactive Flows, Berlin, Germany: Springer-Verlag*, 2008.

[49] SF Jones, GM Evans, and KP Galvin. Bubble nucleation from gas cavities-a review. *Advances in colloid and interface science*, 80(1):27–50, 1999.

[50] D. G. KARAMANEV. Equations for calculation of the terminal velocity and drag coefficient of solid spheres and gas bubbles. *Chemical Engineering Communications*, 147(1):75–84, 1996.

[51] Irvin M Krieger and Thomas J Dougherty. A mechanism for non-newtonian flow in suspensions of rigid spheres. *Transactions of the Society of Rheology*, 3(1):137–152, 1959.

[52] R Krishna, M.I Urseanu, J.M van Baten, and J Ellenberger. Rise velocity of a swarm of large gas bubbles in liquids. *Chemical Engineering Science*, 54(2):171 – 183, 1999.

[53] GDC Kuiken. *Thermodynamics of Irreversible Processes. Applications to Diffusion and Rheology*. John Wiley Sons, Chichester, 1995.

[54] D Kunii and O Levenspiel. 1991, fluidization engineering.

[55] Horace Lamb. *Hydrodynamics*. Cambridge university press, 1895.

[56] Irving Langmuir. The adsorption of gases on plane surfaces of glass, mica, and platinum. *J. Am. Chem. Soc.*, 40(9):1361–1403, 1918.

[57] Brian Edward Launder. On the computation of convective heat transfer in complex turbulent flows. *ASME, Transactions, Journal of Heat Transfer*, 110:1112–1128, 1988.

[58] Brian Edward Launder and Dudley Brian Spalding. The numerical computation of turbulent flows. *Computer methods in applied mechanics and engineering*, 3(2):269–289, 1974.

[59] Der-Tsai Lee and Bruce J Schachter. Two algorithms for constructing a delaunay triangulation. *International Journal of Computer & Information Sciences*, 9(3):219–242, 1980.

[60] Evgeny Mikhailovich Lifshitz, LP Pitaevskii, and VB Berestetskii. Course of theoretical physics. *Statistical physics*, 5, 1980.

[61] Rainald Löhner and Paresh Parikh. Generation of three-dimensional unstructured grids by the advancing-front method. *International Journal for Numerical Methods in Fluids*, 8(10):1135–1149, 1988.

[62] E Loth. Numerical approaches for motion of dispersed particles, droplets and bubbles. *Progress in Energy and Combustion Science*, 26(3):161–223, 2000.

[63] RG Lunnon. Fluid resistance to moving spheres. *Proceedings of the Royal Society of London. Series A, Containing Papers of a Mathematical and Physical Character*, 110(754):302–326, 1926.

[64] J. Lyklema. *Fundamentals of Interface and Colloid Science: Solid-Liquid Interfaces*. Fundamentals of Interface & Colloid Science. Elsevier Science, 1995.

[65] P Mars, JJF Scholten, P Zwietering, DD Eley, H Pines, and PB Weisz. Advances in catalysis, vol. 14, 1963.

[66] J.C. Maxwell. On the dynamical theory of gases. *Philosophical Transactions of the Royal Society of London*, 157:49–88, 1867.

[67] Alan D McNaught and Andrew Wilkinson. Compendium of chemical terminology: Iupac, 1997.

[68] A Messadi, N Dhouibi, and H Hamda. A new equation relating the viscosity arrhenius temperature and the activation energy for some newtonian classical solvents. *Journal of Chemistry*, 2015.

[69] J Milewski, A Miller, and K Badyda. The control strategy for high temperature fuel cell hybrid systems. 2010.

[70] I. Müller. *Thermodynamics*. Interaction of Mechanics and Mathematics. Pitman Publishing Limited, London, 1985.

[71] R. I. Nigmatulin. Spatial averaging in the mechanics of heterogeneous and dispersed systems. *International Journal of Multiphase Flow*, 5(5):353–385, 1979.

[72] T. Nitta, T. Shigetomi, M. Kuto-Oka, and T. Katayama. An adsorption isotherm of multi-site occupancy model for homogeneous surface. *Journal of chemical engineering of Japan*, 17(1):39–45, 1984.

[73] Arthur A Noyes and Willis R Whitney. The rate of solution of solid substances in their own solutions. *Journal of the American Chemical Society*, 19(12):930–934, 1897.

[74] CD Ohl, A Tijink, and A Prosperetti. The added mass of an expanding bubble. *Journal of Fluid Mechanics*, 482:271–290, 2003.

[75] Vít Orava, Ondřej Souček, and Peter Cendula. Multi-phase modeling of non-isothermal reactive flow in fluidized bed reactors. *Journal of Computational and Applied Mathematics*, 289:282–295, 2015.

[76] CW Oseen. Ueber die stokes scheformel, und ueber eine venvandte aufgabe in der hydrodynamik. *Ark. Math. Astronom. Fys*, 6, 1910.

[77] A Werner Preukschat. *Measurements of drag coefficients*. PhD thesis, California Institute of Technology, 1962.

[78] Miroslav Puncochar, Marek C Ruzicka, and Miroslav Simcik. Bubble swarm rise velocity in fluidized beds. *Chemical Engineering Science*, 152:84–94, 2016.

[79] K. R. Rajagopal and A. R. Srinivasa. On thermomechanical restrictions of continua. *Proceedings of the Royal Society of London A: Mathematical, Physical and Engineering Sciences*, 460(2042):631–651, 2004.

[80] K. R. Rajagopal and L. Tao. *Mechanics of mixtures*, volume 35 of *Series on Advances in Mathematics for Applied Sciences*. World Scientific Publishing Co. Inc., River Edge, NJ, 1995.

[81] A. J. Ramirez-Pastor, J. L. Riccardo, and V. D. Pereyra. Adsorption thermodynamics with multisite occupancy at criticality. *Langmuir*, 16(26):10167–10174, 2000.

[82] VH Ransom and JD Ramshaw. Discrete modeling considerations in multiphase fluid dynamics. Technical report, EG and G Idaho, Inc., Idaho Falls (USA), 1988.

[83] JF Richardson and WN Zaki. The sedimentation of a suspension of uniform spheres under conditions of viscous flow. *Chemical Engineering Science*, 3(2):65–73, 1954.

[84] L. L. Romanielo, S. Arvelos, F. W. Tavares, and K. Rajagopal. A modified multi-site occupancy model: evaluation of azeotropelike behavior in adsorption. *Adsorption*, 21(1):3–16, Feb 2015.

[85] W. Rudzinski and D.H. Everett. *Adsorption of Gases on Heterogeneous Surfaces*. Academic Press Ltd, San Diego, 1992.

[86] Leonard M.C. Sagis. Dynamic behavior of interfaces: Modeling with nonequilibrium thermodynamics. *Advances in Colloid and Interface Science*, 206:328 – 343, 2014.

[87] Olaf Schenk and Klaus Gärtner. Solving unsymmetric sparse systems of linear equations with pardiso. *Future Generation Computer Systems*, 20(3):475 – 487, 2004. Selected numerical algorithms.

[88] L. Schiller and Z. Naumann. Uber die grundlegenden berechnungen bei der schwerkraftaufbereitung. *Z. Ver. Deut. Ing.*, 77:318–326, 1933.

[89] MP Schwarz and WJ Turner. Applicability of the standard k-ε turbulence model to gas-stirred baths. *Applied Mathematical Modelling*, 12(3):273–279, 1988.

[90] LE Scriven. Dynamics of a fluid interface equation of motion for newtonian surface fluids. *Chemical Engineering Science*, 12(2):98–108, 1960.

[91] G. Shen and J.A. Finch. Bubble swarm velocity in a column: a two-dimensional approach. *Chemical Engineering Science*, 52(19):3287 – 3293, 1997.

[92] Martin Stuart Silberberg, Randy Duran, Charles G Haas, and Arlan D Norman. *Chemistry: The molecular nature of matter and change*, volume 4. McGraw-Hill New York, 2006.

[93] M Simcik and MC Ruzicka. Added mass of dispersed particles by cfd: Further results. *Chemical Engineering Science*, 97:366–375, 2013.

[94] M Simcik, MC Ruzicka, and J Drahoš. Computing the added mass of dispersed particles. *Chemical Engineering Science*, 63(18):4580–4595, 2008.

[95] O Simonin and PL Viollet. Modelling of turbulent two-phase jets loaded with discrete particles. *FG Hewitt, et al., Phenomena in multiphase yow*, page 259, 1990.

[96] J.C. Slattery. *Interfacial Transport Phenomena*. Springer Verlag, New York, 1990.

[97] J.C. Slattery, L. Sagis, and E.-S. Oh. *Interfacial transport phenomena*. Springer, Berlin, 2007.

[98] J.C. Slattery, L. Sagis, and E.S. Oh. *Interfacial Transport Phenomena*. Springer US, 2007.

[99] John C Slattery. Flow of viscoelastic fluids through porous media. *AIChE Journal*, 13(6):1066–1071, 1967.

[100] John C Slattery. Single-phase flow through porous media. *AIChE Journal*, 15(6):866–872, 1969.

[101] JOHN C SLATTERY. Interfacial transport phenomena invited review. *Chemical Engineering Communications*, 4(1-3):149–166, 1980.

[102] John C Slattery. *Advanced transport phenomena*. Cambridge University Press, 1999.

[103] A Sokolichin, G Eigenberger, and A Lapin. Simulation of buoyancy driven bubbly flow: established simplifications and open questions. *AIChE Journal*, 50(1):24–45, 2004.

[104] DB Spalding and MR Malin. A two-fluid model of turbulence and its application to heated plane jets and wakes. *Physicochemical Hydrodynamics*, 5:339–361, 1984.

[105] J Stefan. Über das gleichgewicht und bewegung, insbesondere die diffusion von gemischen. *Philosophical Transactions of the Royal Society of London*, 63:63–124, 1871.

[106] Jeffrey I Steinfeld, Joseph Salvadore Francisco, and William L Hase. *Chemical kinetics and dynamics*, volume 3. Prentice Hall Englewood Cliffs (New Jersey), 1989.

[107] George Gabriel Stokes. *On the effect of the internal friction of fluids on the motion of pendulums*, volume 9. Pitt Press, 1851.

[108] AH Techet. 2.016 hydrodynamics. *Lecture Notes*, 2005.

[109] A Tomiyama, A Sou, I Zun, N Kanami, and T Sakaguchi. Effects of eötvös number and dimensionless liquid volumetric flux on lateral motion of a bubble in a laminar duct flow. *Advances in multiphase flow*, 1995:3–15, 1995.

[110] C. Truesdell and W. Noll. The non-linear field theories of mechanics. In S. Flüge, editor, *Handbuch der Physik*, volume III/3. Springer, Berlin, 1965.

[111] Clifford Truesdell. *Rational thermodynamics*. Springer Science & Business Media, 2012.

[112] Graham B Wallis. Inertial coupling in two-phase flow: macroscopic properties of suspensions in an inviscid fluid. *Multiphase Science and Technology*, 5(1-4), 1990.

[113] Eric W. Weisstein. Tree. From MathWorld–A Wolfram Web Resource.

[114] Blaine Benjamin Wescott and Carl John Engelder. The catalytic decomposition of formic acid. *The Journal of Physical Chemistry*, 30(4):476–479, 1926.

[115] Igor Yuranov, Nordahl Autissier, Katerina Sordakis, Andrew F. Dalebrook, Martin Grasemann, Vít Orava, Peter Cendula, Lorenz Gubler, and Gábor Laurenczy. Heterogeneous catalytic reactor for hydrogen production from formic acid and its use in polymer electrolyte fuel cells. *ACS Sustainable Chemistry & Engineering*, 6(5):6635–6643, 2018.

List of publications

1. *Multi-phase modelling of non-isothermal reactive flow in fluidized bed reactors*; Vít Orava, Ondřej Souček, Peter Cendula; Journal of Computational and Applied Mathematics, 289:282-295, 2015.

2. *Heterogeneous catalytic reactor for hydrogen production from formic acid and its use in polymer electrolyte fuel cells* Igor Yuranov, Nordahl Autissier, Katerina Sordakis, Andrew F. Dalebrook, Martin Grasemann, Vít Orava, Peter Cendula, Lorenz Gubler, Gábor Laurenczy; ACS Sustainable Chemistry & Engineering, 6(5):6635-6643, 2018.

3. *A continuum model of heterogeneous catalysis: thermodynamic framework for multicomponent bulk and surface phenomena coupled by sorption*; Ondřej Souček, Vít Orava, J. Málek, D. Bothe; under review in the International Journal of Engineering Science.